Slag-Metal Reactions
During
Flux Shielded Arc Welding

by

Chang-Shung Chai

B.S., Fu-Jen University
(1973)

M.A., Temple University
(1977)

SUBMITTED IN PARTIAL FULFILLMENT
OF THE REQUIREMENTS FOR THE
DEGREE OF

DOCTOR OF PHILOSOPHY

at the

© MASSACHUSETTS INSTITUTE OF TECHNOLOGY

September 1980

Signature of Author_____
Department of Materials Science and Engineering
August 8, 1980

Certified by_____ _____
Thomas W. Eagar
Thesis Supervisor

Accepted by_____ _____
Regis M. N. Pelloux
Chairman, Departmental Committee

ABSTRACT

SLAG-METAL REACTIONS DURING
FLUX SHIELDED ARC WELDING

by

CHANG-SHUNG CHAI

Submitted to the Department of Materials Science and
Engineering on August 8, 1980 in partial fulfillment of
the requirements for the degree of Doctor of Philosophy
in Materials Engineering.

The thermodynamic and kinetic parameters controlling the
chemical composition of weld deposits produced during flux
shielded arc welding have been studied. The primary process
studied was submerged arc welding using fused neutral fluxes
although several bonded neutral fluxes were also tested.

A statistical analysis of the effect of the SAW operating
parameters on the manganese, silicon and oxygen recovery has
been performed. The results indicate that wide variations in
the weld metal chemistry may occur depending upon the choice
of operating parameters. In the case of oxygen, the recovery
level varied from 210 ppm to 580 ppm when using a calcium
silicate flux, while the variation for a manganese silicate
flux was 670 ppm to 1740 ppm. Variation in silicon and manga-
nese contents was of similar magnitude, indicating the
complexity of slag-metal reactions which occur during welding.

The effective temperature of the weld pool is estimated
to be $2000^{\circ}C$ from both the SiO_2 and the MnO reaction
equilibria, provided that the surface Mn content is used
instead of the bulk Mn content when computing the MnO reaction
temperature. The bulk Si analysis may be used when computing
the SiO_2 reaction temperature due to the uniform spatial
distribution of Si in the weld metal. It may be concluded

that the slag and the metal reach an effective equilibrium at the interface but not in the bulk.

A thermodynamic equilibrium model has been developed to predict the range of possible Mn and Si contents in the weld metal for a given flux, electrode and base metal chemistry. The data from over one hundred welds were fit to this model with considerable success. Furthermore, the predicted slag-metal equilibrium composition has been verified for twelve different fluxes. It is concluded that this model is capable of defining the limits of Mn and Si changes. In order to reduce the predicted range generated from the thermodynamic model, a mass balance restriction was also used. In some, but not all, cases, the range can be reduced significantly by this.

The mechanisms controlling alloying element transport between the slag and the weld metal have been investigated. From the spatial distributions of Mn and Si in the metal phase and MnO and SiO_2 in the slag phase, it is concluded that the rate limiting step is in the slag phase rather than in the metal phase. The transport coefficient and the effective boundary layer thickness of Mn in the metal phase are estimated to be 10^{-3} cm^2/s and 1 mm respectively, while in the slag phase, the value are on the order of 10^{-4} cm^2/s and 0.35 mm for both MnO and SiO_2.

In computing the mass balance, the sources of alloying elements were equated to the sinks of these elements. The relative important of each of the sinks has been established for the first time. One conclusion of this analysis is that alloying the weld metal by reaction from a neutral flux is not an efficient method, especially if highly alloyed weld metal is desired.

The plasmadynamic oxygen potential of welding flux components was studied using CaF_2-oxide binary fluxes. SiO_2 and MnO are found to be major contributors of oxygen, while CaO is the stablest oxide of the eight different oxides exaimed. The oxygen potentials of fused and bonded fluxes were also investigated. It is concluded that the oxygen pontential of bonded flux is higher than that of fused flux due to the greater homogeneity and lower oxygen activity of the individual components in the fused flux.

Thesis Supervisor: Thomas W. Eagar
            Title: Associate Professor
                     of Materials Engineering

TABLE OF CONTENTS

TABLE OF CONTENTS (continued)

TABLE OF CONTENTS (continued)

LIST OF TABLES

LIST OF TABLES (continued)

LIST OF FIGURES

LIST OF FIGURES (continued)

LIST OF APPENDICES

ACKNOWLEDGEMENTS

I wish to express my sincere appreciation to Professor Thomas W. Eagar for his guidance and encouragement throughout the past years. The subject of this thesis sparked from his suggestions, while he supervised closely most of the areas covered and provided many very useful remarks that shaped its final form. Aside that, the unselfish help of Professor Eagar and his wife, Pamela, in my wedding ceremony was unforgettable in my life. The assistance of Mr. Bruce Russell with the construction of the water cooled copper trough has been invaluable to me. Finally, I wish to thank my family and my wife, Man-Lih who indirectly contributed to this work through their love during the past years.

I. INTRODUCTION

During the past fifty years, welding has grown from a relatively uncommon, untrusted method of joining metals to a common and, in many cases, a most reliable metals joining process. By far the commonest welded material is steel, which offers a wide variety of properties at a reasonable cost. These properties are developed through control of the chemical composition and of the processing which the steel undergoes during manufacture. In recent years, base metal properties have been improved significantly through minor changes in composition coupled with major new processing techniques. An entire new family of steel designated as high strength low alloy (HSLA) has been developed for use in pipelines, ship-building, heavy construction equipment and so forth. Welding technology is having difficulty in matching these advances in base metal properties.

An ideal weld is one in which the properties of the weld metal exactly duplicate the properties of the base metal. Unfortunately, a weld is effectively a casting and as such does not retain the characteristics of the base metal as a result of prior processing. For this reason, the structure and properties of the weld metal are determined primarily through control of the chemical composition of the deposit.

-15-

As the processing of the base metal becomes more advanced, the required properties in the weld metal have become increasingly difficult to achieve. In particular, the factors controlling weld metal chemistry are poorly understood resulting in an empirical approach to the problem. The purpose of the present study is to develop an improved understanding of the chemical changes occurring during flux shielded welding. In this way, it is hoped that a more rational control of the weld metal chemistry and, hence, improved properties may be achieved.

A wide variety of steel is used in engineering structures. This requires an equally wide variety of weld deposits. The composition of each deposit is determined by the compositions of the electrode, the flux and the base metal. The effect of selected elements on mechanical properties, notch toughness and weldability of steel may be indicated as follows:

Carbon: Carbon is the most important alloying element in steel. Increased amounts of carbon increase the hardness, the strength (both yield and ultimate) and the response to heat treatment(hardenability). However, the addition of carbon causes many undesirable effects including reduction in elongation, in notch toughness and in weldability. The reduction in weldability is due to an increase in the hardness of the heat affected zone and an increase in susceptibility to both hot and cold cracking. Because of these adverse effects,

the carbon content of a weldable steel is normally limited to below 0.25%(1,2,3,4).

Manganese: Manganese is added to steel, because it is moderately deoxidizing, and it improves the notch toughness. An increase in manganese up to around 1.2% results in an improvement in notch toughness, but Mn contents over 1.6% cause a rapid deterioration notch toughness(5). Such a reduction in toughness is often due to banding caused by segregation in the ingot. Manganese is also known to reduce hot cracking in the weld metal and in the heat affected zone by reacting with sulphur. Manganese increases hardenability, which in the presence of high carbon content may be detrimental to weldability(1,2).

Silicon: The main function of silicon in steel is to act as a deoxidizer, but the addition of silicon also causes a reduction in elongation and increases the tendency to hot cracking. Up to 0.6% silicon has little effect on notch toughness, but an addition of silicon over 0.6% causes an increase in the transition temperature(1,2). Silicon is an inexpensive strengthening agent in steels, but most welding codes restrict the maximum silicon level to 0.5%. The reason for this restriction is probably historical rather than technical(1,2,6,7).

Oxygen: The effect of oxygen on notch toughness is complex, because it may be found in either a dissolved form

which increases the transition temperature or as inclusions which lower the upper shelf energy. In either case, oxygen has a detrimental effect on fracture toughness. Oxygen may also lead to formation of porosity, particularly in low silicon steel, to promotion of high temperature brittleness and to a decrease in elongation (1,2,6,8). It is common practice to reduce the amount of oxygen in the weld metal by adding deoxidizers such as silicon, manganese and aluminum to the flux and/or the electrodes.

As mentioned above, the mechanical properties of a steel weldment are controlled by the chemistry of the weld metal and the process parameters. The variability of the mechanical properties is increased by gross differences in the weld deposit chemistry resulting from a poor understanding of chemical reactions which occur during the welding process. The central aim of the study which is presented here is a determination of the factors which influence the weld metal composition during flux shielded arc welding. The study hinges upon the assumption that a neutral point or equilibrium condition exists at which metal transport between the slag and the metal phase is zero. Once such weld and flux compositions are determined, several kinetic factors are investigated in order to determine why the weld does not always attain this equilibrium. Five primary approaches have been taken in studying this problem.

Approach 1: Screening experiment

The welding process includes many variables which may affect the weld deposit composition. In order to assess accurately the variables which are of most significance, a screening experiment was performed. This experiment provided the direction needed for the following steps:

Approach 2: Equilibrium point

The basic assumption that a single equilibrium point exists was modelled thermodynamically and tested experimentally.

Approach 3: Mass balance

In some cases, the range of permissible weld metal compositions as predected by thermodynamic model is broad. In order to reduce the predicted range, mass balance has been proposed as an additional restriction upon the weld metal composition.

Approach 4: Kinetics

In order to understand why the predicted equilibrium is not always attained, the spatial distributions of Mn and Si in both the metal and the slag phases have been investigated. The results of this study are then compared with the initial assumptions of the thermodynamic equilibrium model in order to test for consistency.

Approach 5: Plasmadynamic oxygen potential

Finally, the plasmadynamic oxygen potential of CaF_2-oxide

binary flux systems were also investigated. This study aided
in understanding the effect of various flux components on the
reactivity of more complex fluxes.

II. PREVIOUS WORK

Manganese, silicon and oxygen contents undergo the greatest changes during flux shielded welding. As a result, several previous investigators have studied reactions involving these species. Most of this work has been empirical, although in some of the work the investigators have attempted to classify the chemical activities of the fluxes through an index such as excess acidity or basicity. These former studies have been only partly successful in predicting the chemical behavior of welding fluxes(7,9-22).

2.1 Types of submerged arc welding fluxes

The terms "welding flux" and "welding slag" may be considered by some as synonymous. Based on the definition of American Welding Society, flux is a material used to prevent, dissolve or facilitate removal of oxides and other undesirable substances. There is no AWS definition of the term welding slag. For the purpose of discussion in this study, flux is used to describe the material prior to welding and slag is used to describe the fused residue remaining after welding. The term "neutral flux" as used in this study denotes a flux whose chemical recovery in the weld metal is independent of the welding voltage. Implied in this definition is the fact that the weld metal chemistry is independent of the volume of

flux melted(*). Fluxes containing ferroalloy or metal powder additions alter weld deposit compositions as the voltage is changed and are classified as "active fluxes".

The main types of submerged arc welding fluxes are fused, bonded, agglomerated and pressed powder fluxes. Aside from differences in production, there are certain inherent advantages and disadvantages of each. These will be described briefly.

2.1.1 Fused flux:

In the preparation of fused fluxes, the raw materials are dry mixed and melted in an electric furnace. After melting, the melt is usually poured onto chill plates and crushed to the specified particle size. The advantages of fused fluxes are the following(19,20,23):

1) Extremely good chemical homogeneity.

2) Fines may be removed without changing the composition of the flux.

3) Volatiles are absent, producing a quiescent slag pool during welding with relatively little gas evolution.

4) Most fused fluxes are nonhygroscopic, thus simplifying storage problems.

5) The unfused portion may be collected after welding and used again without significant change in flux

---

(*)The quantity of flux consumed during welding increases as the welding voltage increases even though the volume of weld metal remains essentially constant.

-22-

composition due to particle size or density
segregation.

The primary disadvantage of fused fluxes is the inability to
add deoxidizers and ferroalloys without segregation.

2.1.2 Bonded flux:

Raw materials for producing bonded fluxes are ground to
approximately 100xD(*), dry mixed and then bonded by addition
of potassium silicate or sodium silicate. The resulting mix-
ture is then dried at a relative low temperature. The advan-
tages of this type of flux are the following(19,20,23):

1) The low bonding temperatures permit the extensive
   use of metallic deoxidizers and ferroalloys, and

2) The flux can be color coded.

The disadvantages of the bonded fluxes are the following:

1) Fines cannot be removed for fear of altering the
   flux composition.

2) The flux has a tendency to pick up moisture due to
   the potassium silicate or sodium silicate binding
   agents.

3) The flux may evolve significant quantities of gas
   during welding.

(*)To provide a quantitive measurement of flux particle sizes,
flux manufacturers usually mark the largest and smallest mesh
numbers. For example, 100xD means that flux particle sizes
range between 100 mesh and dust (less than 250 mesh)

2.1.3 Agglomerated flux:

Agglomerated fluxes are similar to the bonded fluxes except that the agglomerated flux is bonded with a ceramic which is cured at temperatures in excess of $760^{\circ}C$. The advantages and the disadvantages are almost the same as those of bonded fluxes except that the use of deoxidizers and ferro-alloys is limited due to the relatively high temperatures involved in the manufacturing process(19,20,23).

2.1.4 Pressed powder flux:

In the manufacture of pressed powder fluxes, the chemicals are dry mixed, compressed and baked. The advantages and disadvantages are the same as those of bonded fluxes, except that the binder is not required(20).

The historical development, the role, the physical properties and the welding characteristics of submerged arc welding fluxes have been reviewed by Jackson(19) and Garland (20).

2.2 Slag-metal reactions during welding:

A major advance in systematizing the study of slag-metal reactions during welding was begun by Christensen and Chipman(10) who have indicated that the effective weld pool temperature is approximately $1900^{\circ}C$ based upon tungsten-molybdenum thermocouple measurements and $2000^{\circ}C$ based upon pseudoequilibrium chemical reaction measurements. Belton, Moore and Tankins(12) have reported a metal pool temperature

of 2300°C based upon tungsten-rhenium thermocouple measure-
ments and 2000°C based upon chemical equilibrium measurements.
Up to now, the true slag-metal equilibrium in welding has not
been determined, although several authors have tried to
measure it(10,12,14,15,24-26).

2.2.1 Welding flux basicity:

Ever since Christensen and Chipman showed a consistent
variation of silicon and manganese mass indices with excess
acid content of their fluxes, investigators of welding fluxes
have classified their fluxes by a basicity index, although the
basicity index concept itself is imprecise. Many basicity
indices have been defined (27,28,29). An official basicity
index has been defined by the International Institute of
Welding (IIW) as

$$BI = \frac{MgO+CaF_2+CaO+BaO+SrO+Na_2O+K_2O+Li_2O+1/2(MnO+FeO)}{SiO_2+1/2(Al_2O_3+TiO_2+ZrO_2)} \quad (1)$$

Eagar has modified this formula slightly, by removing
CaF_2 from the above formula. He believes that CaF_2 is neutral
in terms of reactions involving silicon, manganese and oxygen.
In addition, this change allows the IIW basicity index to be
used with some of the thermodynamic data developed in
steelmaking.

Welding investigators have found an empirical rela-
tionship between the basicity index and the oxygen content in

the weld metal. This is shown in Figure 1(7,11), where the basicity index has been defined by Eagar's method. Several investigators have tried to explain the weld metal oxygen content based upon the composition of the flux. It has been claimed that SiO_2(7), FeO(7) and CaO(17) may each control the oxygen content of the weld metal. The mechanism of this control is not always explained.

It has been proposed to the IIW that welding fluxes be classified based upon their oxygen potential rather than their basicity index; however, this would be difficult as it cannot presently be agreed which flux components affect the oxygen content of the weld metal.

2.2.2 The SiO_2 reaction:

As noted previously, several authors have suggested effective reaction temperatures based upon specific chemical reactions, e.g., the SiO_2 reaction:

$$SiO_{2(\ell)} = \underline{Si} + 2\underline{O} \qquad (2)$$

is generally believed to attain an effective temperature of $2000\,^{0}C$ in acidic fluxes(12). The spatial distribution of silicon has also been investigated by previous authors(10,12, 14,15) and found to be uniform. The spatial distribution of SiO_2 in the slag phase has not yet been investigated.

2.2.3 The MnO reaction:

Several authors have found that the MnO reaction:

$$MnO_{(\ell)} = \underline{Mn} + \underline{O} \qquad\qquad (3)$$

does not appear to reach a single effective equilibrium temperature(10,14,15). Others have investigated the manganese reaction in welding and found that the spatial distribution of manganese in the weld metal appears to be nonuniform(10,14,15, 18). The spatial distribution of MnO in the slag phase has not been investigated.

Christensen(10,14,15) has found that there is a trend for the manganese mass action index to increase as welding travel speed increases; however, North(18) and Thier(26) have shown that there is no effect between weld metal manganese content and the travel speed.

2.2.4 The CaO reaction:

The so called stable oxides such as CaO or SiO_2 may become unstable at the high temperatures encountered in welding. These temperatures may be estimated to be around $2000^\circ C$ in the weld metal pool and 8000 K in the plasma. North(17) has claimed that the source of oxygen in the weld metal is mainly CaO which decomposes at these temperatures, although his fluxes were blended and contained $CaCO_3$ as the source of CaO. It is likely that the increased weld metal oxygen content in his study resulted from decomposition of the carbonate and not from decomposition of the CaO. Iwamoto et al(30) have reported that CaO has no effect on the weld metal oxygen content but has a significant effect

on the weld metal nitrogen content. No explanation has been made on their report.

2.2.5 Pseudo-equilibrium measurement:

The multiple bead pad technique has been used by several authors to determine slag-metal equilibria during welding (14,26). This technique consists of making several weld beads one on top of another. Each successive layer has a smaller amount of base metal dilution and, hence, the steady state flux-electrode compositions may be established on the topmost bead. Six to eight layers are commonly used. However, it should be noted that the weld metal chemistry obtained by this method can reach only a steady state and not an equilibrium. Equilibrium can be achieved only if the initial electrode composition is in equilibrium with the flux. Otherwise, slag-metal reactions occur and the constant feeding of new electrode material into the weld pool creates a disruption of the weld pool chemistry.

2.3 Comparisons of slag-metal reactions between steelmaking and welding processes:

Molten metal-slag reactions and slag-metal equilibria have been studied much more extensively in steelmaking than in welding. The available activity data of metal oxide systems, which have been used in this research, are listed in Table 1. While much work has been done to clarify whether mass transport or interfacial chemical reactions determine the overall slag-metal reaction rates in steelmaking, it is

believed that the former is usually more significant(31,32).

As an example, consider the reaction of MnO in a steelmaking

slag with silicon in the molten iron bath. Daines and

Pehlke(33) investigated the rate of this reaction and observed

a pronounced effect of stirring with a small activation

energy. They estimated that the reaction may be controlled by

the diffusion of Mn in the liquid iron and that the reaction

reaches equilibrium within ninety minutes at $1550^{\circ}C$.

Due to the high temperature, the shorter time scale

and the presence of a plasma in the arc welding process, the

Mn reaction in welding may be controlled by some other process

such as a gas-liquid(i.e., plasma-metal) reaction rather than

the slag-metal reactions observed in steelmaking. Due to

ignorance of the true slag-metal equilibrium and the dif-

ficulties presented by the higher temperatures and by control

of the plasma composition in flux shielded arc welding, vir-

tually no studies have been made on the slag-metal kinetics of

the welding process.

2.4 Metallic mist in the welding slag:

It has been noted by several investigators(16,20) that

the welding slag contains metallic inclusions. These inclu-

sions have been given the name "metallic mist". An example of

this mist in shown in Figure 2.

In order to measure the average chemical composition of

the slag, several authors(10,12) have used either magnetic or

liquid density separation techniques to extract the metallic
inclusions from the slag. There is no information about the
chemical composition of metallic particles in the slag phase
nor is any explanation of the reason for mist formation given.
In order to understand the mechanism by which the metallic
mist forms, one must investigate the significant welding para-
meters which affect the volume fraction and chemical com-
position of the metallic mist. This information is necessary
in any study of slag-metal equilibrium and kinetics as the mist
may present a significant source or sink of alloying elements.
Given such data, it may be possible to deduce the mechanism by
which the metallic particles are formed in the slag. Such an
understanding is essential in determining the overall mass
balances of manganese and silicon in the welding process.

2.5 Weld metal chemical composition control:

Several authors(14,24,25,26) have attempted to correlate
the weld metal and electrode compositions with the flux com-
position in flux shielded arc welding. They have achieved a
rough fit of the data under certain welding conditions;
however, their work has been empirical and has not provided a
general solution to the problem of predicting weld metal com-
position from the composition of the starting materials. Some
examples may be illustrated as following: Kokh(25) has
attempted to use thermodynamic calculations and a computer
analysis to predict the weld metal composition. His conclu-
sions were the following:

1) The data obtained by calculation are only qualita-
tively reliable.

2) The result largely depends upon the method of com-
puter calculation and partially upon a factor
which Kokh defines as the retardation coefficient of
the reaction. The value of this factor is unknown
a priori. The retardation coefficient is introduced
in order to take account of the deviation of the true
extent of the reaction from the expected equilibrium
point.

Heuschkel(24) tried to obtain a correlation between the weld
metal and the flux composition for several kinds of welding
fluxes. His results produce a wide variation of manganese and
silicon contents. As an example, the silicon content ranged
between 0.2% and 0.55% at 40% SiO_2 and the manganese content
ranged between 0.9% and 1.8% at 40% MnO for several fluxes.
No explanation has been given. Thier (26) has also developed a
flux diagram which is first generated from empirical measure-
ments made under different welding conditions for a certain
flux. After exerimentally determining this flux diagram, it is
claimed that the weld deposit chemistry can be predicted by
comparing the given welding condition with the flux diagram.
This flux diagram must be developed a new for each flux
composition. Each previous author has concluded that there is
no chance of calculation of final weld metal composition by
metallurgical thermochemistry.

Overall, previous attempts to predict the weld metal composition from that of the initial electrode, flux and base metal chemistries have little practical value. As a result, it is still not possible to control the manganese and the silicon contents in the weld metal without extensive experimentation.

III. EXPERIMENTAL PROCEDURES

As mentioned previously, in order to quantify the weld deposit chemistry, several items of contradiction and confusion must be clarified. Up to now, it is not possible to predict the weld metal chemistry from the composition of the the starting materials. Initially it was necessary to conduct a screening experiment in order to assess the significance of the many welding process variables. After selection of the most important variables from this study, an experiment was performed to verify the proposed thermodynamic model of the slag/weld metal equilibrium. Studies of the reaction kinetics were found to be necessary in order to set more reasonable working limits on the weld deposit chemistry. Finally, the oxygen potential of the metal oxides in the fluxes was investigated in order to provide a better understanding of the stability of the flux components. An outline of the procedures for each of these experiments follows:

1) The initial experimental program was based upon a twenty-trial Plackett-Burman screening experiment design using eleven independent variables(34). The screening experiment was used to define the most important variables controlling weld metal composition for further testing with a minimum amount of initial testing. The eleven factors examined in this study were [1] voltage, [2] current, [3] travel

speed, [4] electrode diameter, [5] base plate thickness, [6]
flux thickness, [7] flux composition, [8] electrode tilt
angle, [9] polarity, [10] electrode stick out and [11] argon
shielding. Values used for these factors and their assign-
ments for each trial are shown in Table 2 and 3. The
measured responses to these eleven factors included [1]
penetration, [2] bead height, [3] bead width, [4] arc
stability, [5] contact angle, [6] flux consumption, [7]
electrode melting rate, [8] weld metal oxygen content, [9]
weld metal manganese content, [10] weld metal silicon
content, [11] weld metal carbon content and [12] volume
fraction of metallic mist.

2) The second part of the experimental program involved
making welds with an electrode and baseplate of identical
composition. This was necessary because it was desired to
perform a test in which the initial weld metal composition
was not affected by the amount of dilution. Unfortunately,
it is not practical to procure welding plates and electrodes
of identical composition. As a result, the artificial base-
plate experiment was developed. In this experiment, an elec-
trode of desired composition was cut into 0.8 meter sections
and straightened. Bundles of eight to ten of these rods
were then tied with fine iron wire. This artificial base-
plate was then placed on a water cooled copper trough. The
spool of the remaining electrode was then mounted on the

welding machine, flux was added and a weld was made. In this way, a weld could be made with an electrode and baseplate of identical composition. The current pick up from the rod bundle to the copper trough was not adequate, and it was found necessary to connect the welding current lead directly to the bundle. A picture of this experimental setup is shown in Figure 3. The artificial baseplate experiment was then used to verify the equilibrium thermodynamic predictions and the mass balance which are presented in the next chapter. A standard set of operating conditions was selected for this experiment, the values of which are given in Table 4.

3) The third part of the experimental program involved investigation of the mechanism of metallic mist formation in the slag phase. The volume fraction of the metallic mist and slag inclusions was measured with a Jolyce Lobel Image Analyzer, and the chemical composition of the metallic particles was measured by the electron microprobe using a five micron beam size. The data from this experiment were used in performing the mass balance.

4) The fourth part of the experimental program involved investigation of the spatial distributions of Mn and Si in the metal phase and the MnO and the SiO_2 in the slag phase in hope of determining the possible transport controlling mechanisms in the flux shielded arc welding process. This

was done by analysis in the electron microprobe. The standard operating conditions were 15kV, 30nA and 30 seconds counting time or approximately 60000 counts per datum point.

5) The fifth part of the experimental program involved investigation of the effect of flux composition on the weld metal oxygen content. Binary mixtures of CaF_2 and metal oxides were used. CaO, MnO, SiO_2, MgO, Al_2O_3, TiO_2, Na_2O and K_2O were investigated. The welding conditions were the same as those given in Table 4.

6) The final portion of the experimental program involved investigation of the difference in slag-metal reactions between blended and fused fluxes. Two blended fluxes were supplied by Combustion Engineering Corporation. A portion of each of these blended fluxes was melted in a graphite crucible in order to produce a fused flux of identical composition. The experimental design was the same as that of the artificial baseplate experiment as described above.

3.1 Equipment:

A Linde VI-800 power supply and Linde EH-10 electrode feeder/control assembly were used for all experiments. The VI-800 is a three phase, constant potential, transformer/ rectifier type dc power supply capable of supplying up to 800 amperes at 43 volts at 100% duty cycle. Current was varied by changing the speed of the electrode feed motor.

3.2 Materials:

The chemical composition of the welding electrodes and

the base metals used in the first and the fifth parts of the experimental program are shown in Table 5. The chemical compositions of the electrodes used in the second part of the experimental program are shown in Table 6.

The weldments from the 3.22% Si plate and electrode were made by hand rather than by automatic machine due to the short length of the electrode which was available. This electrode was saw cut directly from the 3.22% plate.

Two commercial fused fluxes which had quite different basicity indices were chosen for the first part of the experimental program. Two experimentally produced and four commercially produced fused fluxes were used in the second part of the experimental program. Typical chemical compositions of these fluxes are given in Table 7. Several binary fused fluxes were used in the fourth part of the experimental program, the chemical compositions of which are given in Appendix 1. Fluxes were baked at 300^{0}C for at least twelve hours before use and were always used immediately after removal from the oven to prevent moisture contamination. Excess flux was returned to the oven immediately.

3.3 Flux preparation:

The preweighed raw materials were dry mixed in a V-blender at a rotational frequency 35 cycles per minute for half an hour. Part of this premixed flux was put in a graphite crucible and heated with a 30 kW induction power

supply. The experimental apparatus is shown in Figure 4. When the flux was melted and had densified, additional flux was added to the crucible, the flux was held molten for approximately ninety minutes to achieve homogeneity. The fused flux was then cooled to room temperature while in the crucible. It was then removed and scarfed with a grinding wheel to remove surface contamination. After this cleaning process, the fused flux was crushed in a jaw crusher and screened to less than 30 mesh particle size(0.52mm diameter).

3.4 Sampling:

Samples were taken from the weld bead by sawing. The oxide surface film was removed by grinding. The location of the sample is shown in Figure 5.

Weld metal samples were mounted in bakelite and polished for electron microprobe chemical analysis. These samples always included the entire weld cross section as shown in Figure 6(a).

Samples of the fused slag to be used for electron microprobe analysis were mounted in bakelite and polished. These also included the entire slag cross section as shown in Figure 6(b).

The microprobe samples were also used for image analysis of the second phase particles in both the weld metal and the slag.

3.5 Chemical analysis:

The manganese and silicon of the starting electrodes and the deposited weld metals were analyzed by atomic absorption spectroscopy. The estimated error of this technique is $\pm 5\%$ of the measured content. The oxygen content of the weld metal was analyzed in a Leco vacuum fusion apparatus. The estimated error of. this technique is $\pm 5\%$ of the measured oxygen content. The chemical compositions of the flux and the slag were analyzed in the electron microprobe. The estimated error was $\pm 5\%$ of the measured value for the high range(over 15%) and $\pm 2\%$ of the measured value in the low range(below 5%).

3.6 Volume fraction of metallic mist in the welding slag and oxide inclusions in the weld metal:

The volume fraction of metallic mist in the slag phase was analyzed with a Jolyce Lobel image analyzer. The analysis was performed over the entire cross sectional area of the sample. The estimated error was $\pm 10\%$ of the measured value.

3.7 Definitions of terms used in the screening experiment:

The definitions of penetration, bead height, bead width and contact angle are illustrated in Figure 7. Arc stability was monitored by a technique suggested by G. Uttrachi of Union Carbide Coorporation. His technique uses a storage oscilloscope operated in the X-Y rather than the usual Y-time mode. The current oscillations of the d.c. arc are input to the X-axis and the d.c. arc voltage is input into

the Y-axis. This results in a plot as shown in Figure 8. The smaller the region of the voltage-current oscillations, the greater is the arc stability. For the purpose of this study, arc stability was given values 1,3 or 5 depending on the extent of the variations, with 1 being the stablest arc. This technique of quantifying arc stability is similar to the approach of Olsen et al, who used the total voltage oscillation range(35).

IV. EXPERIMENTAL RESULTS AND DISCUSSIONS

4.1 Screening experiment: (The first approach)

As mentioned previously, concerning the factors controlling weld metal composition, several contradictions exist in the literature. The first approach as stated in chapter I is to perform a screening experiment to assess accurately the significant welding variables which affect the composition of the weld metal. The results and discussions of this screening experiment follow.

4.1.1 Results:

As described in Chapter III, experimental procedures, the screening experiment was designed to provide a wide range of welding conditions, values of which are given in Table 2. The experiment results of this screening experiment are given in Appendix 2. By comparing Table 2 with Appendix 2, it is seen that changes in the independent parameters produce even greater changes in the dependent parameters. In most cases, the dependent variables show at least a factor of three variation between the maximum and the minimum variables; hence, the experimental limits, given in Table 2, were effective in separating the dependent responses.

The correlation coefficients for all binary combinations of the dependent-independent variables are given in Table 8. The underlined values are those responses which

have been determined to be correlated with 95% confidence.

4.1.2 Discussions:

Of the 198 correlations presented in Table 8, forty-
five are correlated within 95% confidence limits yet only
nine have correlation coefficients above 0.7. The large
number of correlated variables indicates the complexity of
the interactions during flux shielded welding, yet the small
number of strongly correlated variables shows that the
effects of the process changes, although real, are often
subtle.

Discussion of each of the forty-five correlations would
be tedious and probably repetitive. For example, the fact
that weld penetration has been found to be dependent pri-
marily upon welding current, but also upon electrode
diameter and polarity is not new. The correlation of weld
penetration with weld height and electrode melting rate pro-
bably has not been noted previously, but is not suprising
when one considers that the welding current strongly affects
both bead height and melting rate as well as penetration
depth. Hence, these dependent parameters are all interre-
lated through the welding current and the positive correla-
tion results of weld penetration are not surprising.
However, the data also indicate that weld penetration is not
affected by any of the other parameters within the limits of
this study. Specifically, the finding that electrode tilt

angle does not affect depth of penetration is surprising as
electrode tilting does change the penetration charac-
teristics of some GTA welds. An explanation of why tilting
does not affect SAW weld penetration is lacking. It is seen
that the lack of a correlation is often of as much interest as
if a correlation had been found.

Similarly, the parameters affecting weld bead height,
width, contact angle and flux consumption, as indicated in
Table 8, are not unusual. One correlation which may be of
interest is the finding that weld travel speed has as much
effect on electrode melting as electrode extension. This is
curious because it is generally assumed that the phenomena
occurring at the electrode tip are the only factors control-
ling electrode melting rate. This study indicates that the
condition of the base plate may have an effect as well.
Although the correlation between melting rate and travel
speed is weak, it is as strong as the effect of melting rate
on electrode extension which is commonly cited, after
welding current, as the primary factor controlling melting.
In the present study, flux composition was found to have a
stronger effect on melting rate than electrode extension.
This is no doubt due to changes in the ionization potential
of the fluxes, which influence the heat transport to the
electrode tip.

It is interesting to note that flux burden thickness

and electrode tilt angle were not found to be significant
parameters. As with all the correlations presented, this
is true only within the limits of this experiment. In other
situations, these parameters may be significant. For example,
electrode tilt angle is known to be important in multiple
electrode welding; however, the present study is only valid
for single electrode SAW.

The oxygen, manganese and silicon contents of the weld
metal show relatively little correlation with any parame-
ters other than flux composition, welding current and overall
weld metal chemistry. Manganese content was found not to be
dependent upon travel speed, which agrees with the work of
North(18). The carbon content was not found to correlate
with any parameter. The correlation of silicon content with
welding current and plate thickness suggests that the sili-
con reaction kinetics may be dependent upon convection and
cooling in the molten weld pool. The strong correlation
between silicon and oxygen in the weld metal is in agreement
with the mechanism of oxygen transfer proposed by Eagar(7,9).
The other constitutional correlations are not unusual con-
sidering the fact that the manganese, silicon and oxygen reac-
tions are all interrelated. The volume fraction of metallic
mist is correlated only with the flux composition and the weld
metal chemistry.

One of the most suprising findings of this study is the

wide range of weld metal chemistries obtained with operational changes in the welding process. This is particularly true when the major chemistry variable, flux composition, is separated. Table 9 gives the range of observed chemistries for each flux. Carbon, silicon and oxygen are found to vary by a factor of three with a given flux. Hence, even though no single parameter other than flux composition appears to control weld metal chemistry, changes in seemingly insignificant parameters may produce wide variations in weld metal chemistry. This illustrates the difficulty and complexity of trying to determine weld metal chemistry based upon starting material compositions and provides a caution to those claiming specific chemistry properties of a flux. The actual values obtained are dependent upon the process parameters chosen. This finding further illustrates the need for a more fundamental understanding of the kinetic processes controlling weld metal chemistry. Only by understanding the mechanisms of silicon, manganese, oxygen and carbon transfer between the slag and the metal will it be possible to understand the variations observed here.

A practical consequence of these variations in weld chemistry is illustrated in Figures 9 and 10. In each figure the inclusion population of the lowest oxygen and the highest oxygen welds of each flux are compared. It is apparent that the cleanliness of each weld is affected by the operating

parameters; hence, any comparison of weld mechanical proper-
ties should be made with identical weld procedures. Although
commonly required by welding codes, this is seldom observed in
the welding literature.

Finally, it should be noted that even though external
argon shielding was not found to affect weld metal chemistry
significantly, atmospheric contamination of SAW metal is
still a likely possibility(7). In the present study, the
effect of atmospheric contamination appears to have been
overshadowed by other factors. Studies by North et al(17),
confirmed in this work, indicate increased weld metal oxygen
when using pure CaF_2 as a flux. These changes are commonly
on the order of 100 to 300ppm oxygen, which although not
insignificant, were probably too small to be detected in
this screening experiment.

Based upon this screening experiment, it is seen that
the weld deposit chemistry is primarily dependent upon the
flux composition; however, other seemingly insignificant
operating parameters may produce notable changes in the weld
metal chemistry. From the standpoint of the thermodynamics
and the kinetics of the process, the results of the screening
experiment clearly show that the effect of flux on the weld
metal chemistry is thermodynamic and the effect of other
parameters such as voltage, current, travel speed and so
forth, is kinetic. The weld metal chemistry is determined

by the kinetics of the slag-metal reactions operating within the limits placed upon the system by the thermodynamics. Hence, if a true understanding of flux shielded weld chemistry is to be obtained, both the thermodynamics and the kinetics of the process must be studied.

4.2 Thermodynamic equilibrium: (The Second Approach)

From the results of the screening experiment, it is seen that flux chemistry depends most strongly upon the flux composition. In the following section, a new formalism is developed from which to predict slag-metal equilibria during flux shielded arc welding. The predicted equilibria are then compared with the experimental data from both the published literature and from this experimental study.

4.2.1 The theoretical approach:

As noted previously, it is a generally accepted fact that the slag and the metal do not achieve equilibrium during flux shielded welding. For this reason most investigators have chosen an empirical approach to welding flux formulation. An important initial hypothesis of the present work is the belief that equilibrium thermodynamics, while unable to predict the extent of a reaction, should at least be able to predict the direction of the reaction. It is further assumed that much of the slag-metal equilibria developed for steelmaking, are applicable to welding flux studies. Using these hypotheses, a model is developed, using the following assumptions:

4.2.1.1. Assumptions:

1). The effective temperature of chemical reactions in
   the metal pool is 2000°C.

2). An empirical relationship exists between the
   basicity index of the welding flux and the weld
   metal oxygen content as shown in Figure 1.

3). The activity data of steelmaking slags may be
   extrapolated from 1600°C to 2000°C by assuming
   regular solution behavior.

4). The primary reactions of interest are those
   involving silicon, manganese and oxygen.

Each of these assumptions requires some justification.

Assumption 1: In his review of welding fluxes, Jackson
(19) noted that most investigators using thermocouple tech-
niques have measured the maximum weld pool temperature as
2000°C. This temperature is an average value representing the
median between the fusion temperature and the weld pool sur-
face temperature in the arc vicinity, which may be roughly
estimated from metal evaporation data as 2400°C. This esti-
mate is obtained by equating the heat lost by metal vaporiza-
tion as calculated by Cobine and Burger(36) to the heat
transfered to the weld metal pool surface as measured by
Nestor(37). It should be noted that Christensen and
Chipman(10,14,15) and Belton et al(12) found an effective
equilibrium temperature of 2000°C for both MnO and

-48-

SiO_2 reactions in selected fluxes, based upon chemical analysis of the weld metal. Perhaps more important than either of these justifications is the finding which will be presented subsequently that equilibria based upon 2000°C agree with the experimental data while equilibria based upon 1800°C or 2200°C do not. Further justification of this assumption will be given following a discussion of reaction knetics in section 4.6.

Assumption 2: Kubli and Sharav(11) showed that the oxygen content of submerged arc weld metal decreased with increasing flux basicity. Tuliani et al(38) quantified the oxygen content of the weld metal as a function of the International Institute of Welding Flux Basicity Index. Eagar(7) has modified this relationship slightly by omitting the CaF_2 term. The relationship between the weld metal oxygen content and the welding flux basicity index, based upon Tuliani's data and Eagar's BI is shown in Figure 1. Much more data could be added to this graph; however, the trend would not be changed, i.e., the weld metal oxygen content produced with acidic fluxes is strongly dependent upon the BI of the flux, while the oxygen content of the weld metal is essentially independent of basicity index for basic fluxes. In the model presented here the oxygen content of a given flux is estimated a priori from the solid line of Figure 1.

Assumption 3: There are no experimental data to justify

this assumption. This hypothesis is made as a matter of convenience due to lack of any better alternative. It should be noted however that this assumption modifies the slag activities relatively little. For example, the activity of SiO_2 in a 40%CaO-60%SiO_2 melt is changed from 0.8 at 1600°C to 0.75 at 2000°C by assuming regular solution behavior.

Assumption 4: The oxidizing potential of welding fluxes is not controlled entirely by the FeO content of the slag as it is in ironmaking or steelmaking. Although high FeO welding fluxes produce large weld metal oxygen content(10), the oxygen content of welds made with fluxes containing less than 10%FeO is not noticably influenced by the FeO content of the flux(12,38). Eagar has shown that this may be due to the formation of suboxides at high temperatures involved in welding(9). In any cases, almost all commercial submerged arc welding fluxes have low FeO contents (typically less than 2%).

Although free aluminum or titanium in the base metal or welding electrode certainly reacts with the oxygen in the weld metal, the quantity of these strongly deoxidizing elements indicates that little or none of these elements is recovered in the weld metal, but is entirely consumed in either the flux or as inclusions in the weld metal. Similar arguments may be made for the other cations listed in Equation 1.

4.2.1.2 The SiO_2 reaction:

Belton et al.[12] have shown that the weld metal silicon content in acidic fluxes can be represented by the following reaction in the temperature range $1713^{\circ}C$ to $2000^{\circ}C$:

$$SiO_{2(\ell)} = \underline{Si} + 2\,\underline{O}$$

$$\log K = -28360/T + 10.61 \tag{4}$$
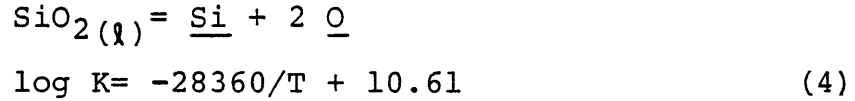
$$K = \frac{[Si][O]^2}{(SiO_2)}$$

where (SiO_2), $[Si]$ and $[O]$ define as activity of SiO_2 and weight percent of Si and O. The standard state for SiO_2 in the slag is pure SiO_2 and the standard state for oxygen and silicon in the weld metal is based upon a one percent solution. Using these data and Belton's observation, the activity of silica in welding fluxes can be determined as a function of the Si and oxygen contents of the weld metal. Neglecting interaction terms, the activity coefficient of silicon, f_{Si}, increases and the activity coefficient of oxygen, f_O, decreases such that $f_{Si}f_O$ remains essentially one for silicon contents less than 3%[31]. This leads to an equation of the form:

$$(SiO_2) = 73.6[Si][O]^2 \tag{5}$$

The plot of this equation is shown in Figure 11. Upon appli-cation of Assumption 2 and Equation 5, the relationship between (SiO_2) and BI is shown in Figure 12. Using Assumption

-51-

3 and the available activity data for several flux systems given in Table 1, the relationship between the equilibrium %SiO$_2$ and the BI for a given weld metal silicon content in each flux system in Table 1 may be generated. An example is shown in Figure 13 for SiO$_2$-FeO-MnO fluxes containing less than 20%FeO. The manganese silicate system is one of the principal types of fluxes used in welding. Similar SiO$_2$ equilibrium plots generated in this research for other flux systems are given in Appendix 3.

4.2.1.3 The MnO reaction:

A similar analysis as used for the silicon reaction may be applied to the MnO reaction:

$$MnO_{(l)} = \underline{Mn} + \underline{O}$$
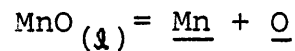
$$\log K = -12760/T + 5.68 \tag{6}$$

$$K = \frac{[Mn]\,[O]}{(MnO)}$$

Again, neglecting interaction terms due to the small interactions between Mn and oxygen in iron base materials(39), and also due to the small amount of oxygen present in the weld metal, we obtain:

$$(MnO) = 0.86\,[Mn]\,[O] \tag{7}$$

The plot of this equation is shown in Figure 14. Using

-52-

Assumption 2 and Equation 7, the relationship between a_{MnO} and the BI may be calculated as shown in Figure 15. Application of Assumption 3 and using the relationship between the equilibrium %MnO and the BI for a given weld metal manganese content, the equilibrium plot may be generated for each flux system in Table 1. An example of the $CaO-MnO-Al_2O_3$ flux system is given in Figure 16. The MnO equilibrium plots for other flux systems generated in this research are given in Appendix 4.

As will be seen later, the equilibrium calculations based upon the above discussions are capable of predicting the trend of the chemical reactions which occur between the slag and the metal during submerged arc welding.

4.2.2 Experimental verification of the theory:

Experimental verification of the proposed theoretical equilibria is necessary if only because the assumptions themselves are not easily verified. The value of any theory is in proportion to its ability to provide accurate predictions of the parameters of interest. To this end two separate verification techniques were used.

First, slag-metal reaction data available from the literature were used to determine if the theory is capable of predicting the trend of Mn and Si transfers for a wide range of flux, electrode and baseplate compositions. This test is thought to demonstrate the generality of the theory.

Second, the accuracy of the theory was investigated by measurement of the extent of the Mn and the Si transfer as a function of the electrode/baseplate composition. This test measures the ability of the theory to predict the specific equilibrium compositions. As will be seen subsequently, the theory withstood each of these tests with remarkable success.

4.2.2.1 Verification by using data in the literature:

Data on commercially useful fluxes have been used in this work(12,14,15,17,18,38,40-48) to test the validity of these calculated equilibria. The data represent a wide range of conditions, e.g., the flux basicity varies from 0.2 to 4.0, the Mn in the base metal and in the electrode varies from 0.01% to 3.1% and the Si varies from 0.002% to 1.0%.

If the percent MnO in the flux is over the equilibrium percent MnO, as predicted by a plot such as Figure 16, then the MnO in the flux will decompose and transfer Mn into the weld metal. Similarly, if the actual amount of MnO in the flux is less than this predicted equilibrium value, the system will change such as to increase the MnO in the flux, and the Mn in the weld metal will be deoxidizing. It is impossible for both the flux and the weld metal to gain or lose both MnO and Mn unless large sinks and sources of Mn are present. As an example, consider a welding flux composed of $30.67\%CaO-4\%MnO-65.3\%Al_2O_3$ and an electrode and baseplate with an average composition of 0.5%Mn. The BI of

this welding flux is 1.0 based upon Equation 1. According to

Figure 16 the equilibrium Mn content in the weld metal is 2%

if the flux basicity is 1.0 for a $CaO-MnO-Al_2O_3$ flux with

4%MnO. Because the initial Mn content of the electrode and

the baseplate is 0.5%, one would expect that the measured weld

metal Mn content will be between 0.5% and 2% if the equili-

brium approach is correct. If the final measured weld metal

Mn content is measured as 1%, then we may define the change in

the Mn as $Mn_f - Mn_i = \Delta Mn$. ΔMn is a measure of the change in the

weld metal Mn due to a slag-metal reaction. It is a response

to a stimulus. In our example, $\Delta Mn = 1.0 - 0.5 = 0.5\%$. In a simi-

lar manner $\Delta^* MnO$ is defined as the difference between the ini-

tial MnO of the flux and the final equilibrium MnO correspond-

ing to the final Mn content in the weld metal, i.e., $\Delta^* MnO =$

$MnO_i - MnO_{f,eq}$. In our example the %MnO in a $CaO-MnO-Al_2O_3$ flux

with BI 1.0 in equilibrium with a weld metal of 1.0% final Mn

is 1.8%, and $\Delta^* MnO = 4 - 1.8 = 2.2\%$, $\Delta^* MnO$ is a measure of the

deviation of the initial slag composition from the final

equilibrium MnO corresponding to the final weld metal

composition. It is the stimulus which produces the ΔMn

response. Plotting the response versus the stimulus gives an

effect. If the calculated equilibrium is correct, a positive

stimulus should have a positive response and a negative stimu-

lus should have a negative response. If ΔMn is plotted versus

$\Delta^* MnO$, all data points confirming the calculated equilibrium

should lie within quadrants I and III. Any responses in quadrants II and IV violate the hypothetical equilibrium. It is seen in Figure 17 that all the experimental data points fall within the I and III quadrants, confirming the predicted equilibrium. The argument for a ΔSi-Δ^*SiO2 plot is identical. The result is shown in Figure 18. Again all the data points fall within the I and the III quadrants. It is seen that the hypothetical equilibrium gives very good agreement with experiment for a wide range of fluxes, electrodes and base-plates.

Based upon the above results, it is possible to predict whether the weld metal will gain or lose Mn and Si for a given flux, electrode and base metal chemistry. Unfortunately, this technique does not make it possible to quantify the extent of this change. However it is possible to put limits on these changes. In the previous example (see Figure 16), the limit of ΔMn will be 2-0.5=1.5%, since a change greater than this value would indicate that the weld metal had gained enough Mn to overshoot the equilibrium. Here the equilibrium Mn content is 2% which corresponds to the initial flux composition shown in Figure 16, and the initial Mn content of the wire and base metal is 0.5%. Hence, one would expect the final Mn content of the weld metal to lie between these limits. The limits of Δ^*MnO will be 4-0.4=3.6%. Here the initial %MnO in the flux is 4% and the equilibrium %MnO corresponding to the initial Mn

-56-

content of the electrode and the base metal is 0.4% as shown in Figure 16. The value of ΔMnO is obtained from the flux, the electrode and the base metal chemistries in conjunction with the equilibrium plot(Figure 16) assuming a dilution factor of 0.5. Figure 19 is an example of these limits calculated for both Mn and Si for a commercial flux.

An advantage of using the definitions of ΔMn, Δ^*MnO, ΔSi and Δ^*SiO_2 as described here is that these conventions indicate overshoot of ΔMn or ΔSi past the equilibrium value, $Mn_{i,eq}$, by causing the data to plot in the II and IV. Using this convention, it is impossible for the weld metal to gain Mn while the flux also gains MnO. To clarify this point, consider the same example as before, i.e., a $CaO-MnO-Al_2O_3$ flux of BI 1.0 and initial weld metal composition of 0.5%Mn. In our prediction, the final weld metal should be between 0.5 and 2%Mn or ΔMn_{max}=1.5%. If the final weld metal manganese change is beyond this range, e.g. Mn_f=2.5%, then $\Delta Mn = Mn_f - Mn_i$ 2.5-0.5=2% and $\Delta^*MnO = MnO_i - MnO_{f,eq}$=4-6=-2%. The datum point falls within the second quadrant. Alternatively, if Mn_f=0%, then $\Delta Mn = Mn_f - Mn_i$=0-0.5=-0.5% and $\Delta^*MnO = MnO_i - MnO_{f,eq}$=4-0=4%. This datum point falls within the fourth quadrant and a change in the weld metal Mn content away from equilibrium is indicated. These cases are ruled out by defining Δ^*MnO as $MnO_i - MnO_{f,eq}$ rather than as $\Delta MnO = MnO_i - MnO_{i,eq}$. Since the data points shown in the Figure 17 and Figure 18 all follow the

-57-

equilibrium prediction without exception, it may be concluded that the calculated equilibrium is consistent with the law of mass conservation.

It is worthy of note that a similar analysis using thermodynamic data based upon 1800°C would not yield good agreement, while an analysis based upon an equilibrium temperature of 2200°C, compresses the data so as to obscure any trends. An example of assuming 1800°C is shown in Figure 20. Obviously, it is impossible that the weld metal loses elements while the slag also loses the same metal oxide, hence, the predictions lying in the second quadrant are worthless. Based upon the above arguments and the empirical fit of the data shown in Figures 17 and 18, 2000°C is a reasonable equilibrium temperature for the reactions.

From the above analyses, all the data points fall within the first and the third quadrants for both the SiO_2 and the MnO reactions. This confirms that the initial assumptions are suitable for this thermodynamic approach. The equilibrium plots shown in Appendix 3 and 4 are verified in the general case by the wide varieties of commercial data which have been used here. It is concluded that the proposed theory is generally capable of predicting the direction of the slag-metal reactions which occur during flux shielded welding. It is now necessary to verify the accuracy of several individual equilibrium points.

4.2.2.2 The accuracy of the equilibrium Mn and Si predictions:

Although the previous test confirms the generality of the theory, it does not prove the accuracy of the predictions. Indeed, there is considerable scatter of the data within quadrants I and III of Figure 17 and 18. This scatter may be explained in part by the non-equilibrium nature of the slag-metal reactions in welding. Nonetheless, it is of interest to determine the accuracy with which the theory can predict not only the gain or loss of Mn or Si from the weld pool, but also the composition at which the change in composition is expected to be zero.

Several authors have attempted to study slag-metal reactions during welding by producing a pyramid of weld beads, of which each succeeding layer is diluted by a smaller fraction of the base metal(10,14,15,26). In this way, it is claimed that the final flux/electrode equilibrium may be attained. This is not necessarily true; the pyramid of weld beads leads to a steady state weld metal composition rather than an equilibrium composition. This is caused by the continuous disruption of the weld pool chemistry by the melting electrode. Only if the electrode is of a composition which corresponds to equilibrium with the flux will metal transfer between the electrode and the slag be zero. In all other cases, the transfer reaches a steady state which is a balance between the rate of the slag-metal reaction and the rate of

weld pool dilution caused by the melting electrode.

In order to overcome the difficulties with the pyramid bead test, it is desirable to have an electrode and a baseplate of identical composition; hence, dilution effects may be neglected. Such identical electrode/baseplate compositions are very difficult to obtain. Instead, it was decided to create an artificial baseplate by bundling seven or eight lengths of electrode and placing these on a water cooled copper trough. The setup is shown in Figure 3. In this way, welds may be made with an electrode and base plate of identical composition. A series of welds is made, varying the Mn or Si content of the electrode until a given flux produces no net change in the deposit chemistry as compared with the electrode chemistry. This composition represents the composition of Mn or Si in equilibrium with the chosen flux. In practice it is convenient to vary either the Mn or the Si content without attempting to hold the composition of the other element constant. This ignores the interaction effects between the Mn and Si recoveries; nonetheless this approach was found to be useful.

In this experiment, four laboratory fused fluxes which were designated F-1, F-2, MIT-1 and MIT-2 two commercial fused fluxes designated F-3 and F-4 were used. F-1 contained 42.53% SiO_2-15.7% MnO-41.77% CaO with BI=1.17. The theoretically predicted equilibrium point of this flux is 1.83% Mn and 0.33%

Si based on Appendix 4-a and Appendix 3-a, respectively. The
experimental results for flux F-1 are shown in Figures 21 and
22 for Mn and Si, respectively. Based on the experimental
results, the measured equilibrium point is 1.85% Mn and 0.28%
Si. Due to a lack of experimental activity data for SiO_2 in
the $CaO-SiO_2-MnO$ system, the activity data for SiO_2 in this
flux system was taken by calculation from the Gibbs-Duhem
equation(49). This may be the reason for the error between
the predicted and the measured Si equilibrium values, although
the agreement is remarkably good in any case.

The second flux, F-2 contained 39.53% SiO_2-7.7% MnO-
-23.15% CaO-29.62% Al_2O_3 with BI=0.5, which has a theoretical
predicted equilibrium value of 0.40% Mn and 0.25% Si based on
Appendices 3-b and 2-b. The experimental results shown in
Figures 23 and 24 give measured equilibrium points of 0.44% Mn
and 0.28% Si. Again the agreement between measured and pre-
dicted Mn equilibrium and Si equilibrium is very good.

The third flux, F-3, which is a commercial formulation
containing 50% SiO_2-40% MnO-5% CaF_2-3% CaO with BI=0.46, has a
predicted equilibrium point of 1.1% Mn and 0.80% Si based on
the graphs shown in Appendices 4-a and 3-c. The measured
results shown in Figure 25 and 26 give the equilibrium point
as 1.27% Mn and 0.95% Si. The error here is somewhat greater,
most likely due to the greater complexity of the commercial
formulation. Nonetheless, the agreement is still reasonable.

The fourth flux, F-4, again of commercial use, containing 36% SiO_2-47% CaO-0.14% MnO-9.8% CaF_2-5.0% Na_2O with BI=1.45 has a predicted equilibrium point of 0% Mn and 0.32% Si based on Appendix 3-d. The measured result in Figure 27 shows the equilibrium point is 0.25% Si. It is not possible predict the equilibrium Mn content, because the initial percent MnO in the fourth flux is almost zero. However, the experimental results are shown in Figure 28. The error in the silicon content as measured by Figure 25 is probably due to assuming an activity of SiO_2 based only upon the CaO-SiO_2 flux system. The commercial flux is more complex, containing 9.8% CaF_2 and 5% Na_2O in this case. If more accurate SiO_2 activities were available, the error may be reduced.

Two bonded fluxes were supplied by Combustion Engineering Corporation and were designated as MIT-1-B and MIT-2-B. In order to compare the reactivities of bonded fluxes with fused fluxes, a portion of each of these bonded fluxes was fused by induction. The fused fluxes were designated as MIT-1-F and MIT-2-F. The flux composition is given in Table 7. It will be noted that the basicity index of each flux is 0.52, yet due to the different flux systems of each, the predicted equilibrium Mn and Si contents vary markedly.

The theoretical equilibrium point of flux MIT-1 is 0.2% Mn and 0.12% Si based upon the graphs shown in Appendices 4-b and 3-f. The experimental results for MIT-1 shown in Figures

29 and 30 give measured equilibrium points of 0.18% Mn and
0.17% Si for MIT-1-B and 0.15% Mn and 0.25% Si for MIT-1-F.
Considering the complexity of the formulation of MIT-1, the
agreement between the predicted value and the measured value
is good for both the bonded and the fused fluxes.

The predicted equilibrium point of flux MIT-2 is 0% Mn
and 1.3% Si based upon Appendix 3-d. The experimental results
shown in Figure 31 and 32 give a measured Mn equilibrium of
less than 0.31% while the equilibrium Si is 1.08% and 1.18%
for bonded and fused fluxes respectively. It is not possible
to measure the exact equilibrium Si content in this case,
because the available Si content of most commercial welding
electrodes does not exceed 1.0%. Nonetheless, the experimen-
tal data do suggest that the equilibrium Si content is greater
than 1.0% which is consistent with the predictions.

Similar experimental data have been taken by Thier using
the pyramid bead technique in order to overcome the dilution
factor(26). His results which are given in Figure 33 for flux
LW280 show an experimental equilibrium point of 1.25% for Mn
and approximately 0.7% for Si. The dilution factor was
claimed to be smaller than 1%. The basicity index of LW280 is
0.85 as may be calculated from the composition which is given
in Table 7. This flux has a theoretical equilibrium point of
1.25% Mn and 0.5% Si based upon Appendices 4-b and 3-f,
respectively. The agreement between experimental and pre-
dicted equilibrium values is again quite good, especially if

one considers the complex formulation of this flux. The experimental equilibrium carbon content for Thier's tests is approximately 0.05%. This must be due to carbon contamination in Thier's flux as thermodynamic analysis predicts that CO will be evolved from all weld metals. In fact, carbon is added to cast iron welding fluxes in order to maintain a high carbon content in the cast iron. Thier's results also show that the equilibrium point is not affected by the welding conditions. It is only affected by the flux composition. This indicates that the effects of the welding parameters are kinetic while the definition of the flux equilibrium point is thermodynamic. His results also show that welding travel speed has no effect on manganese recovery which confirms the result of the screening experiment. While his results also show some effect of current and voltage on weld metal composition, these effects are small and could not be detected in the screening experiment as only one electrode composition was chosen.

Christensen(14) has also performed pyramid-bead experiments. His experimental results are given in Figure 34. The measured equilibrium points of flux a, c, d, e and f are 0.1% Mn, 0.1% Mn, 0.2% Mn, 1.55% Mn and 0.56% Mn respectively. The predicted values from the formalism presented here are 0% Mn, 0% Mn, 0% Mn, 1.75% Mn and 0.38% Mn, respectively. Due to the small amount of MnO in the fluxes a, c and d, the

predicted equilibrium Mn values are zero(*). Nonetheless the experimental and the predicted equilibrium values are in good agreement for these fluxes. Flux f clearly shows that the welding conditions have no effect on the equilibrium point which is in agreement with Thier's results. It may be concluded that only one set of welding conditions is necessary to verify the equilibrium point.

Overall, comparisons between the theoretical and the experimental equilibrium chemistry are given in Table 10 for all the fluxes investigated in this study. The average error is estimated to be around 15% with a maximum absolute deviation of 0.20% in Mn and 0.15% in Si. Considering the simplicity of the model, the predictions appear to provide remarkably good agreement with the experimental data. It can also be seen that the equilibrium thermodynamic approach may also be applied to the bonded flux as well as to the fused flux.

As presented the analysis applies only to neutral submerged arc welding fluxes with CaF_2 content less than 20%. Furthermore, the analysis is less precise with highly basic fluxes, because the chemical activities of SiO_2 and MnO converge at high basicities and experimental error in analysis

---

(*) As will be discussed subsequently, fluxes with zero initial MnO or SiO_2 generally do not provide accurate equilibrium predictions.

result in greater errors in the equilibrium prediction. In addition, the weld metal oxygen content changes little in the highly basic fluxes, this also reduces the sensitivity of the analysis. One should use care in applying the equilibrium plots generated in this research as higher experimental error would be expected in the high basicity region. The extent of the error depends upon the flux system: For example the SiO_2-MgO-Al_2O_3 system has maximum useful basicity of 0.6, while others such as the SiO_2-CaO-Al_2O_3 system may be used for basicities up to 2.0.

It is seen that equilibrium thermodynamics is capable of defining the limits of Mn and Si changes during flux shielded arc welding using fused fluxes. The predicted ranges of permissible Mn and Si change for several commercial fused fluxes are shown in Appendix 5. In some cases, these limits are quite narrow and the model provides nearly a quantitative estimate of the changes, and may be of use in selecting combinations of flux/electrode/baseplate a priori. In other cases, these limits are rather broad and an understanding of the mass balance is necessary in order to narrow the observed changes. This leads to the third approach studied in this work.

4.3 The mass balance: (The third approach)

As shown in section 4.2, the thermodynamic equilibrium model is capable of predicting the direction, if not the magnitude, of the change in silicon and manganese during submerged arc welding with neutral fluxes. In the case in which the initial weld metal chemistry is near the equilibrium point, the predicted range of permissible weld metal chemistry is quite narrow and the extent of change in the weld deposit chemistry is more predictable as may be seen in Figures 21 to 32. This provides nearly a quantitative estimate of the changes. On the other hand, when the initial weld metal chemistry is farther away from the equilibrium point, the predicted limit is rather broad and the extent of changes in the weld metal chemistry is less predictable as may be seen in Figures 21 to 34. This latter situation is unsatisfactory.

It was hypothesized that part of the variation in weld metal alloy recovery might be due to sources or sinks of alloying elements in the process. For this reason, a mass balance was performed on Mn and Si. In addition, it is thought that such a mass balance provides a useful starting point for future studies of alloyed(or so called "active") fluxes.

4.3.1 The Mn balance:

Considering the possible sources and sinks in any process, the total initial weight of an element should be

equal to the total final element weight. In the submerged arc welding process using neutral flux, the possible sources of manganese include the flux, the electrode and the baseplate. The possible sinks include the metallic mist in the slag, slag inclusions in the weld metal and metal vaporization. Taking all of these sources and sinks into account, a mass balance may be written by equating the total initial alloying element with the total amount of alloying element in the final weld.

Total initial manganese=Total final manganese

$$Mn,i+0.77k(MnO,i)=Mn,f+0.77k(MnO,f)$$
$$+k(D_m/D_g)(Mn,m)(V,m)$$
$$+0.77(D_s/D_m)(MnO,s)(V,s)$$
$$+\delta_{Mn} \qquad (8)$$

Here, Mn,i=the initial weld metal Mn content.

MnO,i=the initial MnO content in the flux.

k=the ratio of slag weight to weld metal weight.

Mn,f=the final weld metal Mn content.

MnO,f=the final MnO in the slag.

D_m=the density of metallic mist or weld metal.

D_s=the density of slag inclusion in the weld metal.

V,m=the volume fraction of metallic mist in slag phase.

V,s=the volume fraction of slag inclusions in the weld metal.

δ_{Mn}=a factor used to account for other sinks of alloying element such as metal evaporation.

-68-

The above formulation is valid only for neutral fluxes.
Some additional considerations should be taken into account
when using alloyed flux. These will be discussed later.

Equation 8 can be rearranged and expressed as follows:

$$0.77k(\Delta MnO) = \Delta Mn + k(D_m/D_g)(Mn,m)(V,m)$$

$$+0.77(D_s/D_m)(MnO,s)(V,s)$$

$$+\delta_{Mn} \qquad (9)$$

Here $\Delta MnO = MnO,_i - MnO,_f$ and $\Delta Mn = Mn_f - Mn_i$ as defined before.
This formulation may be divided into four categories as
shown in Table 11. Category A in which both ΔMn and ΔMnO are
positive implies that the weld metal gains manganese and the
slag loses manganese oxide; Category B represents the situ-
ation when the weld metal loses manganese and the slag gains
manganese oxide; Category C represents the situation when
both the weld metal and the slag gain manganese while cate-
gory D represents loss of Mn in both the weld metal and the
slag.

The experimental data for volume fraction of metallic
mist and slag inclusion are given in Appendices 7 and 8. The
chemical composition of the flux, the slag, the weld metal
and the metallic mist are given in Appendix 7. D_m is approx-
imately 7.8 g/cm^3, D_g or D_s is approximately 3.3 g/cm^3
in these experimental fluxes.

The experimental results are shown in Table 12. In
Table 12, the first column represents the total manganese

change in the slag, i.e. $0.77k(\Delta MnO)$. A positive value means that the slag loses MnO and a negative value means that the slag gains MnO based on the earlier definition. The second column represents the total manganese change in the weld metal; a positive value means that the weld metal gains manganese and a negative value means that the weld metal loses manganese. The third column represents the content of manganese in the metallic mist of the slag phase, i.e. $k(D_m/D_g)(Mn,m)(V,m)$. The fourth column represents the content of manganese in the slag inclusions of the metal phase, i.e. $0.77(D_s/D_m)(MnO,s)(V,s)$. The last column represents the other unknown contributions in the slag-metal reaction process. A positive value of this last quantity means that unknown sinks exist such as metal vaporization and a negative value means that the sources other than the flux, the electrode and the base metal exist.

From the first and second columns of Table 12, it is seen that only situations in which ΔMn and ΔMnO are both positive or both negative exist. This demonstrates that only cases A and B of Table 11 are found in the submerged arc welding process when using neutral fluxes. The unknown source of Mn, i.e., category C, is not found or expected as it is a non-physical situation. The strong sink of Mn, i.e., case D, is not observed experimentally, although there is no fundamental reason to exclude it. In case A, the gain

of the element in the weld metal is less than the decomposition of the metal oxide as seen from column 1 and 2 in Table 12 which implies that a sink is present. It also suggests that alloying the weld metal by neutral flux is not an efficient method as a portion of the alloy content is lost to the sink. In case B, it is seen that the loss of the manganese in the weld metal is almost fully converted to oxide in the slag. This is probably due to the presence of a high oxygen potential within the arc region which rapidly oxidizes the Mn metal.

All the values in the third column of Table 12 are comparatively small which shows that the metallic mist is not an important sink of Mn. The chemical composition of the metallic mist was investigated by the electron microprobe as described in the experimental procedures section. The results are given in Appendix 7 which shows that iron is the major component. This suggests that the mist is formed by weld metal spatter rather than by decomposition of the flux. If the formation mechanism is due to flux decomposition, one would expect the metallic mist to be high in manganese or silicon content as the oxides of these metals are abundant in the slag; however, this is not the case. This formation mechanism of the metallic mist is quite different from that of the mist as described by Jackson et al(16). They found that a metallic mist was formed by reduction of oxide spe-

cies by the graphite crucible when manufacturing the flux by an arc melting process. In Jackson's case, there is an abundance of carbon in the graphite crucible and much atmospheric oxygen is available, both of which combine to form carbon monoxide. This carbon monoxide reduces the flux. In the arc welding process, the quantity of carbon is limited, and the quantity of carbon monoxide formed cannot explain the volume of metallic mist formed.

As may be seen from column 4 of Table 12, slag inclusions were found to be a relatively important sink in this study especially in the case where the weld metal gains manganese. The formation of slag inclusions is a complex process, much more work needs to be done in this area in the future. Probably most important for this study is to apply the results of the mass balance to limit the permissible range of weld metal chemistry as predicted by the thermodynamic model presented earlier. This will be shown subsequently.

The last column of Table 12 shows positive values which implies that the unknown sources are not found. The unknown sinks such as gas evolution may be important, especially in the case when large amounts of MnO are decomposed.

4.3.2 The Si balance:

Using the same procedures as shown for the Mn balance, the mass balance of Si in neutral submerged arc fluxes can be written as:

$$0.47k(\Delta SiO_2) = \Delta Si + k(D_m/D_g)(Si,m)(V,m)$$
$$+0.47(D_s/D_m)(SiO_2,s)(V,s)$$
$$+\delta_{si} \qquad\qquad (10)$$

The notation is the same as used in the Mn balance. The experimental results are given in Table 13. These data also show that 1) the metallic mist is not an important sink, 2) slag inclusions are a relatively important sink, 3) the unknown sinks such as gas evolution may be important when large amounts of SiO_2 are decomposed and 4) neither unknown sources nor strong sinks are found in the Si balance. All of the findings from the Si balance are in agreement with the Mn balance as discussed in section 4.3.1.

4.3.3 The application of the mass balance:

As seen previously, thermodynamic equilibrium controls the direction of slag-metal reaction in flux shielded arc welding processes. This equilibrium provides a means of establishing working limits for the weld metal chemistry. In addition, the weld metal chemistry must also obey the mass balance as discussed previously. The mass balance places a restriction on the weld metal chemistry in addition to that imposed by the thermodynamics. Combination of both the thermodynamic equilibrium and the mass balance should provide a narrower working limit. The following discussions will focus on the application of these principles.

As shown from Tables 12 and 13, only two cases are found experimentally, viz.:

Category A: The weld metal gains an element(Mn or Si)
and the slag loses the conjugate metal
oxide (MnO or SiO_2):

In this case, Equations 9 and 10 can be written as

$$0.77 \; k_{(exp)}(\Delta MnO) \geqslant \Delta Mn \qquad\qquad (11\text{-}a)$$

$$0.47 k_{(exp)}(\Delta SiO_2) \geqslant \Delta Si \qquad\qquad (11\text{-}b)$$

for the Mn or Si balance, respectively, because the contribu-
tion of sinks in Equations 9 and 10 are all positive. We may
define a theoretical k value as

$$k_{(th)} = \frac{\Delta Mn}{0.77(\Delta MnO)} \qquad\qquad (12\text{-}a)$$

$$\text{or} \; k_{(th)} = \frac{\Delta Si}{0.47(\Delta SiO_2)} \qquad\qquad (12\text{-}b)$$

for the Mn and the Si balances. Here ΔMn, ΔMnO, ΔSi and SiO_2
are the experimentally measured values. The difference bet-
ween $k_{(th)}$ and $k_{(exp)}$ is that $k_{(th)}$ is calculated from the
experimentally measured weld metal chemistry while $k_{(exp)}$ is
a direct measurement of the ratio of the slag weight to the
weld metal weight. Comparing Equations 11 and 12, yields

$$k_{(exp)} \geqslant \frac{\Delta Mn}{0.77(\Delta MnO)} = k_{(th)} \qquad\qquad (13\text{-}a)$$

$$\text{or} \; k_{(exp)} \geqslant \frac{\Delta Si}{0.47(\Delta SiO_2)} = k_{(th)} \qquad\qquad (13\text{-}b)$$

If no sinks are present, the equal sign holds. The physical

meaning of Equation 13 is that it is necessary to have more slag present than the theoretical value in order to obtain a sufficient amount of weld metal Mn or Si to place the experimental prediction in the first quadrant of the $\Delta Mn-\Delta MnO$ plot or $\Delta Si-\Delta SiO_2$ plot(cf. Figure 17 and 18).

Category B: The weld metal loses an element(Mn or Si) and the slag gains the conjugate metal oxide(MnO or SiO_2):

In this case, the increase of metal oxide in the slag phase is controlled by the loss of an element in the weld metal. Equation 9 and 10 can be written as

$$-\Delta Mn > -0.77k_{(exp)}(\Delta MnO)$$

$$-\Delta Si > -0.47k_{(exp)}(\Delta SiO_2)$$

which is equivalent to

$$k(exp) < \frac{-\Delta Mn}{0.77(-\Delta MnO)} \qquad (15-a)$$

$$\text{or } k(exp) < \frac{-\Delta Si}{0.47(-\Delta SiO_2)} \qquad (15-b)$$

Here, $-\Delta Mn$, $-\Delta MnO$, $-\Delta Si$ and $-\Delta SiO_2$ are positive due to the original sign convention. The physical meaning of Equation 15 is that it is necessary to have more metal to react in order to obtain a sufficient amount of metal oxide in the slag if the experimental results are to fall within the third quadrant of the $\Delta Mn-\Delta MnO$ plot or the $\Delta Si-\Delta SiO_2$ plot. In both of the above situations, the equal sign implies that

-75-

no sink is present. In all other cases a sink is present.

Based upon the above formulations, it is seen that

1) In the first quadrant of the permissible range plot,

$k_{(exp)}$>$k_{(th)}$ for both the Mn and the Si balance.

2) In the third quadrant of the permissible range plot,

$k_{(exp)}$<$k_{(th)}$ for both the Mn and the Si balance.

This relationship can be verified by comparing $k_{(exp)}$ as given

in Appendix 9 to the value of $k_{(th)}$ calculated from Equation

13. The result is shown in Figures 35 and 36. Actually, this

result is not surprising, as it follows directly from the

results in Table 12 and 13 which show the presence of sinks.

If sources have been presented, the data points would have

fallen above the line.

Based upon this understanding, the restriction region

imposed by the mass balance is shown schematically in Figure

37 assuming $k_{(th)}$=0.5. As seen from Figure 37, this addi-

tional restriction reduces the permissible working limit. The

efficiency of this mass balance restriction depends upon each

flux system and is only valid for neutral fluxes. Some addi-

tional considerations need to be taken into account for

alloyed fluxes which will be suggested from a theoretical

point of view later.

4.4 The predicted range of manganese and silicon in the
weld metal:

In this section, the results of Approach 2(Equilibrium

point) and Approach 3(Mass balance) will be combined in order

to provide a reasonable range of manganese and silicon in the weld metal. The detail procedures are as follows:

1) Using the thermodynamic approach discussed in the section 4.2, it is possible to predict the equilibrium weld metal Mn or Si content for a given flux. With this information, one may determine the direction in which the chemical reaction will proceed. Furthermore, it is possible to predict a maximum range of compositional change for each specific flux/ electrode/baseplate combination. As an example, if the predicted equilibrium manganese and silicon of the weld metal are 1.83% and 0.33%, respectively, for Flux-1, and if the initial manganese of the base metal/ electrode, taking dilution into account is 1%, then the weld metal manganese content will range between 1% and 1.83%Mn. Referring to Appendix 4-a, we see that the flux will lose at most 5.5%MnO (15.7%-10.2%). Using the same procedures for the other initial base metal chemistries used with Flux-1, we may predict the ranges as shown in Figure 38. The predictions for silicon in the weld metal, using Flux-1 are also shown in Figure 39 for several initial base metal silicon contents.

2) Using the mass balance, it is possible to reduce the range of the predictions shown in Figures 38 and 39. Superimposing values of constant k onto Figures 38 and 39, gives the results shown in Figures 40 and 41. Typical values for k lie between 0.7 and 0.3. This reduces the expected

variation in the metal oxide sharply, although the permissible variation in the weld metal analysis is not changed much. As an example, consider a weld made with Flux F-1 in which k is measured as 0.5. From the previous study we know that the the actual weld metal analysis as defined by ΔMn should lie below the line k=0.5. If $Mn_{,i}$=1.0%, the equilibrium thermodynamic prediction requires that ΔMn-ΔMnO lie within triangle abc. As noted previously, this gives a maximum variation in ΔMn of 0.83% when ΔMnO equals zero. The mass balance places a further restriction that the ΔMn-ΔMnO result will lie within triangle abp. This reduces ΔMn_{max} from 0.83% to 0.67% as shown in Figure 40. In some cases, the range can be reduced significantly although in others the improvement is much less.

In summary, it is possible to predict the range of the weld metal Mn and Si contents by the following procedures. First, equilibrium thermodynamics is used to predict the direction of the weld metal composition change. Second, a mass balance is used to restrict this range to more manageable limits. If the predicted point is in the first quadrant of the ΔMn-ΔMnO plot, i.e., if the weld metal gains the element or the slag loses the metal oxide, the predicted change should lie on or below the experimentally measured k line. In the submerged arc welding process, normally k is smaller than 0.5, so if $k_{(exp)}$ is not available, it is reasonable to assume k=0.5 in the first quadrant. In the

case of $\Delta Mn-\Delta MnO$ in the third quadrant, i.e., loss of alloying element from the weld metal, the operating point should also be below the k line. If k=0 is assumed, the predicted range is the same as that obtained by thermodynamic prediction.

4.5 <u>The effects of welding conditions on the weld metal chemistry</u>:

In order to control the weld deposit chemistry, the correlation between the weld metal chemistry and the welding conditions has been investigated by previous authors (10,15, 18,26). They have found that the range of deviation of the weld metal chemistry is different for different welding conditions and is also dependent upon the initial electrode chemistry. No explanation has been made and contradictions exist. If the understanding of weld metal equilibrium presented here is accurate, one should be able to explain the contradictions which were found by the previous authors. A selection of some of their results is summarized in Table 14. As seen from Table 14, a larger spread was found in the final weld metal manganese content if the initial manganese content was farther from the equilibrium point.

It is understood from Section 4.2 that if the initial choice of electrode/baseplate chemistry is close to the thermodynamic equilibrium point of the flux, then the limits placed upon the process by the thermodynamic model are quite narrow. One would not expect any significant change of the

weld metal chemistry. In such a case, there will be not an effect of kinetic factors on the weld metal chemistry. On the other hand, if the initial choice of the electrode/ baseplate chemistry deviates significantly from the flux equilibrium point, one may expect that kinetic factors will play an important role in determining the weld deposit chemistry. This is the reason why the previous authors found that in some cases welding conditions had significant effects on the weld deposit chemistry, in other cases the effects was minor. Furthermore, this is also the reason why the data points farther away from the equilibrium point are much more scattered as seen from Figures 22 through 35 in this experimental study. These results further confirm that the effect of welding conditions is one of kinetic control and the effect of flux is one of thermodynamic control of weld metal chemistry.

It is also seen that the travel speed has no effect on the weld metal chemistry. This confirms the results of the screening experiment in section 4.1. The effect of travel speed on the weld metal chemistry found by Christensen(15) was due to the fact that the welding voltage and current were not constant in his experiment. The effect of welding current on the weld deposit chemistry is larger than that of welding voltage which also confirms the finding of the screening experiment. While the effects of current and voltage in the screening experiment are relatively smaller

than that shown in Table 14, this is due to the fact that only one electrode composition was chosen in the screening experiment.

Based upon the above results, it is concluded that the weld metal chemistry would be more predictable when the initial weld metal chemistry is near the equilibrium point. However, if the initial chemistry deviates significantly from the equilibrium content, the weld deposit chemistry is likely to be controlled by the welding kinetics which results a more complex situation. This leads to the fourth approach of investigating the kinetics.

4.6 Kinetics: (The fourth approach)

As seen in the description of the thermodynamic equilibrium model(section 4.2), the new equilibrium formalism is quite successful in predicting the direction and the permissible extent of both the manganese and the silicon reactions; however,the actual extent of the reactions is determined by kinetic factors rather than thermodynamic factors and hence is more difficult to predict. Prediction of the equilibrium state is a necessary starting point for study of the kinetic processes governing the approach to equilibrium. At present, the welding process is not understood well enough to predict the exact extent or the mechanisms controlling of the weld metal chemistry. In the following section several aspects of kinetic control of the weld pool are investigated.

4.6.1 The possible transport controlling mechanisms:

The slag-metal reactions occuring during flux shielded arc welding may include the following steps:

1) transport of reactants to the slag-metal-plasma interface:

    a) bulk transport in the metal phase.

    b) bulk transport in the slag phase.

    c) bulk transport in the plasma phase.

2) interfacial reactions:

    a) plasma-metal reactions which include dissociation, association, adsorption, vaporization and chemical reaction at the plasma-metal pool and the plasma-electrode tip.

    b) plasma-slag reactions which also include dissociation, association, adsorption, vaporization and chemical reaction.

    c) slag-metal reactions.

3) transport of products in the plasma region.

4) transport of products in the bulk:

    a) transport of products from the interface to the bulk metal phase.

    b) transport of products from the interface to the bulk slag phase.

A schematic representation of the entire process is shown in Fig. 42. It may be argued that transport in the gas phase should be faster than that in the solid and the liquid phases. This rules out transport in the plasma region as the rate determining step. Furthermore, due to the much higher temperature in the plasma region, the rate of plasma-slag and plasma-metal reactions are expected to be more rapid than that of slag-metal reactions.

The spatial distributions of silicon and manganese in the weld metal have been measured by several investigators (12,14,15,18), and it has been found that the distribution of silicon is uniform but the distribution of manganese is not. Due to the uniform distribution of silicon in the metal phase, previous authors have suggested that the transport rate of silicon in the weld metal is rapid. No other studies have been made in this area. In order to understand the possible transport controlling mechanisms of Mn and Si between the slag and the metal phases, it is also necessary to investigate the spatial distributions of SiO_2 and MnO in the slag phase.

4.6.2 Experimental results:

A selection of experimental results of the spatial distributions in both the slag and the metal phases is shown in Figure 43 and 44, while a more complete set of data is given in Appendix 5. The silicon distribution in the metal phase is uniform in all cases except when the 3.22% Si plate and electrode are used. The manganese distribution in the metal phase is uniform in some cases, but in general it is non-uniform. In the slag phase, the spatial distribution of both SiO_2 and MnO is non-uniform in all the cases investigated.

4.6.3 Discussions:

4.6.3.1 Transport processes both in slag and in metal phases:

The above experimental results confirm the findings of

previous investigators that the distribution of silicon in

the metal phase is uniform and that of Mn is not. However,

the results of the weld made with a 3%Si plate and electrode

show that the distribution of silicon in the weld metal is

also non-uniform. This non-uniform distribution of silicon

is due to the large deviation between the initial 3.22% Si

and the equilibrium 0.33% Si. This suggests that the uni-

form distribution of silicon in the weld metal which was

found by the previous investigators may be due to the fact

that commercial steel baseplate and electrodes are usually

limited to 0.5% Si, which does not provide a large deviation

between the initial Si and the equilibrium Si. At such small

deviations, the amount of mass transfer is not large and the

process reaches an effective equilibrium. Furthermore, the

experimental data of Figures 43 and 44 also show that the

distribution of manganese in the metal phase is uniform if the

initial Mn content lies in the vicinity of the chemical

equilibrium point as defined previously. This also suggests

that the non-uniform distribution of Mn commonly found by the

previous authors may be due to the large manganese chemistry

variation in commercial steels, i.e., 0% to 1.6% which provi-

des a greater possiblity of large deviation between initial

and equilibrium Mn content. Considering that the diffusion

coefficients of silicon and manganese in the steel are of the

same order of magnitude and one may   conclude that the

transport rates of Si and Mn in the metal phase are competitive. This differs from the conclusion of the previous investigators that the Si transport is fast. Their conclusions were based upon the uniform spatial distribution of silicon found in the weld metal phase, which has been shown in this study to be more a function of the usually small changes in the silicon content of the weld metal rather than to be a result of an enhanced reaction rate.

In order to clarify whether mass transport is slower in the weld metal phase or in the slag phase, it is necessary to investigate the spatial distribution in both phases. If the transport of a species in the slag phase is much slower than in the metal phase, we may expect the spatial distribution of the species to be uniform in the metal phase while remaining non-uniform in the slag phase and vice versa. The results in Figure 43 and 44 show that the spatial distributions of Mn and Si in the weld metal are uniform while the spatial distributions of MnO and SiO_2 are not. This indicates that transport in the slag phase is slower than that in the metal phase as would be expected from bonding considerations. It is still not clear from the results of this investigation whether MnO or SiO_2 transport in the slag phase is the slowest transport step. More work needs to be done in this area.

Up to now, no diffusion data have been estimated or

measured in welding due to the complexity of the

process. In order to estimate the transport coefficient of Mn

and Si in both the slag and the metal phases, several assump-

tions have been made:

1) The transport time in the metal phase is estimated

   from the solidification time. In addition, the soli-

   dification time for the slag phase was assumed to be

   equal to the transport time in the metal phase. The

   solidification time is given as (2)

$$S_t = \frac{L H_{net}}{2\pi k \rho c (T_m - T_o)}$$ (16)

Here S_t=solidification time, the time lapse from beginning

to end of solidification at a fixed point in the weld
metal. (s)

L=heat of fusion. $(J\ mm^{-3})$

H_{net}=net energy input $(J\ mm^{-1})$

k=thermal conductivity of the metal $(J\ mm^{-1}\ s^{-1}\ K^{-1})$

ρ=metal density $(g\ mm^{-3})$

c=specific heat of solid metal $(J\ g^{-1}\ K^{-1})$

T_m=melting temperature of the metal (K)

T_o=the uniform initial temperature of the sheet or

   plate (K)

For the experimental conditions used, the solidification

time is approximately

$$S_t = \frac{2 \times 1830}{2\pi(0.028)(0.0044)(1510-25)^2} = 2.15 \text{ seconds}$$

By comparison with any casting process, weld metal solidification is extremely rapid. Even in a severely chilled ingot or casting, the solidification time is several seconds, while, for many castings, solidification time is on the order of minutes or hours.

2) The area under the spatial distribution curve divided by the transport time is approximately equal to the mass flow rate, J(*). A schematic illustration is shown in Figure 45.

3) Using a linear approximation of Fick's first law:

$$J=-Ddc/dx=-D(C_s-C_b)/\delta \qquad (17)$$

We may define a transport distance, δ.

The estimated values of J, δ and (C_s-C_b) are given in Table 15. Substituting these estimated values of J, δ and (C_s-C_b) into equation (17) gives the values of D listed in Table 15. The solidification time of the slag should be longer than 2.15 seconds because the melting point of the slag is lower than that of base metal; however, the estimate here is only approximate, and the real diffusion coefficient will be lower than the estimated value in the slag phase. The analysis does indicate that transport in the slag phase is at least an order of magnitude slower than that in the metal phase.

---

* In many cases J is called a flux but in the present case such terminology is avoided for obvious reasons.
The estimated values of J, δ and (C_s-C_b) are given in

Using data from the steelmaking literature the diffusion coefficient of Mn or Si in the metal phase is estimated to be on the order of $10^{-4}\text{cm}^2/\text{s}$ and that in the slag phase is of the order of $10^{-6}\text{cm}^2/\text{s}$ (39,50). Comparing the data estimated from steelmaking and this experiment, it is seen that the mass transport in the welding process is several times greater than that in steelmaking process. In arc welding processes, the weld pool is stirred vigorously by the electromagnetic forces induced by the welding current. This forced convection is very important in enhancing welding transport phenomena. Apps and Milner(51) found the heat transfer to be several times greater in the weld pool than could be accounted by thermal conduction alone. We may conclude that the diffusion or heat transfer in the welding process is primarily controlled by forced convection, arising from the Lorentz forces acting on the weld pool.

4.6.3.2 Equilibrium at the slag-metal interface:

A unique equilibrium constant exists at every temperature for each reaction. If equilibrium at a single temperature exists, the equilibrium constant calculated from the composition of the reacting species will be the same. This "effective" reaction temperature provides a method of estimating whether the equilibrium is achieved or not. In the following section, the concept of an effective equilibrium reaction temperature for the SiO_2 and MnO reactions is discussed.

1) The SiO$_2$ reaction:

As seen in section 4.6.2, the bulk and the surface silicon contents in the weld metal do not vary markedly; hence,it does not make much difference whether surface or bulk Si is used in the calculation. Nonetheless, the distribution of SiO$_2$ in the slag is non-uniform,and the effective reaction temperature will depend upon whether bulk or surface compositions are used. In most cases however, the largest difference between the bulk and the surface SiO$_2$ in the slag is less than 3%. This 3% difference does not affect the activity of SiO$_2$ in the slag significantly; hence, the equilibrium reaction temperature for the SiO$_2$ reaction may be calculated using bulk analyses for the weld metal and the slag. Using activity of SiO$_2$ in each flux system as estimated from steelmaking data, the effective SiO$_2$ reaction temperatures during welding may be calculated.

Iwamoto et al.(30) have studied the oxygen distribution of the weld metal by using IMA (ion microprobe analysis) with Ar$^+$ as the ionic source. The results of four different weldments showed that the deviation between point and bulk weld metal oxygen contents was within 30ppm as shown in Figure 46. The bulk weld metal oxygen contents measured by Leco fusion apparatus were between 550ppm and 600ppm in Iwamoto's experiment. This suggests that the oxygen content in the weld metal is uniform which means that the bulk oxygen con-

tent can be used in instead of the surface oxygen content.

Based on the above discussions, the effective reaction
temperatures of the SiO_2 reaction were estimated by Eq.2
from the data in the published literature(12,14,15,16,45,48),
and the results are shown in Figure 47. A uniform reaction
temperature of $2000^{\circ}C$ is obtained for the SiO_2 reaction.
Several of the welds of Figure 47 were produced with 3%
silicon iron base plate, using high basicity fluxes. The
experimental conditions are given in Table 4 and the results
are shown in Table 16. This combination would be expected
to deviate from equilibrium more than most commercial
welding combinations. The fact that $2000^{\circ}C$ still represents
a reasonable choice of equilibrium temperature verifies the
uniformity of the SiO_2 equilibrium which occurs during
welding. The data in Figure 47 confirm the results of
Belton et al. that the SiO_2 reaction achieves an effective
equilibrium reaction temperature of $2000^{\circ}C$ over a wide range
of weld metal chemistry and flux composition(12). These data
also show that the SiO_2 reaction is extremely rapid in that
it does reach an effective equilibrium even when one percent
silicon is transferred from the slag to the metal or vice
versa.

2) The MnO reaction:

The spatial distribution of Mn in the weld metal is not
uniform as noted by previous investigators. Since it is the

surface Mn content that determines the equilibrium in slag-metal reactions, the use of bulk Mn may result in large errors in the analysis. Unfortunately, the bulk Mn content was used by previous investigators in determing the effective reaction temperature. This account for the wide range of findings. It will be shown subsequently that it is necessary to use surface Mn content instead of bulk Mn in the chemical reaction calculation.

The distribution of MnO in the slag phase is also non-uniform. In most cases, the largest difference between bulk and surface MnO content is within 3%. This 3% difference will not affect the activity of MnO in the slag phase significantly except in low MnO fluxes; hence, the bulk MnO may be used in the estimation of the effective temperature. The experimental results of bulk Mn, surface Mn and oxygen weld metal content are given in Table 17 for two different fluxes. The calculated effective reaction temperatures are given in Figure 48. It is seen that the MnO reaction reaches equilibrium at the slag-metal interface at an average reaction temperature 2000°C. This is consistent with the SiO_2 reaction. The comparison of the equilibrium constants obtained by using bulk Mn and surface Mn is also given in Table 17. A much wider range of reaction temperatures is obtained when the bulk Mn content is used in the calculation.

If the weld metal gains manganese, the surface Mn content
be larger than that of the bulk due to the requirement
of diffusion from the surface to the bulk. This also
implies that the effective temperature estimated from the bulk
Mn content will be lower than that estimated from the surface
Mn content. On the other hand, if the weld metal loses
manganese, the surface Mn will be less than the bulk Mn
content. This means that the effective temperature esti-
mated from the bulk Mn content will be higher than that
estimated from the surface Mn content. This is the reason
why previous investigators suggested that a single effective
MnO reaction temperature is not attained during welding.

Based upon the above discussions, it is concluded that
the weld metal surface Mn content should be used in the
calculation of effective reaction temperature and that a
single effective reaction temperature is obtained for both
the MnO and for the SiO_2 reactions. This implies that
equilibrium exists at the slag-metal interface. This is
further confirmation of the validity of the initial
assumption of $2000°C$ as the equilibrium reaction temperature
chosen in section 4.2.1.1. From the above discussions
describing the spatial distributions of Mn and Si in the
metal and the slag phases, and the effective equilibrium at
the slag metal interface, it may be concluded that the rate
determining step in flux shielded arc welding reactions is

bulk transport of metal oxides in the slag phase. The data are insufficient to determine whether diffusion of MnO or SiO_2 is more important in establishing the final weld metal chemistry. Further study in this area would be desirable.

4.7 The oxygen potential of CaF₂-oxide flux systems:
(The fifth approach)

Based upon the screening experiment, it was found that the flux composition has the most significant effect on the weld metal oxygen content. In order to understand the oxygen potential of the flux and the relative stability of various oxides in the welding process, binary CaF_2-oxide flux systems have been investigated. At the same time, the effect of CaF_2 on the weld metal oxygen content has also been investigated.

The weld metal oxygen content produced with binary CaF_2-oxide systems is shown in Figure 49. The welding conditions and the chemical composition of the electrode and baseplate used for these experiments are given in Table 4 and 5. The oxygen contribution due to each oxide or the relative oxide stability can be ranked on an increasing order as shown in Table 18.

4.7.1 The oxygen potential:

CaO is the stablest oxide examined in this study. The weld metal oxygen contents produced using 70%CaF_2-30%CaO and pure CaF_2 are essentially identical which implies that

CaO makes no contribution to the weld metal oxygen content. This contradicts to the results of North(17). Heuschkel(24) has shown that the weld metal oxygen content increases drastically with increasing CO_2 content in the argon shielded GMA process. Previous investigators(17) have shown that the weld metal oxygen content increases as the $CaCO_3$ content of the flux is increased. From the present study, it is seen that the increasing weld metal oxygen content is due to the carbonate decomposition, i.e., $CaCO_3=CaO+CO_2$. The CO_2 gas from the carbonate decomposition is the main source of the high weld metal oxygen content observed by North. It is clear that if a given flux has a component which is decomposed by the plasma into a suboxide, the oxygen content in the weld metal will be higher than that expected. This is consistent with the prediction of Eagar(7,9).

The weld metal oxygen content is related to the oxide stability. The stabler the oxide, the lower will be the oxygen content of the weld metal. The trend of oxide stability predicted by steelmaking thermodynamics does not coincide with that of arc welding processes as shown in Table 18. This implies that consideration of slag-metal reactions alone is not sufficient to explain the oxygen content observed in the weld metal. Oxygen transport in the arc welding process is more complex. In the arc welding process, the presence of the arc plasma has a significant effect on

the weld metal oxygen content. It is for this reason that
it is necessary to specify an empirical weld metal oxygen
content from the previous theoretical treatment of section
4.1. It is not possible to calculate the weld metal oxygen
content based upon steelmaking thermodynamics. However,
once the oxygen content is known, it may be used to predict
the Mn and Si contents of the weld metal.

The oxygen potential of MgO is much higher in the weld-
ing process than would be expected from steelmaking data.
This high oxygen potential with MgO in the arc welding pro-
cess is no doubt due to the high temperature of welding
which causes oxides of volatile species such as Mg to
decompose readily. This suggests that in order to explain
the weld metal oxygen content, not only slag-metal reactions
but also the decomposition of the slag by the plasma need
to be considered. Slag-metal reactions can provide a
general trend but this trend can be altered signifi-
cantly by decomposition of species such as $CaCO_3$ and MgO.

SiO_2 and MnO are the major oxygen contributors in the
flux due to their lower free energy of formation as pre-
dicted from steelmaking thermodynamics and also due to the
formation of suboxides such as SiO. This suggests that in
order to lower the weld metal oxygen content, these low
stability oxides need to be removed as much as possible.
Unfortunately, silica in particular is very inexpensive and
imparts many desirable operating features to the flux.

The oxygen potential of fused and bonded fluxes was also compared by the artificial baseplate experiment technique. The flux preparation and experimental conditions are the same as mentioned in section 4.2.3.2. The weld metal oxygen contents for these trials are given in Table 19 for MIT-1-B and MIT-1-F. The mean value and standard deviation of weld metal oxygen content are 0.061 ± 0.016% for MIT-1-B and 0.051 ± 0.020% for MIT-2-F. A statistical analysis(52) of these populations indicates that not only is the mean value of the oxygen content higher in the bonded fluxes than that in the fused fluxes but the difference is more than can be expected from experimental error alone. This is probably due to the inhomogeniety of the bonded flux as well as the lower activity of the individual components in the fused fluxes. The bonded flux is made up of individual oxide minerals which are separated from other components on a microscopic scale. The bonded flux is not a single phase, and the activity of each oxide would be higher than in a fused flux. This means that the bonded flux possesses a higher oxygen potential while in the case of fused fluxes, the manufacturing process produces a uniform melt which may be considered as a single phase or nearly so. The components in this flux have lower oxide activity. On the other hand, if the flux contains volatile species such as carbonates, then the flux may have a much higher oxygen potential. Fused

fluxes will not have such species. The bonded flux will not have this advantage. Based upon this understanding, the bonded flux can be expected to always have a higher oxygen potential than that of a fused flux of identical composition.

4.7.2 The effect of CaF_2 on the oxygen potential:

Figure 49 shows that the oxygen content in the weld metal is proportional to the oxide content in the binary CaF_2-oxide flux. This implies that CaF_2 does reduce the oxygen potential potential of flux if only by a dilution effect. The higher the oxygen potential of the oxide, the more significant is the effect of CaF_2 on the overall oxygen content of the weld metal. With oxides such as SiO_2 and MnO, an additional 10% CaF_2 could reduce the oxygen content by 100ppm. In the case of high stability oxides such as CaO, CaF_2 has little or no effect on the weld metal oxygen content. This suggests that the effect of CaF_2 on flux oxygen potential strongly depends upon the flux composition. CaF_2 has a significant effect only if the flux contains a relatively unstable oxide species such as SiO_2, MnO, MgO and Al_2O_3. This contribution of CaF_2 to weld metal oxygen recovery makes the treatment of CaF_2 in welding fluxes difficult in a thermodynamic sense. It is still not clear whether CaF_2 should be included in the basicity index or not.

The oxygen content of the weld metal using these fluxes is far below that of most commercial fluxes due to a com-

paratively small portion of the metal oxide in these laboratory fluxes.

From this investigation, it is found that the CaF_2 does lower the weld metal oxygen content but that the effect of CaF_2 on the basicity index is still not clear. Further experiments are necessary to study the function of CaF_2 in welding fluxes.

4.8 The suggested approaches of alloying weld metal through the alloyed fluxes:

The previous discussions are only suitable for neutral fluxes. A different model should be used for alloyed flux, however, understanding the behavior of the neutral flux is a prerequisite for investigating the alloyed flux. Some correlation between these two kinds of fluxes can be expected especially when considering two extreme situations of the alloyed fluxes. First, assume that the alloy elements within the alloying flux remain completely in the slag during welding, i.e., no reaction occurs. This is equivalent to the neutral flux because the alloy elements in the slag have no effect. We may expect the neutral flux model would apply in this extreme case. Second, assume that the alloy elements in the slag are totally transferred into the weld metal. This is the same as using a highly alloyed electrode in conjunction with a neutral flux, i.e., changing the initial metal composition but without changing the equilibrium point of the flux. If the alloyed flux follows either one of these two extreme cases, the neutral flux behavior can be used to pre-

dict the alloyed flux behavior. Unfortunately neither of
these two extreme cases are met in practice.

Two different approaches may be taken in analyzing the
flux equilibrium when using alloyed fluxes.

1) Fix the initial weld metal chemistry while changing
   the equilibrium weld metal chemistry:

In this case, the initial weld metal chemistry is calcu-
lated based upon the electrode/base metal chemistry and the
dilution factor. This is the same procedure as used with
neutral fluxes. The final equilibrium weld metal chemistry of
the alloyed flux would be higher than that of the neutral flux
due to the presence of the elements in the alloyed flux. In
this approach, the problem will become one of how to estimate
the new equilibrium point. If we are able to estimate the
equilibrium point, it will become possible to give the per-
missible working limits as before. The schematic represen-
tation of this approach is given in Figure 50. Point A in
Figure 50 represents the initial weld metal Mn which may be
estimated as before, i.e.,

$$Mn_i = DMn_b + (1-D)Mn_e$$

Here D=dilution factor, Mn_b=baseplate Mn content, Mn_e=electrode
Mn content. Point A is a fixed point in this approach. Point B_o
represents the equilibrium point of the neutral flux which may
be obtained as shown in section 4.2. This point is equivalent
to zero percent recovery of the alloyed element in the alloyed
flux. This point is independent of the value of k. Point B_1,
represents an equilibrium point representing 100% recovery.

The location of this point is strongly dependent upon the k value. The larger the value of k is, the higher the B_1 value will be. The actual equilibrium point of alloyed flux must lie between B_0 and B_1. It is a function of both the k value and the efficiency of alloy recovery from the flux. Let us assume B^* is the equilibrium point of the alloyed flux (cf. Figure 50). In this case the final weld metal Mn content must lie between A and B^*. The difficulty with this approach is that a means of calculating B^* needs to be developed.

From the mass balance point of view, the k value would be important because larger k implies more alloying element is available to participate in the reaction. This further implies that the welding process parameters such as welding voltage may significantly affect the weld metal chemistry in the alloyed flux, because welding voltage is the most important parameter affecting the flux consumption. This is quite different from the neutral flux. As we have seen before, variation of k does not restrict the weld metal chemistry very effectively in neutral fluxes. It is also necessary to consider the oxidation and the evaporation of alloy element in the slag when applying the mass balance. These sinks may be more important in alloyed fluxes than in neutral fluxes.

2) Fix the equilibrium point and change the initial weld metal chemistry:

In this approach, we assume that the equilibrium point

-100-

of the alloyed flux is the same as that of the neutral flux.
The effect of the alloying element within the flux is
taken into account by adjusting the initial weld metal
chemistry. The schematic representation of this approach is
given in Figure 51. The minimum initial weld metal chem-
istry is produced by the neutral flux when the recovery is
zero. This is given as point A in Figure 51.
The maximum initial weld metal chemistry is produced in the
case of full recovery, i.e., when the alloyed element is
totally transfered into the weld metal as shown by point A.
This point also depends upon the k value. In this approach,
the problem is to determine the initial weld metal chemistry
which must lie between A_1 and A, in Figure 51. If one assumes
that A^* is the adjusted initial point, then the permissible
weld metal Mn will range between B_0 and A^*.

These two approaches are different; which one is better
depends upon which one fits the experimental data better.
The recovery may be expected to vary in a large range
depending upon the welding conditions which influence the
value of k and also upon the physical properties of the flux
which influence alloy recovery. Kinetic factors may be quite
different between the neutral and the alloyed fluxes. These
possibilities need to be investigated experimentally in
future work.

Based upon the above discussions, the possibility of optimizing recovery by using equilibrium percent MnO in flux and alloying with Mn metal would be better than using all Mn metal. Because the equilibrium percent MnO in flux would prevent the weld metal from losing the Mn element and the additional Mn alloy in flux would enforce the weld metal Mn recovery. If using all Mn metal in the flux, one would not be able to guarantee that the weld metal will gain the manganese due to the transfer coefficient of Mn alloy in the flux could be ranged between zero and one. In the case of non-transfer, i.e., no reaction occurs, the weld metal will lose the Mn element because none MnO in the flux and no effect of Mn alloy in the flux. Further study of active fluxes is necessary in this area.

V. Conclusions

In order to understand slag-metal reactions in the flux
shielded arc welding process, the effects of process variables,
thermodynamics, kinetics, mass balance and flux oxygen potential
have been investigated. This study has resulted in the
following conclusions:

1) The flux composition is the most important process variable
   which affects the weld metal chemistry.

2) Process changes are interrelated and can produce signifi-
   cant changes in weld metal chemistry. The recovery of Mn is
   independent of welding speed which agrees with the result
   of North and Thier but contradicts the conclusion of
   Christensen. The contradiction between these authors has
   been explained.

3) The flux composition exerts thermodynamic control over the
   weld metal chemistry while process variables exert kinetic
   control over the extent of the reaction. But CaF_2 may
   influence the weld deposit chemical composition through
   kinetic means by reducing the viscosity of the flux and
   thereby increasing mass transfer by forced convection.

4) The thermodynamic equilibrium point is a function only of
   flux composition, and is independent of the welding
   operating conditions.

5) A thermodynamic model has been proposed. The generality
   and the accuracy of this model have been verified by

comparison with data in the available literature and with
new experimental results. It is concluded that this model
is able to predict the permissible range of weld metal Mn
and Si contents based upon the flux, the electrode and the
baseplate chemistry.

6) The distribution of SiO_2 and MnO in the slag phase have
been investigated for the first time and have been found to
be non-uniform. The mass transport coefficient in the slag
is several orders of magnitude greater in the welding pro-
cess than in the steelmaking process due to the strong con-
vection induced by electromagnetic forces. Mass transport
in the liquid metal phase is even faster than in the slag
phase; hence, the controlling step for metal transport
between the slag and the metal is transport in the slag
phase.

7) The effective reaction temperature for both the SiO_2 and
the MnO reactions is 2000°C provided surface compositions
and not bulk compositions are used to compute the
equilibrium constant.

8) A mass balance provides some improvement in restriction of
the permissible range of the weld metal chemistry which
was predicted by the thermodynamic model. The mass balance
also shows that the metallic mist is not an important sink
while slag inclusions in the metal phase are important sinks
in some cases.

9) Bonded fluxes have higher a oxygen potential than fused fluxes due to higher homogeneity and lower oxygen activity in the fused fluxes.

10) CaF_2 may reduce the oxygen potential of oxide components in the flux. Its effectiveness depends upon the stability of oxide.

11) The weld metal oxygen content has been investigated using CaF_2-oxide flux systems. CaO is the stablest oxide and SiO_2/MnO are the least stable oxides of the eight oxides investigated.

VI. Summary

The structure and properties of the weld metal are
determined primarily through control of the weld deposit
chemistry. Unfortunately, the factors controlling the weld
metal chemistry are pooly understood, resulting in an empiri-
cal approach to control the weld deposit chemistry. The pur-
pose of the study as presented is to develop an improved
understanding of weld metal chemistry control.

A screening experiment has been performed in order to
understand the important controlling factors. It was found
that the direction of slag-metal reaction is controlled by
thermodynamic factors which are related to chemistry of the
system, while the extent of the reaction is controlled by
kinetic factors which are related to the operating parameters
of the process. A thermodynamic equilibrium model has been
presented. Although not capable of predicting the magnitude of
the Mn and the Si changes in the weld metal, it is capable of
predicting the gain or loss of these elements over a wide
range of flux/electrode/baseplate compositions. A mass balance
has also been presented which is found to impose an additional
restriction on the weld metal chemistry. Combination of both
thermodynamic equilibrium model and the mass balance, produced
the best prediction of final weld metal composition. The model
represents a significant advance in our ability to predict and

control the slag-metal reactions in the submerged arc welding process.

The plasmadynamic oxygen Potentials of several oxides commonly found in commercial welding fluxes have also been investigated. The results provide an indication of oxide stability which may be helpful for the future investigators.

VII Suggestions for the future work

1) Further work needs to be done in order to extend both the thermodynamic and the mass balance models to active submerged arc welding fluxes and to other welding processes such as shielded metal arc or flux cored arc welding.

2) In order to clarify the plasmadynamic oxygen potential of the flux, it is necessary to investigate the plasma behavior in the arc region. Only in this way will it be possible to understand the plasma-metal reactions which occur.

3) Further study of welding kinetics is needed to clarify the competition between the Mn and the Si reactions.

4) Slag inclusions are an important sink of alloyed element in some cases. In order to understand the mechanisms controlling the growth of slag inclusion, further experiments are necessary.

5) CaF_2 has a dilution effect on the flux oxygen potential, but this effect depends upon the stability of the oxides present. Further experiments are necessary to study the function of CaF_2 in welding fluxes.

VIII REFERENCES

1. R.D. Stout and W.D. Doty. Weldability of Steel. Welding Research Council, New York, N.Y., 1978.

2. C. Weisman. Welding Handbook, Volume 1. Seventh Edition, American Welding Society, Miami, FL., 1976.

3. P.R. Kirkwood,"Weld Metal Composition Control," Welding J., Aug. 1969, p.328-s.

4. J. Heuschkel, "Composition Controlled, High-Strength, Ductile, Toughness, Steel Weld Metals," Welding J., Aug. 1964, 0.361-s.

5. G.M. Evans, "Effect of Manganese on the Microstructure and Properties of All-Weld-Metal Deposits," Welding J., Vol. 59, No. 3, 1980, p.67-s.

6. P.D. Blake, "Oxygen and Nitrogen in Weld Metal," Welding Research International, Vol. 9, No.1, 1979, p.23.

7. T.W. Eagar, "Sources of Weld Metal Oxygen Contamination During Submerged Arc Welding," Welding J., Vol. 57, No.3, 1978, p.76-s.

8. Y. Ito, M. Nakanishi and N. Katsumoto, "Effect of CaF_2 in Flux on Toughness of Weld Metal Relation between CaF_2 Content in Welding Flux and Impure Gas Content in Weld Metal," The Sumitomo Search, No.16, Nov. 1976, p.78.

9. T.W. Eagar, "Oxygen and Nitrogen Contamination During Arc Welding," in Weldments: Physical Metallurgy and Failure Phenomena. R.J. Christoffel, E.F. Nippes and H.D. Solomon eds. General Electrical Co., 1979, p.31.

10. N. Christensen and J. Chipman, "Slag-Metal Interaction in Submerged Arc Welding," WRC Bulletin, No. 15, January 1953.

11. R.A. Kubli and W.B. Sharav, "Advancements in Arc Welding of High Impact Steels," Welding J., Vol. 40, No. 11, 1963, p.497-s.

12. G.R. Belton, T.J. Moore and E.S. Tankins, "Slag-Metal Reactions in Submerged Arc Welding," Welding J., Vol.42, No. 7, 1963, p.289-s.

13. W.J. Lewis and P.J. Rieppel, "Flux and Filler-Wire Developments for Submerged Arc Welding HY-80 Steel," Welding J., Vol. 40, No. 8, 1961, p.337-s.

14. N. Christensen, "Spatial Distribution of Manganese, Silicon, Chromium and Oxygen in Submerged Arc Weld Deposits," Contract DA-91-591-EUC 3455, U.S. Despt. of Army, European Research Office, Nov. 1965.

15. N. Christensen, "Spatial Distribution of Manganese, Silicon, Chromiun and Oxygen in Submerged Arc Weld Deposits," Contract DA-91-591-EUC 2797, U.S. Dept. of Army, European Research Office, March, 1964.

16. C.A. Butler and C.E. Jackson, "Submerged Arc Welding Characteristics of the CaO-TiO$_2$-SiO$_2$ System," Welding J., Vol. 46, p.448-s.

17. T.H. North, H.B. Bell, A. Nowicki and I. Craig, "Slag/ Metal Interaction, Oxygen and Toughness in Submerged Arc Welding," Welding J., Vol.57, No.3, 1978, p.63-s.

18. T.H. North, "The Distribution of Manganese Between Slag and Metal During Submerged Arc Welding," Welding Research Abroad, 23(1), January, 1977, p.2

19. C.E. Jackson, "Fluxes and Slags in Welding," WRC Bulletin, No. 190, December, 1973.

20. J.G. Garland and N. Bailey, "Fluxes for Submerged Arc Welding Ferritic Steels: A Literature Survey," The Welding Institute, Member Report M/84/75, 1975.

21. J.H. Palm, "How Fluxes Determine the Metallurgical Properties of Submerged Arc Welds" Welding J., July, 1972, p.358-s.

22. T. Boniszewski, "Basic Fluxes and Deoxidation in Sub- merged Arc Welding of Steel," Metal Construction and British Welding J., April, 1974, p.128.

23. W.H. Kearns. Welding Handbook, Volume 2. Seventh Edition, Miami, FL., 1978.

24. J. Heuschkel, "Weld Metal Composition Control," Welding J., Aug. 1969, p.328-s.

25. B.A. Korh, "Thermodynamic Calculation of Alloying From the Slag and Deoxidisation of the Metal During Welding," Automatic Welding, Vol. 30, No. 7, 1977, p.16.

26. H. Thier, "Metallurgical Reactions in Submerged Arc Weldings," Proceedings of the Conference on Weld Pool Chemistry & Metallurgy, The Welding Institute, London, April, 1980, p.271.

27. N.N. Potapov and S.A. Kurlanov, "A Quantitative Evalution of the Basicity of Welding Fluxes," Welding Production, No.9, 1978, p.6.

28. N. Iwamoto, "Structure of Slag-Basicity of Slag," Trans. of JWRI, Vol. 3, No. 2, 1974, p.89.

29. C. Wagner, "The Concept of the Basicity of Slags," Met. Trans. B. Vol. 6B, Sep. 1975, p.405.

30. N. Iwamoto, T. Taira, K. Akao, Y. Tsunawaki and Y. Makino, "Study on Minor Elements in Weld Steel with Submerged Arc Welding Using Fluxes of the System $(CaO)-MnO-SiO_2$," Trans. of JWRI, Vol. 7, No. 1, 1978, p.49.

31. K. Niwa and T. Yokokawa, in Chemical Metallurgy of Iron and Steel, A Symposium, The Iron and Steel Institute, London, 1973, p.77.

32. Y. Kawai and K. Mori, "Equilibrium and Kinetics of Slag-Metal Reactions," Trans. ISIJ, Vol. 13, 1973, p.303.

33. W.L. Daines and R.D. Pehlke, "Kinetics of Manganese Oxide Reduction from Basic Slags by Silicon Disoloved in Liquid Iron," Trans. AIME, 242, 1969, p.565.

34. R.L. Plackett and J.P. Burman, "The Design of Optimum Multifactorial Experiments," Biometrika, 33, 1946, p.305.

35. D.D. Schwemmer, D.L. Olson and D.L. Williamson, "The Relationship of Weld Penetration to the Weld Flux," Welding J., May 1979, p.153-s.

36. J.D. Cobine and E.E. Burger, "Analysis of Electrode Phenomena in the High Current Arc," J. Appl. Phys. 26(7) 1955, p.895.

37. O.H. Nestor, "Heat Intensity and Current Density Distributions at the Anode of High Current, Inert Gas Arcs," J. Appl. Phys., Vol. 33, No. 5, May 1962, p.1938.

38. S.S. Tuliani, T. Boniszewski and N.F. Eaton, "Notch Toughness of Commercial Submerged Arc Weld Metal," Welding and Metal Fabrication, Aug. 1969, p.327.

39. J.F. Elliott, M. Gleiser and V. Ramakrisna. _Thermo-chemistry for Steelmaking_. Vol. II. Addison Wesley Publishing Co. Reading, MA. 1963.

40. J.G. Garland and R.P. Kirkwood, "Metallurgical Factors Controlling Weld Metal Toughness in the Seam Welding of Line Pipe," in _Welding of Line Pipe Steels_, K.H. Koopman, ed., Welding Research Council, New York, NY, 1977, p.176.

41. S.F. Baumann, J.R. Sawhill and M. Nakabayashi, "Wire and Flux Development for Seam Welding of HSLA Line Pipe," ibid., p.56.

42. W.K.C. Jones, "Reheat Cracking Susceptibility of Some 2Cr-Mo Submerged Arc Welding Metal," _Welding J._, 55(2), 1976, p.42-s.

43. A.P. Bennett and P.J. Stanley, "Fluxes for Submerged Arc Welding of Q.T. 35 Steel," _British Welding J._, Feb. 1966, p.59.

44. G. Uttrachi, Union Carbide Corp., Astabula, Ohio, Private Communication, 1977.

45. J.G. Garland P.R. Kirkwood, "A Reapprisal of the Relationship Between Flux Basicity and Mechanical Properties in Submerged Arc Welding," _Welding and Metal Fabrication_, April, 1976, p. 217.

46. N. Bailey, "Effect of Wire Composition and Flux Type on Solidification Cracking When Submerged Arc Welding C-Mn Steel," _Welding Research International_, Vol. 8, No. 3, 1978, p.240.

47. J.G. Garland and N. Bailey, "Solidification Cracking During the Submerged Arc Welding of Carbon-Manganese Steels," _Welding Research International_, Vol. 8, No. 3, 1978, p. 240.

48. J.G. Garland and P.P. Kirkwood, "Towards Improved Submerged Arc Weld Metal Toughness," _Metal Construction_, Vol. 7, No. 6, p.320.

49. G.J.W. Kor, "Equilibrium Between Liquid Mn-Si Alloys and $MnO-SiO_2-CaO-MgO$ slags," _Met. Trans. B._ Vol. 10B, Sep., 1979, p.367.

50. H. Keller and K. Schwerdtfeger, "Tracer Diffusivity of Si in $Cao-SiO_2$ Melts at $1600°C$," _Met. Trans. B._, Vol. 10B, Dec. 1979, p.551.

51. D.R. Miller and R.L. Apps, "A Note on the Behavior of Liquid Metal Under the Arc," British Welding J., Vol. 10, 1963, p. 348.

52. S.L. Meyer. Data Analysis for Scientists and Engineers. John Wiley & Sons Inc., NY., 1975.

53. F.D. Richardson. Physical Chemistry of Melts in Metallurgy. Vol. I. Academic Press, NY., 1974.

54. H. Fujita and S. Maruhaski, "Equilibrium between $FeO-MnO-SiO_2$ slags and molten Iron," Tetsu-To-Hagane, 56, 1970, p.830.

55. S. Maruhashi, "Equilibrium between $FeO-MnO-Al_2O_3$ Slags and Molten Iron," Tetsu-To-Hagane, 57, 1971, p.891.

56. R.H. Rein and J. Chipman, "Activities in the Liquid Solution $SiO_2-CaO-MgO-Al_2O_3$ at 1600°C," Trans., AIME., vol. 233, 1965, p.415.

57. E. Martin, O.I.H. Abdelkarim, I.D. Somerville and H.B. Bell, "The Thermodynamics of Melts Containing MnO, FeO, CaO, TiO_2 and SiO_2," in Metal-Slag-Gas Reactions and Processes, Z.A. Foroulis and W.W. Smeltzer, eds., The Electrochemical Society, Princeton, N.J., 1975, p.1.

58. H.E. McGannon, ed., The Making, Shaping and Treating of Steel, 9th Edition, U.S. Steel, 1971.

Table 1: The available activity data used in this study

System	Temperature(^{0}C)	Reference
$MnO-SiO_2$	1500-1600	39
$CaO-SiO_2$	1600	39
$MnO-CaO-Al_2O_3$	1560	53
$CaO-MnO-SiO_2$	1650	39
$FeO-MnO-SiO_2$	1560	54
$CaO-Al_2O_3-SiO_2$	1700	39
$SiO_2-MgO-Al_2O_3$	1600	56
$SiO_2-CaO-MgO$	1600	56
$CaO-FeO-SiO_2$	1550	56
$FeO-MnO-TiO_2$	1475	57
$MnO-CaO-TiO_2$	1500	57
$MnO-TiO_2-SiO_2$	1500	57
$SiO_2-CaO-Al_2O_3-MgO$	1600	56
$SiO_2-MnO-CaO-Al_2O_3$	1650	58
$SiO_2+P_2O_5-CaO+MnO+MgO-FeO+Fe_2O_3$	1500	58

Table 2: Independent variables and values which were
chosen for the screening experiment

		(+)	(−)
X(1):	Voltage	30 volts	20 volts
X(2):	Current	500 amperes	300 amperes
X(3):	Welding travel speed	48.4cm/min.	29.8cm/min.
X(4):	Electrode diameter	W-1	W-2
X(5):	Plate thickness	B-1	B-2
X(6):	Flux thickness	4 cm.	2 cm.
X(7):	Flux composition	F-3	F-4
X(8):	Tilt angle (leading direction)	15 degree	0 degree
X(9):	Polarity	DCRP	DCSP
X(10):	Stick out	2.5 cm.	1.5 cm.
X(11):	Argon shielding	yes	no

Table 3:   Twenty-Run Plackett-Burman Design

Run	Mean	X1	X2	X3	X4	X5	X6	X7	X8	X9	X10	X11	X12	X13	X14	X15	X16	X17	X18	X19
1	+	+	+	−	−	+	+	+	+	−	+	−	+	−	−	−	−	+	+	−
2	+	+	−	−	+	+	+	+	−	+	−	+	−	−	−	−	+	+	−	+
3	+	−	−	+	+	+	+	−	+	−	+	−	−	−	−	+	+	−	+	+
4	+	−	+	+	+	+	−	+	−	+	−	−	−	−	+	+	−	+	+	−
5	+	+	+	+	+	−	+	−	+	−	−	−	−	+	+	−	+	+	−	−
6	+	+	+	+	−	+	−	+	−	−	−	−	+	+	−	+	+	−	−	+
7	+	+	+	−	+	−	+	−	−	−	−	+	+	−	+	+	−	−	+	+
8	+	+	−	+	−	+	−	−	−	−	+	+	−	+	+	−	−	+	+	+
9	+	−	+	−	+	−	−	−	−	+	+	−	+	+	−	−	+	+	+	+
10	+	+	−	+	−	−	−	−	+	+	−	+	+	−	−	+	+	+	+	−
11	+	−	+	−	−	−	−	+	+	−	+	+	−	−	+	+	+	+	−	+
12	+	+	−	−	−	−	+	+	−	+	+	−	−	+	+	+	+	−	+	−
13	+	−	−	−	−	+	+	−	+	+	−	−	+	+	+	+	−	+	−	+
14	+	−	−	−	+	+	−	+	+	−	−	+	+	+	+	−	+	−	+	−
15	+	−	−	+	+	−	+	+	−	−	+	+	+	+	−	+	−	+	−	−
16	+	−	+	+	−	+	+	−	−	+	+	+	+	−	+	−	+	−	−	−
17	+	+	+	−	+	+	−	−	+	+	+	+	−	+	−	+	−	−	−	−
18	+	+	−	+	+	−	−	+	+	+	+	−	+	−	+	−	−	−	−	+
19	+	−	+	+	−	−	+	+	+	+	−	+	−	+	−	−	−	−	+	+
20	+	−	−	−	−	−	−	−	−	−	−	−	−	−	−	−	−	−	−	−

X(1):Voltage, X(2):Current, X(3):Welding Speed, X(4):Wire Diameter, X(5):Plate Thickness,
X(6): Flux Thickness,   X(7):Flux Composition, X(8):Tilt Angle, X(9):Polarity,
X(10):Stick Out,, X(11): Argon shielding.

Table 4: Operating Conditions for the artificial
baseplate experiment and the plasmadynamic
oxygen potential experiment

Voltage:	30 volts
Current:	400 ampers
Welding speed:	39.3 cm/sec
Stick out:	2 cm
Polarity:	DCRP
Tilt angle:	zero degree
Argon Shielding:	Yes

Table 5: Electrode and baseplate compositions used
in the screening experiment and the
plasmadynamic oxygen potential experiment

	Wire diameter or plate thickness	Mn (%)	Si (%)	C (%)	Oxygen (%)
W-1	1/8 inches	0.81	0.27	0.11	0.016
W-2	3/32 inches	1.02	0.26	0.12	0.011
W-3	3/32 inches	1.11	0.11	0.15	0.019
B-1	1.0 inch	1.40	0.37	0.12	0.003
B-2	0.5 inches	1.37	0.37	0.13	0.002
B-3	1.0 inch	0.06	3.22	0.03	0.009

Table 6: Average electrode compositions used in the
artificial baseplate experiment. L, LD, HB,
A and AS represent Lincoln, Linde, Hobart,
Airco and Page welding companies respectively.

	Mn(%)	Si(%)	Oxygen(%)
L-61-3/32	1.07	0.23	0.011
L-60-3/32	0.49	0.01	0.02
L-61-1/8	1.03	0.21	0.016
L-50-3/32	1.34	0.63	.
L-70-1/8	0.79	0.01	
L-61-1/8	0.81	0.27	0.016
LD-40-1/8	2.04	0.02	
LD-81-1/8	1.07	0.06	
LD-36-3/32	2.24	0.10	
LD-81-3/32	1.18	0.18	0.019
LD-44-1/8	2.30	0.02	
LD-44-3/32	2.33	0.02	0.01
LD-81-1/8	1.11	0.11	
LD-80-3/32	0.45	0.03	0.01
LD-82-1/16	1.15	0.50	
LD-85-1/16	1.35	0.55	0.01
LD-86-1/16	1.60	0.72	
HB-25-3/32	0.63	0.30	0.02
HB-28-3/32	1.38	0.65	
A-7-1/8	0.07	0.02	
A-7-3/32	0.16	0.02	
AS-25-1/16	1.40	0.42	0.01
AS-28-1/16	1.78	0.70	
X-1/8	0.12	0.40	
AS-6-1/16	0.35	0.10	

Table 7: Flux compositions examined in this study
(LW280 from reference 26 and F-a to F-f
from reference 14)

	F-1 (wt. %)	F-2 (wt. %)	F-3 (wt. %)	F-4 (wt. %)	MIT-1 (wt.%)	MIT-2 (wt.%)	LW280 (wt.%)	F-a (wt.%)	F-c (wt.%)	F-d (wt.%)	F-e (wt.%)	F-f (wt.%)
$CaCO_3$	---	---	---	---	0.14	---	---	---	---	---	---	---
CaO	41.77	23.15	3	47	5.25	31.92	22.04	32	24.4	28.7	7.8	39.9
CaF_2	---	---	5	9.8	13.71	---	5.23	2	6.8	3.53	7.25	8.0
Na_2O	---	---	---	5.0	4.46	1.86	---	---	---	---	---	---
MgO	---	---	---	---	9.38	0.07	11.59	10	---	---	---	---
MnO	15.7	7.7	40	0.14	3.05	0.09	6.68	0.2	0.15	0.18	34.8	4.3
Fe_2O_3	---	----	---	---	0.10	0.38	0.70	0.3	0.60	0.23	1.11	0.24
Al_2O_3	---	29.62	---	---	43.37	0.18	15.7	6	4.0	4.5	4.0	1.90
TiO_2	---	---	---	---	5.31	0.04	0.98	---	---	---	---	---
SiO_2	42.53	39.52	50	36	15.20	65.48	35.54	49	52.5	52.6	38.4	40.0
BI	1.17	0.5	0.46	1.45	0.52	0.52	0.85	0.81	0.45	0.53	0.63	1.02

TABLE 8. Correlation coefficients from the screening experiment

	Penetration	Height	Width	Arc Stability	Contact Angle	Flux Consumption	Melting rate	Oxygen	Manganese	Silicon	Carbon	Volume fraction of metallic mist
Voltage	0.16	-0.33	0.63	-0.52	0.59	0.40	0.02	0.00	-0.13	-0.10	0.21	0.05
Current	0.84	0.62	0.00	0.17	-0.45	0.20	0.79	-0.39	0.25	-0.30	0.41	-0.08
Travel Speed	-0.14	-0.33	-0.37	0.06	0.07	0.20	-0.20	0.01	-0.19	-0.21	0.21	-0.16
Electrode Diameter	-0.21	-0.30	0.38	-0.06	0.29	0.12	-0.05	0.19	-0.03	0.04	0.02	0.03
Plate thickness	0.06	-0.03	-0.04	-0.17	0.10	-0.15	0.15	-0.02	-0.07	-0.40	0.25	-0.08
Flux thickness	-0.04	0.00	0.14	0.06	0.06	0.10	0.01	-0.01	0.23	0.17	-0.15	-0.24
Flux composition	-0.08	0.19	-0.13	0.17	-0.25	-0.01	0.36	0.83	0.75	0.59	-0.31	0.59
Electrode tilt angle	0.06	0.05	0.01	-0.06	-0.11	0.28	0.02	0.00	0.06	0.13	0.41	0.05
Electrode Polarity	-0.33	0.35	-0.29	0.64	-0.34	0.12	0.26	-0.14	-0.10	0.13	-0.12	0.10
Electrode extension	0.16	0.24	-0.27	0.17	-0.19	-0.43	0.20	0.11	0.02	0.22	-0.21	0.22
Argon Shielding	0.0	0.1	0.0	0.2	-0.2	0.3	0.0	0.0	-0.1	0.0	0.03	0.13
Penetration	-	0.48	0.11	-0.12	-0.22	0.01	0.60	-0.37	0.26	-0.29	0.31	-0.16
Height	-	-	-0.43	0.60	-0.88	-0.14	0.82	-0.21	0.36	0.07	0.13	0.34
Width	-	-	-	-0.67	0.70	0.37	-0.10	-0.03	-0.04	-0.10	-0.18	-0.20
Arc Stability	-	-	-	-	-0.74	-0.15	0.32	-0.01	0.12	0.22	0.04	0.24
Contact Angle	-	-	-	-	-	0.16	-0.60	0.05	0.30	-0.18	-0.02	-0.34
Flux consumption	-	-	-	-	-	-	-0.01	-0.19	-0.22	-0.33	0.12	-0.13
Melting rate	-	-	-	-	-	-	-	-0.06	0.46	0.01	0.14	0.31
Oxygen	-	-	-	-	-	-	-	-	0.58	0.75	-0.31	0.48
Manganese	-	-	-	-	-	-	-	-	-	0.63	-0.25	0.30
Silicon	-	-	-	-	-	-	-	-	-	-	-0.34	0.41
Carbon	-	-	-	-	-	-	-	-	-	-	-	-0.22

Table 9: Weld metal chemistry variations observed
with each flux in the screening experiment

Flux type	C(%)	Mn(%)	Si(%)	O(%)
Manganese-silicate (F-3)	0.05-0.15	1.03-1.28	0.33-0.92	0.067-0.174
Calcium-silicate (F-4)	0.07-0.16	0.58-1.09	0.11-0.44	0.021-0.058

Table 10: Comparison of theoretically predicted Mn and
Si equilibrium with the experimentally measured
values. Fluxes F-1, F-2, MIT-1 and MIT-2 are
laboratory compositions. All fluxes were fused,
except MIT-1-B and MIT-2-B. (LW280 from reference
26, F-a, F-c, F-d, F-e and F-f were from reference
14)

flux	BI	Mn(th) (%)	Mn(exp) (%)	Si(th) (%)	Si(exp) (%)
F-1	1.17	1.83	1.85	0.33	0.28
F-2	0.5	0.4	0.44	0.25	0.29
F-3	0.46	1.1	1.27	0.80	0.95
F-4	1.45	0	n.d.	0.32	0.25
MIT-1-B	0.52	0.2	0.18	0.12	0.17
MIT-1-F	0.52	0.2	0.15	0.12	0.25
MIT-2-B	0.52	0	<0.31	1.3	>1.18
MIT-2-F	0.52	0	<0.32	1.3	>1.18
LW280	0.85	1.25	1.25	0.5	$\simeq$ 0.7
F-a	0.81	0	0.1	1.6	n.d.
F-c	0.45	0	0.1	1.0	n.d.
F-d	0.53	0	0.2	1.3	n.d.
F-e	0.63	1.75	1.75	n.d.	n.d.
F-f	1.02	0.38	0.56	0.5	n.d.

Table 11: The four possible cases of change in
Mn and MnO in the metal and slag phases
considered in the mass balance study

	$\Delta MnO\,(+)$	$\Delta MnO\,(-)$
$\Delta Mn\,(+)$	A	C
$\Delta Mn\,(-)$	D	B

Table 12: Results of the Mn mass balance

A. Weld metal gains Mn or slag loses MnO:

weld no.	$0.77k\Delta MnO$ (%)	ΔMn (%)	$k(D_m/D_g)(Mn_{,m})(V_{,m})$ (%)	$0.77(D_s/D_m)(MnO_{,s})(V_{,s})$ (%)	δ_{Mn} (%)
1-1	0.03(±0.1)	0.00	0.02	0.14(±0.14)	-0.13
1-4	0.21(±0.17)	0.01	0.01	0.13(±0.13)	0.06
1-5	0.56(±0.1)	0.15	0.00	0.39(±0.39)	0.02
1-6	0.93(±0.15)	0.35	0.01	0.14(±0.14)	0.27
1-8	1.21(±0.22)	0.33	0.01	0.14(±0.14)	0.43
1-12	1.22(±0.12)	0.22	0.02	0.14(+0.14)	0.84

B. Weld metal loses Mn or slag gains MnO:

weld no.	$0.77k\Delta MnO$ (%)	ΔMn (%)	$k(D_m/D_g)(Mn_{,m})(V_{,m})$ (%)	$0.77(D_s/D_m)(MnO_{,s})(V_{,s})$ (%)	δ_{Mn} (%)
1-11	-0.05(±0.1)	-0.05	0.02	---	-0.02
2-1	-0.22(±0.2)	-0.22	0.00	---	0
2-5	-0.2(±0.18)	-0.28	0.01	0.06	0.01
2-8	-0.47(±0.2)	-0.57	0.00	0.10	0
2-10	-0.06(±0.1)	-0.1	0.00	0.06	-0.02

Table 13: Results of the Si mass balance

A. Weld metal gains silicon or slag loses silica:

weld no.	$0.47k\Delta SiO_2$ (%)	ΔSi (%)	$k(D_m/D_g)(Si_{,m})(V_{,m})$ (%)	$0.47(D_s/D_m)(MnO_{,s})(V_{,s})$ (%)	δ_{Si} (%)
1-1	0.12($\pm$0.08)	0.09	0.02	---	0.01
1-4	0.16($\pm$0.01)	0.09	0.02	---	0.05
1-5	0.09($\pm$0.06)	0.06	0.00	---	0.00
1-6	0.09	0.06	0.02	---	0.01
1-8	0.03	0.00	0.01	---	0.02
1-11	0.18($\pm$0.1)	0.08	0.02	---	0.08
2-1	0.48($\pm$0.13)	0.04	0.01	0.41($\pm$0.2)	0.02
2-5	0.40($\pm$0.11)	0.05	0.01	0.18($\pm$0.1)	0.16
2-8	0.67($\pm$0.12)	0.02	0.01	0.32($\pm$0.15)	0.32
2-10	0.24($\pm$0.12)	0.03	0.01	0.18($\pm$0.1)	0.02
1-12	0.03	0.02	0.01	---	0.00

B. Weld metal loses silicon or slag gains silica:

weld no.	$0.47k\Delta SiO_2$ (%)	ΔSi (%)	$k(D_m/D_g)(Si_{,m})(V_{,m})$ (%)	$0.47(D_s/D_m)(MnO_{,s})(V_{,s})$ (%)	δ_{Si} (%)
11	-0.09($\pm$0.1)	-0.09	---	0.04($\pm$0.02)	-0.04

Table 14: The comparison between deviation range of the weld metal Mn content
and the difference between initial and equilibrium Mn content

Difference between initial and equilibrium Mn, (%)	Spread in final weld metal Mn.(%)	voltage range (volts)	current range (amperes)	speed range (cm/sec)	reference no.
EFFECT OF WELDING SPEED					
1.8	0	26	615	0.25-2.5	19
0.8	0	29	580	0.5-1.3	27
0.3	0	29	580	0.5-1.3	27
0.2	0	29	580	0.5-1.3	27
EFFECT OF WELDING VOLTAGE					
1.8	0.6	26-40	615	---	19
0.8	0.2	25-36	580	0.92	27
0.3	0.1	25-36	580	0.92	27
0.2	0.1	25-36	580	0.92	27
EFFECT OF WELDING CURRENT					
1.8	1.1	26	350-580	---	19
0.8	0.4	29	450-580	0.92	27
0.3	0.2	29	450-580	0.92	27
0.2	0.1	29	450-580	0.92	27
EFFECT OF WELDING SPEED WITHOUT KEEPING VOLTAGE AND CURRENT CONSTANT					
1.95	0.2	24-40	50-1095	0.2-0.5	16

Table 15: The estimated transport rate,J, transport coefficient,D, effective transport thickness,δ and the difference between surface and bulk element content,ΔC for selected welds

weld no.	Metal Phase Manganese				Slag Phase Manganese				Slag Phase Silicon			
	J (cm-%/sec)	δ (mm)	ΔC (%)	D (cm^2/sec)	J (cm-%/sec)	δ (mm)	ΔC (%)	D (cm^2/sec)	J (cm-%/sec)	δ (mm)	ΔC (%)	D (cm^2/sec)
1-1	---	---	---	---	4.5×10^{-3}	0.25	0.77	1.5×10^{-4}	1.1×10^{-2}	0.25	1.41	1.9×10^{-4}
1-2	1.22×10^{-2}	1.33	0.35	4.6×10^{-3}	1.3×10^{-2}	0.38	1.54	3.2×10^{-4}	1×10^{-2}	0.38	1.27	3×10^{-4}
1-4	---	---	---	---	1.1×10^{-2}	0.25	1.93	1.5×10^{-4}	1.2×10^{-2}	0.38	1.41	3.3×10^{-4}
1-5	8.8×10^{-3}	1.02	0.28	3.2×10^{-3}	---	---	---	---	---	---	---	---
1-11	---	---	---	---	1.1×10^{-2}	0.4	0.92	4.8×10^{-4}	---	---	---	---
1S	4.2×10^{-3}	0.51	0.26	8.2×10^{-4}	4.8×10^{-2}	0.4	2.31	8.3×10^{-4}	1.2×10^{-2}	0.51	0.71	8.6×10^{-4}
8S	2.8×10^{-2}	0.15	0.28	1.5×10^{-3}	---	---	---	---	2.8×10^{-3}	0.20	0.19	2.9×10^{-4}
9S	7×10^{-3}	1.0	0.15	4.6×10^{-3}	8×10^{-5}	0.13	0.02	5.2×10^{-5}	3.9×10^{-4}	0.2	0.05	1.6×10^{-4}

Table 16 : Results of weld metal chemistry using
3.22%Si plate

Flux	BI	Mn_f (%)	Si_f(%)	Reaction Temperature(^{0}C)
LD-0091	1.35	0.24	1.69	2029
LD-709-5	1.0	0.37	1.78	2053
$2MnO-SiO_2$	1.17	1.80	1.10	2051

Table 17 : Comparison between reaction temperature
estimated from surface and bulk Mn content
in the weld metal by MnO reaction.
(1-1 to 1-12 from this study, 1 to 36 from
reference 15)

weld no.	Mn,i (%)	Mn,s (%)	Mn,b (%)	Oxygen (%)	T,s (C)	T,b (C)
1-1	1.85	1.85	1.85	0.050	1979	1979
1-2	1.40	1.85	1.50	0.047	1968	1932
1-3	0.09	0.82	0.48	0.068	1896	1812
1-4	1.74	1.75	1.75	0.072	2031	2031
1-5	1.00	1.50	1.15	0.052	1950	1905
1-6	0.85	1.62	1.20	0.062	1992	1941
1-7	0.07	1.50	0.40	0.035	1885	1694
1-8	0.94	---	1.27	0.030	---	1835
1-9	0.98	---	1.40	0.049	---	1928
1-10	0.64	---	1.00	0.060	---	1906
1-11	1.95	1.90	1.90	0.046	1968	1968
1-12	0.88	1.50	1.10	0.056	1962	1910
1	1.15	0.36	0.64	0.086	2050	2164
6	1.26	0.36	0.56	0.077	2031	2115
11	1.08	0.33	0.55	0.068	1994	2088
15	1.10	0.53	0.65	0.084	2119	2158
17	1.01	0.39	0.69	0.071	2031	2138
18	1.11	0.29	0.57	0.053	1929	2047
31	1.25	0.44	0.60	0.063	2031	2088
36	0.96	0.39	0.60	0.090	2074	2158

Table 18: The relative oxide stability
(No.1 is the stablest, No.6
is the least stable)

1. CaO

2. K_2O

3. TiO_2/Na_2O

4. Al_2O_3

5. MgO

6. SiO_2/MnO

Table 19 : Weld metal oxygen content comparison
between bonded and fused fluxes

weld no.	MIT-1-B (%)	MIT-1-F (%)	MIT-2-B (%)	MIT-2-F (%)
1	0.070	0.048	0.104	0.085
2	0.075	0.046	0.098	0.090
3	0.052	0.046	0.100	0.082
4	0.046	0.039	0.119	0.115
5	0.060	0.028	0.168	0.131
6	0.050	0.100		
7	0.052	0.036		
8	0.039	0.074		
9	0.101	0.142		
10	0.060	0.049		
11	0.065	0.050		
12	0.063	0.052		
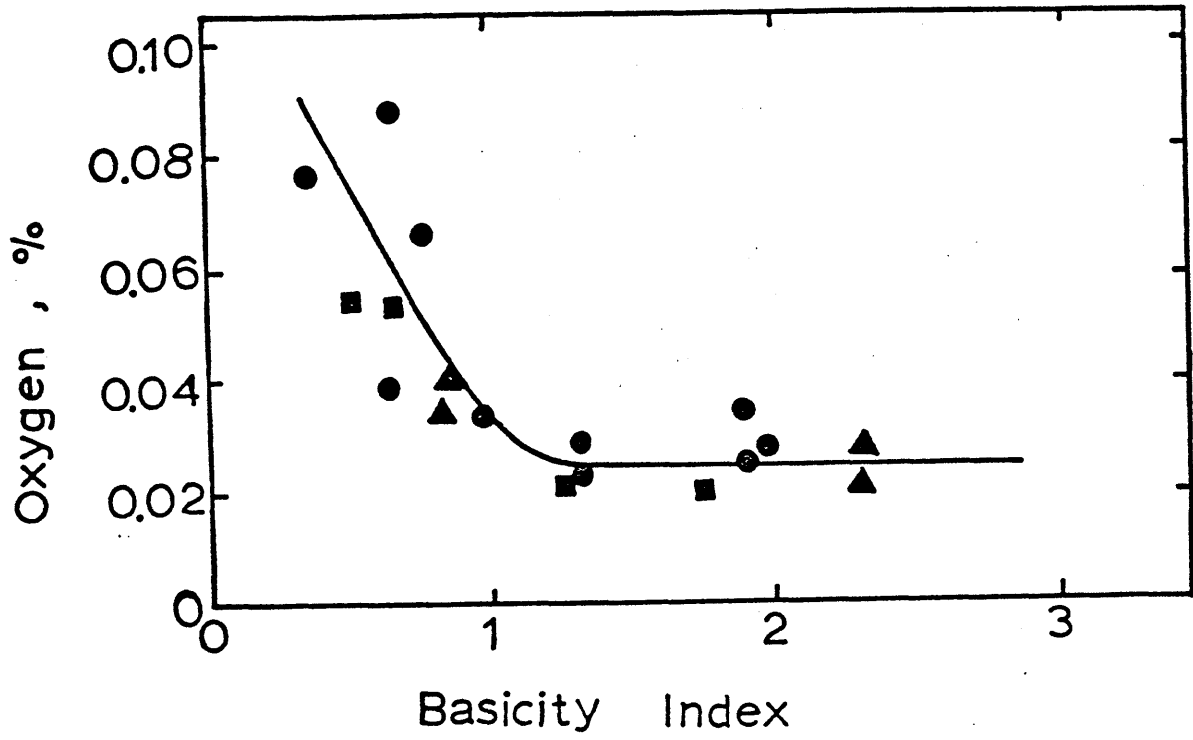
Fig. 1: The empirical relationship between the weld metal
oxygen content and the flux basicity index in
submerged arc welding process.
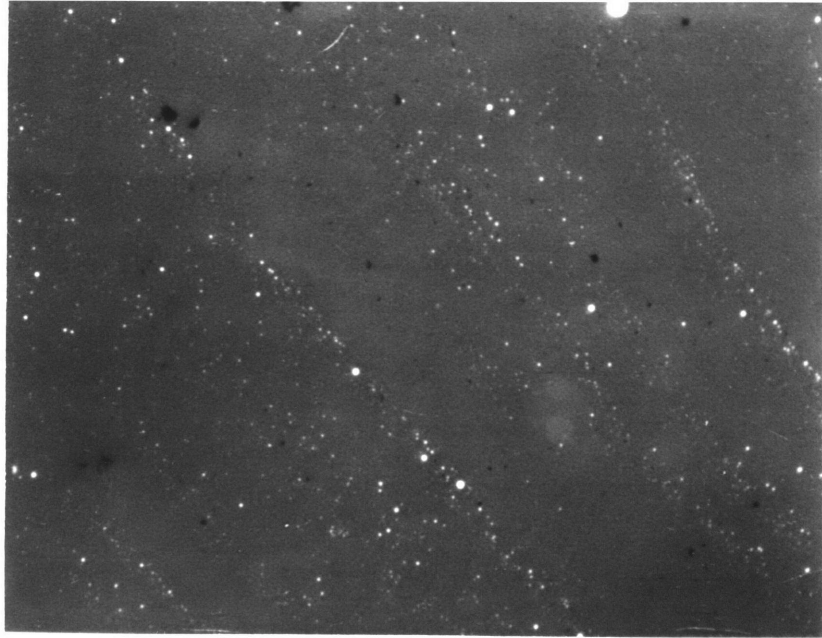
Fig. 2: Typical example of metallic mist in the
slag phase. (103X)
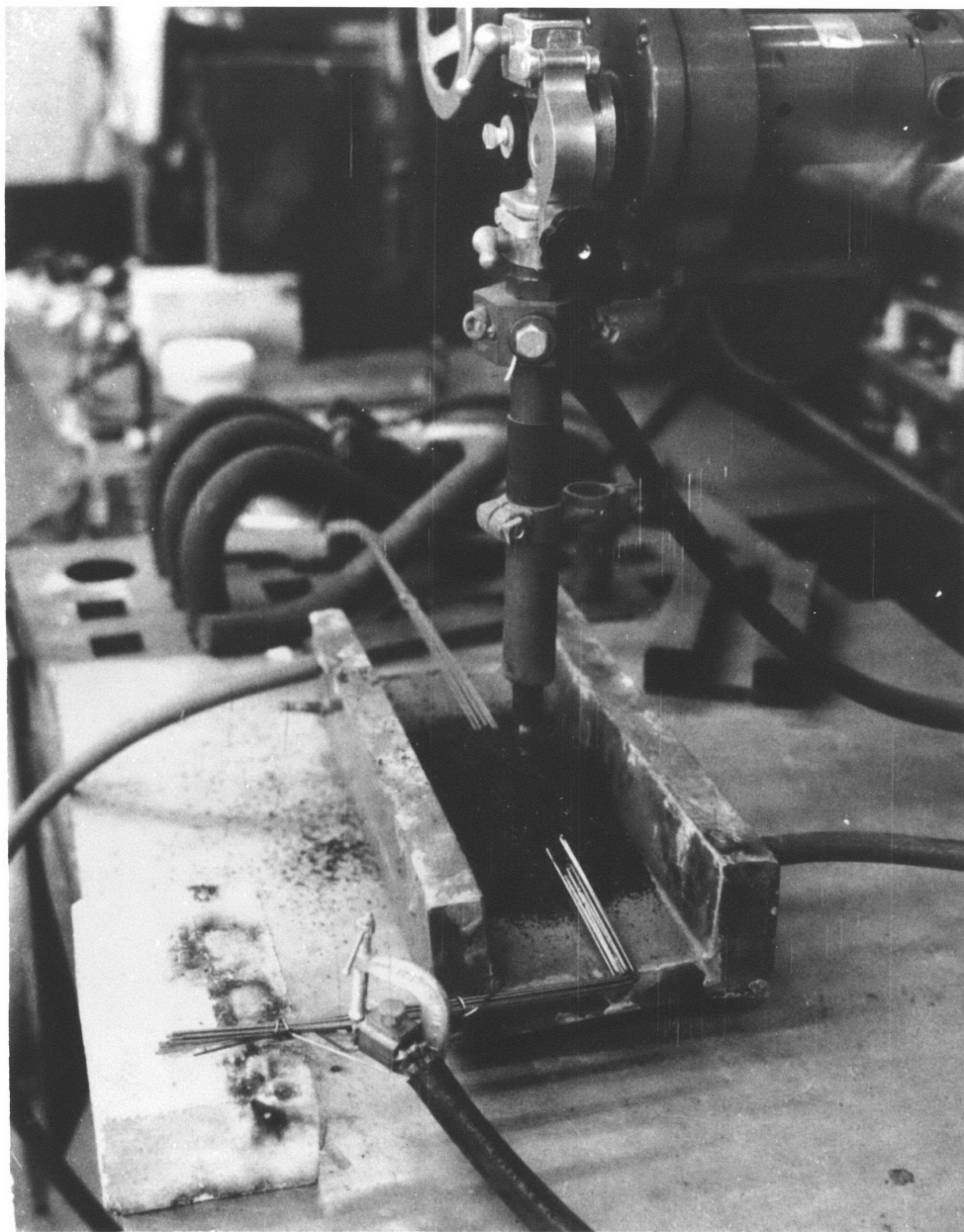
Fig. 3: Setup of artificial baseplate experiment.
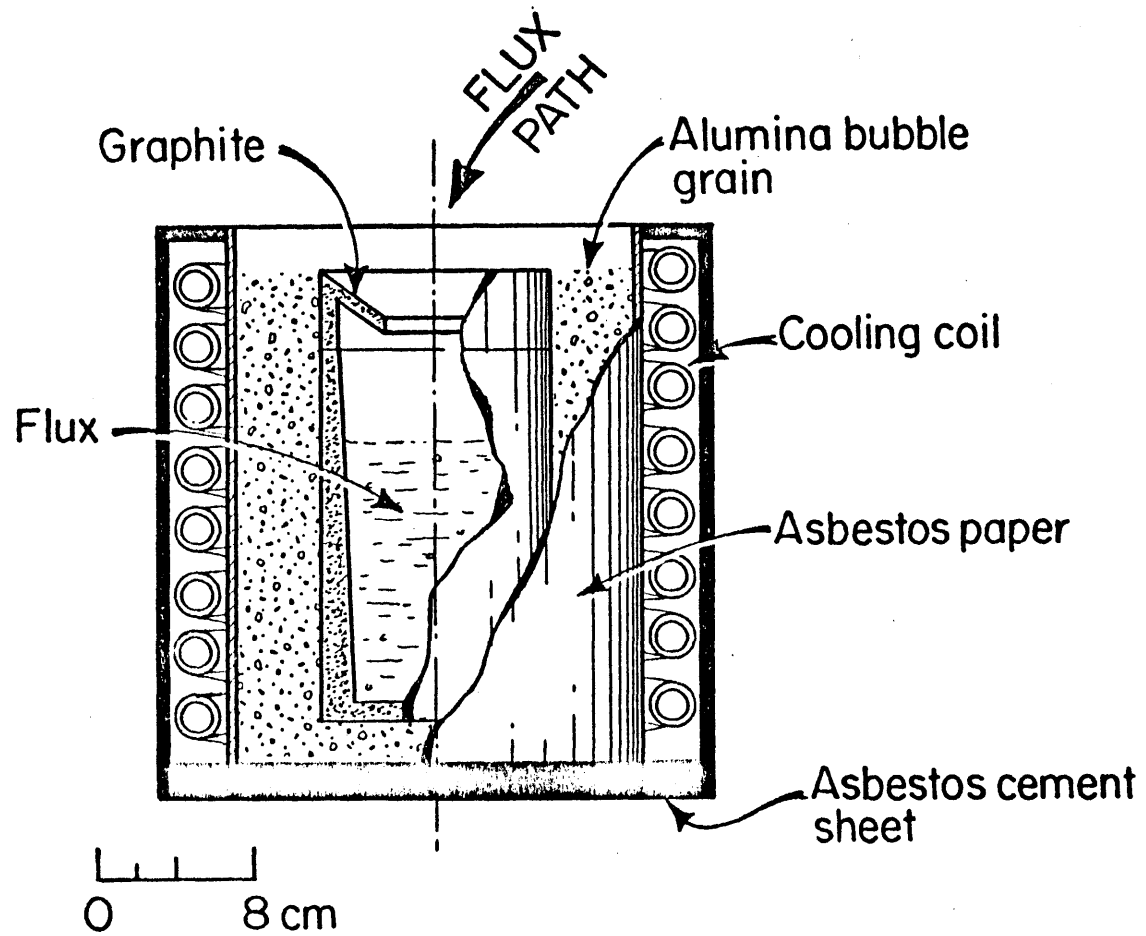
Fig. 4: The schematic drawing of induction melting furnance
used in this study.
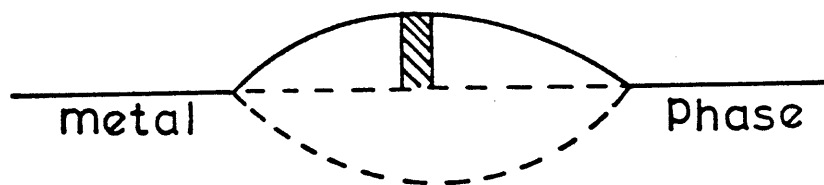
Fig. 5: Shadow area representing the position
of sample used for atomic absorption
chemical analysis.

(a)
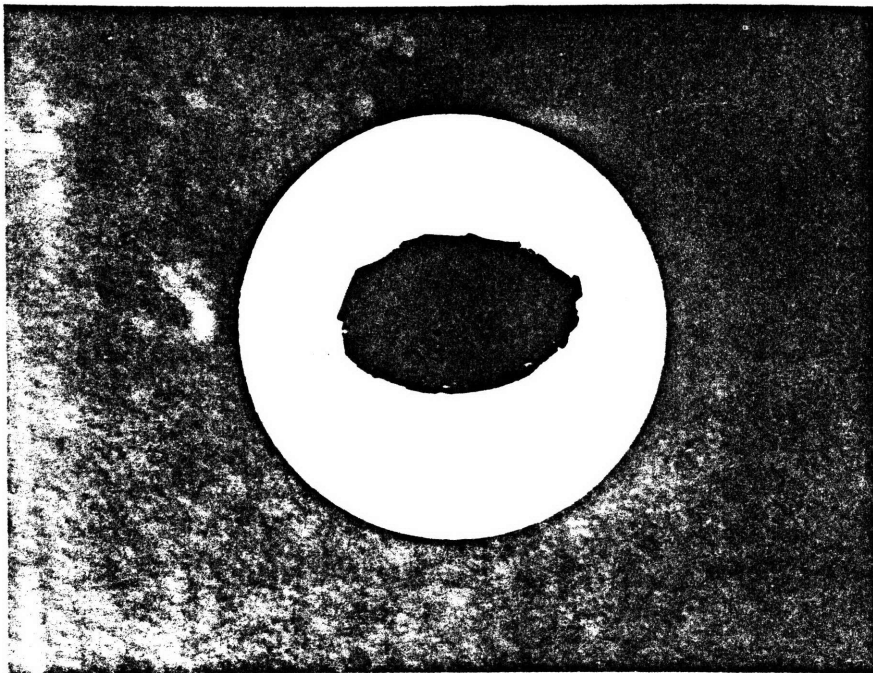
(b)

Fig. 6: Typical sample of (a) slag and (b) weld metal
obtained from artificial baseplate experiment.
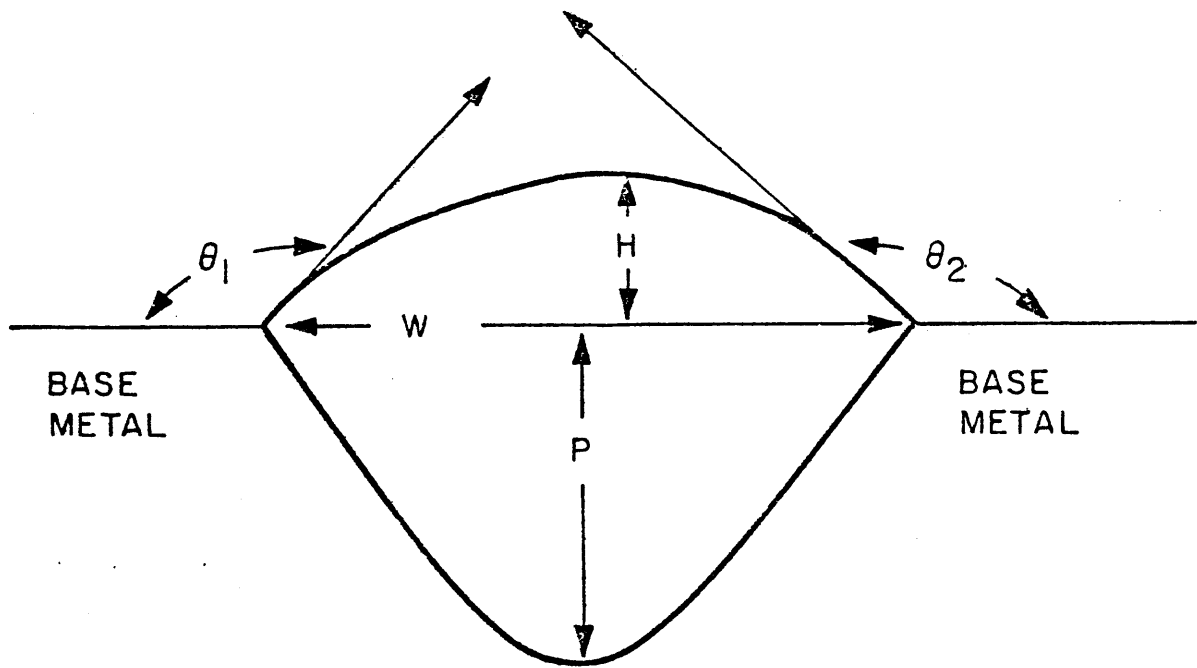
H: Bead Height

P: Depth of Penetration

W: Bead Width

θ: Contact Angle $= (\theta_1 + \theta_2)/2$

Fig. 7: Schematic defining the weld bead shape parameters measured in this study.
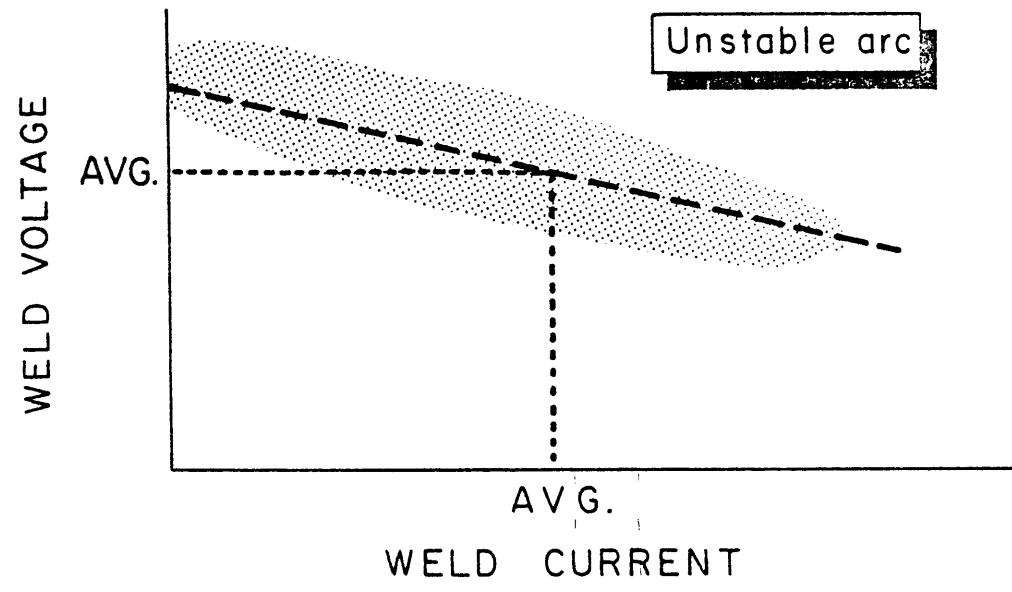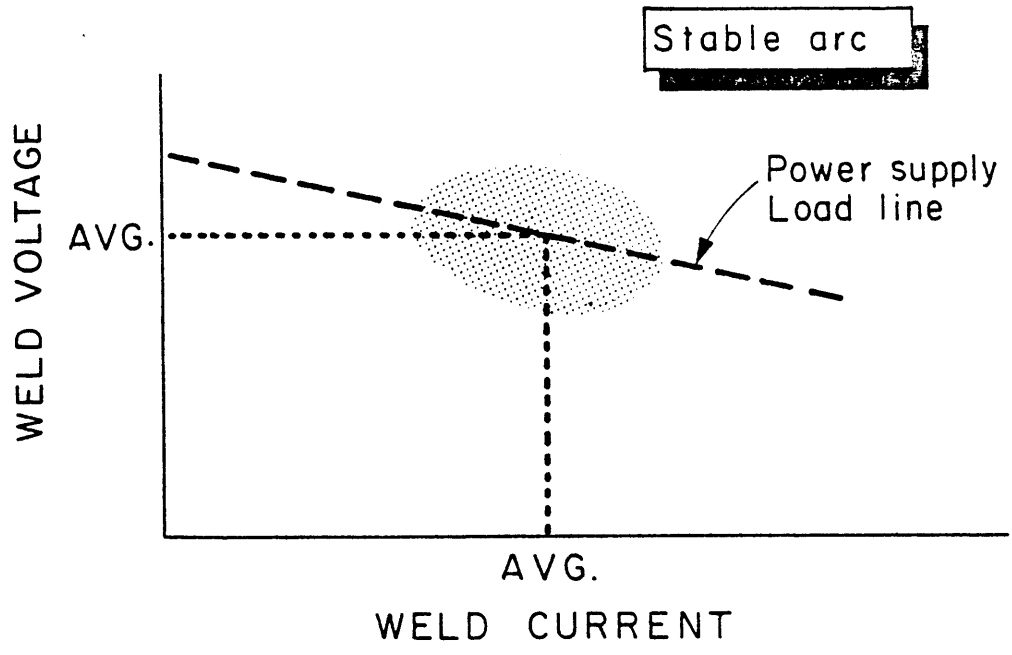
Fig. 8: Schematic of the oscillographic image of DC arcs used to monitor arc stability. Note that unstable arcs often are completely extinguished and may approach double the average welding current on reignition.
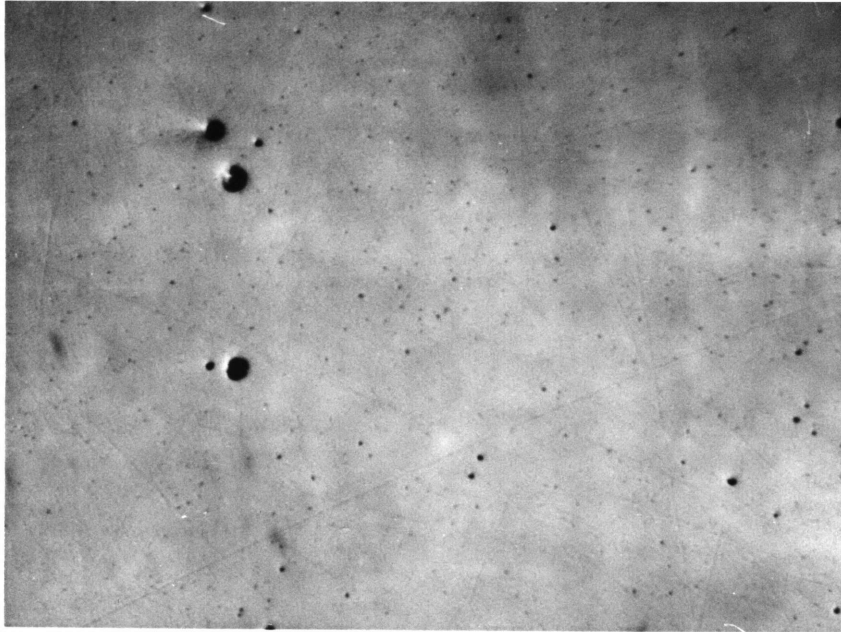
(a)
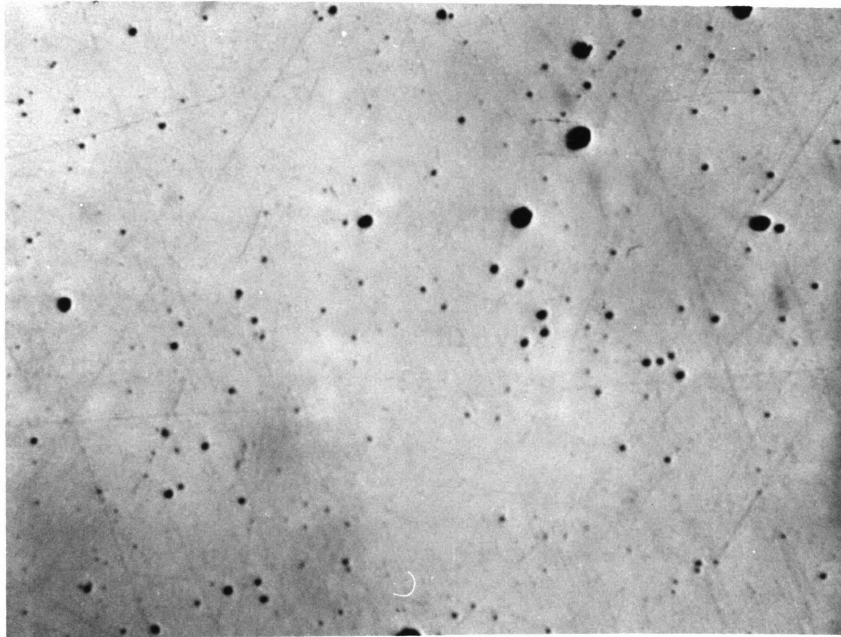
(b)

Fig. 9: Inclusion distribution in weld metal produced
with calcium silicate flux (a) 210 ppm O,
(b) 580 ppm O. (230X).
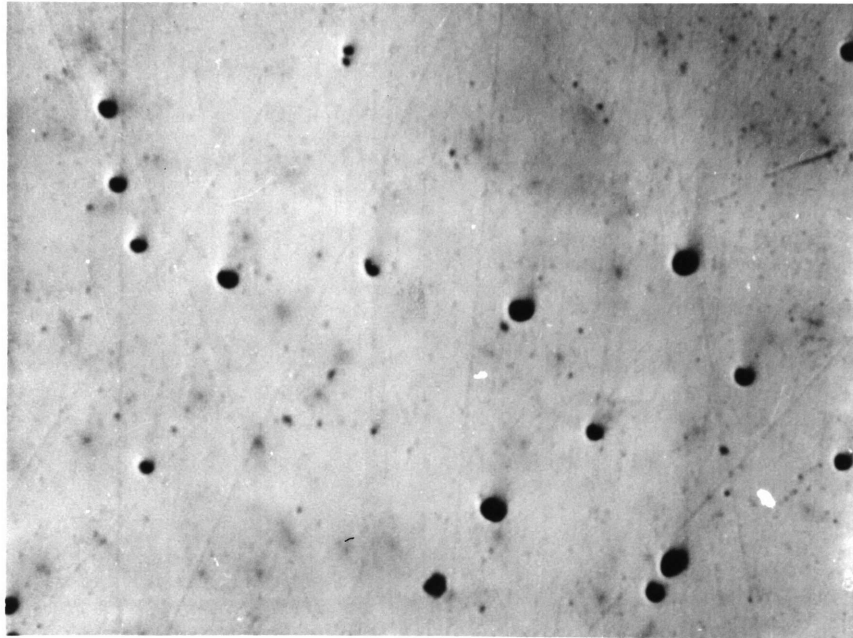
(a)
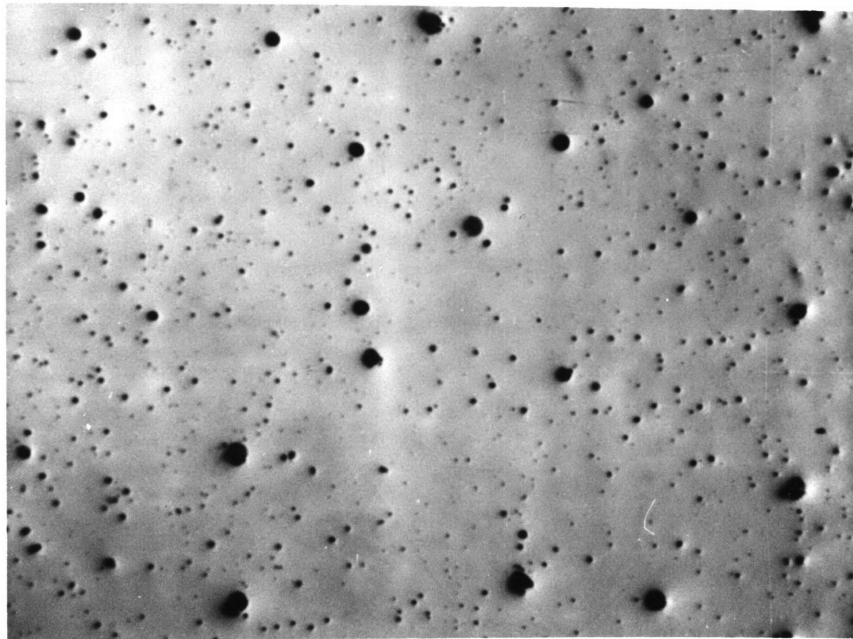
(b)

Fig. 10: Inclusion distribution in weld metal produced
with manganese silicate flux (a) 670 ppm $\underline{O}$,
(b) 1740 ppm $\underline{O}$. (230X)
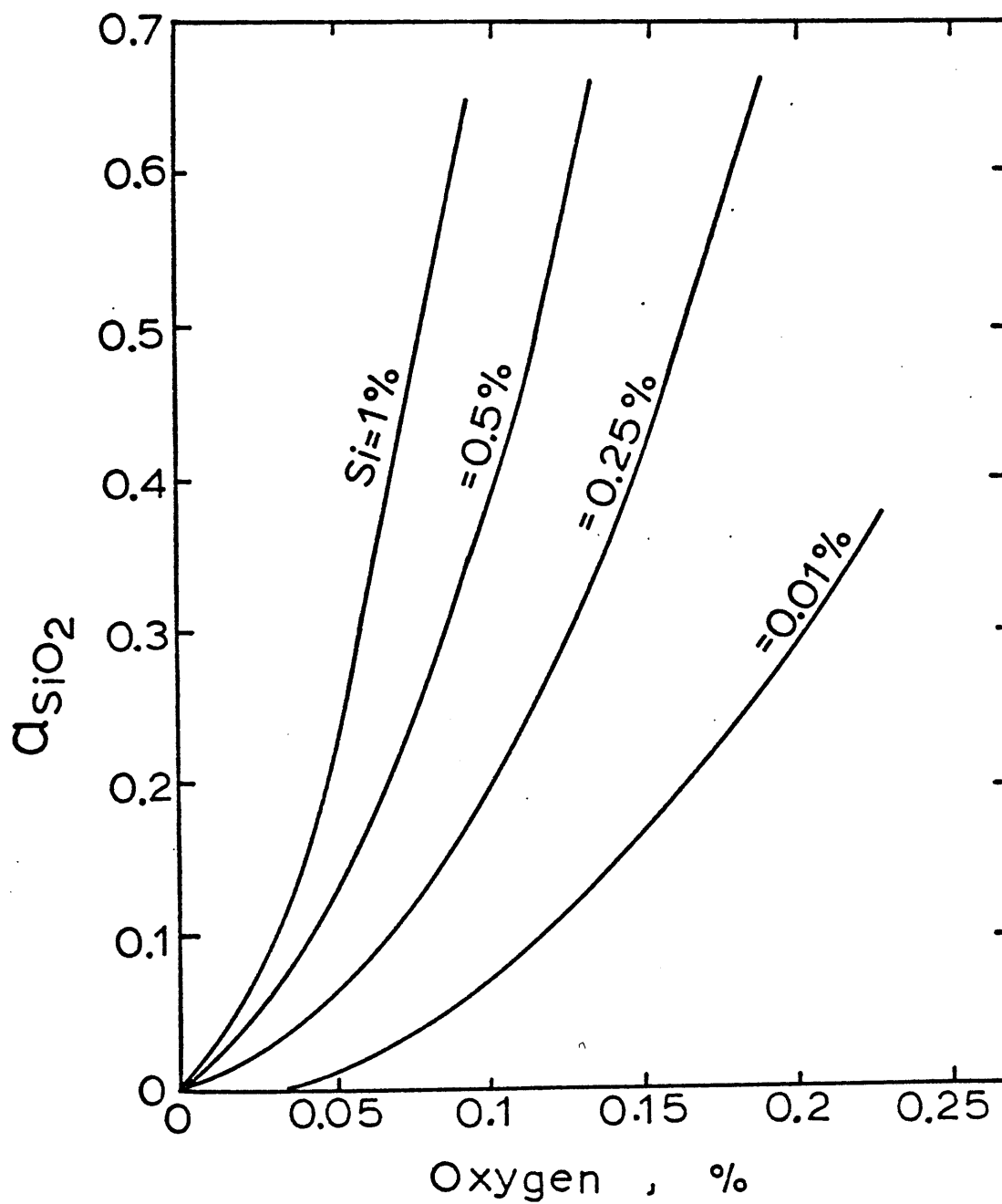
Fig. 11: Graph of the equation $a_{SiO_2} = 73.6 (w/o\ Si)(w/o\ O)^2$
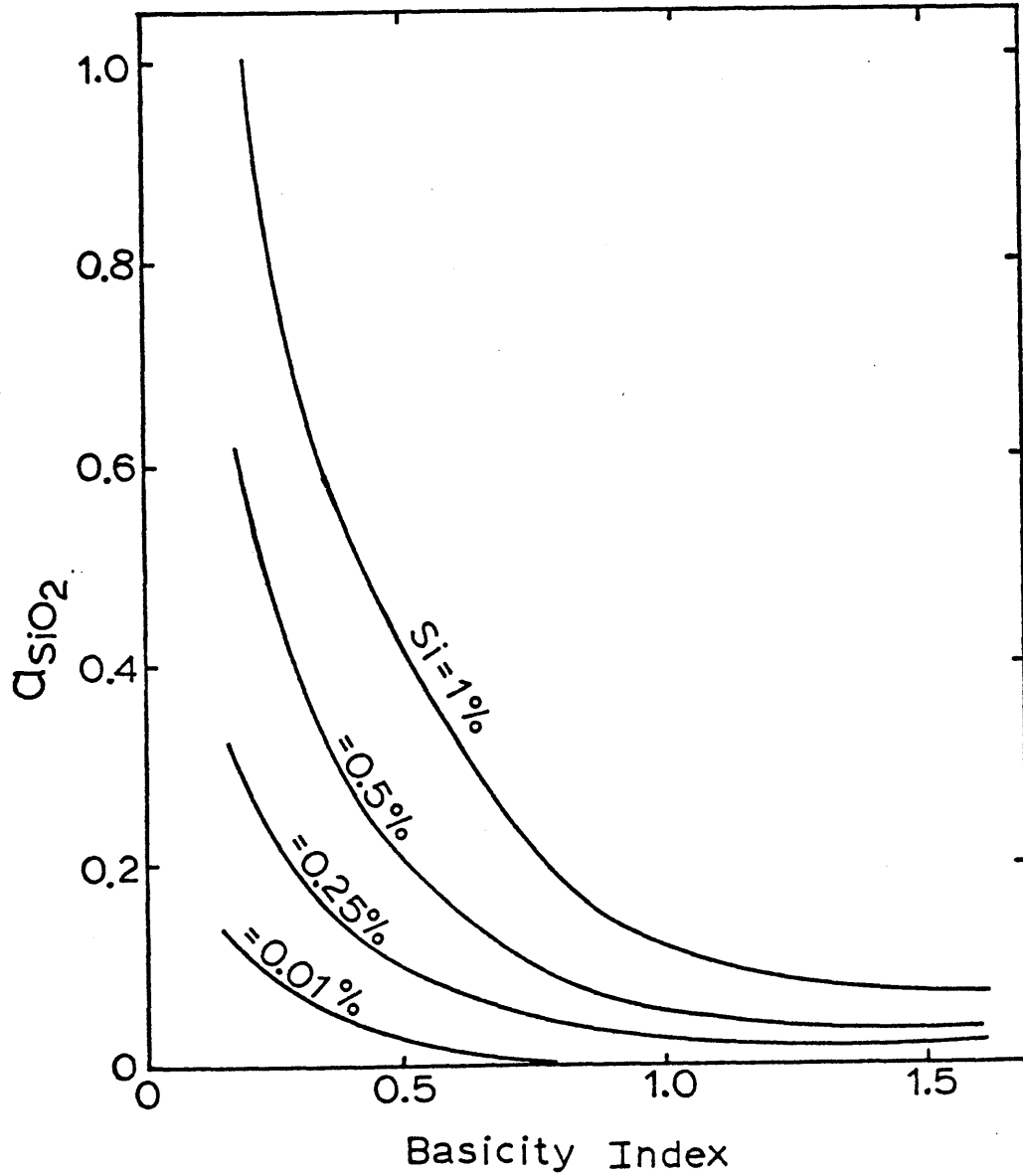
Fig. 12: The relationship between a_{SiO_2} and BI for a given weld metal silicon content at 2000°C.
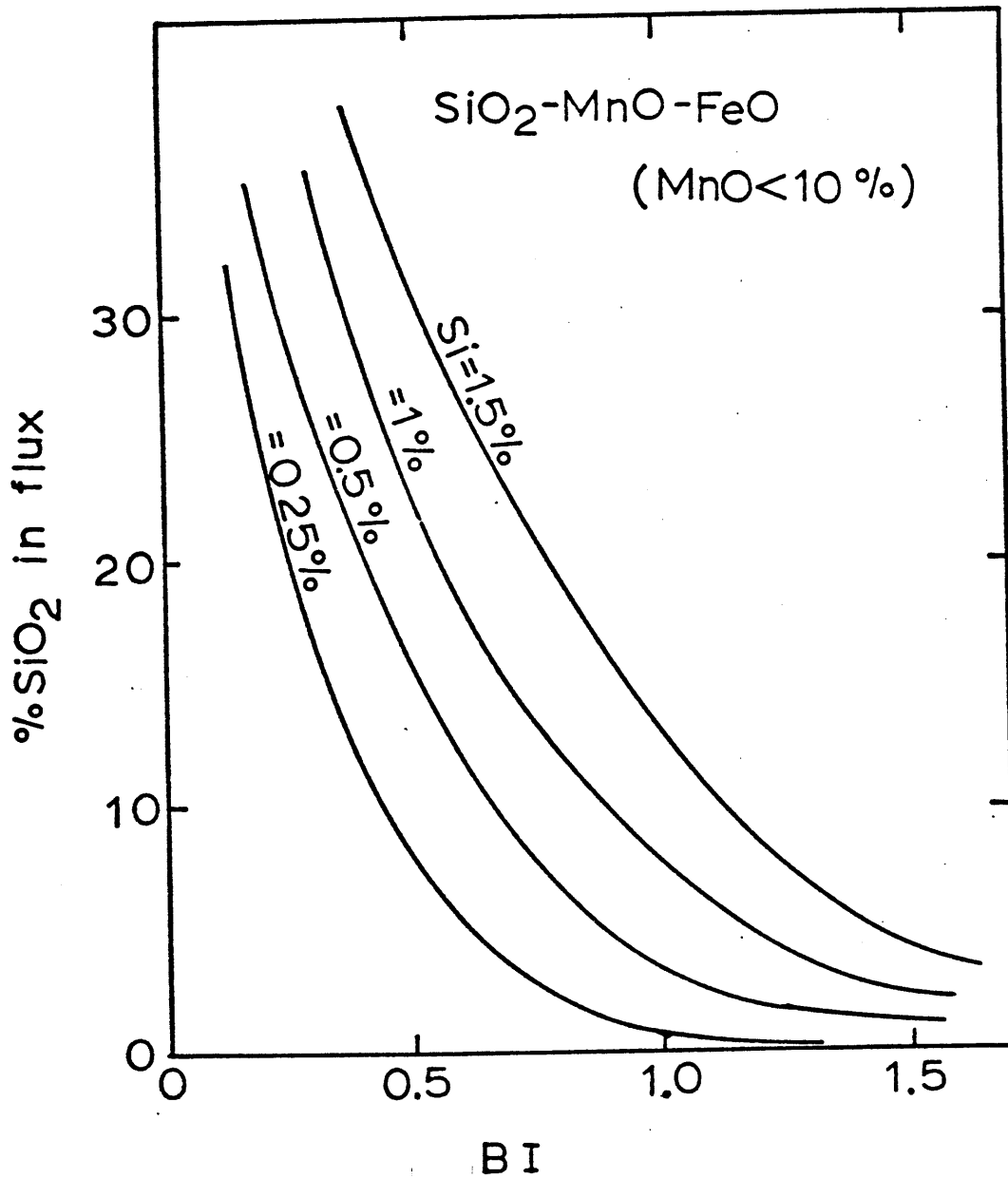
Fig. 13: The relationship between equilibrium %SiO_2 and
BI for a given weld metal Si content at 2000°C
in the SiO_2-MnO-FeO system.
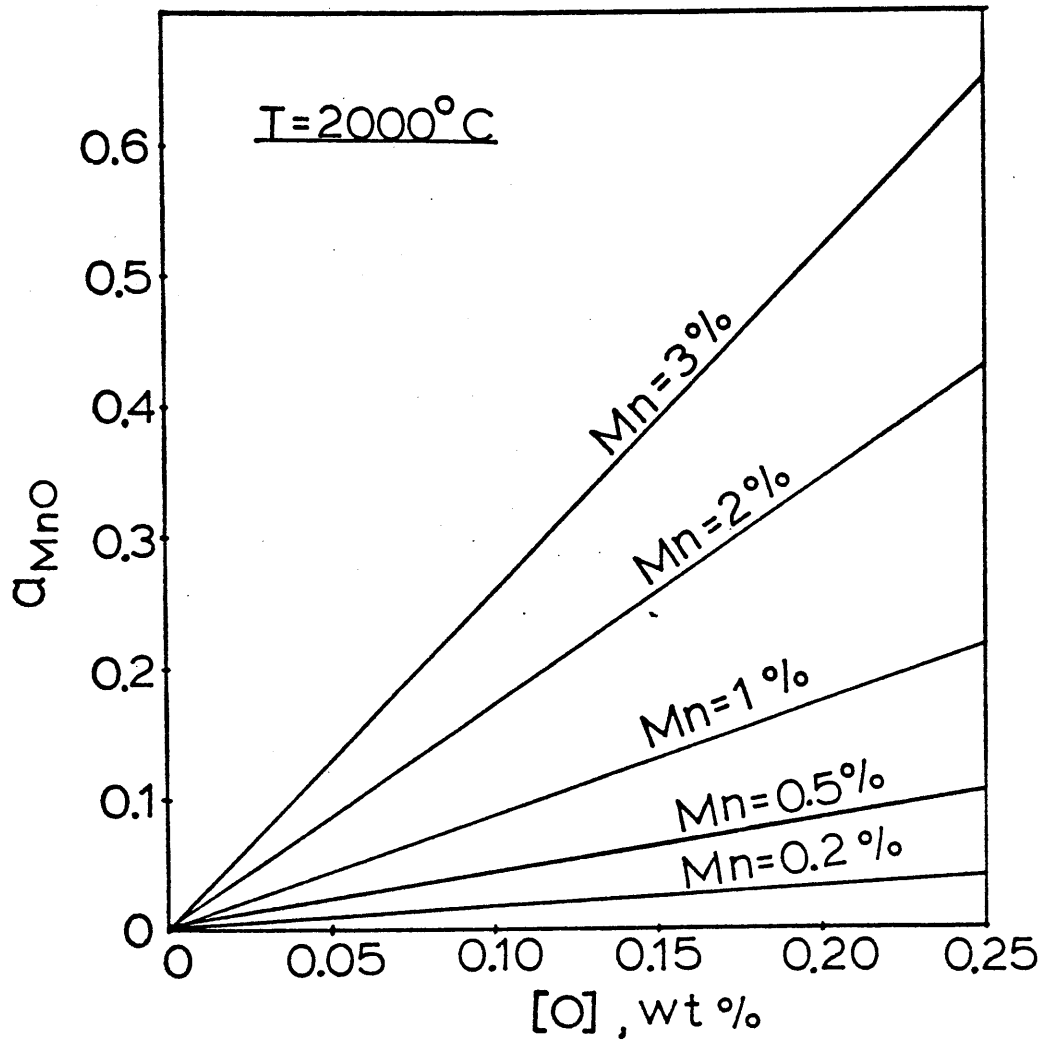
Fig. 14: Graph of the equation $a_{MnO} = 0.86 \,(\text{w/o Mn})\,(\text{w/o O})$.
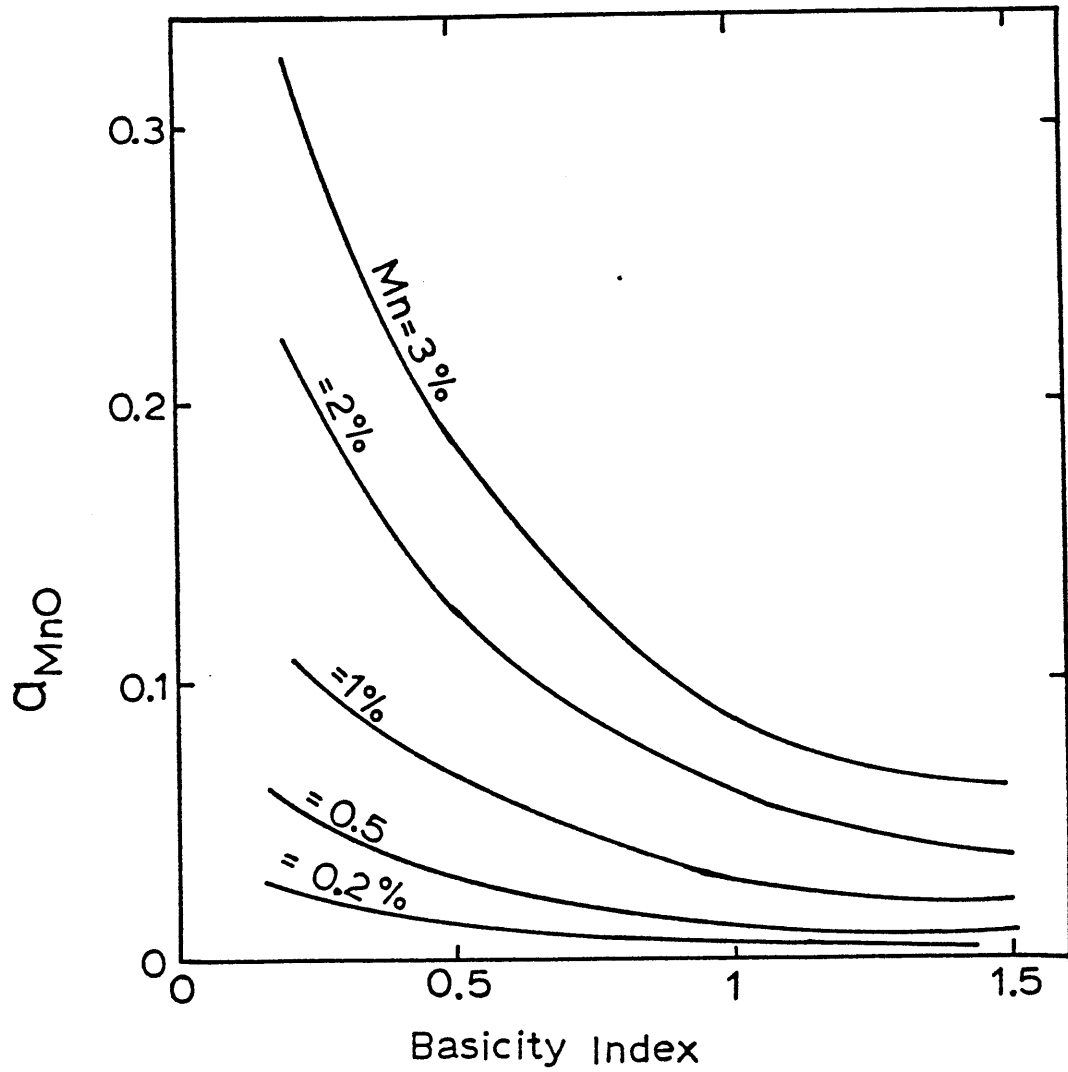
Fig. 15: The relationship between a_{MnO} and BI for a given
weld metal Mn content at 2000°C.
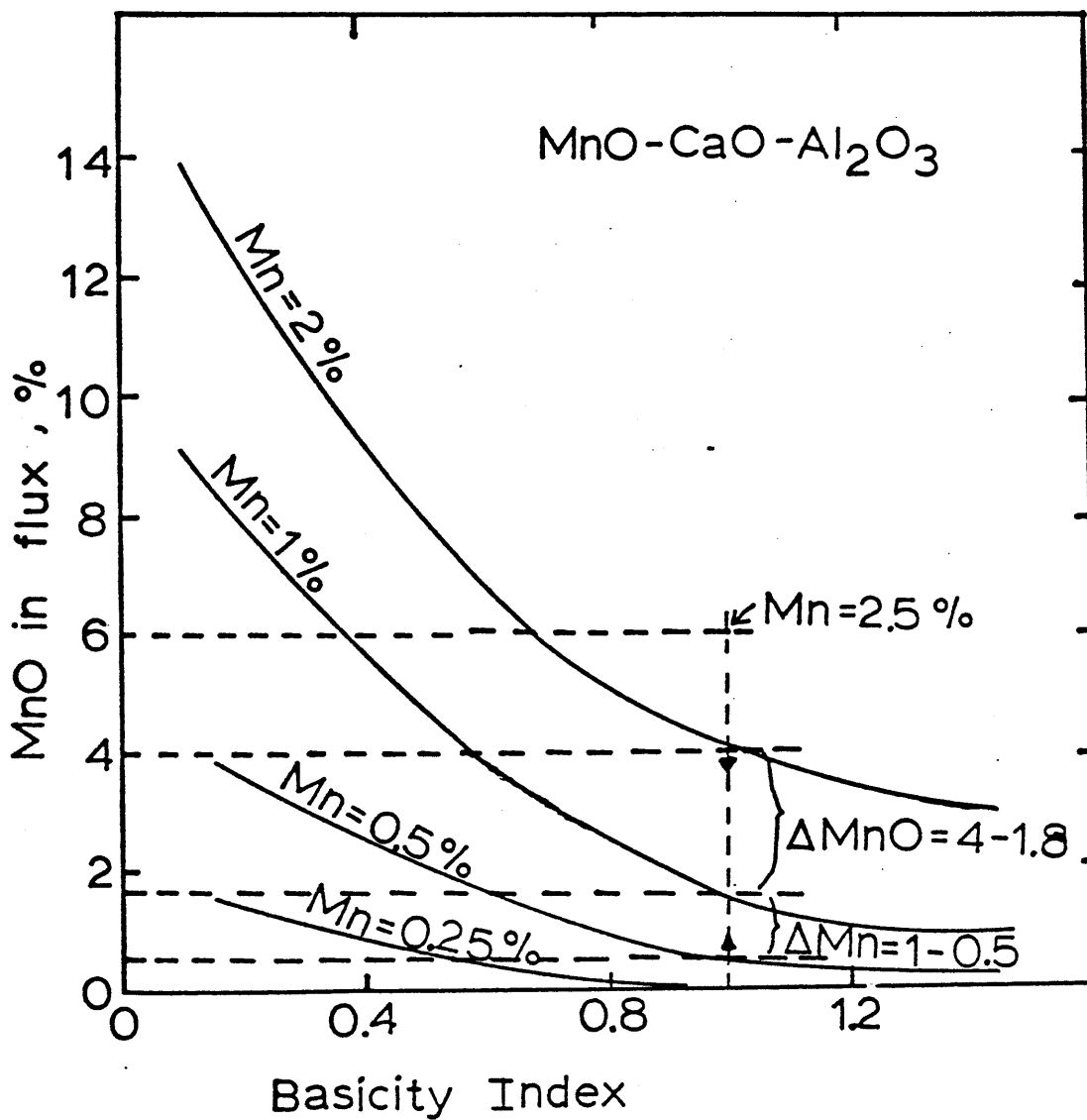
Fig. 16: The relationship between the equilibrium percent MnO and BI for a given weld metal Mn content at 2000°C in the MnO-CaO-Al$_2$O$_3$ system. The dotted lines are presented for reference to discussion in the text.
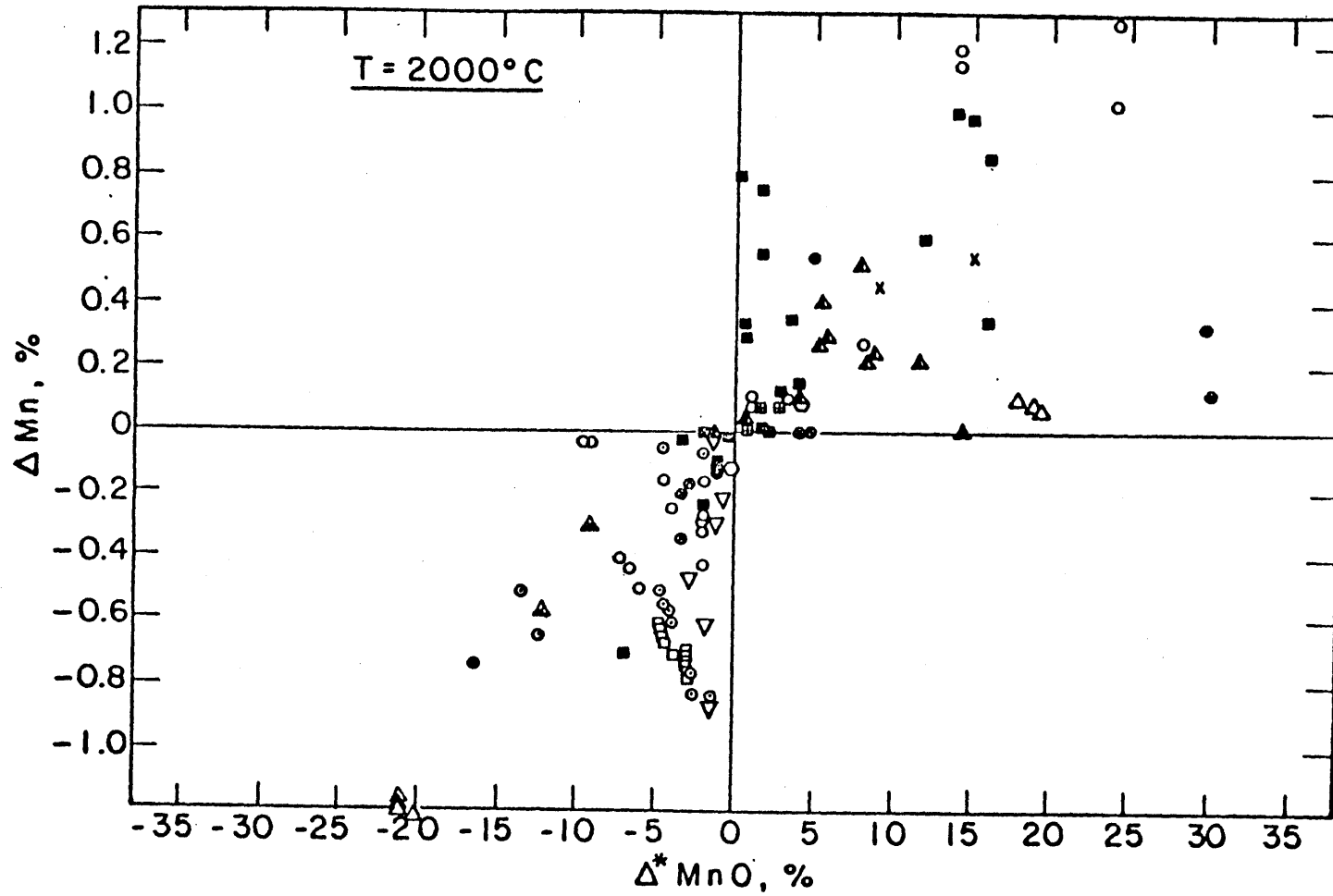
Fig. 17: Variation of change in weld metal manganese, ΔMn, with deviation of
flux MnO from the predicted equilibrium, $\Delta^* MnO$, at 2000°C.
(For list of symbol references see Appendix 10)
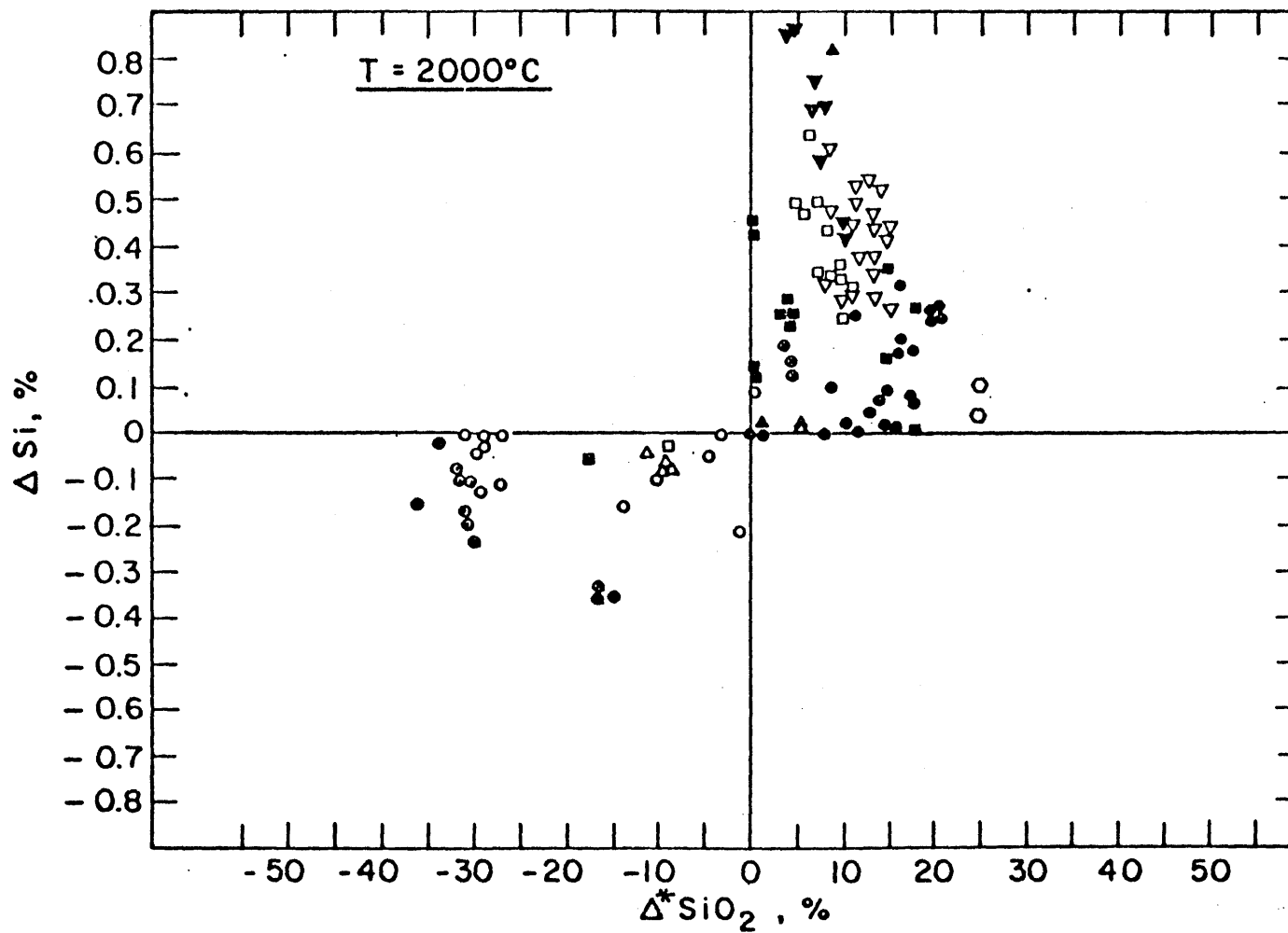
Fig. 18: Variation of change in weld metal silicon, ΔSi, with deviation of flux SiO_2 from predicted equilibrium, $\Delta^* SiO_2$ at 2000°C.

(For list of symbol references see Appendix 10)
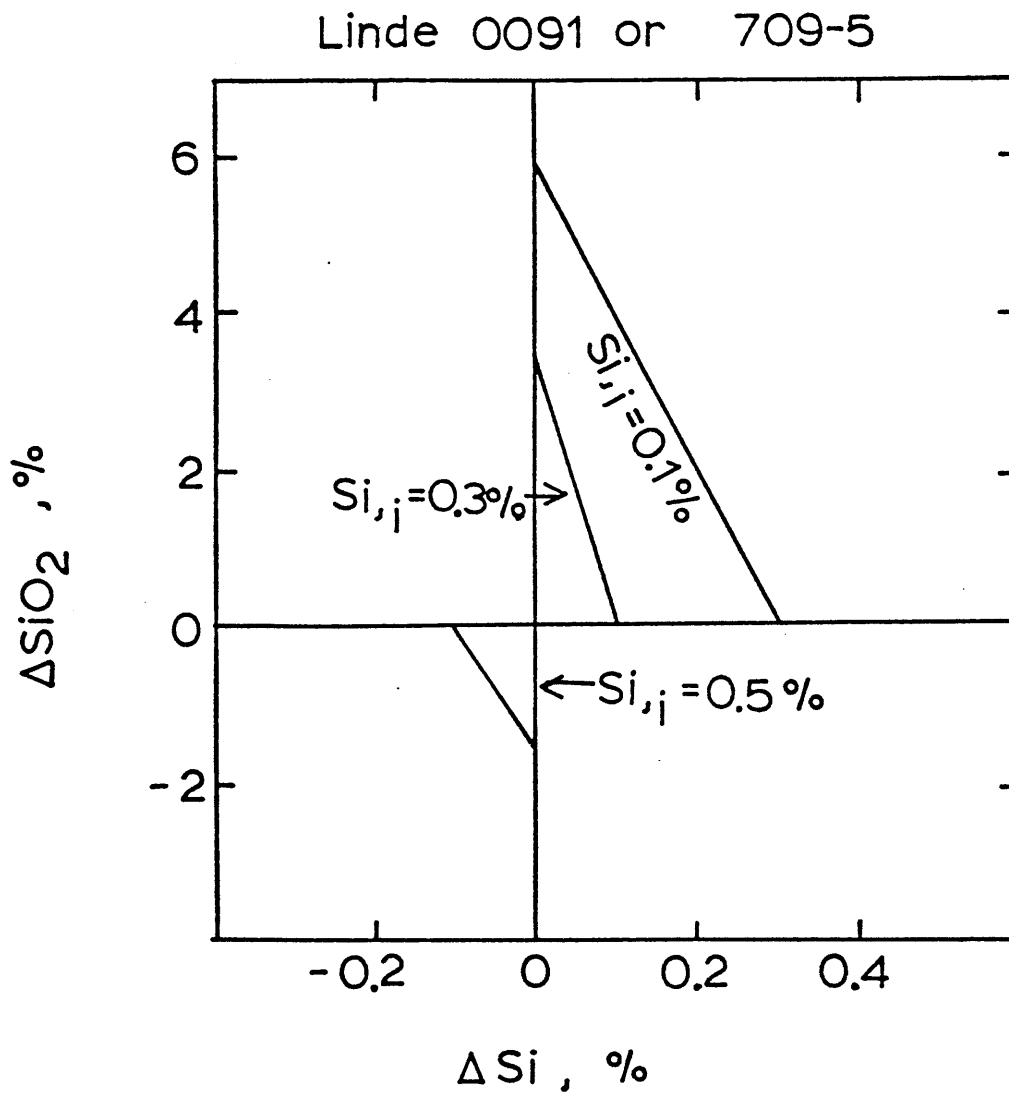
Linde 0091 or 709-5

Fig. 19: The estimated permissible range of change of
Si for weld metal of 0.1%, 0.3% and 0.5%
initial Si when using Linde 0091 or
Linde 709-5 flux.
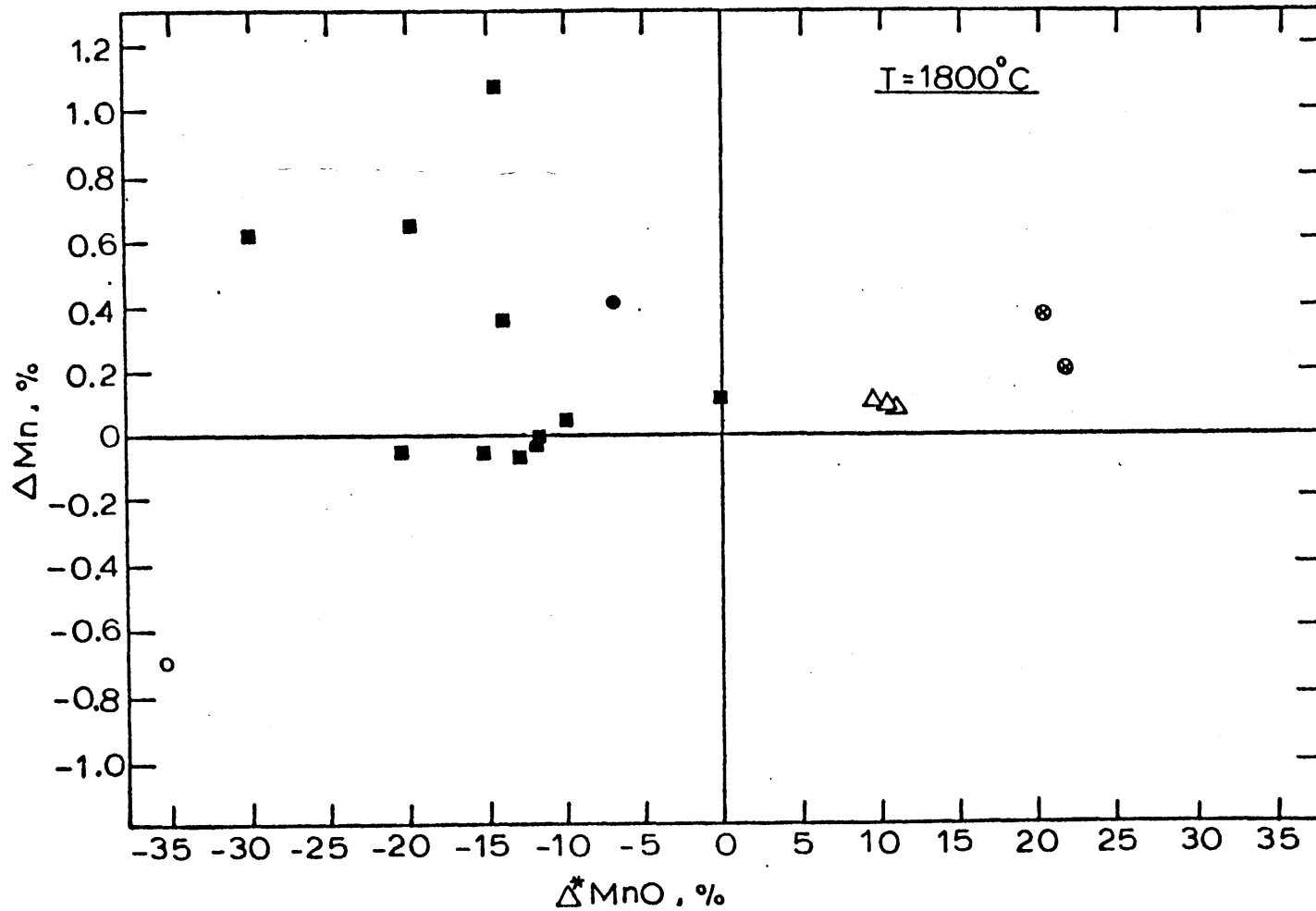
Fig. 20: Variation of change in weld metal manganese, ΔMn, with deviation
of flux MnO from predicted equilibrium, Δ*MnO at 1800°C.
(For the list of symbol references see Appendix 10)
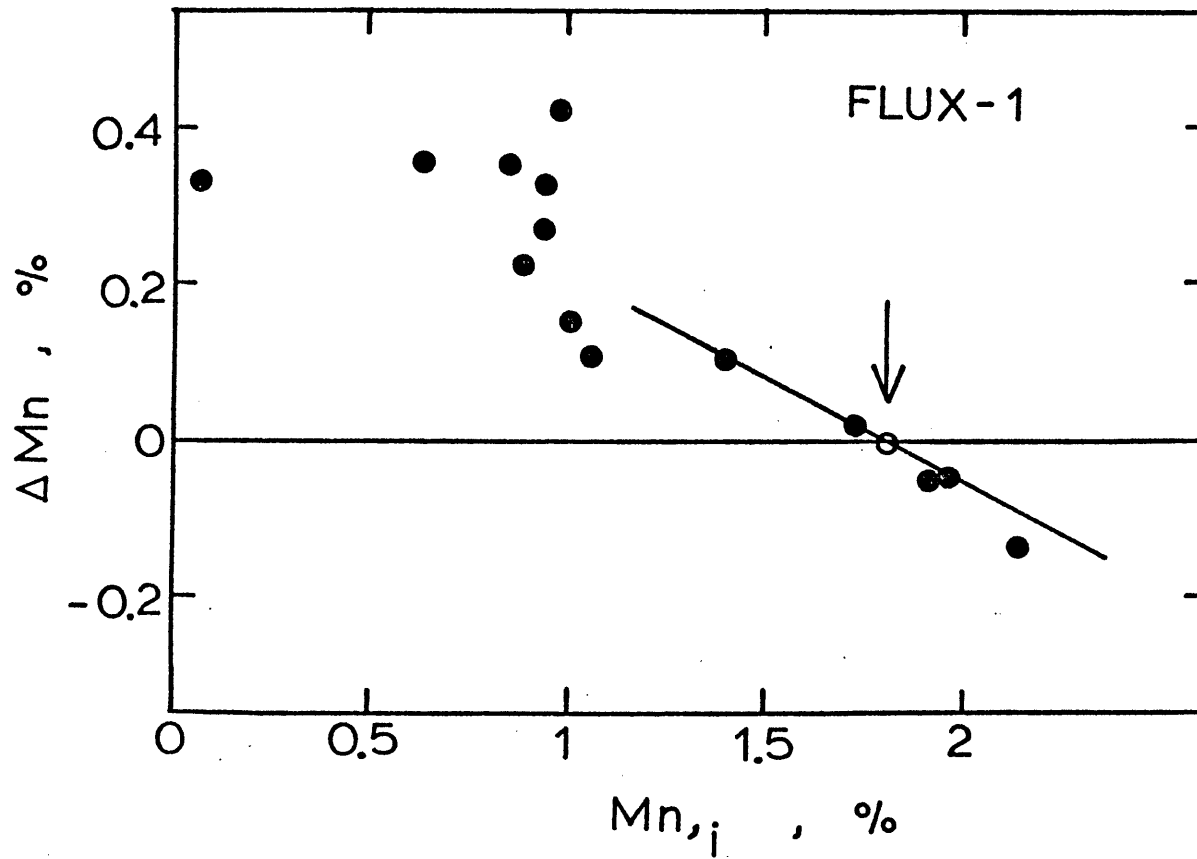
Fig. 21: The change in weld metal manganese content, ΔMn, as a
function of initial Mn content, $Mn_{,i}$, with Flux-1 using
artificial baseplate technique. The arrow denotes the
predicted equilibrium Mn content of Flux-1.
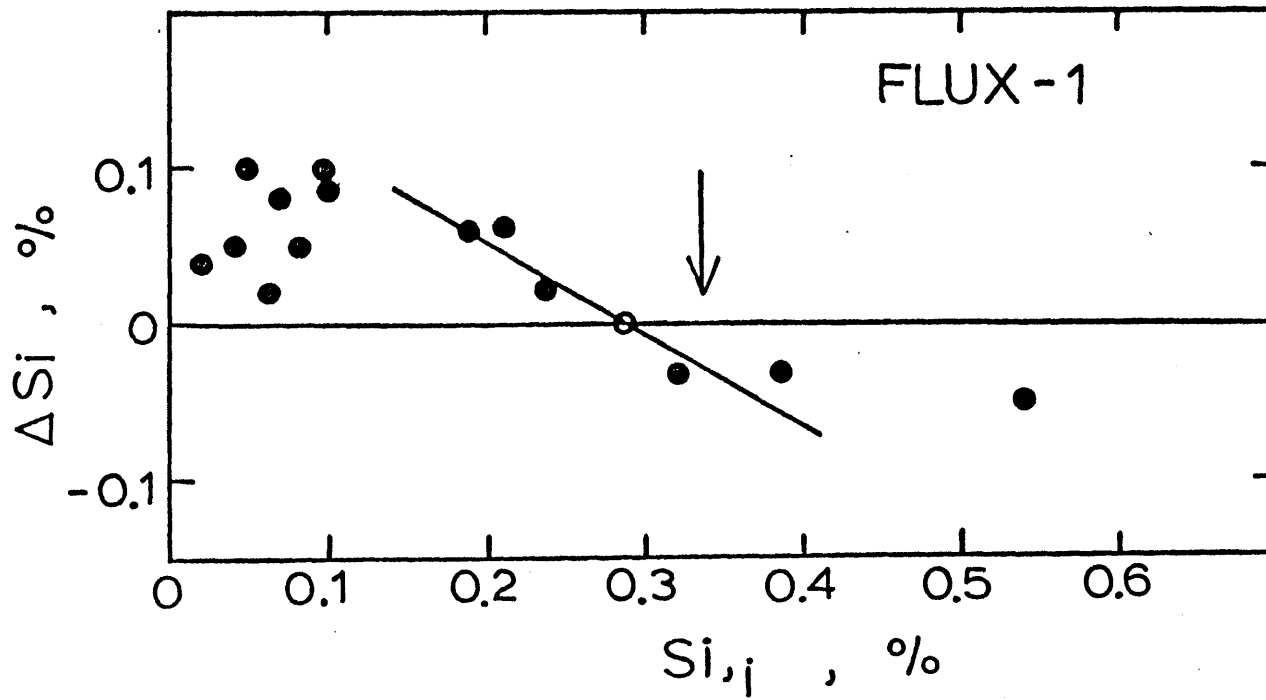
Fig. 22: The change in weld metal Si, ΔSi, as a function of the initial Si content, $Si_{,i}$, measured with Flux-1 using the artificial baseplate technique. The arrow denotes the predicted equilibrium Si content for Flux-1.
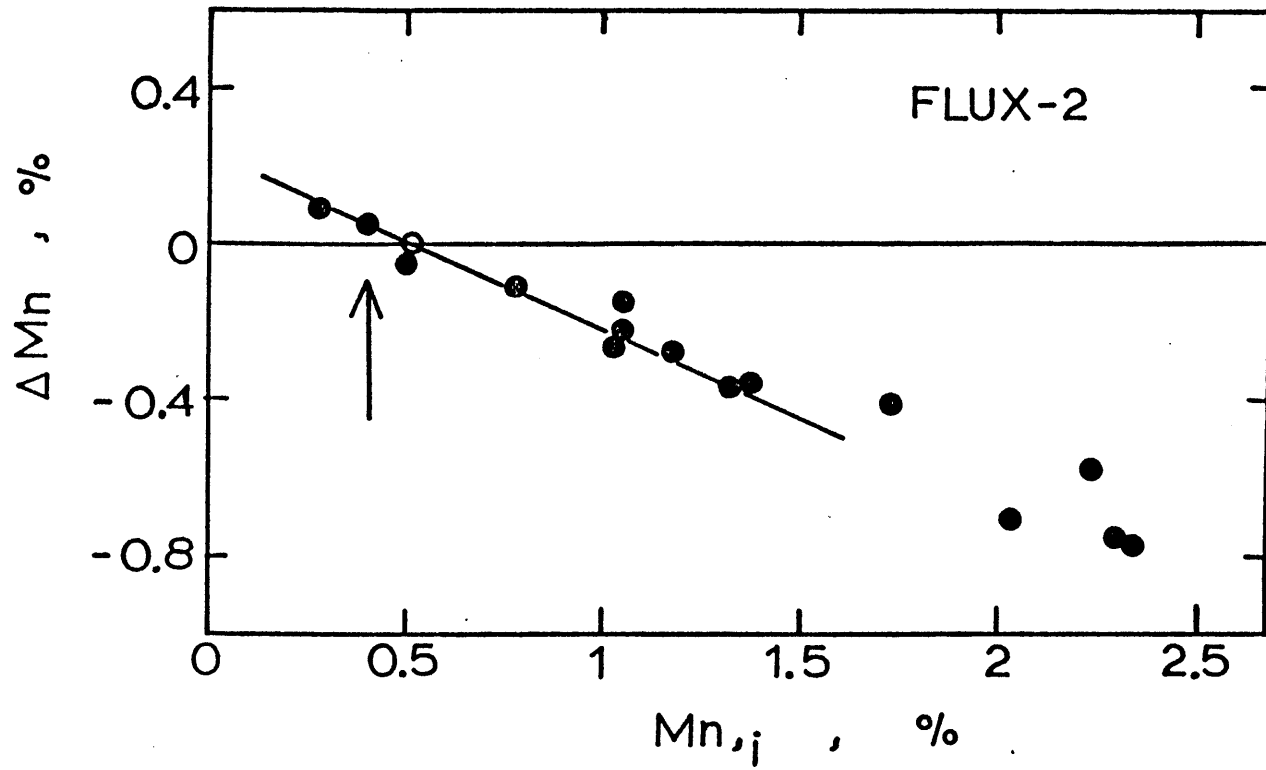
Fig. 23: The change in weld metal Mn, ΔMn, as a function of the
the initial Mn content, Mn_i, measured with Flux-2 using
artificial baseplate technique. The arrow denotes the
predicted equilibrium Mn for the Flux-2.
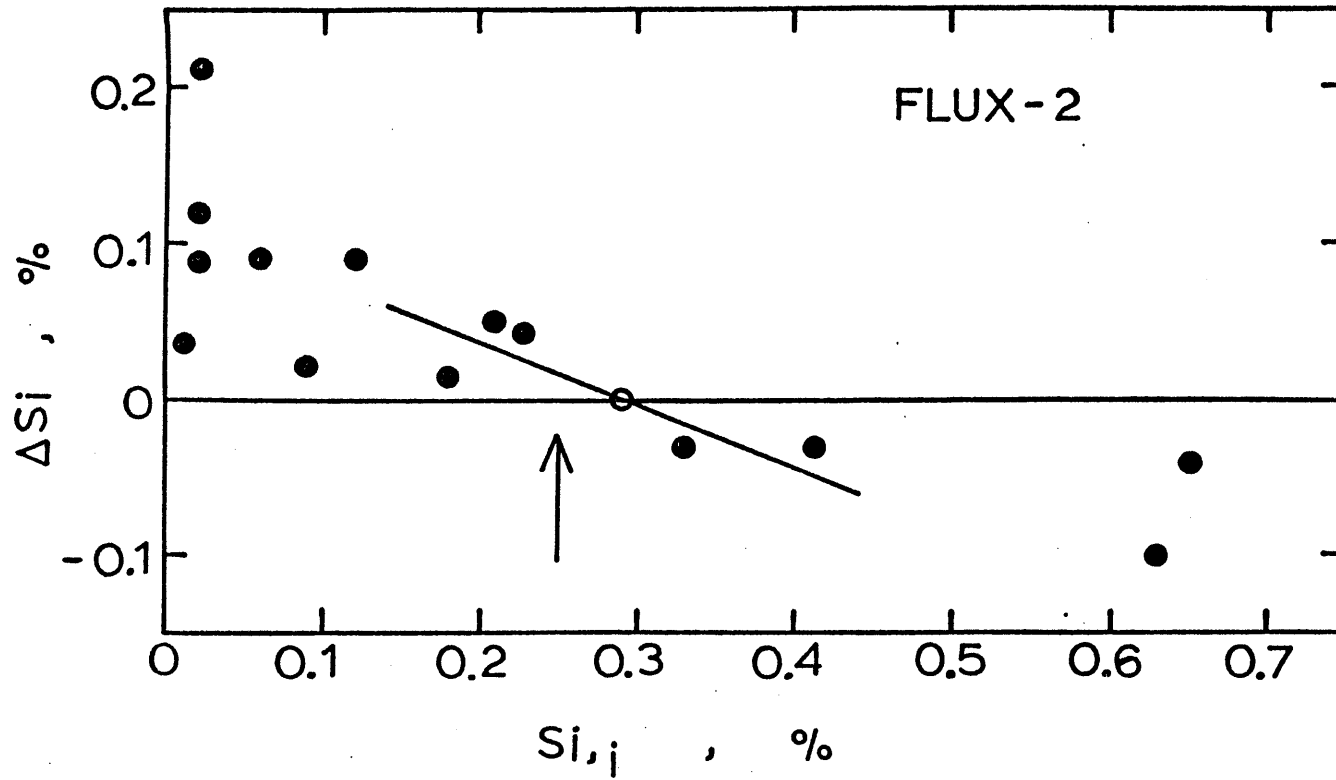
Fig. 24: The change in weld metal Si content, ΔSi, as a function of the initial Si content, $Si_{,i}$, measured with Flux-2 using artificial baseplate technique. The arrow denotes the predicted equilibrium Si for the Flux-2.
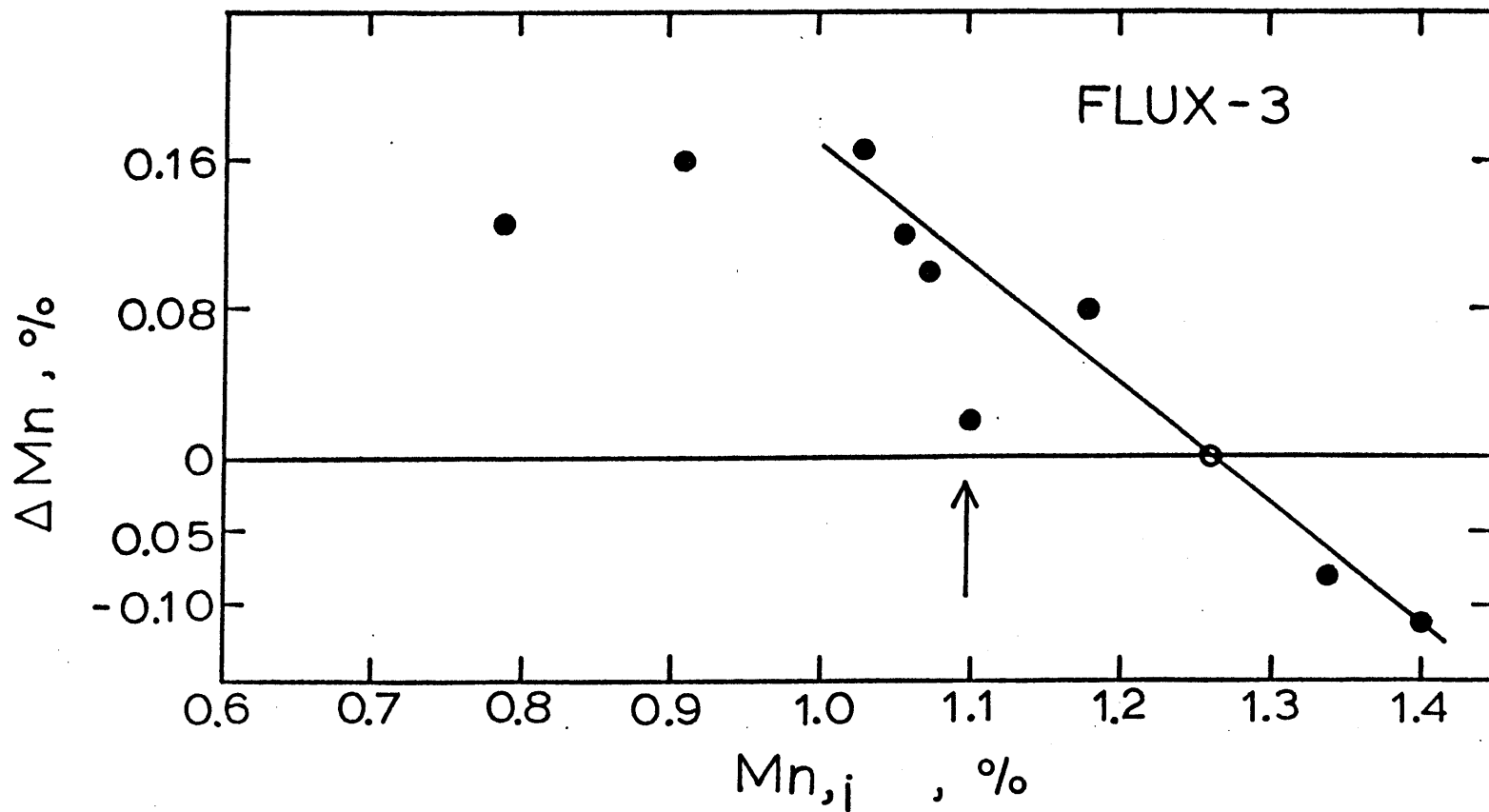
Fig. 25: The change in weld metal Mn, ΔMn, as a function of the initial Mn content, Mn$_{,i}$, measured with Flux-3 using artificial baseplate technique. The arrow denotes the predicted equilibrium Mn content for Flux-3.
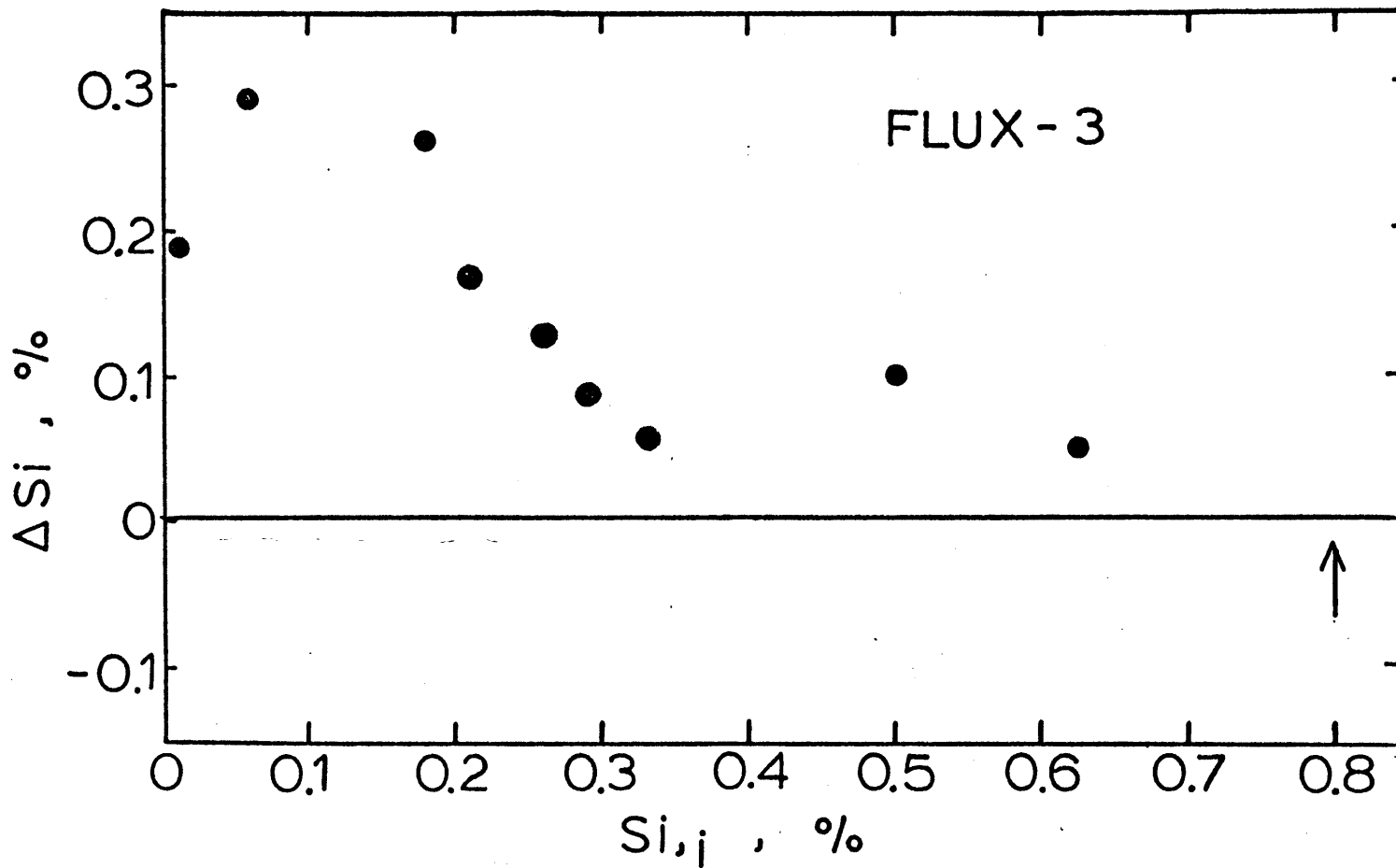
Fig. 26: The change in the weld metal Si, ΔSi, as a function of the initial
Si content, Si,i, measured with Flux-3 using artificial baseplate
technique. The arrow denotes the predicted equilibrium Si content
for the Flux-3.
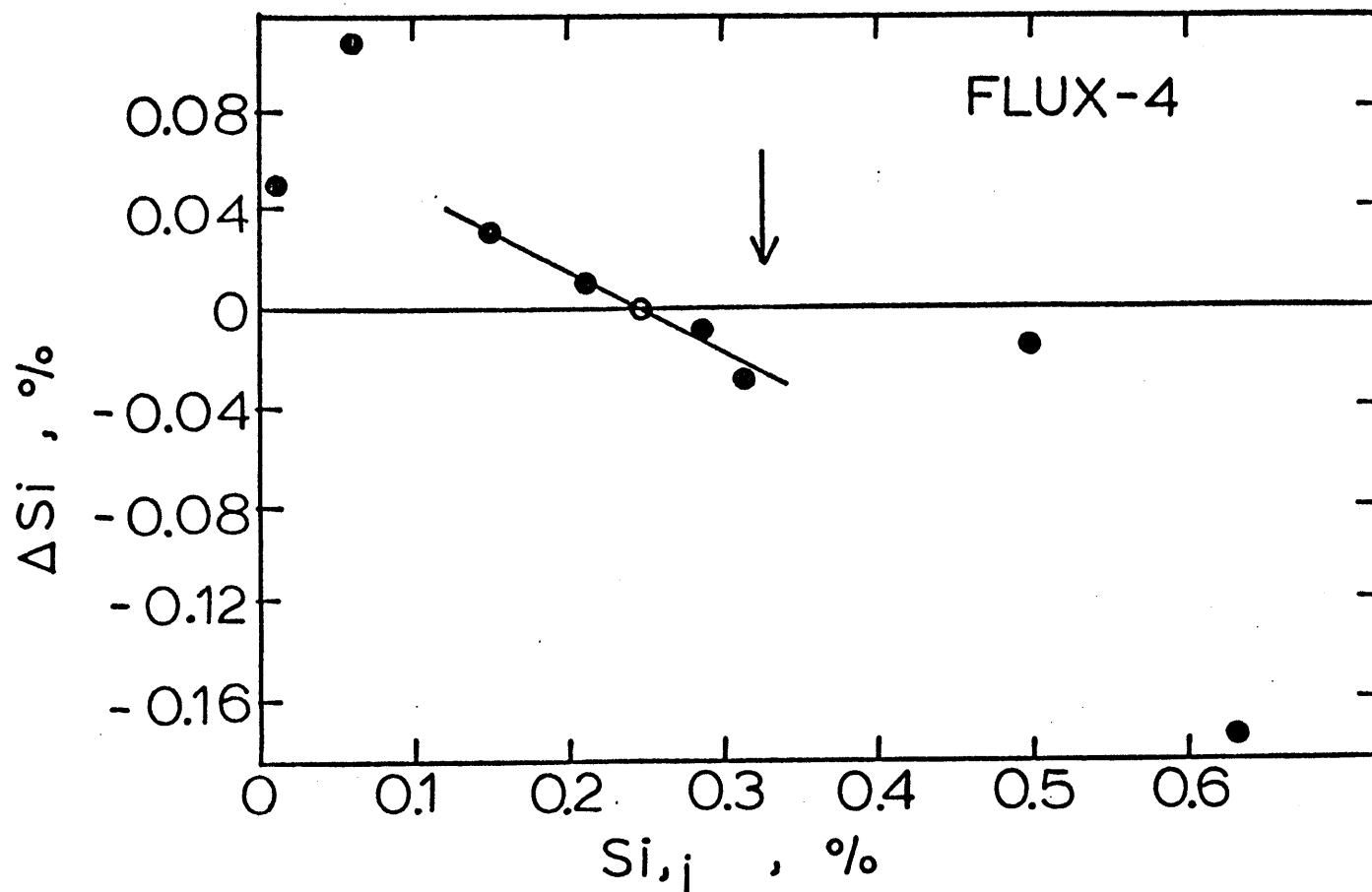
Fig. 27: The change in the weld metal Si, ΔSi, as a function of the initial Si content, $Si_{,i}$, measured with Flux-4 using the artificial baseplate technique. The arrow denotes the predicted equilibrium Si content for the Flux-4.
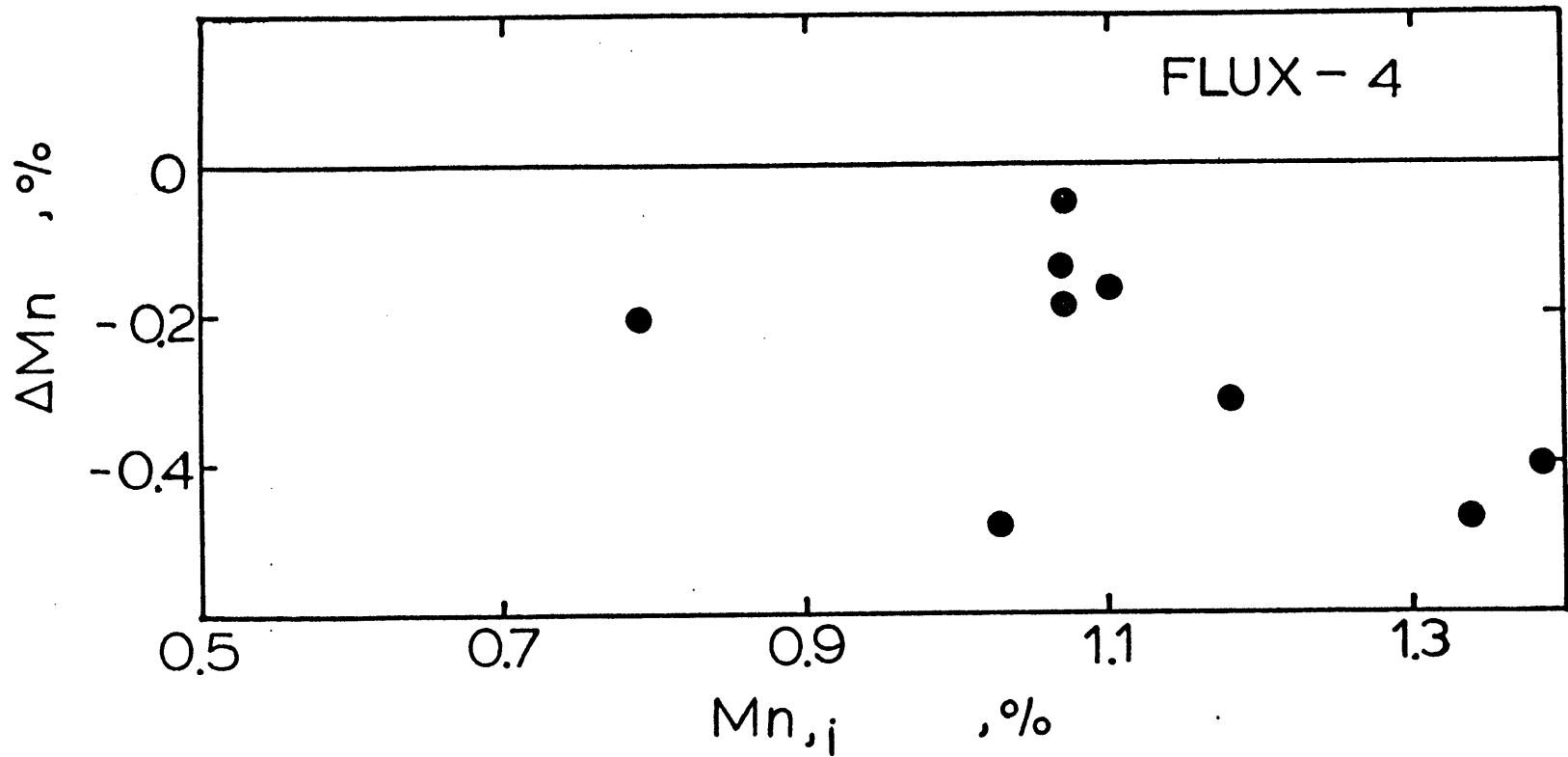
Fig. 28: The change in the weld metal Mn, ΔMn, as a function of the initial Si content, $Mn_{,i}$, measured with Flux-4 using the artificial baseplate technique. The predicted equilibrium Mn content is zero for Flux-4.
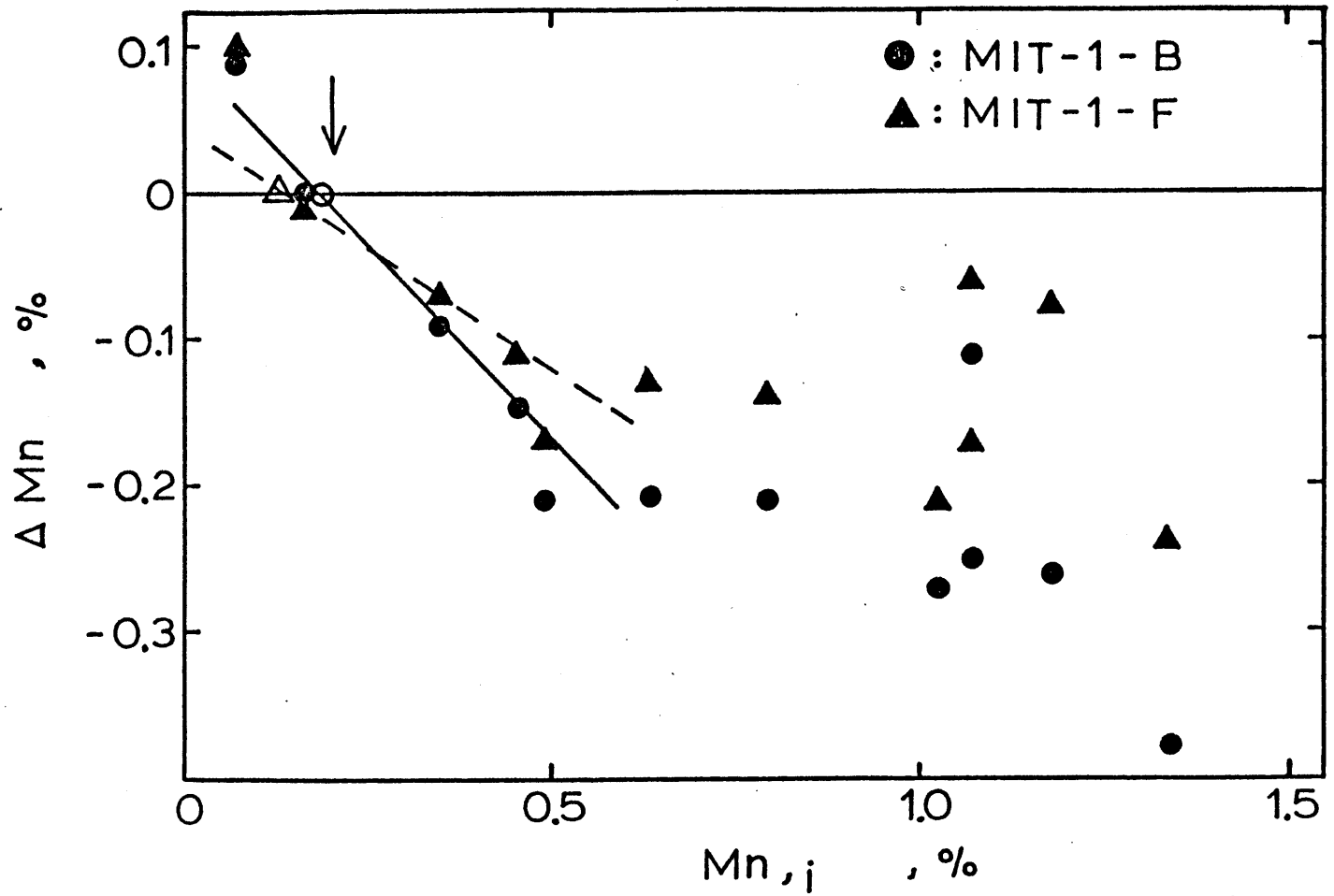
Fig. 29: The change of the weld metal Mn, ΔMn, as a function of the initial
Mn content, Mn_i, measured with Flux MIT-1, both bonded and fused,
using artificial baseplate technique. The arrow denotes the predicted
equilibrium Mn for Flux MIT-1.
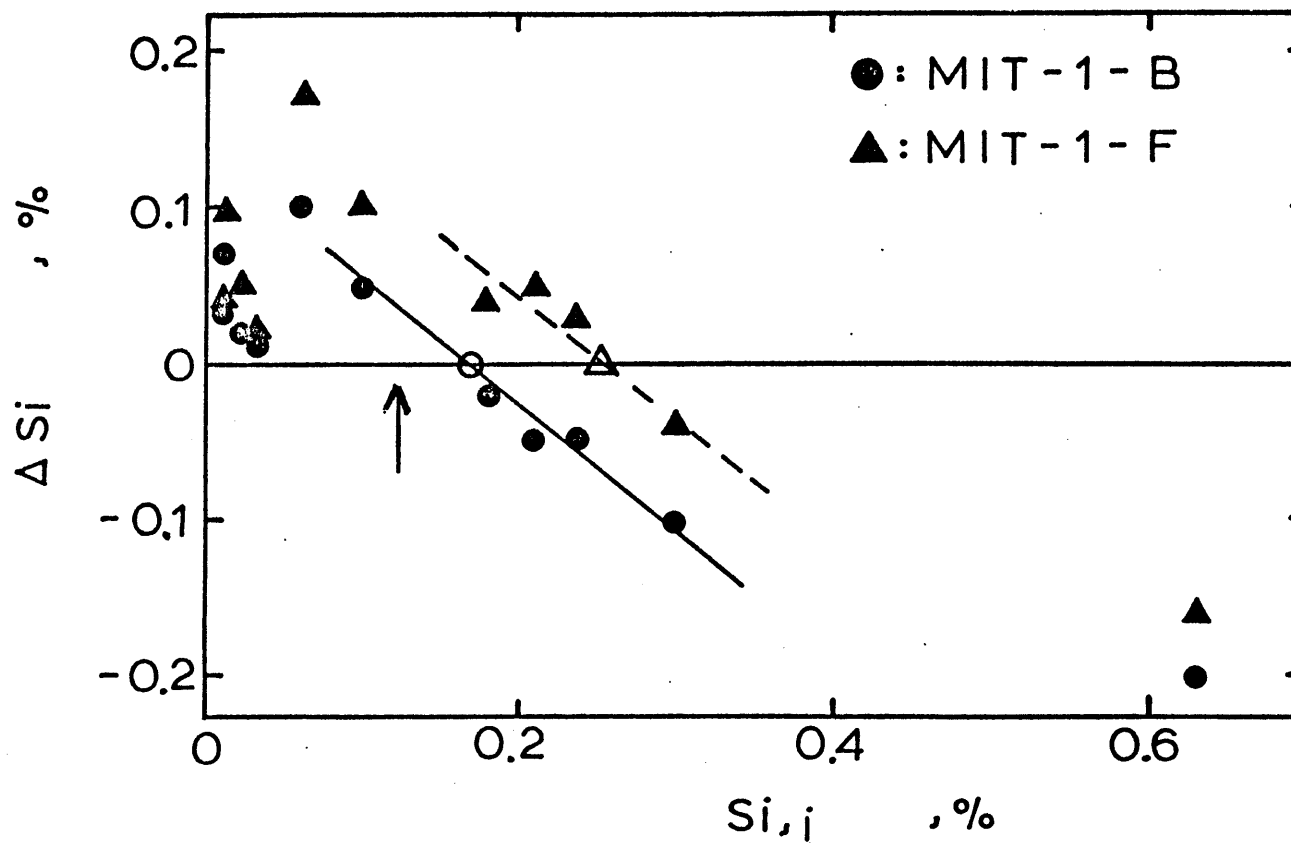
Fig. 30: The change of the weld metal Si, ΔSi, as a function of the initial Si content, Si_i, measured with Flux MIT-1, both bonded and fused, using the artificial baseplate technique. The arrow denotes the predicted equilibrium Si for the Flux MIT-1.
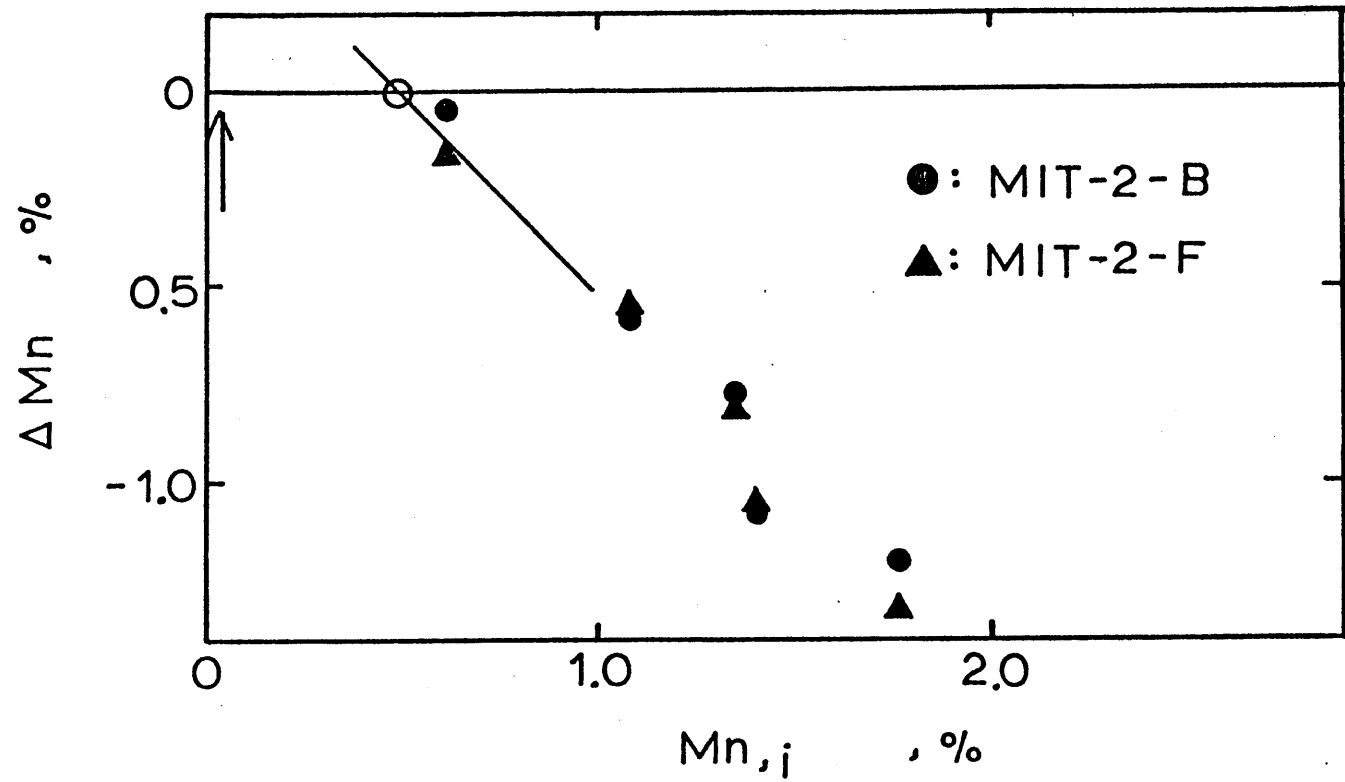
Fig. 31: The change of the weld metal Mn, ΔMn, as a function of the initial
Mn content, Mn_i, measured with Flux MIT-2, both bonded and fused,
using the artificial baseplate technique. The arrow denotes the
predicted equilibrium Mn for the Flux MIT-2.
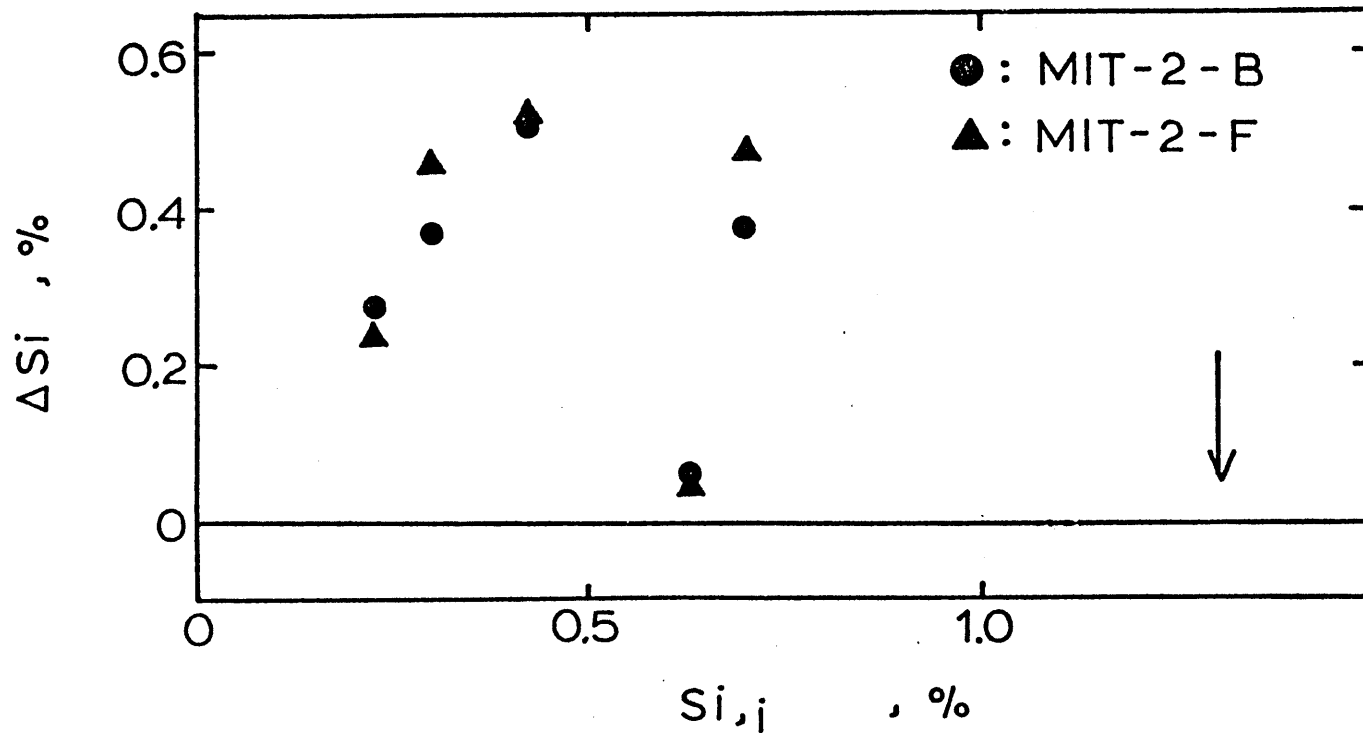
Fig. 32: The change of the weld metal Si, ΔSi, as a function of the initial Si content, Si_i, measured with Flux MIT-2, both bonded and fused, using the artificial baseplate technique. The arrow denotes the predicted equilibrium Si content for Flux MIT-2.
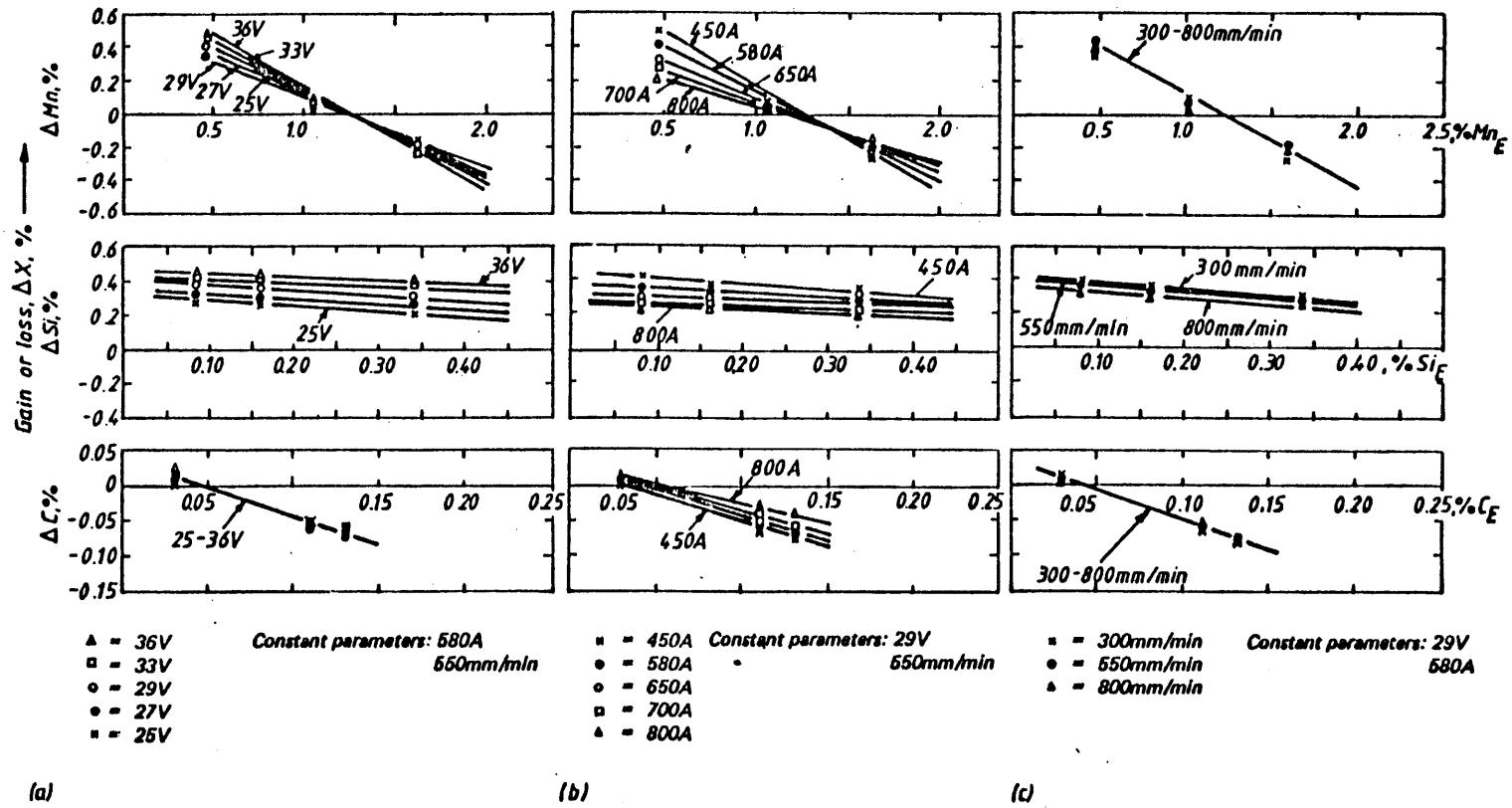
Fig. 33: Influence of (a) voltage, (b) current and (c) welding speed on reactions of Mn, Si and C for Flux LW280. (from reference 26)
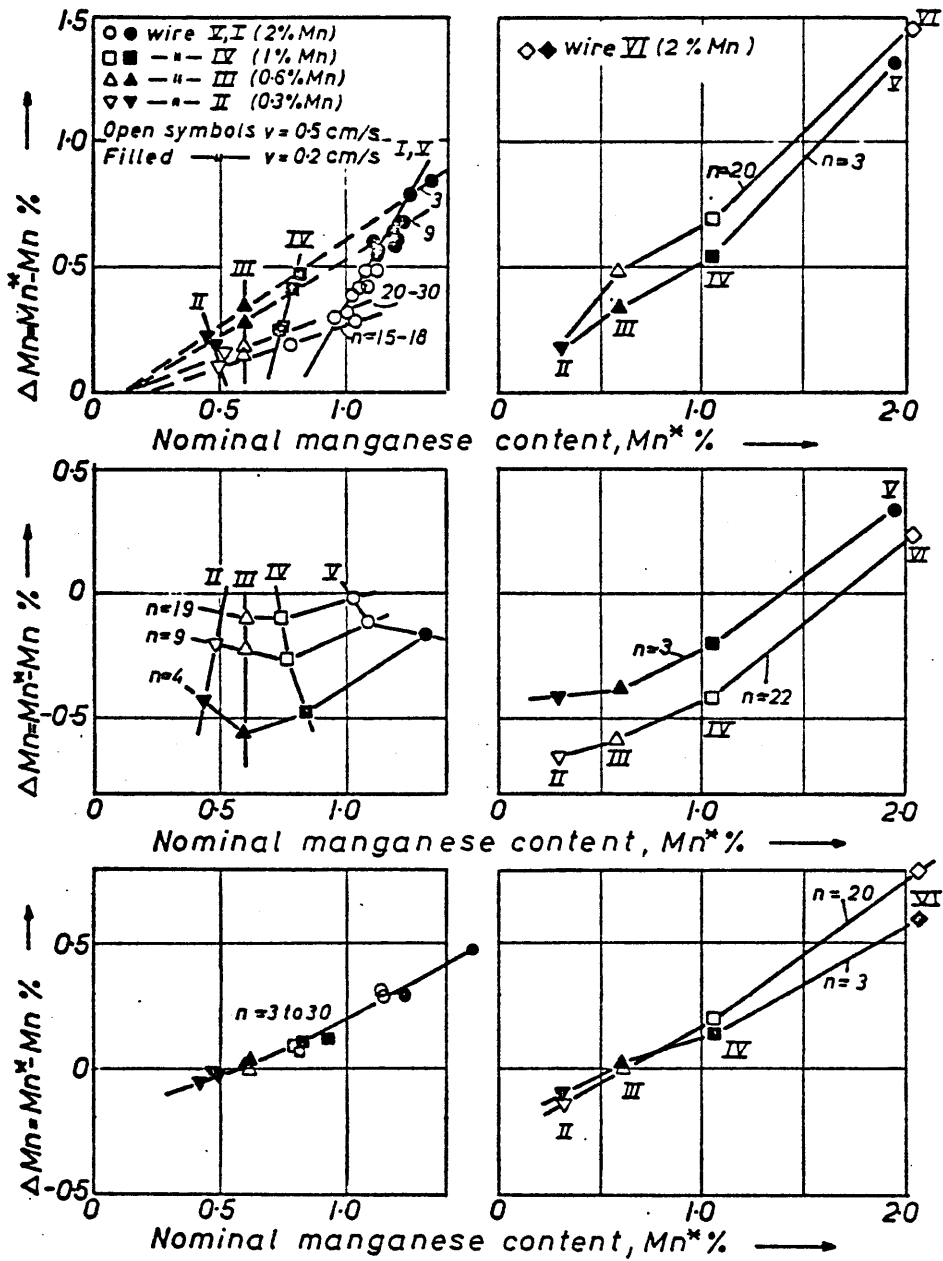
Fig. 34: The displacement of the weld metal Mn content
(From reference 14, upper graphes: flux a, c
and d, central graphes: flux e, lower graphes:
flux f)

-166-
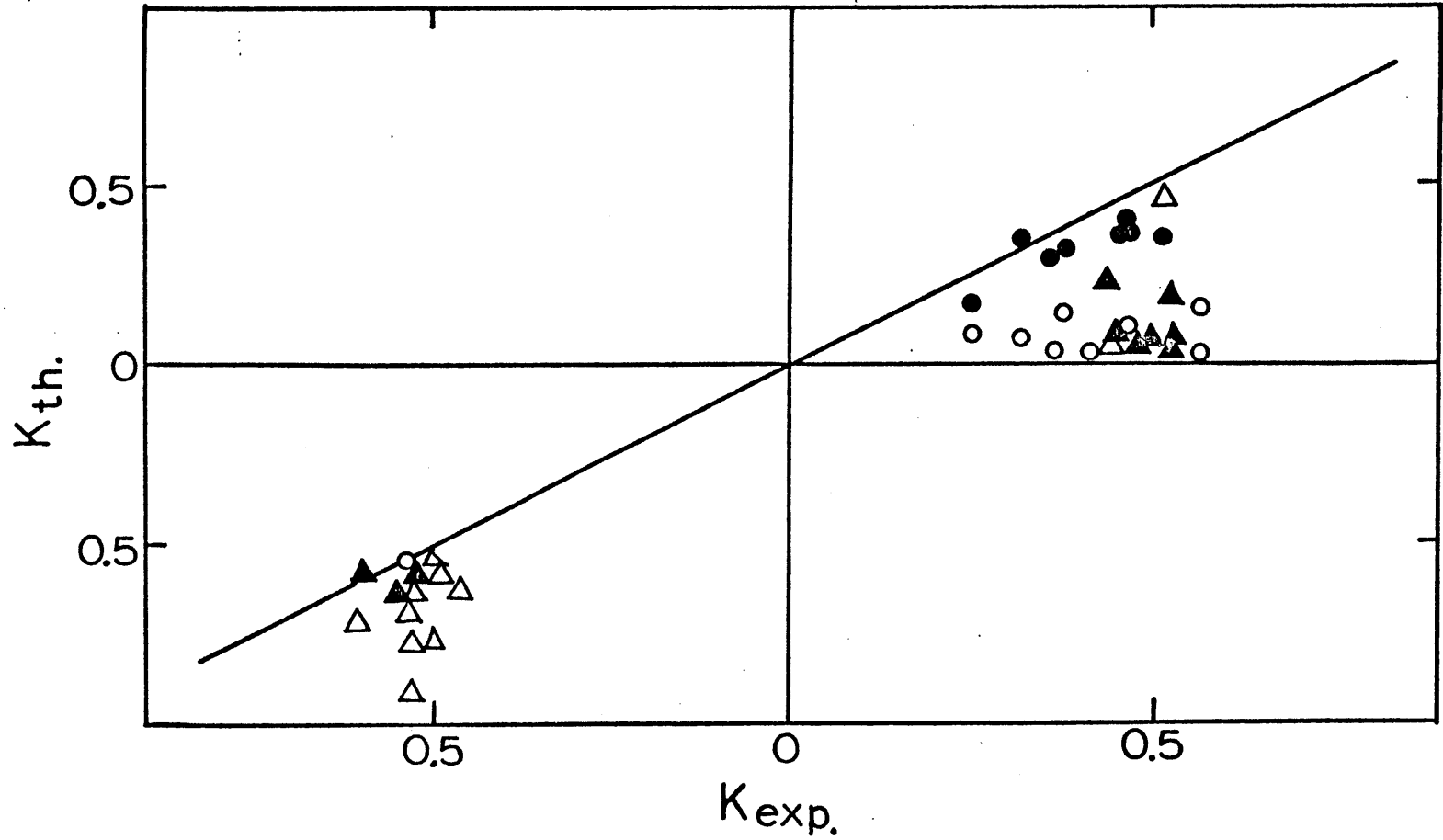
Fig. 35: The relationship between $k_{th.}$ and $k_{exp.}$ (List of symbol references see Appendix 10)
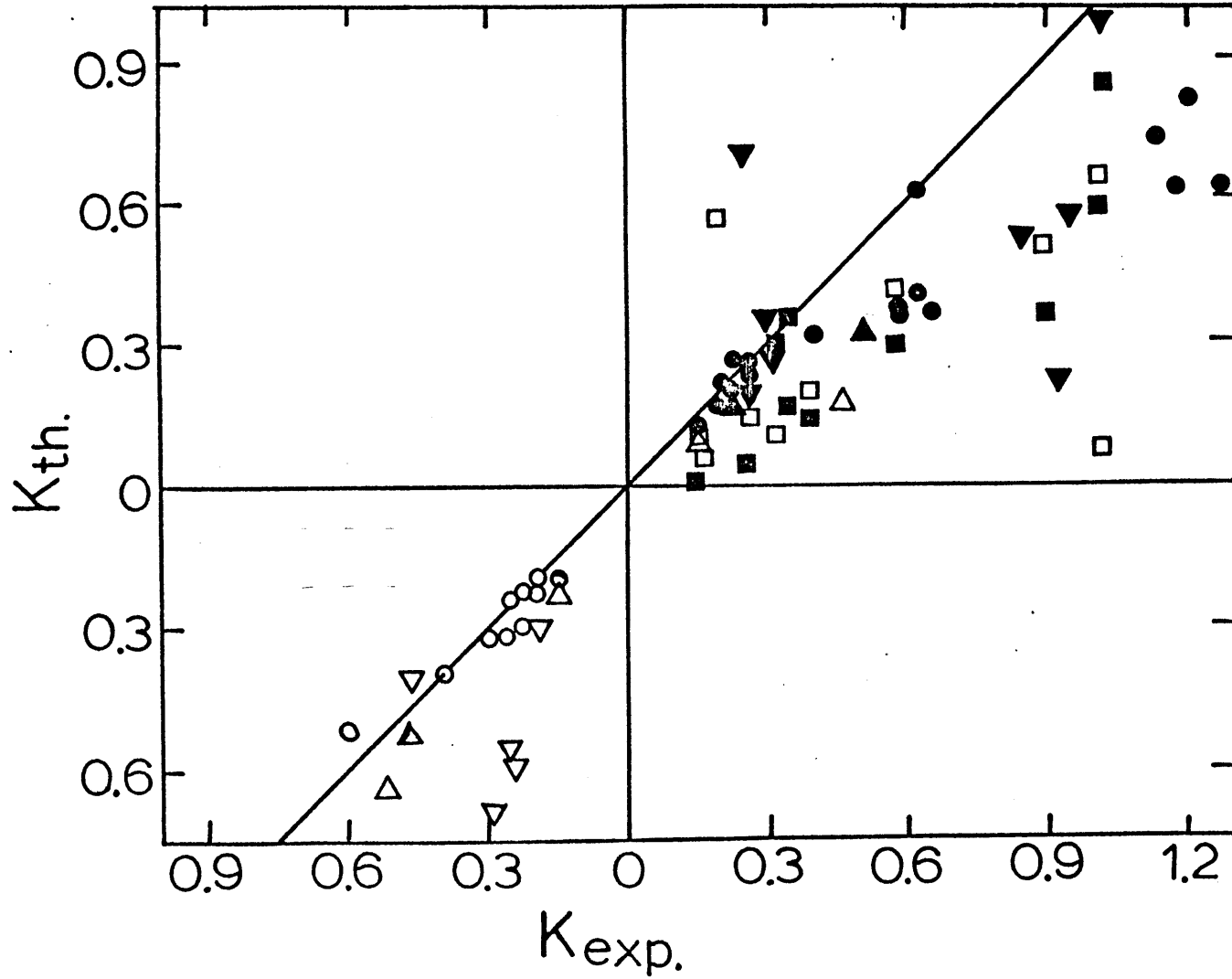
Fig. 36: The relationship between $k_{th.}$ and $k_{exp.}$ (List of symbol references see Appendix 10)
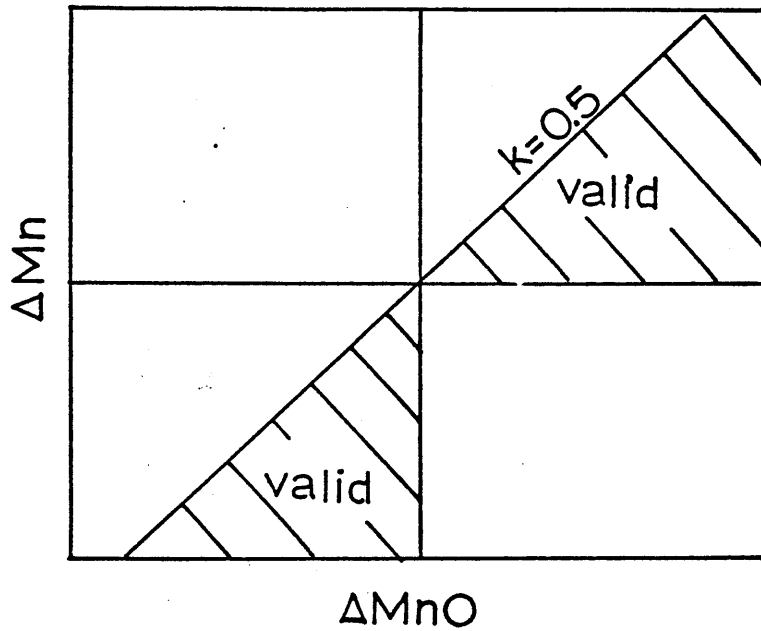
Fig. 37: Schematic representation of the valid
region as restricted by the mass balance.
In the first quadrant, shadow region
represents the $k_{exp.}$ is smaller than 0.5.
In the third quadrant, shadow region
represents that $k_{exp.}$ is larger than 0.5.
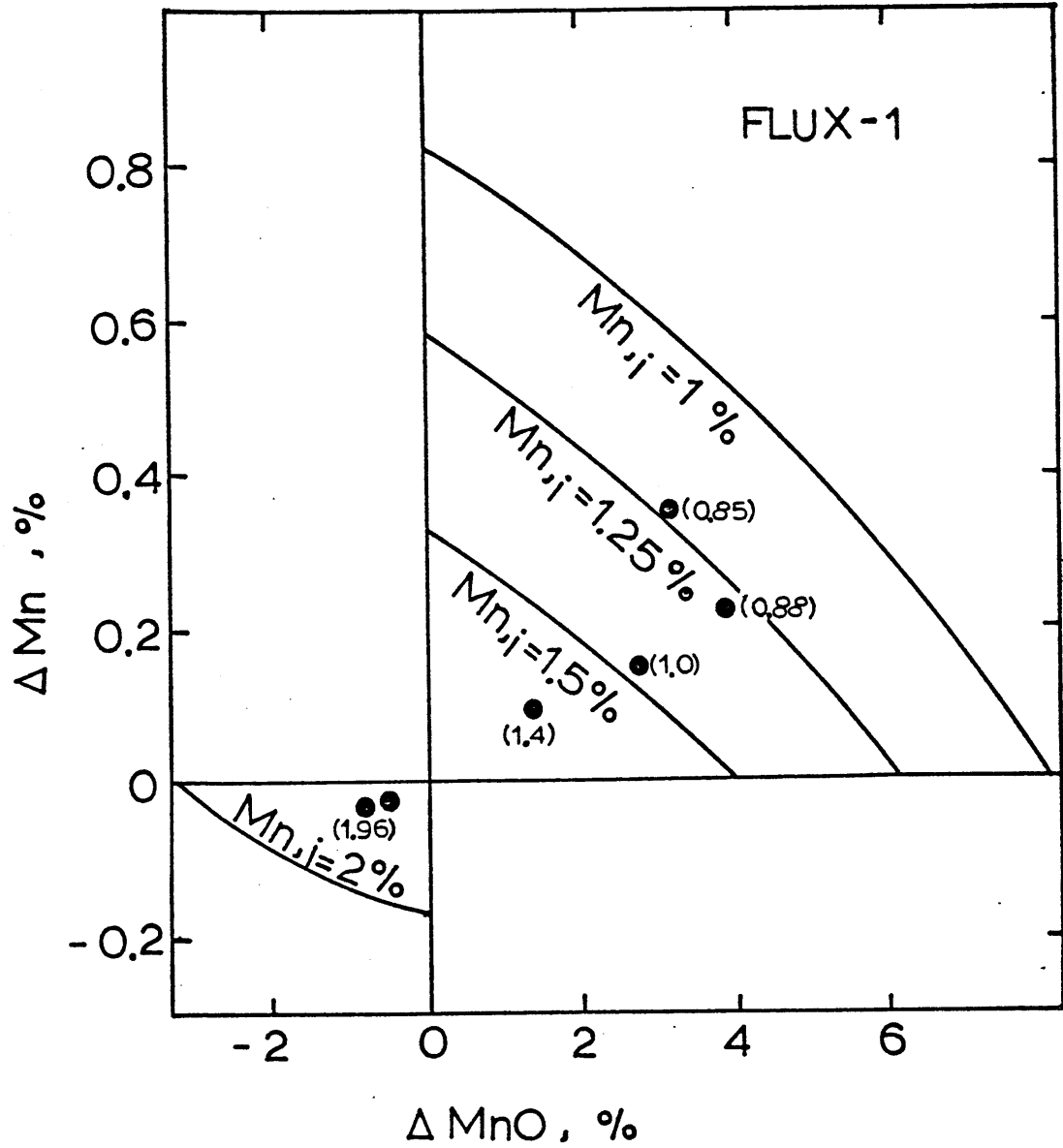
Fig. 38: The permissible weld metal Mn range estimated
from the thermodynamic model using Flux-1 for
a given initial weld metal Mn content. (The
initial Mn content of the datum point is given
within the parenthesis)
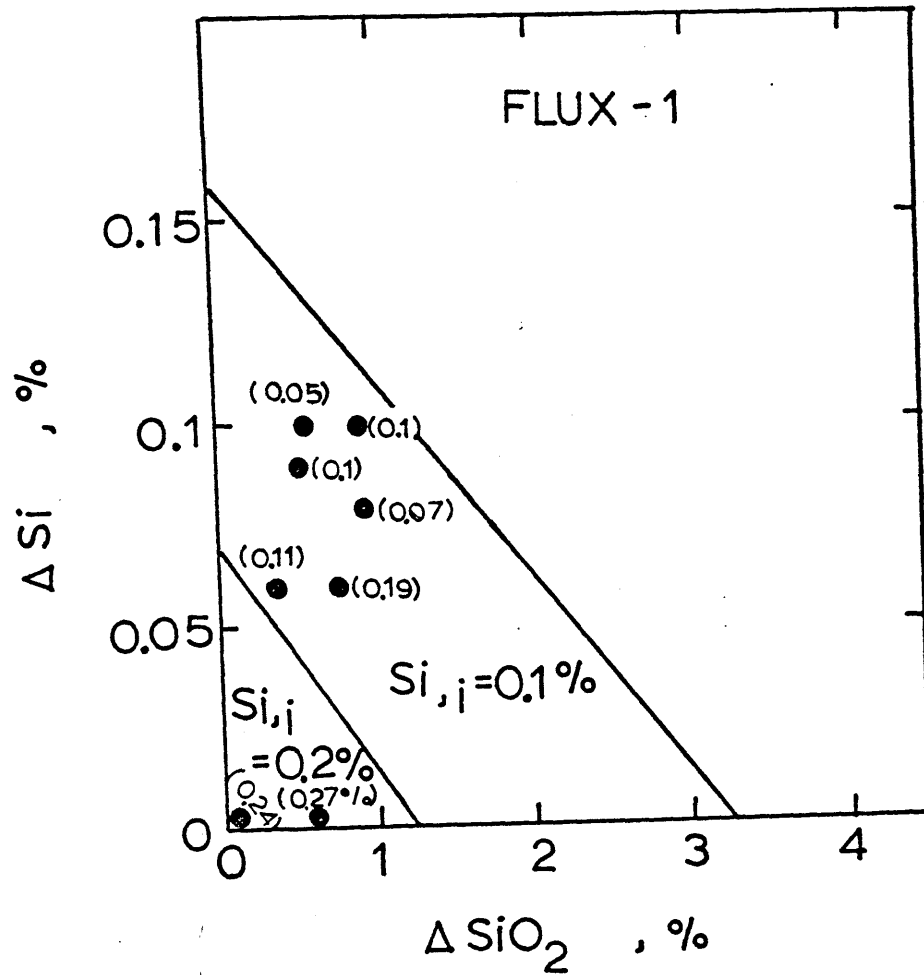
Fig. 39: The permissible weld metal Si range
estimated from the thermodynamic model
using Flux-1 for a given initial weld
metal Si content. (The initial Si content
of the datum point is given within the
parenthesis)
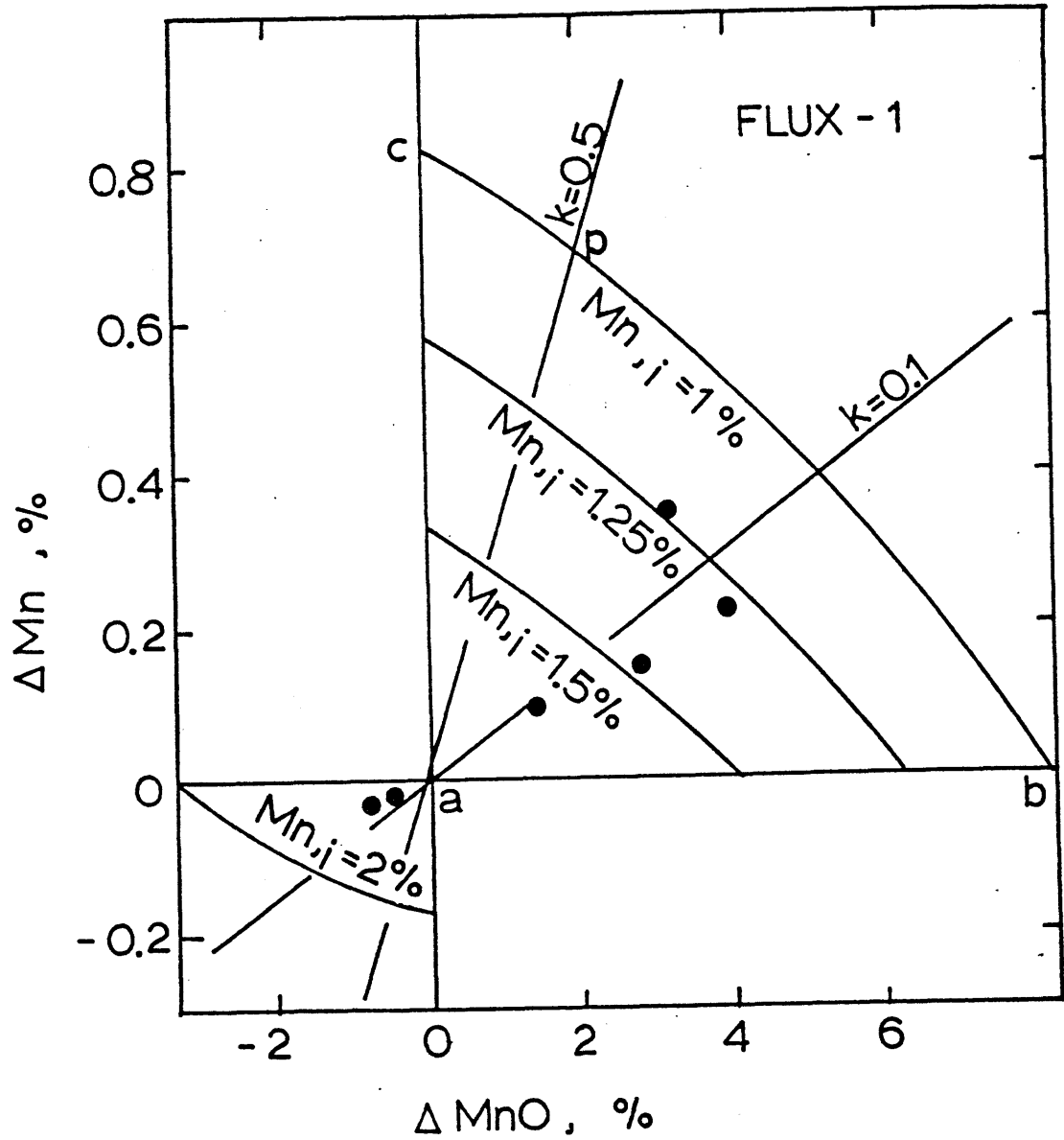
Fig. 40: The permissible weld metal Mn range estimated from the thermodynamic model and the mass balance using Flux-1 for a given initial weld metal Mn content.
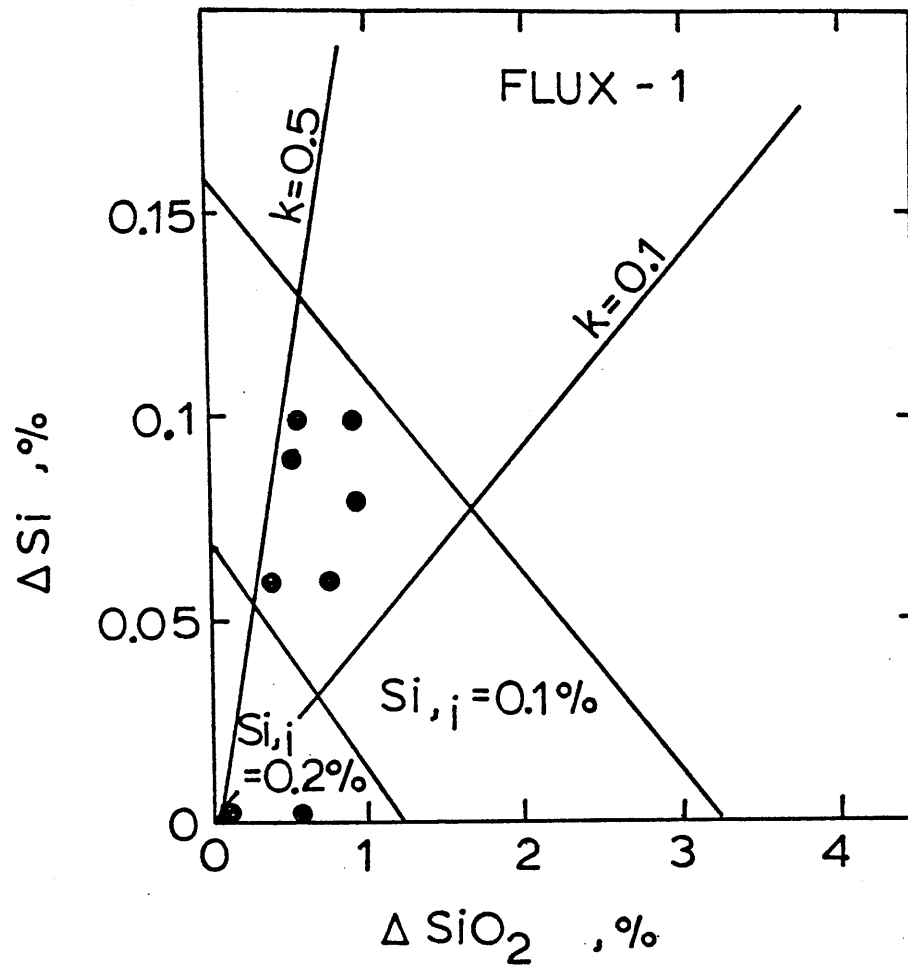
Fig. 41: The permissible weld metal Si range estimated
from the thermodynamic model and the mass
balance using Flux-1 for a given initial
weld metal Si content.
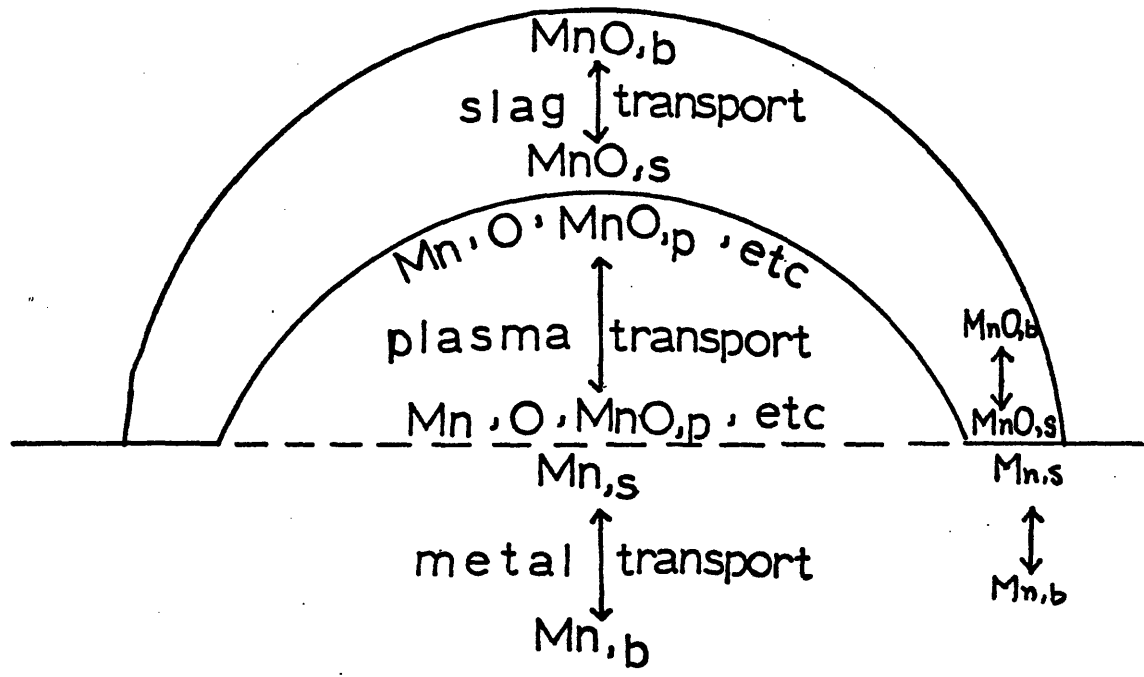
Fig. 42: Schematic representation of slag-metal
reactions in the arc welding process.
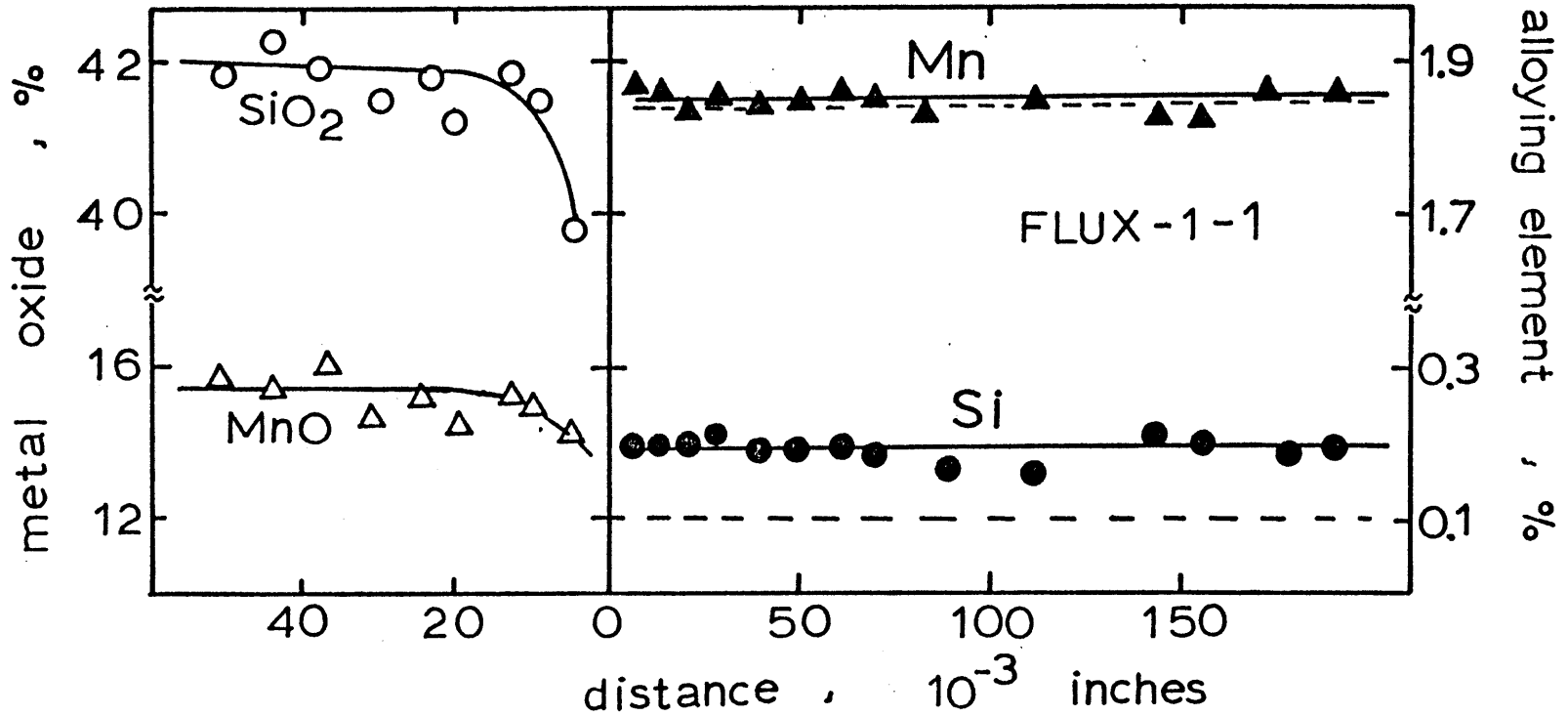
Fig. 43: The spatial distribution of Mn and Si in both the slag and the metal phases for weld 1-1. (dashed lines are the initial values)
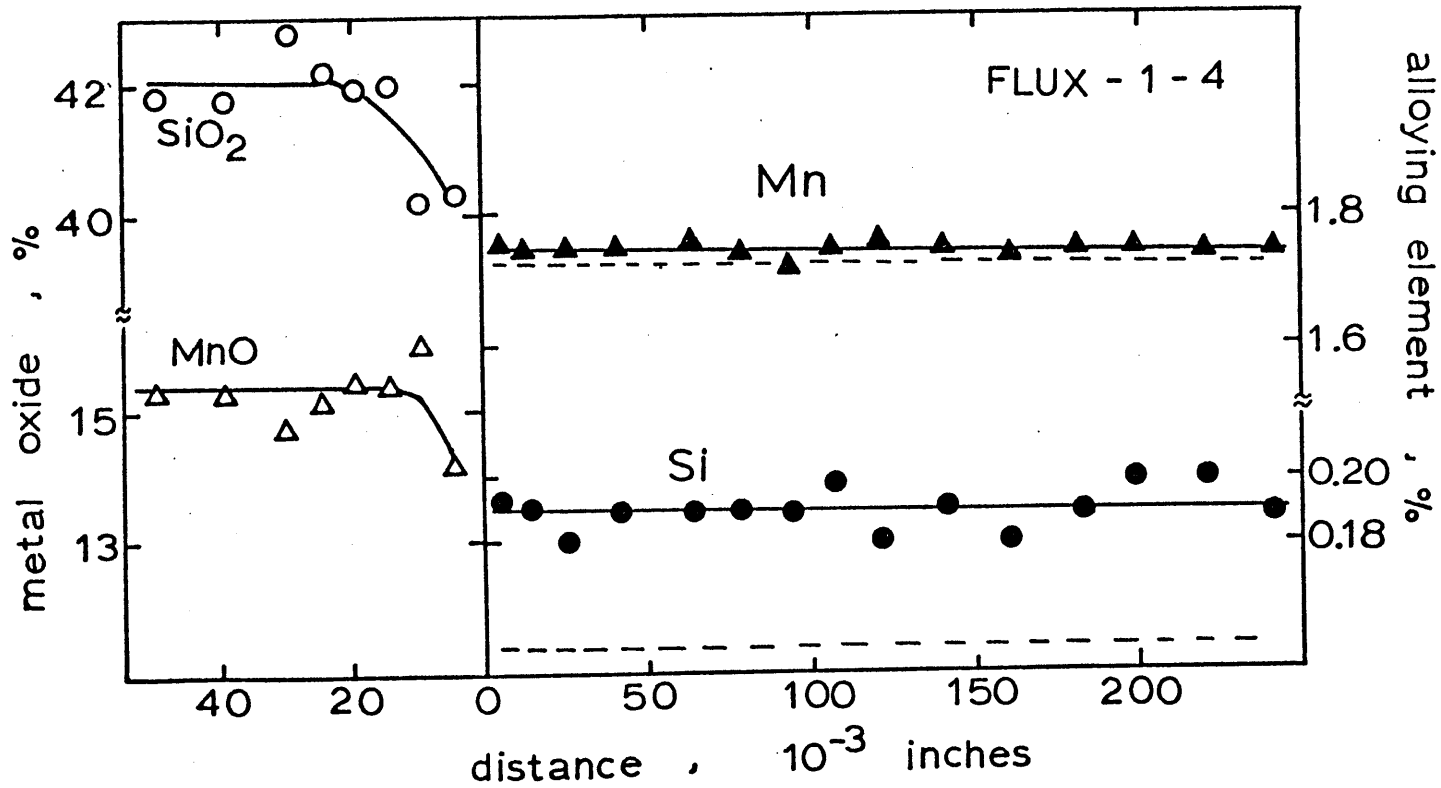
Fig. 44: The spatial distribution of Mn and Si in both the slag and the metal
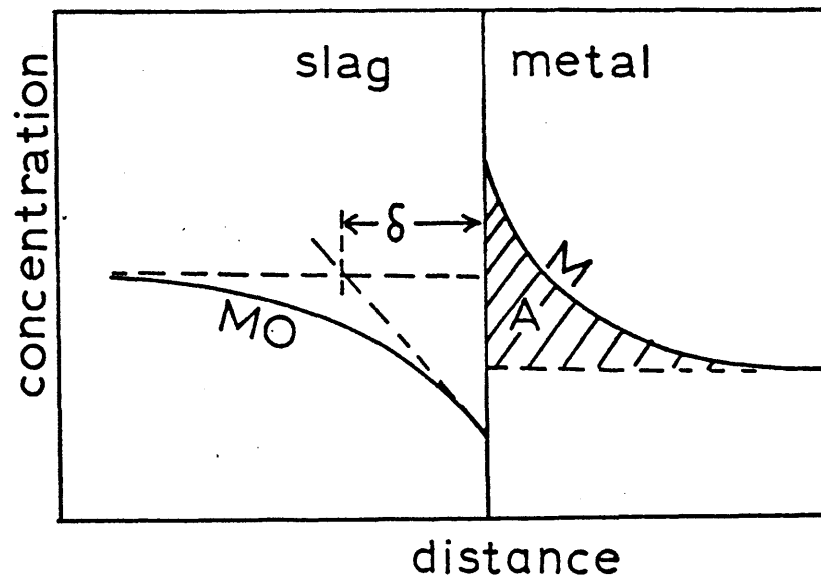phases for weld 1-4. (dashed lines are the initial values)

Fig. 45: Schematic representation of the terms
used in definition of the effective
transport thickness, δ, and the transport
rate.
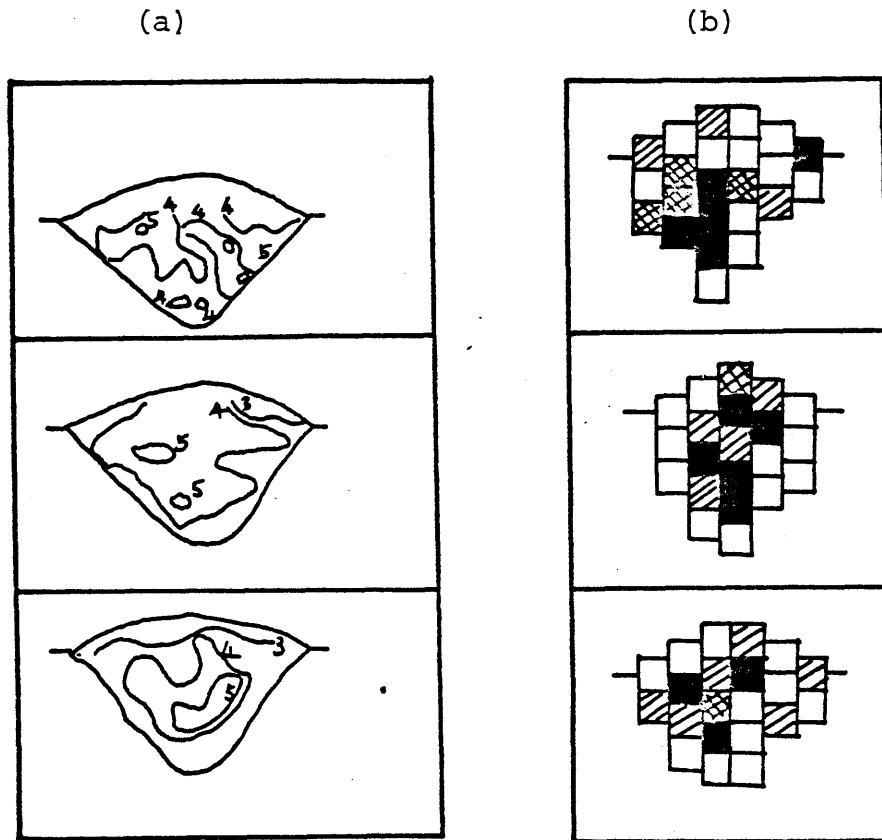
(a)   (b)

Fig. 46: (a) Mapping of oxygen in the weld metal as
               measured by the impulse fusion technique
          (b) Relative concentration of oxygen in weld
               bead.
               ☐ : under average
               ▨ :1-10 ppm over average
               ▧ :11-20 ppm over average
               ■ : over 21 ppm
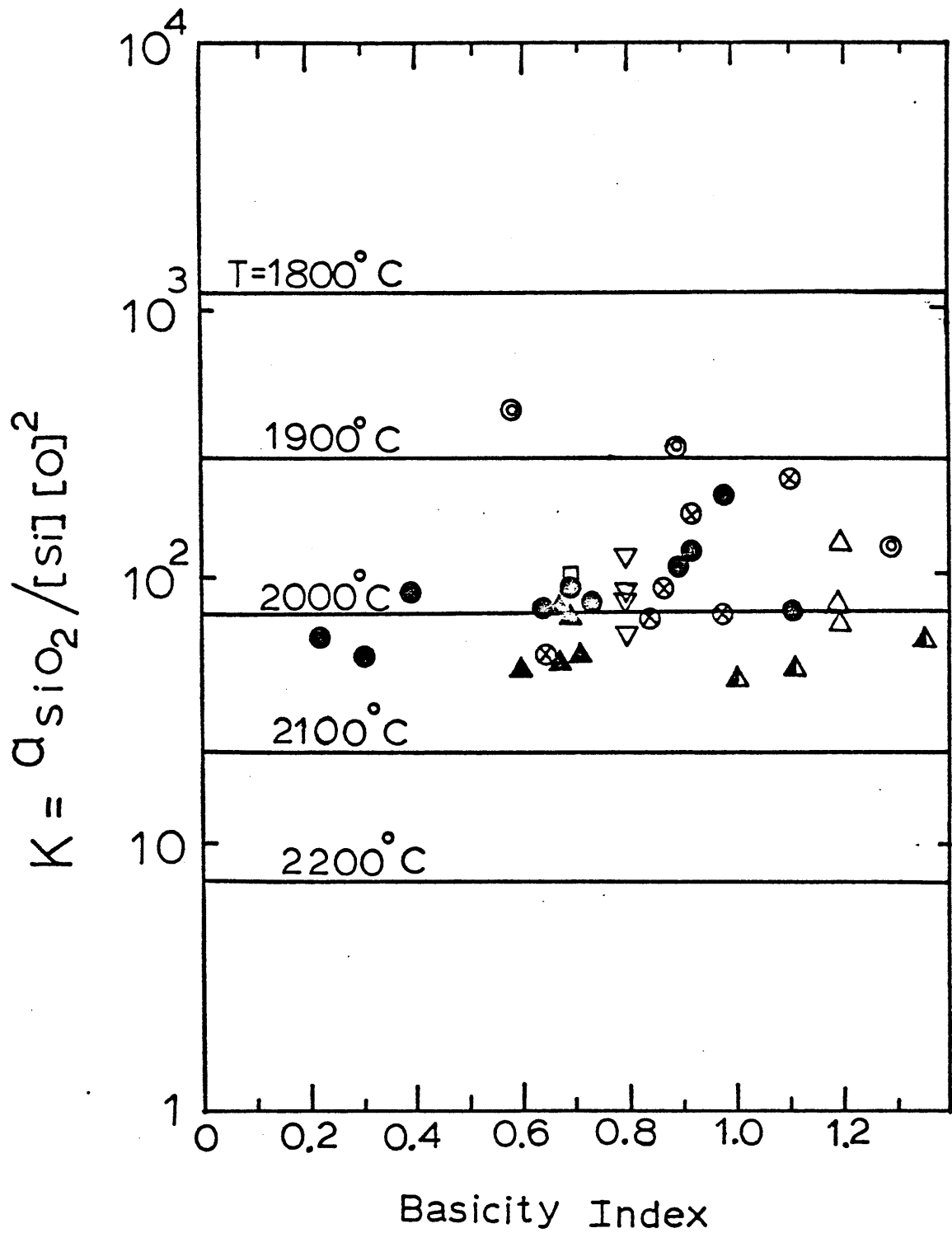   with average 550 ppm (from reference 30)

Fig. 47: The effective weld pool temperature estimated from
the SiO$_2$ reaction equilibrium constant. (for list
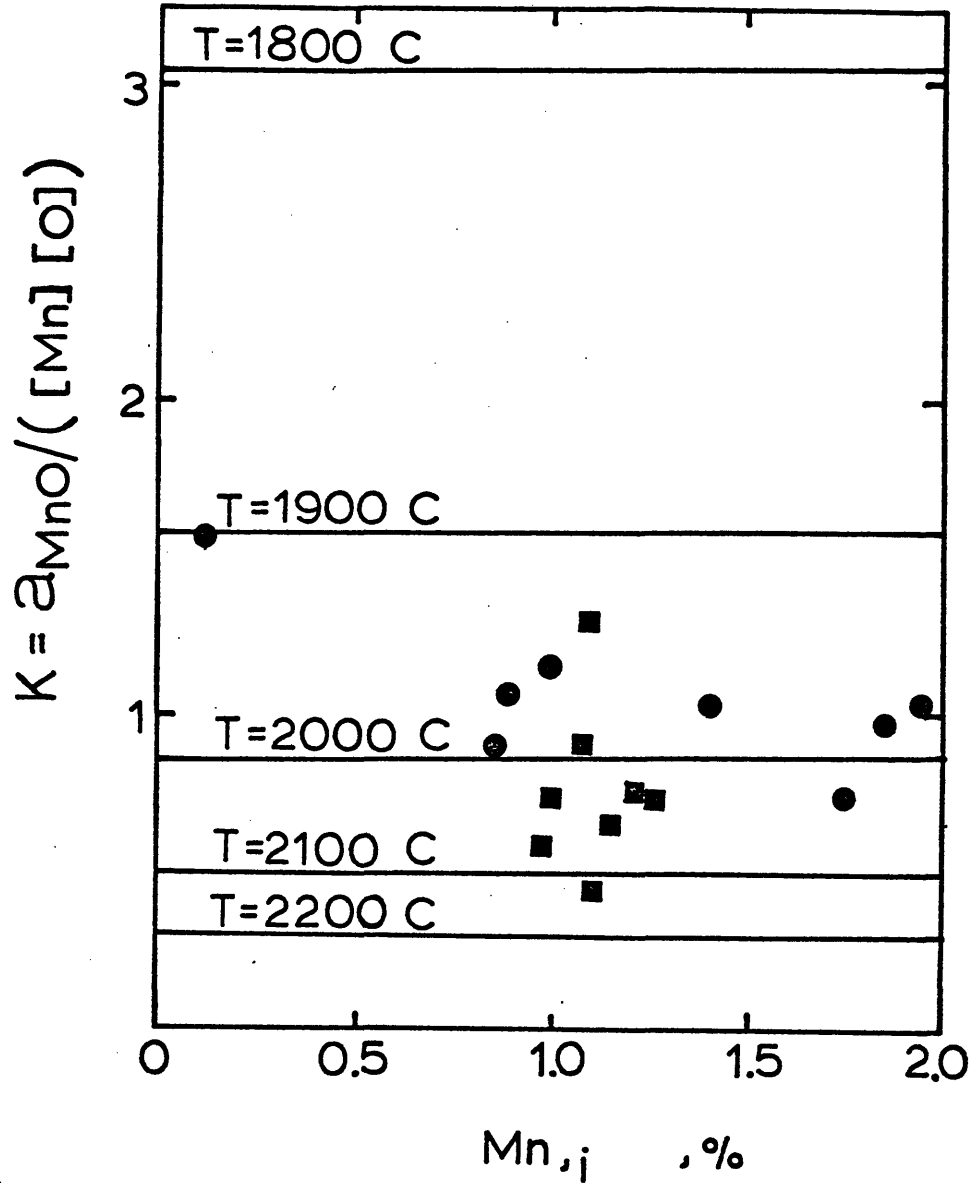of symbols refers to Appendix 10)

Fig. 48: The effective weld pool temperatures estimated
by the MnO reaction equilibrium constant using
weld metal surface Mn content. (square symbols
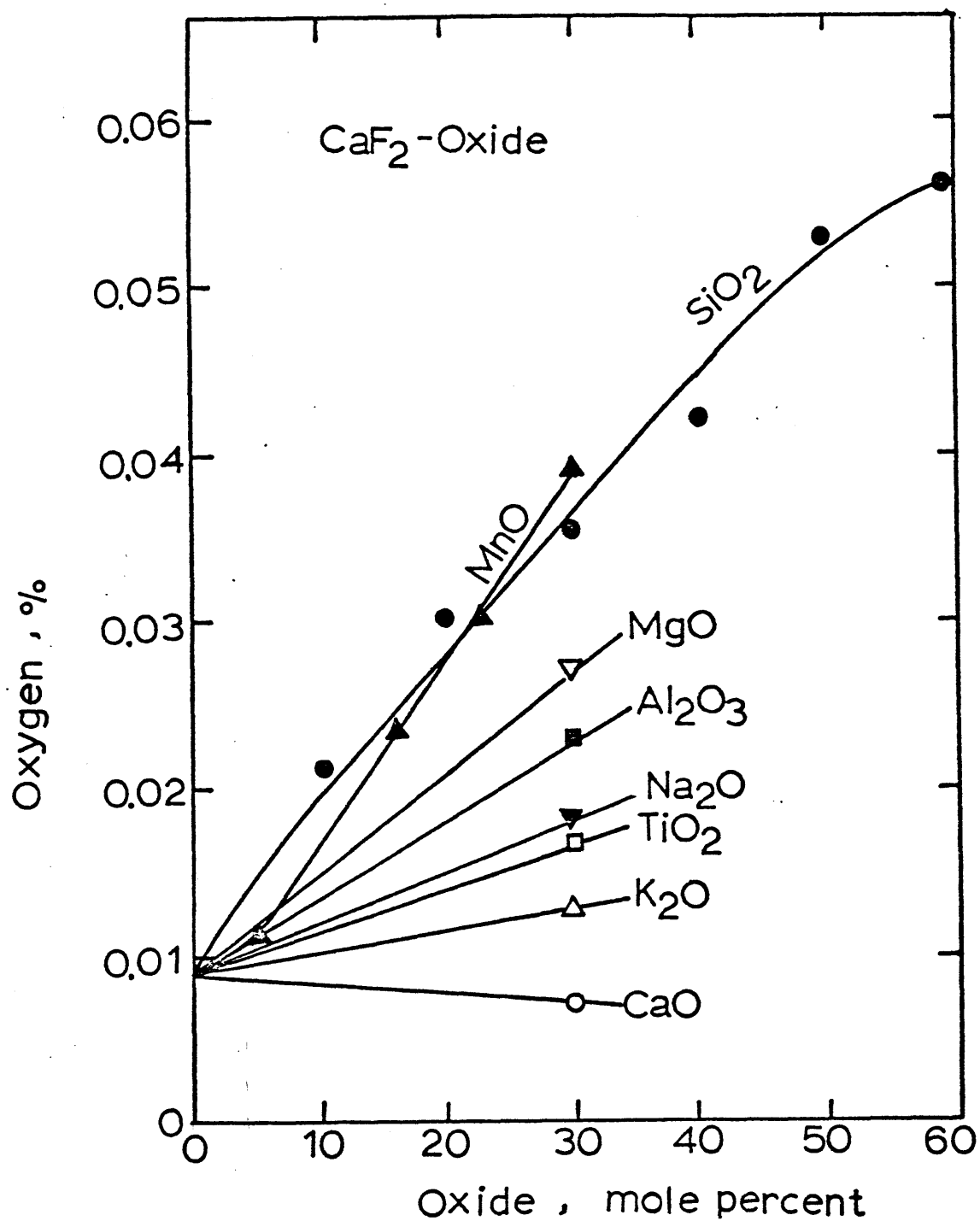from reference 14, circular symbols from this
study)

-180-

Fig. 49: Weld metal oxygen content produced with binary CaF$_2$-oxide flux system.
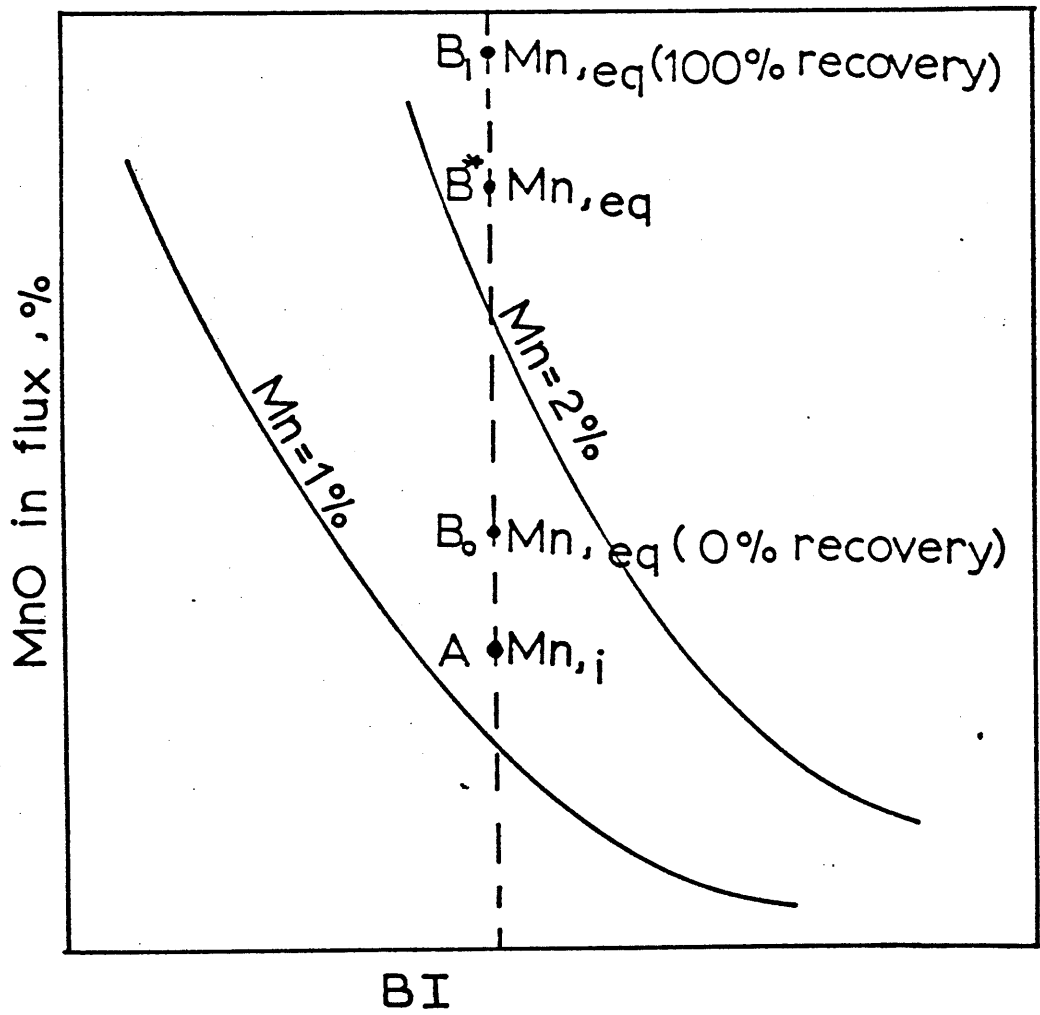
Fig. 50: Schematic representation of fixing initial
weld metal composition used in predicting
the final weld metal composition for alloyed
fluxes. The dotted line is presented for
reference to discussion in the text.

$A_I \, | \, Mn_{,i}$ (100% recovery)

$B_o \, | \, Mn_{,eq}$

$A^* \, | \, Mn_{,i}$

$A \, | \, Mn_{,i}$ (0% recovery)

Mn=2%

Mn=1%

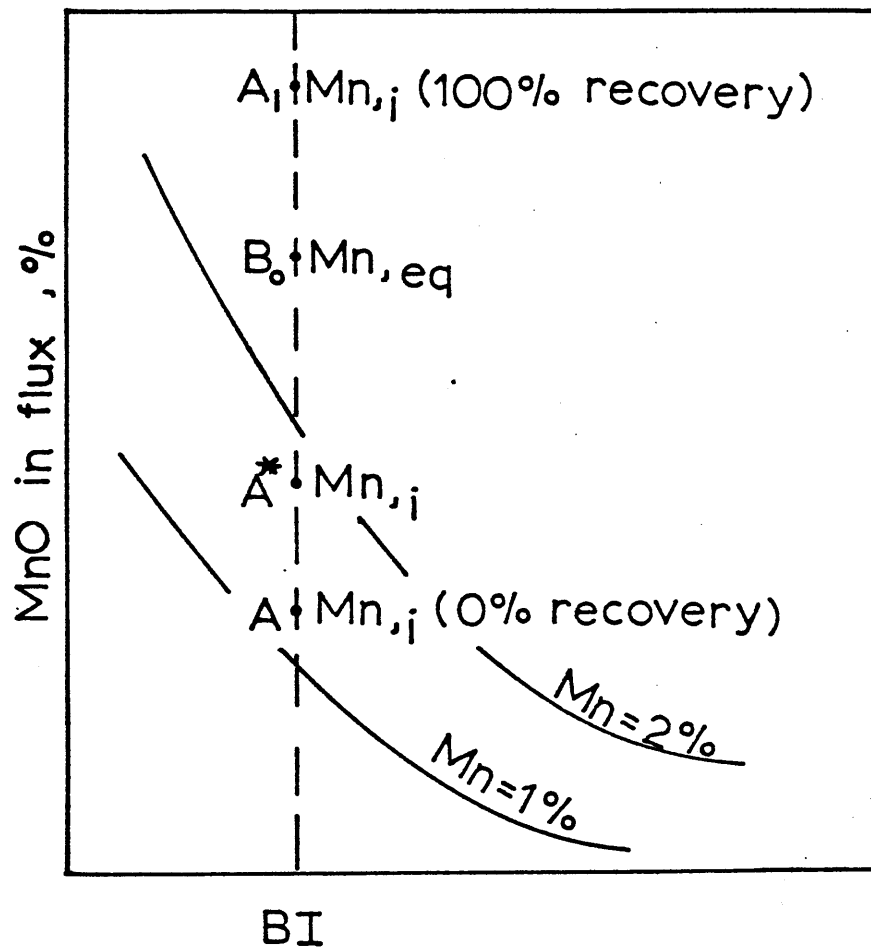MnO in flux , %

BI

Fig. 51: Schematic representation of fixing
        equilibrium point used in predicting
        the final weld metal composition for
        alloyed fluxes. The dotted line is
        presented for reference to discussion
        in the text.

Appendix 1: Results of plasmadynamic oxygen potential experiment using CaF_2-oxide flux systems

| weld	Flux compositions (atomic percent)	weld metal compositions			volume fraction of metallic mist(%)
		Mn(%)	Si(%)	O(%)	
1S	$30\%SiO_2$-$70\%CaF_2$	0.78	0.40	0.035	0.04
2S	$30w/oSiO_2$-$70w/oMnO$	1.78	0.18	0.064	0.48
3S	$30\%TiO_2$-$70\%CaF_2$	1.24	0.22	0.017	---
4S	$30\%Al_2O_3$-$70\%CaF_2$	1.24	0.22	0.023	---
5S	$30\%K_2O$-$70\%CaF_2$	0.93	0.18	0.013	---
6S	$30\%CaO$-$70\%CaF_2$	1.15	0.24	0.007	---
7S	$30\%Na_2O$-$70\%CaF_2$	1.30	0.18	0.018	---
8S	$30\%MgO$-$70\%CaF_2$	0.91	0.22	0.027	0.749
9S	$100\%CaF_2$	0.95	0.25	0.009	0.378
10S	$30\%MnO$-$70\%CaF_2$	1.45	0.04	0.039	---
1MS	$20\%SiO_2$-$80\%CaF_2$	1.24	0.37	0.030	0.05
2MS	$10\%SiO_2$-$90\%CaF_2$	1.20	0.37	0.021	0.06
3MS	$5\%MnO$-$95\%CaF_2$	1.38	0.11	0.011	0.99
4MS	$15.3\%MnO$-$84.7\%CaF_2$	1.48	0.08	0.024	1.26
5MS	$22\%MnO$-$78\%CaF_2$	1.80	0.09	0.030	---
6MS	$60\%SiO_2$-$40\%CaF_2$	0.96	0.52	0.056	---
7MS	$50\%SiO_2$-$50\%CaF_2$	0.77	0.44	0.053	0.08
8MS	$40\%SiO_2$-$60\%CaF_2$	0.88	0.53	0.042	0.14

Appendix 2: Results of the screening experiment

Trial	Penetration (mm)	Height (mm)	Width (mm)	Arc Stability	Contact Angle($^\circ$)	Consumption of Flux(g/sec)	Melting Rate(g/sec)
1	10.5	6.0	16.0	1	125	1.094	2.87
2	1.5	4.0	16.0	3	138.8	1.958	1.784
3	3.0	2.5	12.0	1	137.5	0.718	1.17
4	4.0	5.5	10.0	5	91.8	0.811	2.824
5	7.0	2.0	17.0	1	150.0	2.032	1.558
6	9.0	3.0	13.5	1	145.0	1.373	1.88
7	7.5	3.5	24.0	1	150	1.92	1.787
8	4.0	2.0	11.5	1	141.5	1.489	0.965
9	7.0	6.5	9.0	5	90	0.732	2.06
10	3.5	3.0	12.0	3	134	1.69	1.06
11	8.5	8.5	8.0	5	50	0.615	2.615
12	2.5	4.5	14.0	3	119	0.38	1.98
13	3.0	4.0	11.0	5	119.5	0.9	1.117
14	3.0	2.5	15.0	1	125.5	0.993	1.257
15	3.0	2.0	11.5	5	135	0.904	1.006
16	7.0	6.5	7.0	5	83.5	0.496	2.337
17	7.0	5.0	18.5	3	128	1.99	2.475
18	2.0	2.5	14.0	3	142.5	1.56	1.52
19	4.5	6.5	9.0	5	264.0	3.08	2.23
20	3.5	3.0	15.0	1	142	0.94	1.044

Appendix 2: (continued)

Trial	Weld metal phase				Slag phase, metallic mist		
	Oxygen (%)	Manganese (%)	Silicon (%)	Carbon (%)	Volume fraction of metallic mist (%)	Manganese (%)	Silicon (%)
1	0.085	1.28	0.40	0.10	0.583	1.06	0.33
2	0.102	1.07	0.38	0.05	2.25	2.74	1.23
3	0.054	0.98	0.32	0.12	0.305	0.44	0.54
4	0.086	1.03	0.33	0.14	1.57	---	---
5	0.043	0.92	0.33	0.16	0.256	0.02	0.37
6	0.088	1.23	0.35	0.10	0.26	---	---
7	0.026	1.05	0.32	0.10	0.168	---	---
8	0.058	0.58	0.11	0.13	1.14	0.06	0.32
9	0.027	0.97	0.42	0.11	0.35	0.06	0.57
10	0.033	0.85	0.44	0.12	0.207	0.05	0.33
11	0.087	1.23	0.64	0.12	3.4	---	---
12	0.143	1.19	0.92	0.07	1.5	1.23	0.35
13	0.033	0.91	0.37	0.12	0.147	0.09	0.43
14	0.174	1.21	0.77	0.15	0.914	1.36	0.53
15	0.15	1.11	0.60	0.06	2.12	2.47	1.41
16	0.022	1.09	0.4	0.12	0.335	0.07	0.80
17	0.021	0.82	0.3	0.12	0.335	0.03	0.93
18	0.133	1.11	0.75	0.06	2.12	0.92	0.31
19	0.067	1.11	0.42	0.13	0.564	3.29	1.69
20	0.028	0.9	0.36	0.07	0.139	0.01	0.36
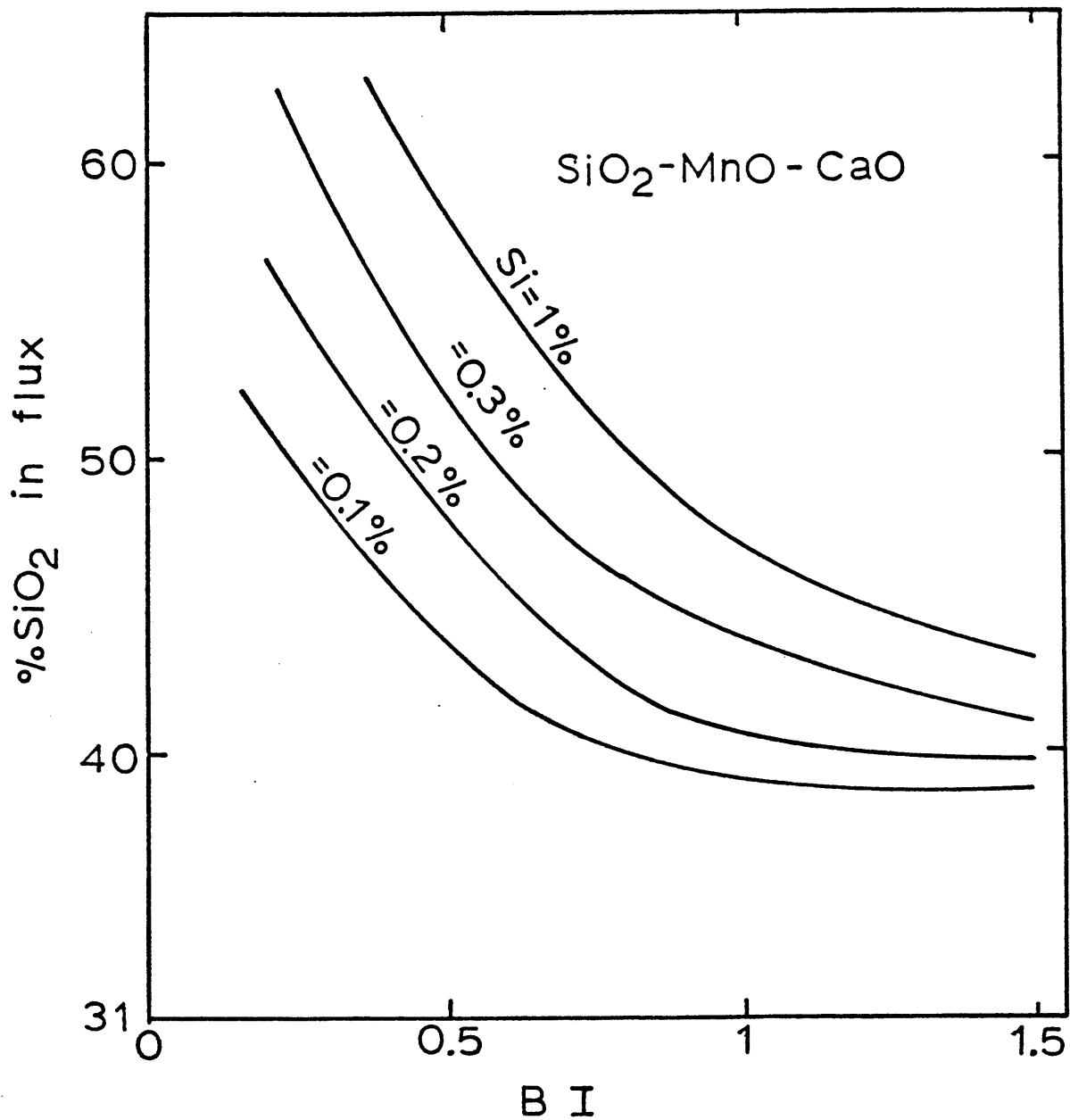
Appendix 3-a: The equilibrium percent SiO_2 at $2000^\circ C$ in the
SiO_2-MnO-CaO system as a function of BI,
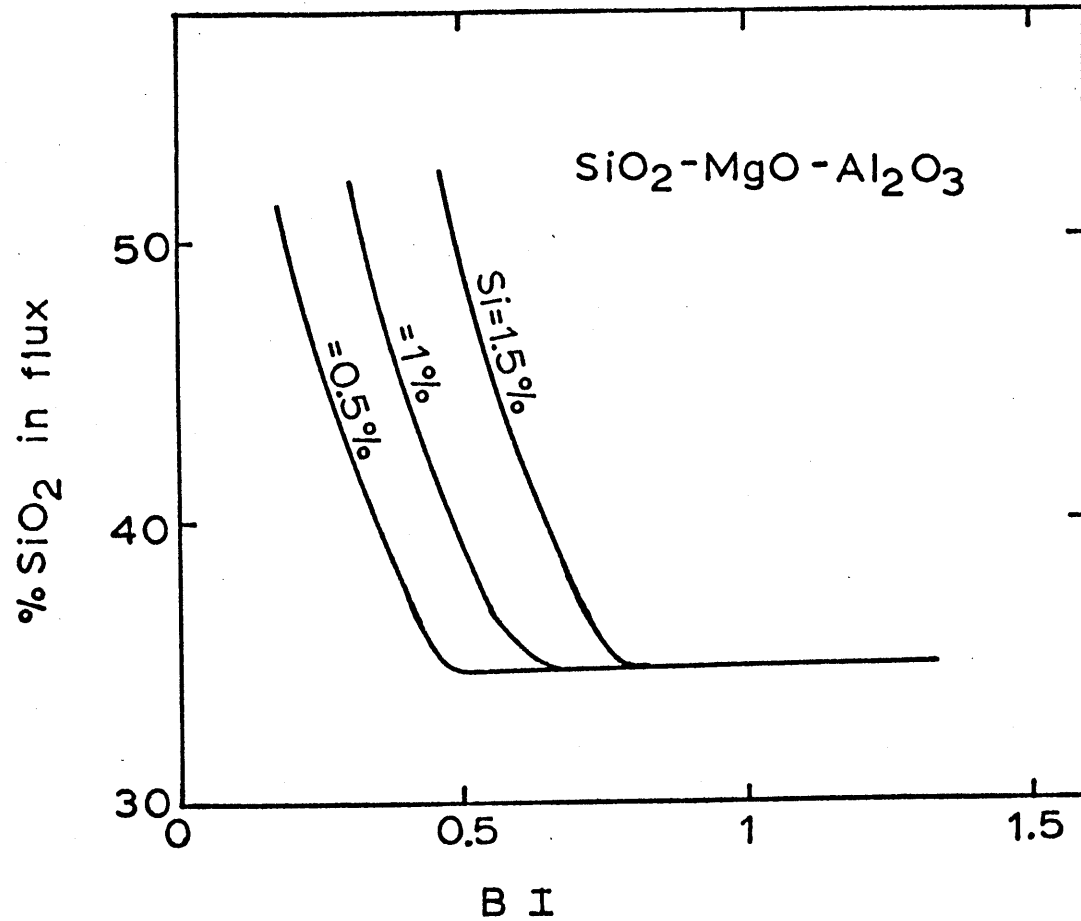assuming 0.1, 0.2, 0.3 and 1% Si in the weld
metal.
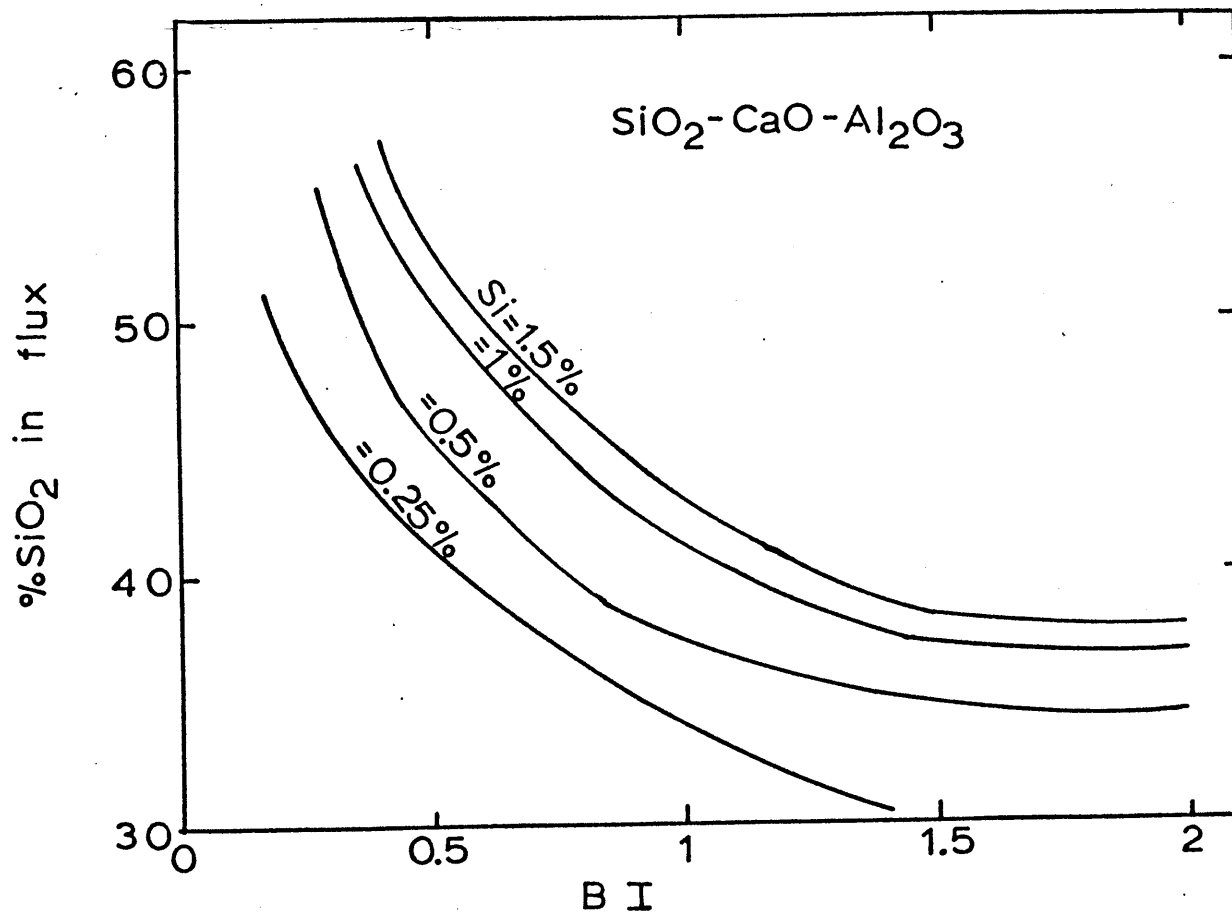
Appendix 3-b: The equilibrium percent SiO_2 at $2000^{O}C$ in the
SiO_2-CaO-Al_2O_3 system as a function of BI,
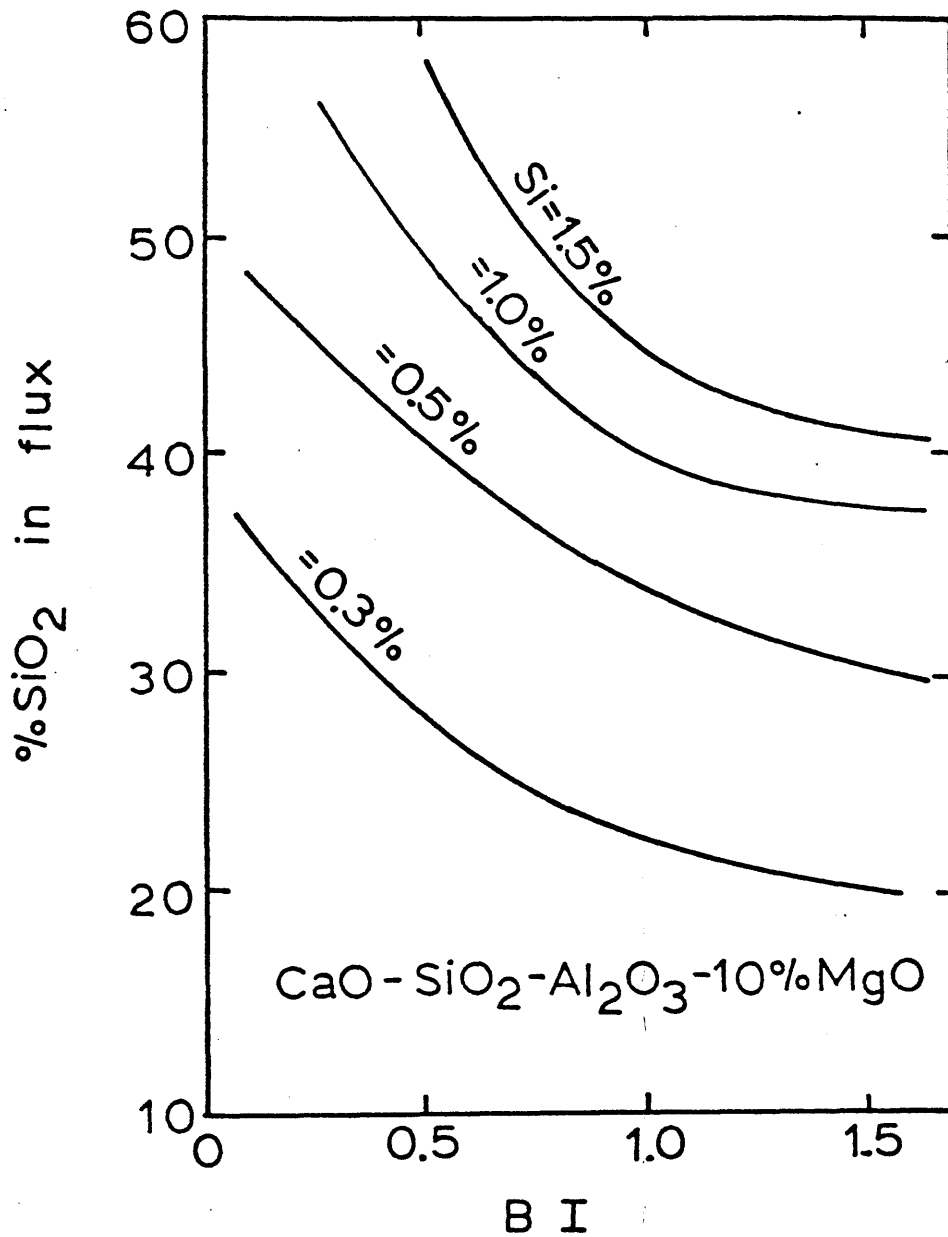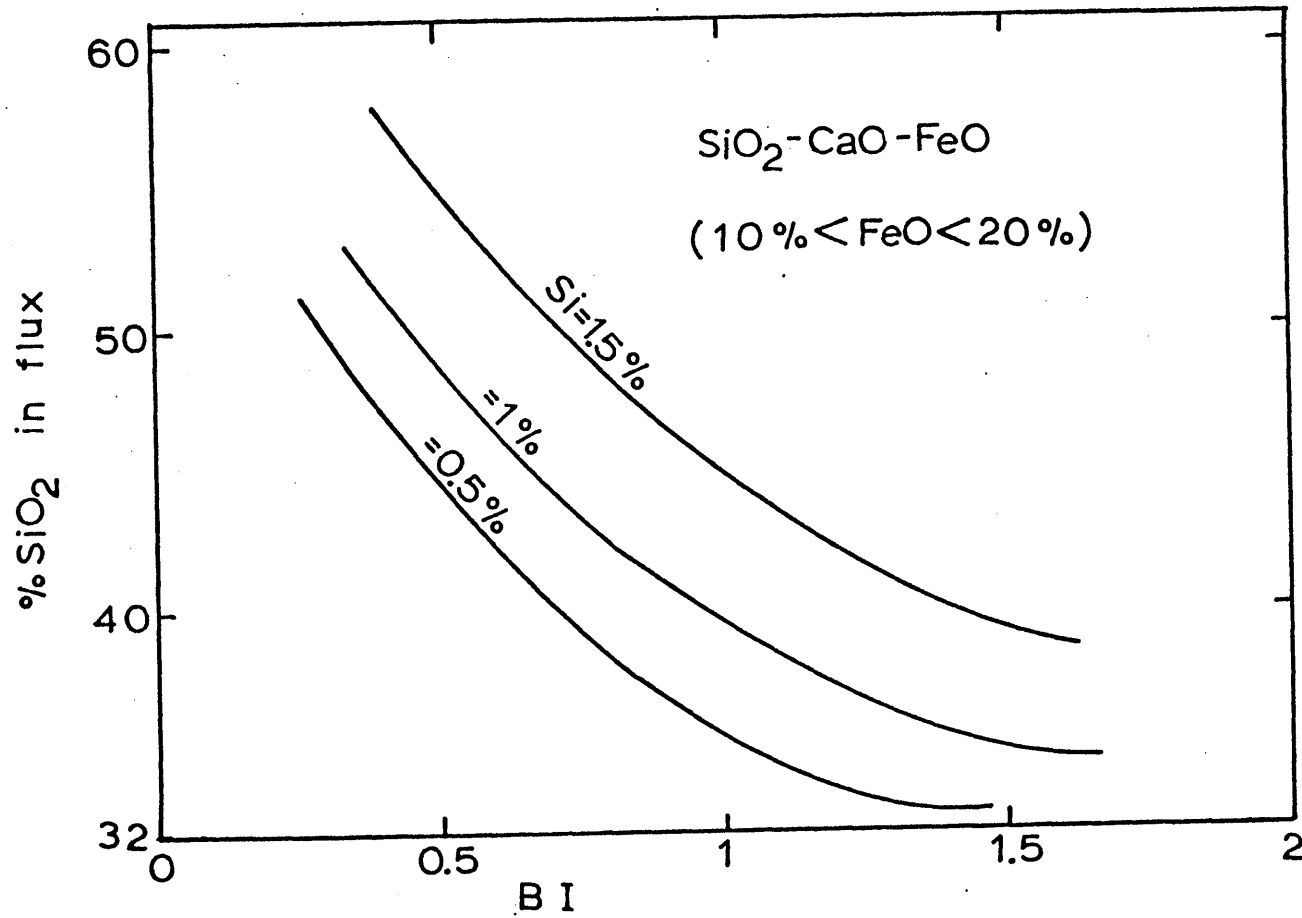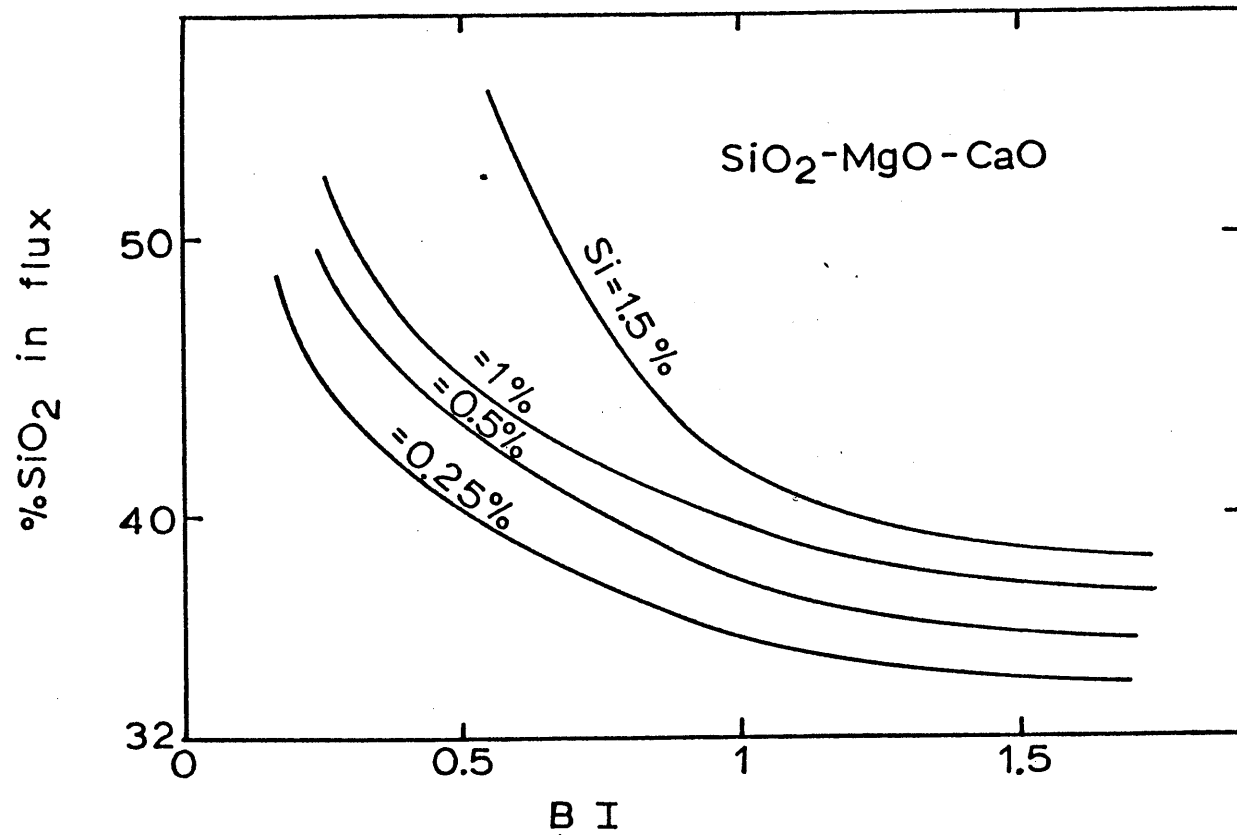assuming 0.25, 0.5, 1 and 1.5% Si in the weld metal.
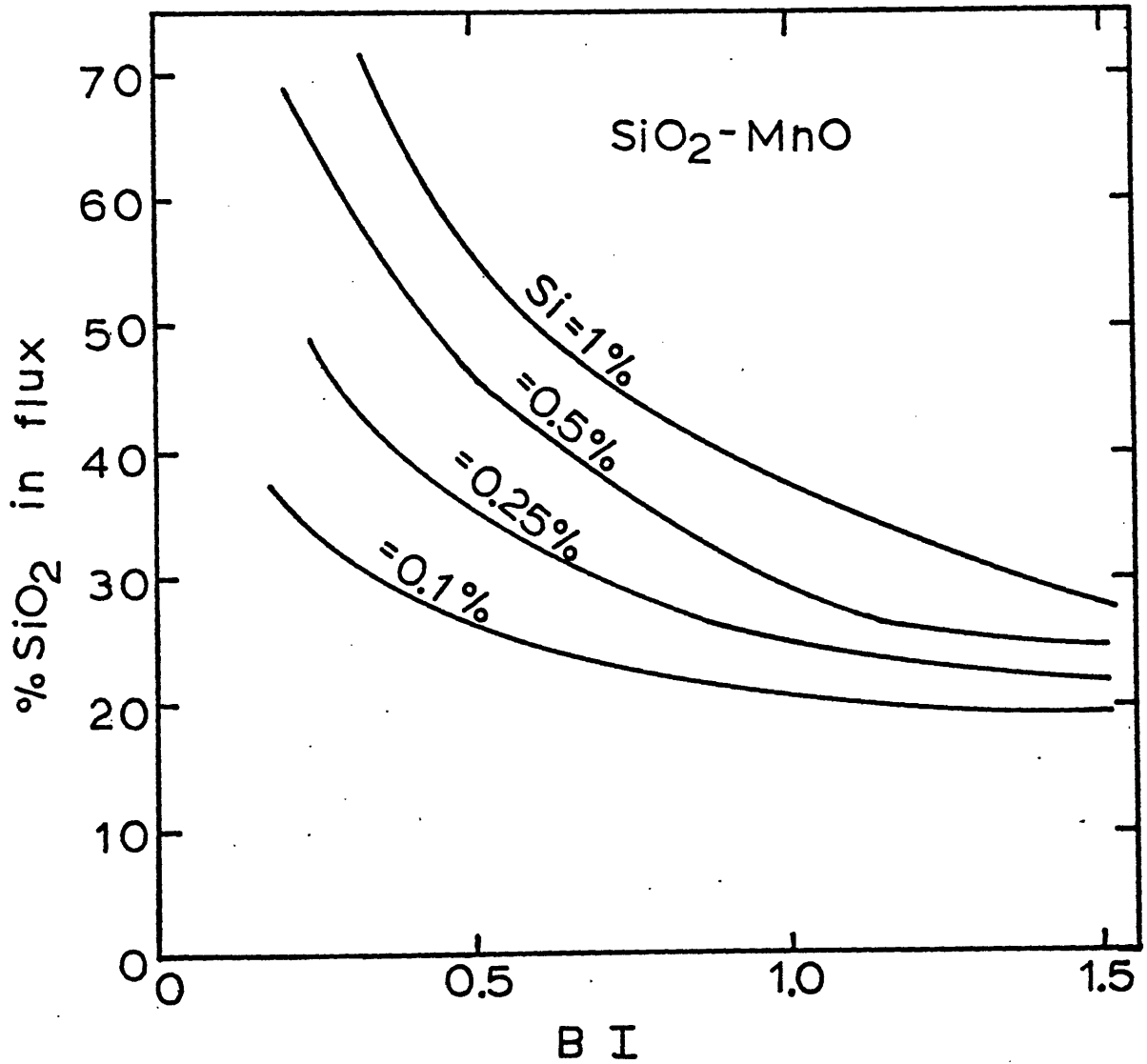
Appendix 3-c: The equilibrium percent SiO_2 at 2000^OC in the SiO_2-MnO system as a function of BI, assuming 0.1, 0.25, 0.5 and 1% Si in the weld metal.
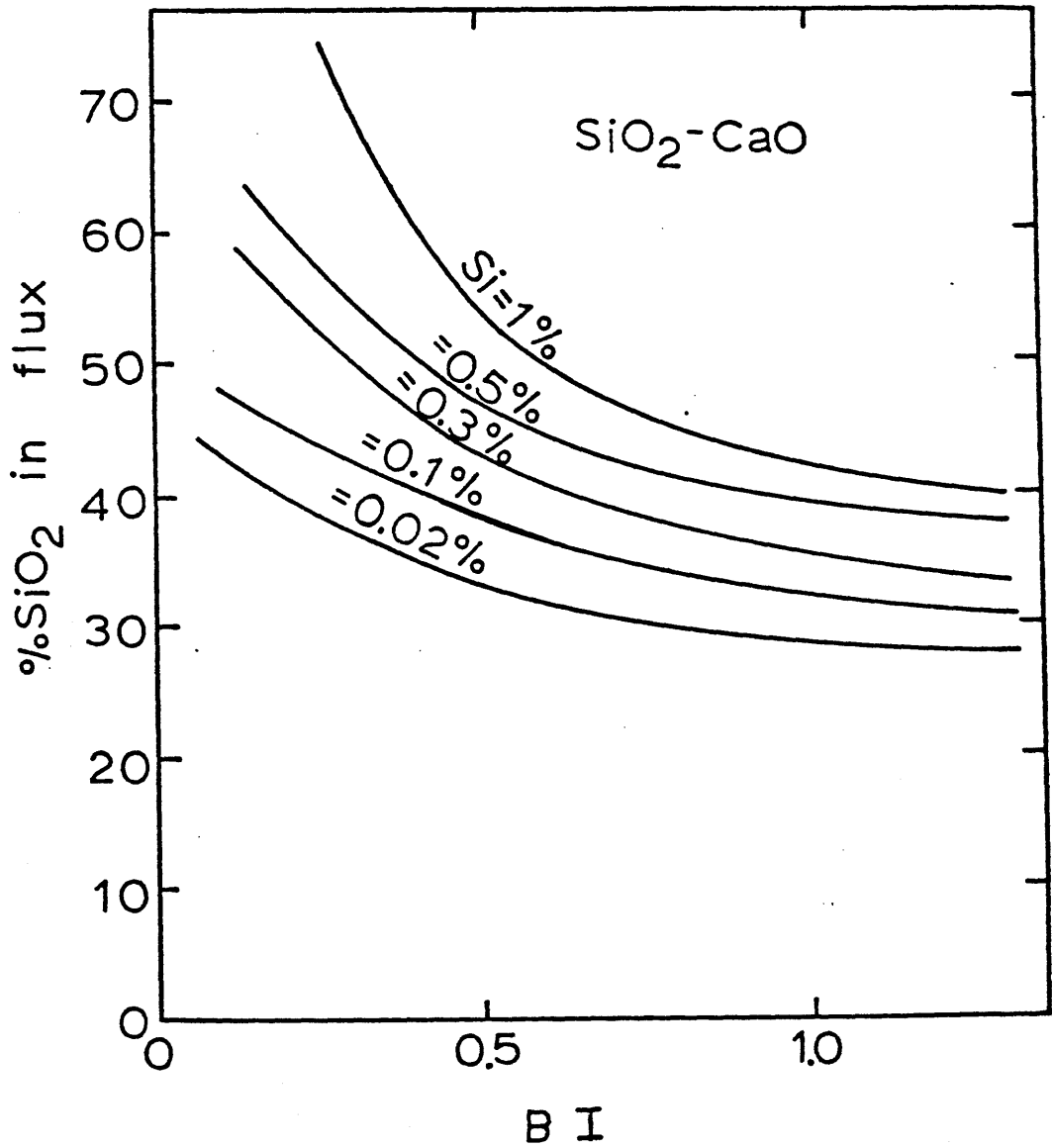
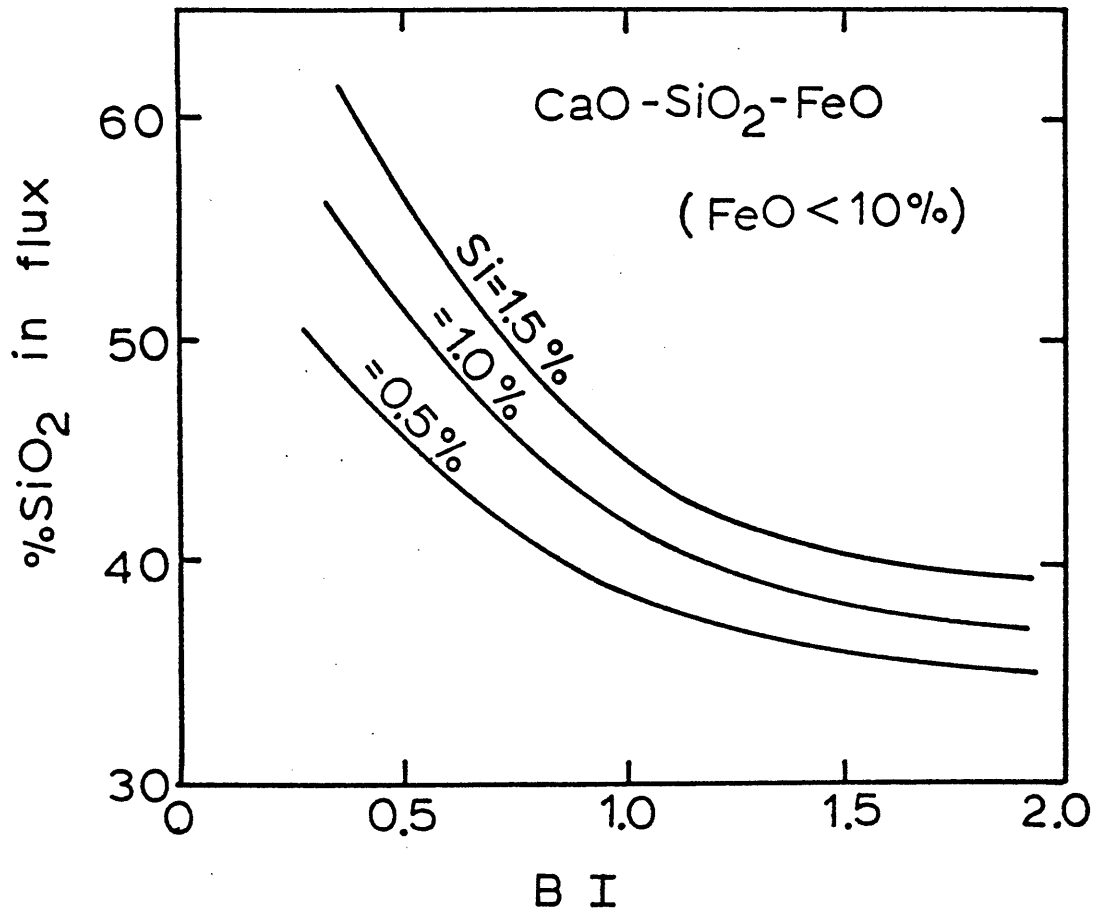Appendix 3-d: The equilibrium percent SiO_2 at $2000^\circ C$ in
the SiO_2-CaO system as a function of BI,
assuming 0.02, 0.1, 0.3, 0.5 and 1% Si in
the weld metal.

Appendix 3-e: The equilibrium percent SiO_2 at 2000°C in the SiO_2-MgO-Al_2O_3 system as a function of BI, assuming 0.5, 1 and 1.5% Si in the weld metal.

Appendix 3-f: The equilibrium percent SiO_2 at $2000^{\circ}C$ in the CaO-SiO_2-Al_2O_3-$10\%MgO$ system as a function of BI, assuming 0.3, 0.5, 1.0 and 1.5% Si in the weld metal.

Appendix 3-g: The equilibrium percent SiO_2 at $2000^{O}C$ in the SiO_2-CaO-FeO ($10\% < FeO < 20\%$) system as a function of BI, assuming 0.5, 1 and 1.5% Si in the weld metal.
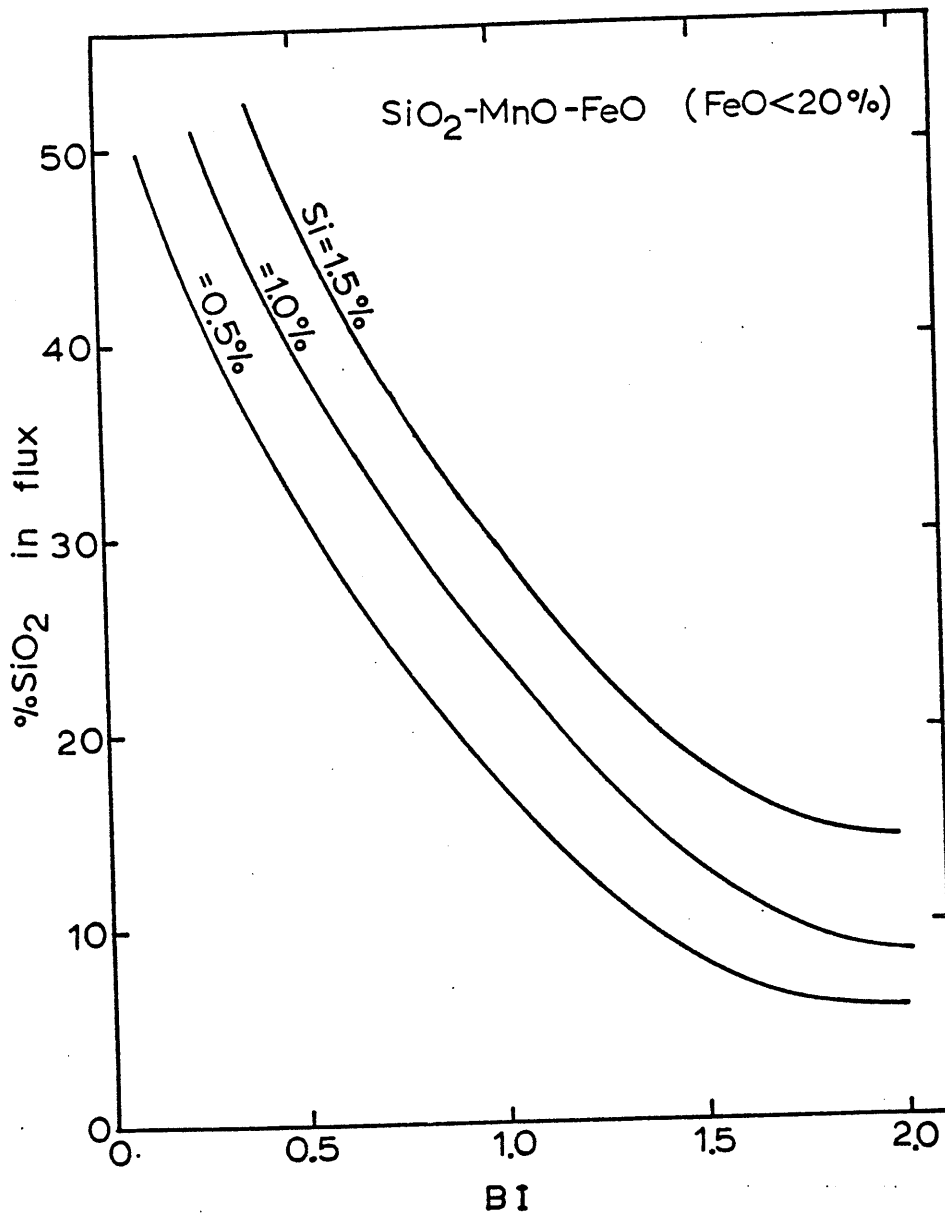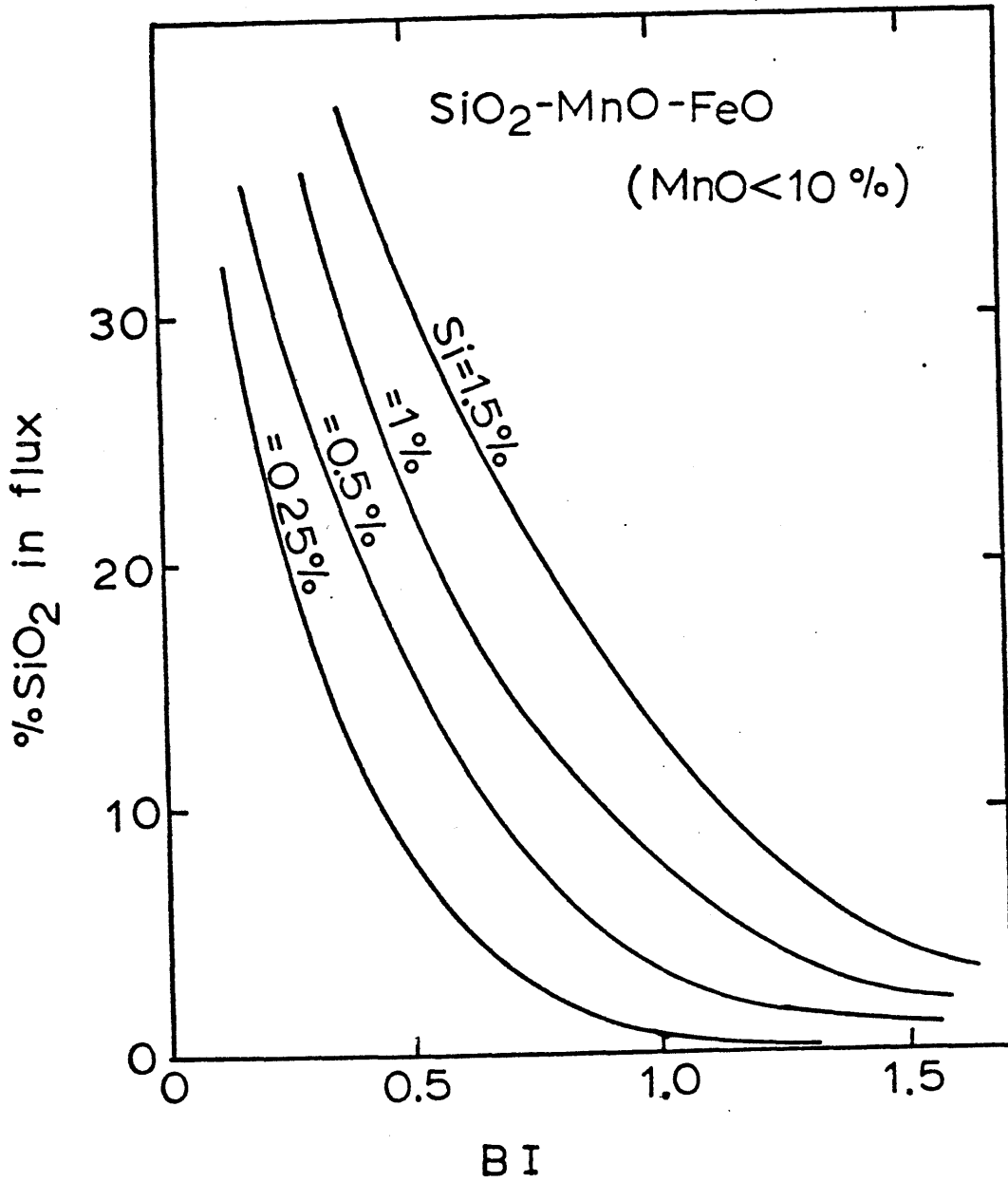
Appendix 3-h: The equilibrium percent SiO$_2$ at 2000°C
in the SiO$_2$-MnO-FeO (FeO<20%) system as
a function of BI, assuming 0.5, 1.0 and
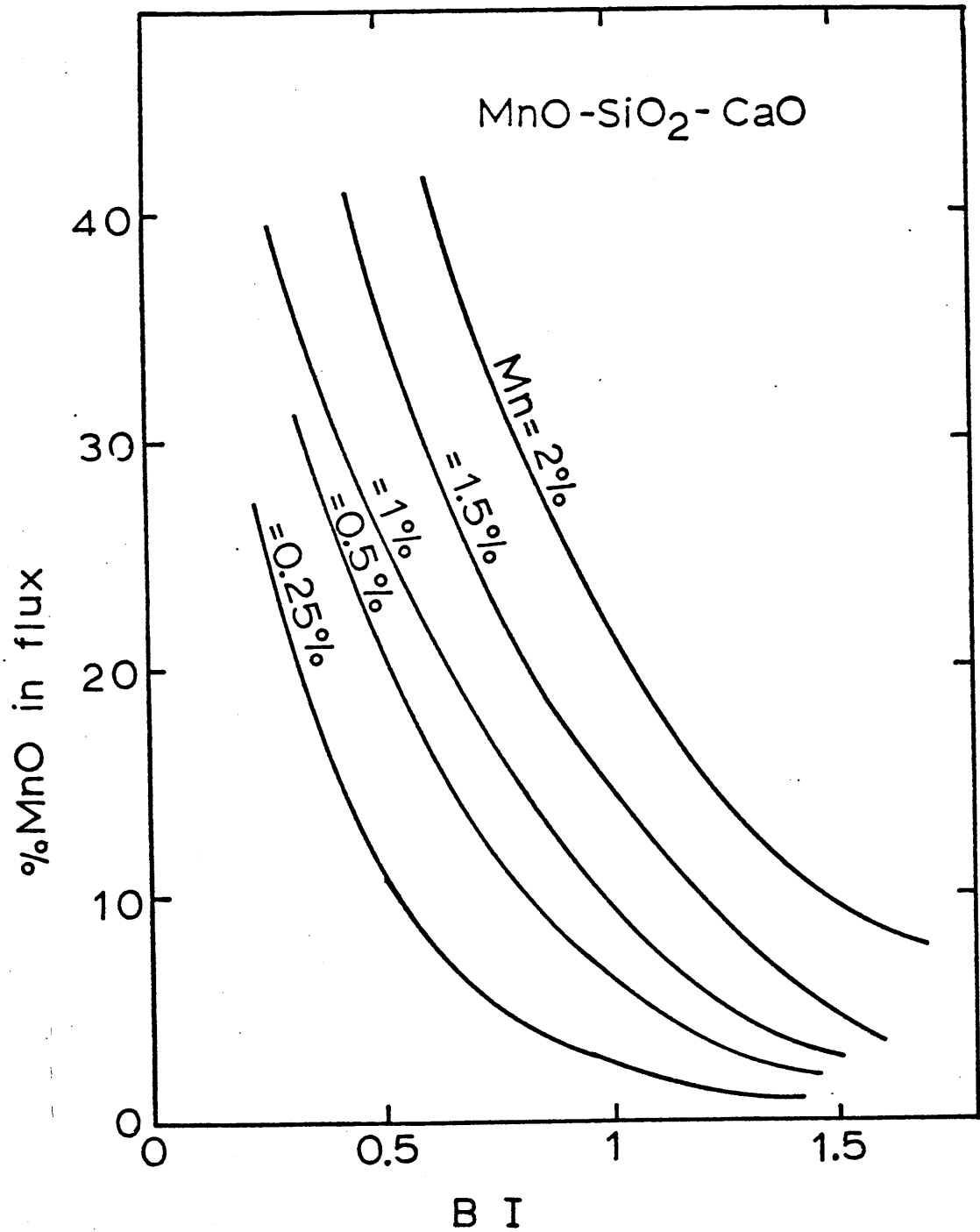1.5% Si in the weld metal.

Appendix 3-i: The equilibrium percent SiO_2 at $2000^{O}C$ in the SiO_2-MgO-CaO system as a function of BI, assuming 0.25, 0.5, 1 and 1.5% Si in the weld metal.
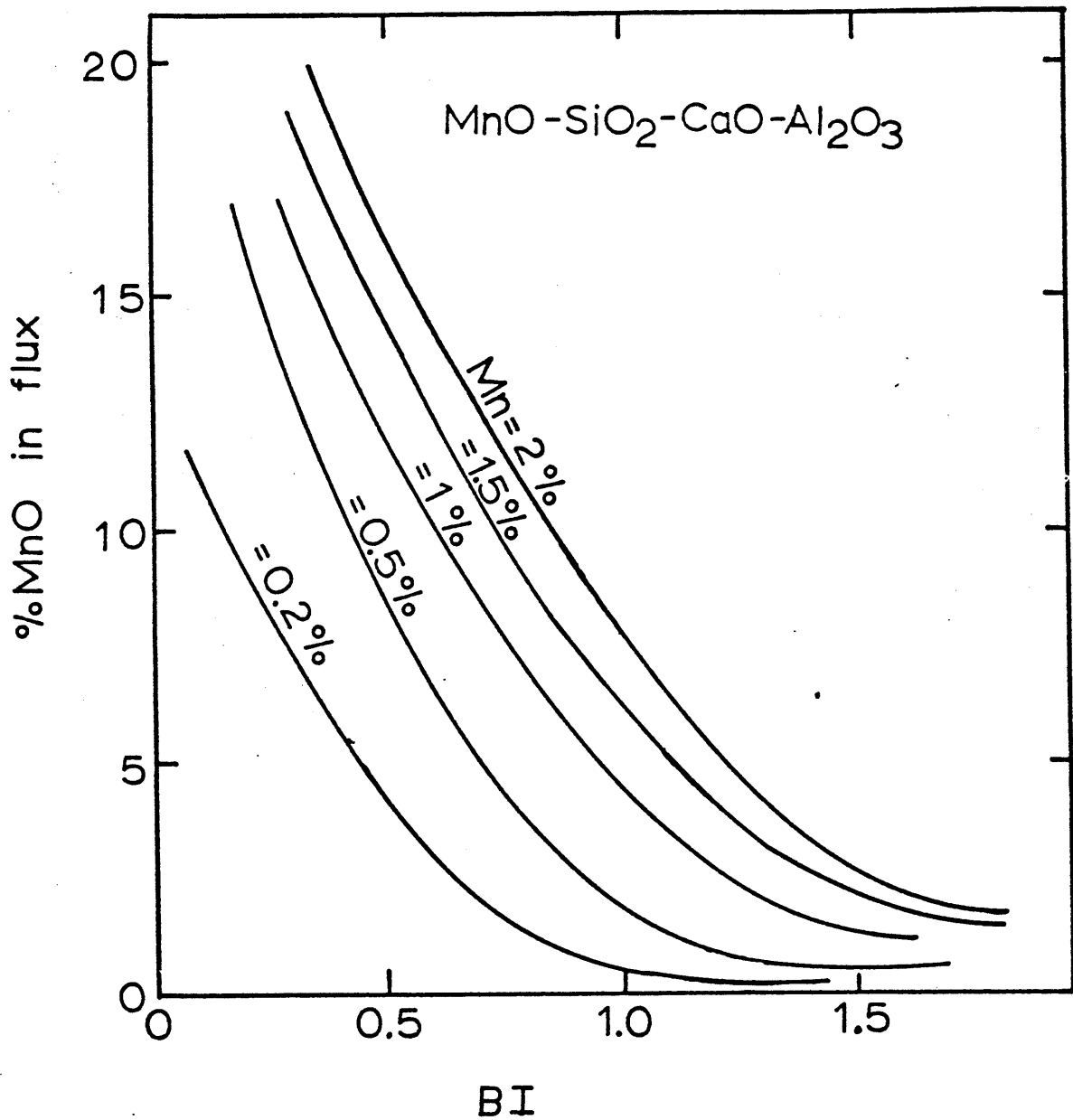
Appendix 3-j: The equilibrium percent SiO$_2$ at 2000°C
in the CaO-SiO$_2$-FeO (FeO<10%) system as
a function of BI, assuming 0.5,1.0 and
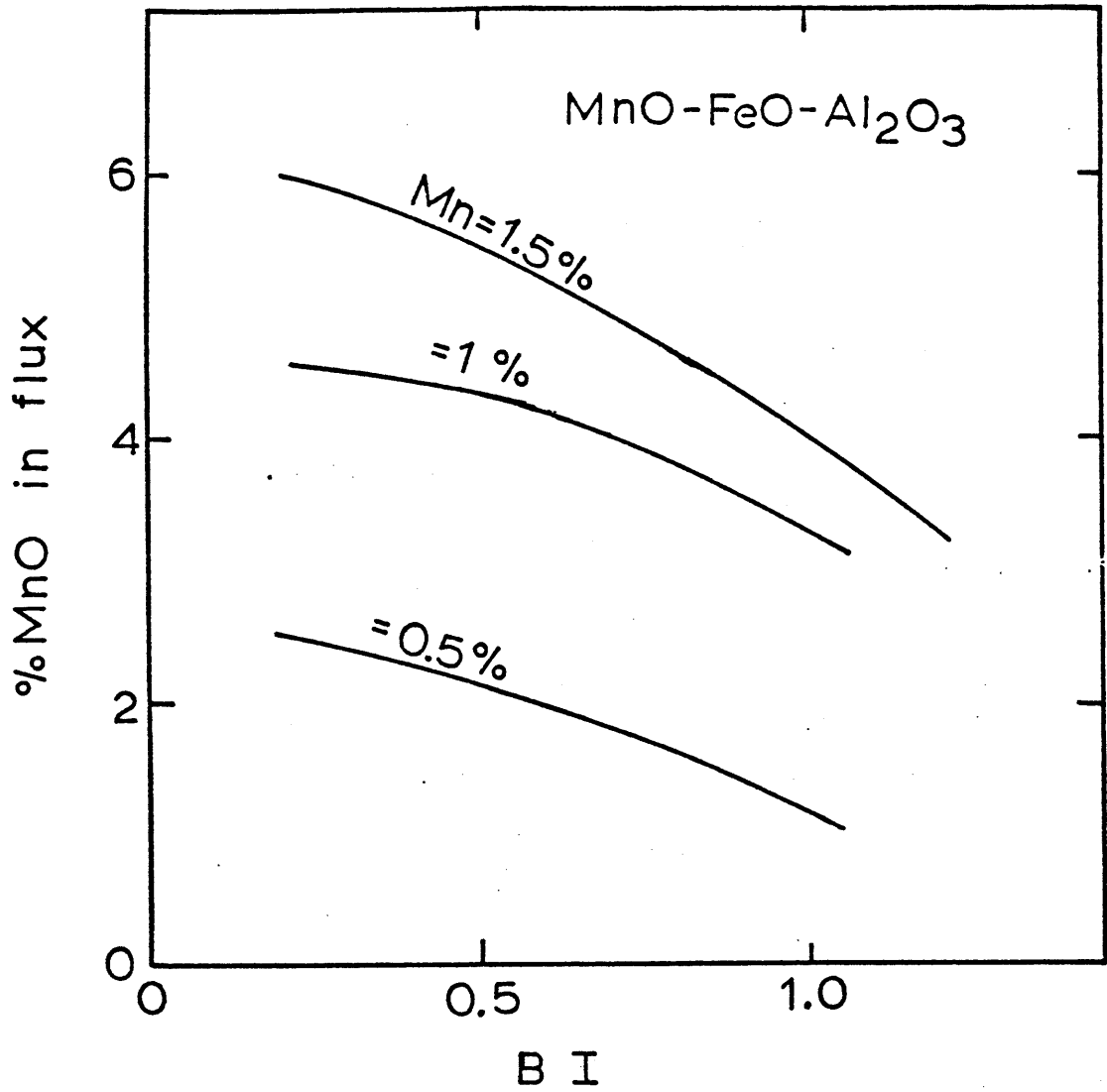1.5% Si in the weld metal.

Appendix 3-k: The equilibrium percent SiO_2 at $2000^\circ C$ in the SiO_2-MnO-FeO (MnO<10%) system as a function of BI, assuming 0.25, 0.5, 1 and 1.5% Si in the weld metal.

Appendix 4-a: The equilibrium percent MnO at 2000°C in the
MnO-SiO$_2$-CaO system as a function of BI,
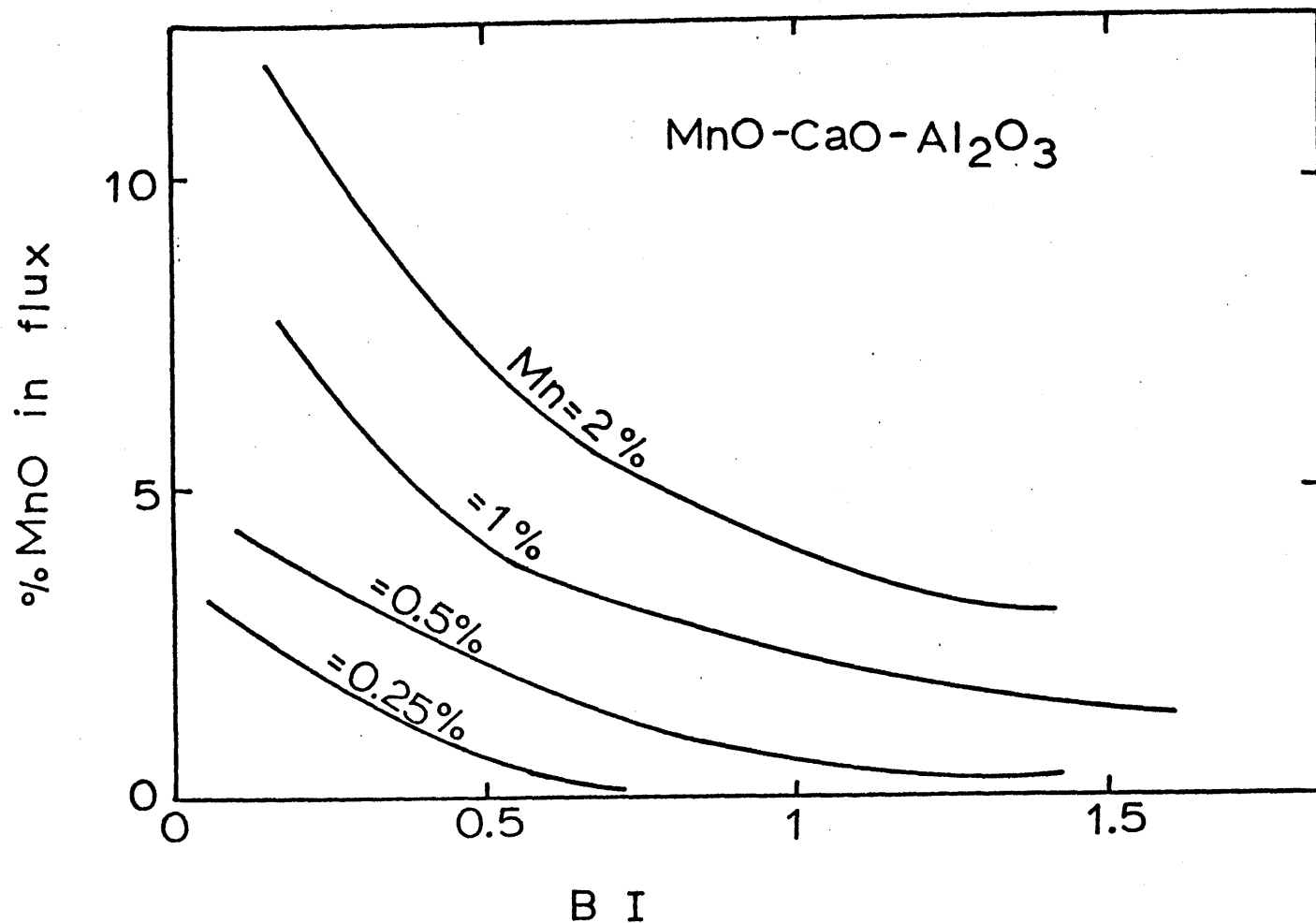assuming 0.25, 0.5, 1, 1.5 and 2% Mn in the
weld metal.

Appendix 4-b: The equilibrium percent MnO at $2000^{\circ}C$ in the MnO-SiO$_2$-CaO-Al$_2$O$_3$ system as a function of BI, assuming 0.2, 0.5, 1, 1.5 and 2% Mn in the weld metal.
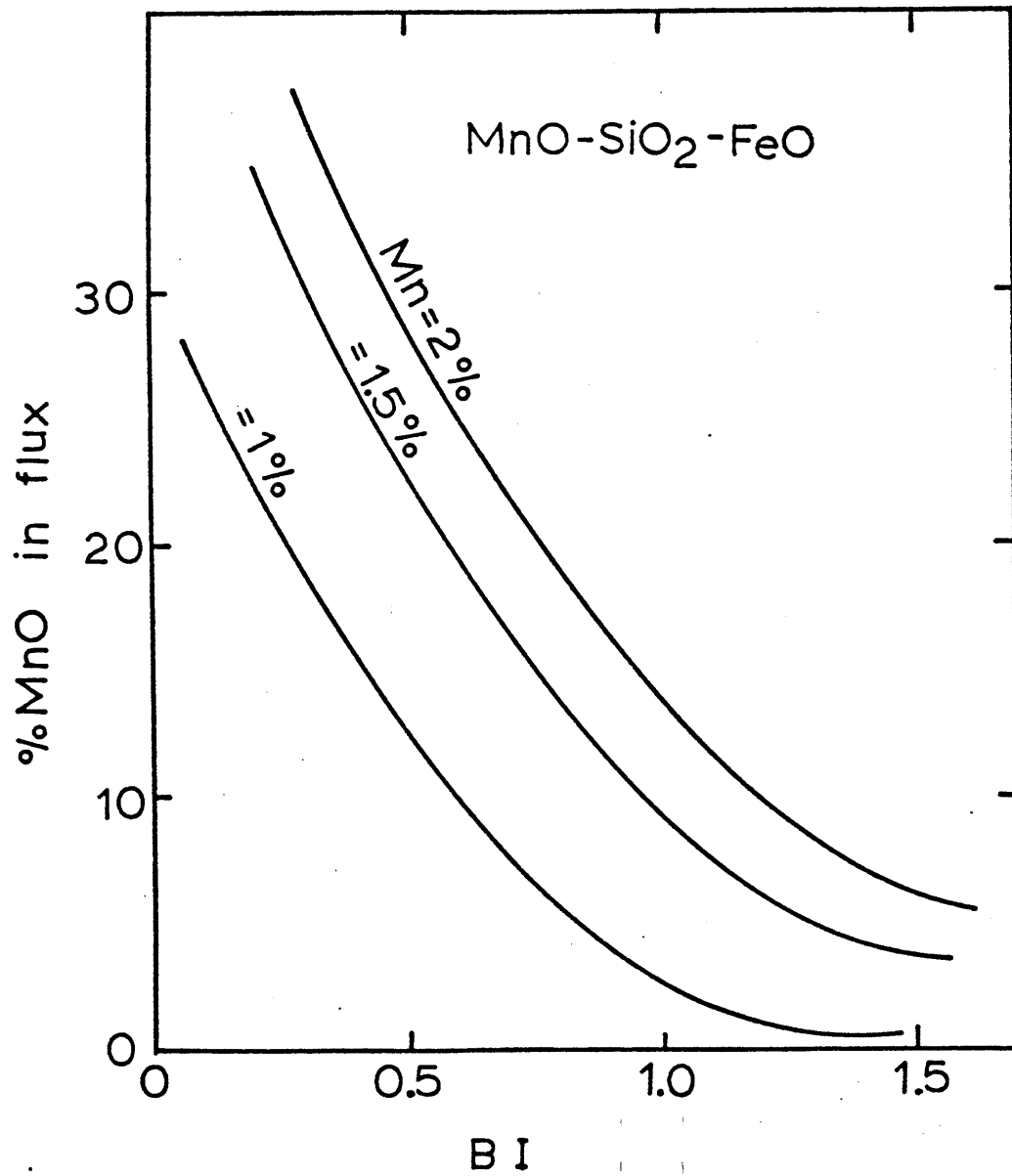
Appendix 4-c: The equilibrium percent MnO at 2000°C in
the MnO-FeO-Al$_2$O$_3$ system as a function
of BI, assuming 0.5, 1 and 1.5 % Mn in the
weld metal.

Appendix 4-d: The equilibrium percent MnO at 2000°C in the MnO-CaO-Al_2O_3 system as a function of BI, assuming 0.25, 0.5, 1 and 2% Mn in the weld metal.
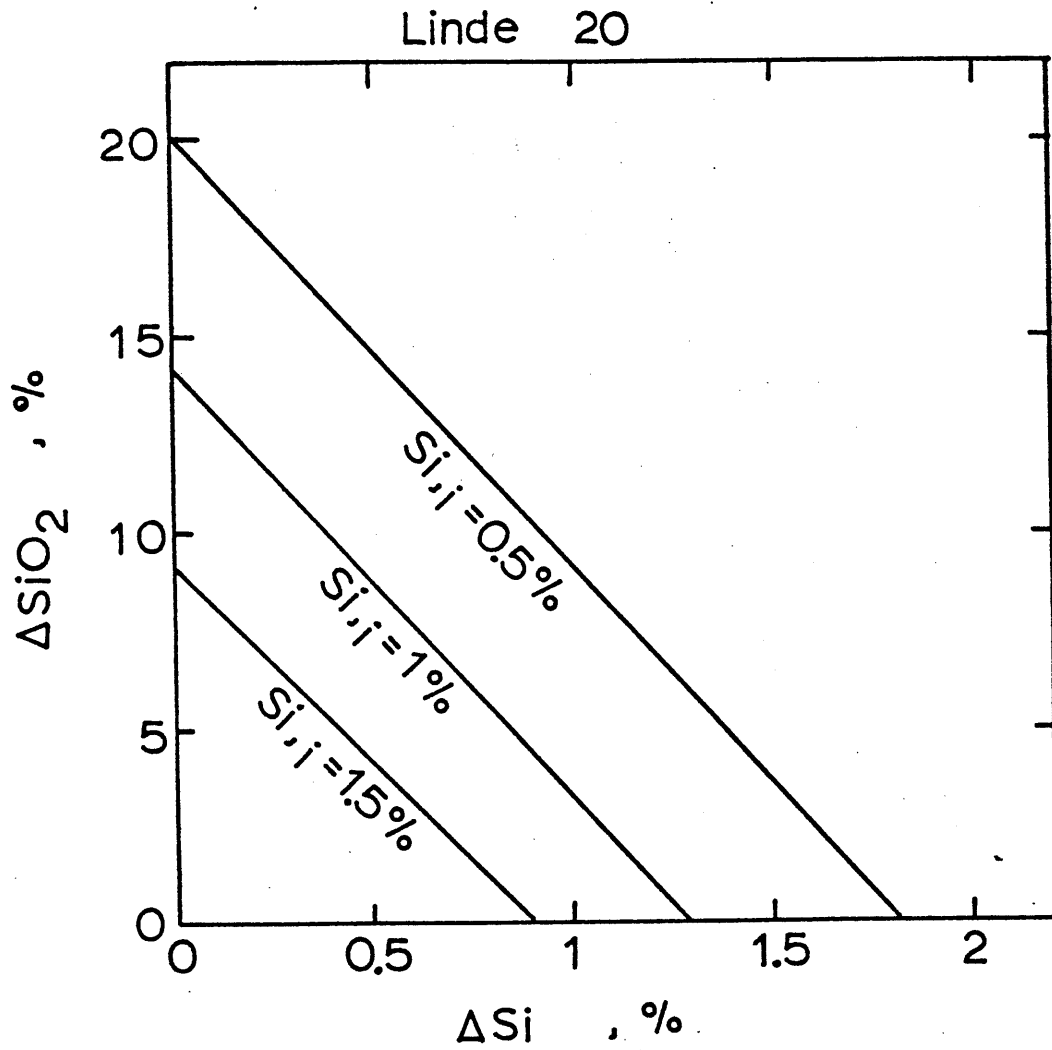
Appendix 4-e: The equilibrium percent MnO at $2000^{O}C$ in the
the MnO-SiO$_2$-FeO system as a function of
BI, assuming 1, 1.5 and 2% Mn in the weld
metal.

Linde 20

Appendix 5-a: The estimated permissible range of change
of Si in the weld metal with 0.5, 1 and
1.5% initial Si for Linde 20 flux.

Linde 50
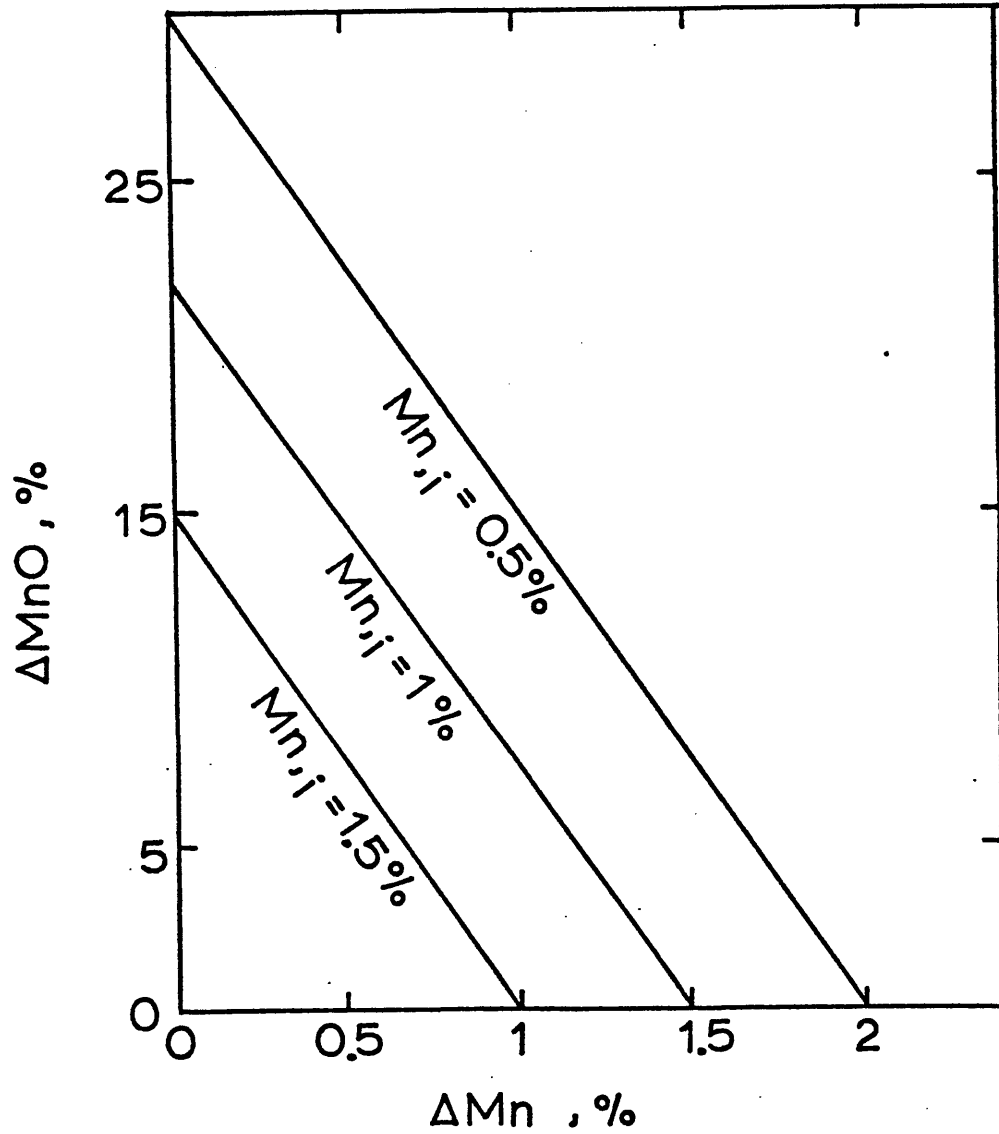
Appendix 5-b: The estimated permissible range of
change of Mn in the weld metal with
0.5, 1 and 1.5% initial Mn for
Linde 50 flux.

Linde 50

Appendix 5-c: The estimated permissible range of change of Si in the weld metal with 0.5, 1 and 2% initial Si for Linde 50 flux.

Linde-60

Appendix 5-d: The estimated permissible range of change of Si in the weld metal with 0.1, 0.3 and 0.5% initial Si for Linde 60 flux.

Linde   60
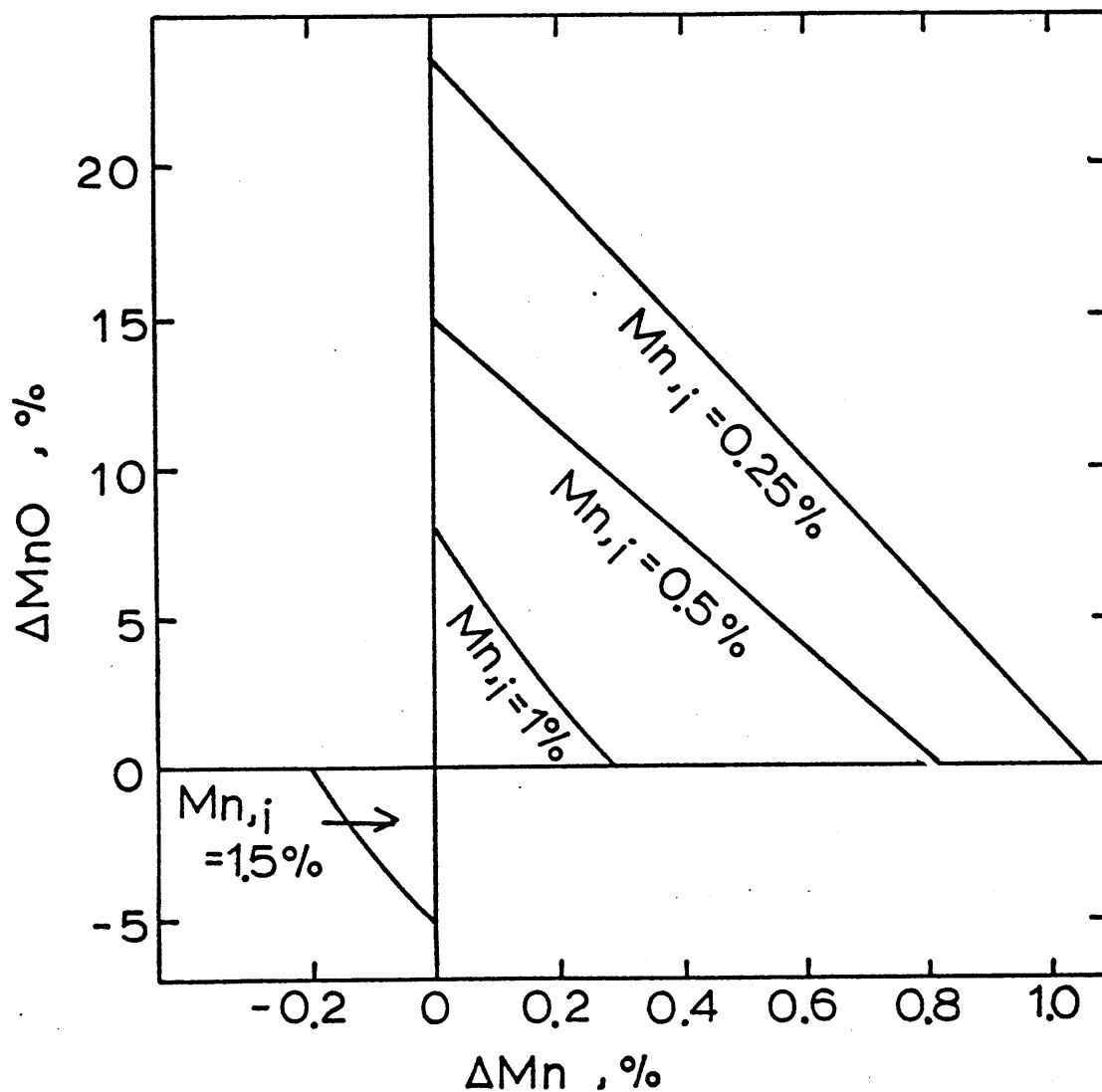
Appendix 5-e: The estimated permissible range of change
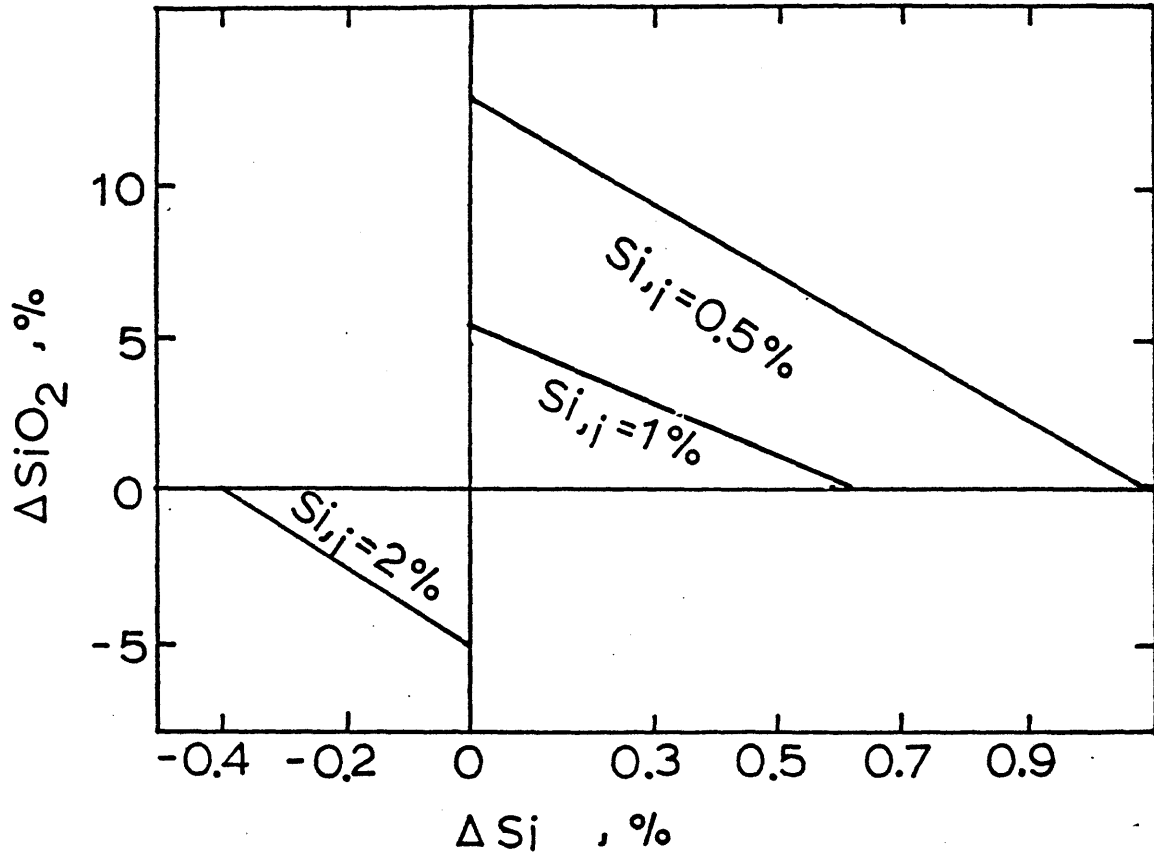of Mn in the weld metal with 0.25, 0.5, 1
and 1.5% initial Mn for Linde 60 flux.
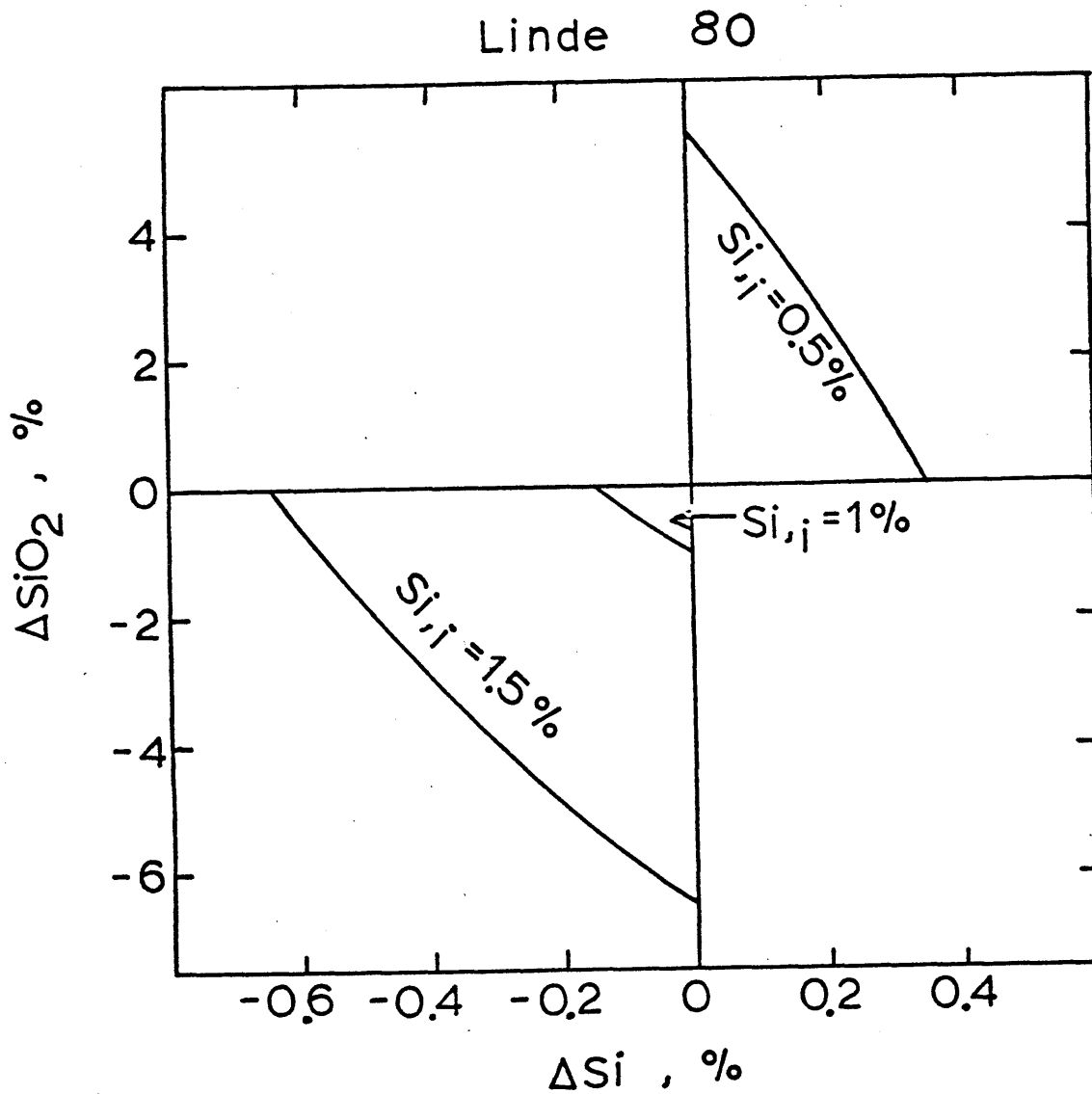
Appendix 5-f: The estimated permissible range of change
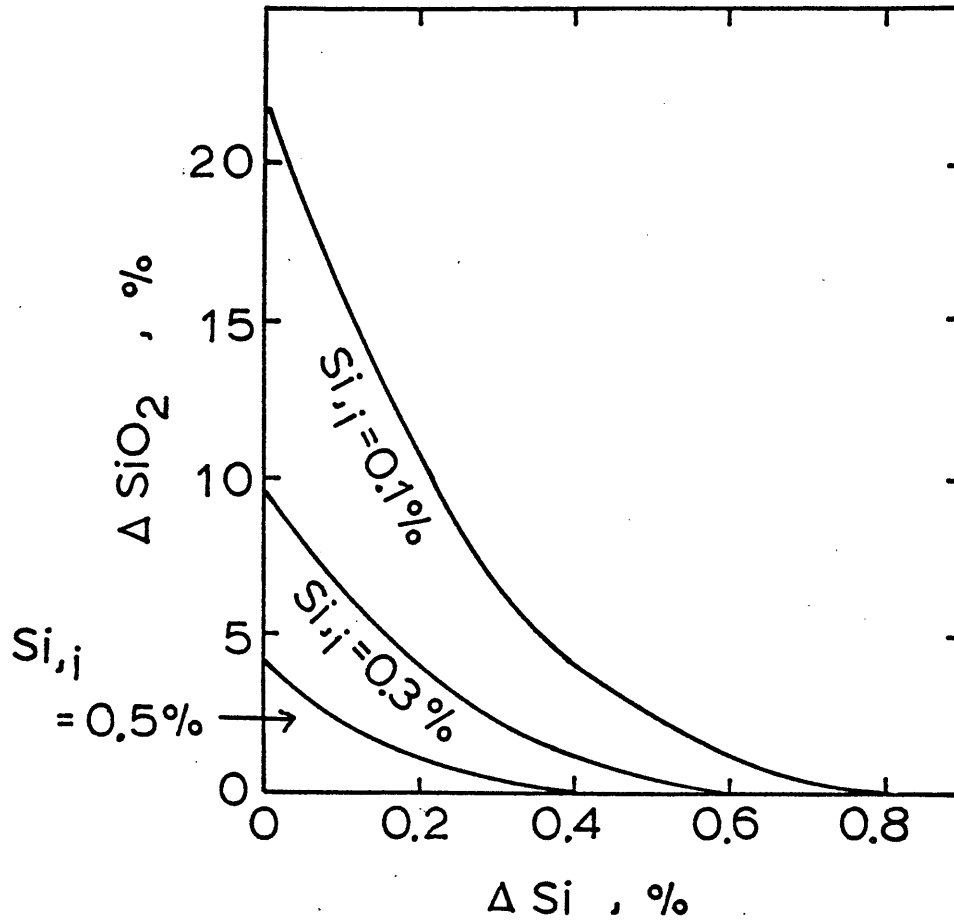of Si in the weld metal with 0.5, 1 and
1.5% initial Si for Linde 80 flux.
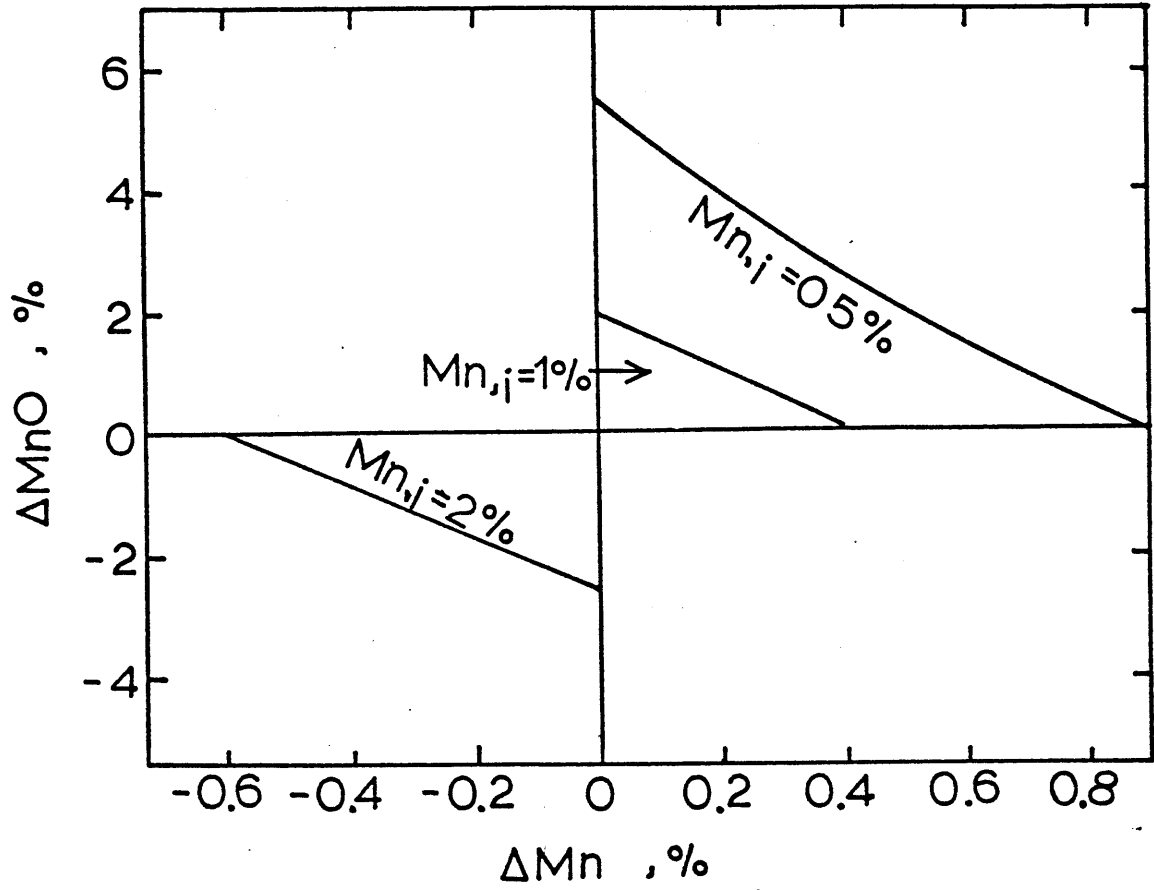
Appendix 5-g: The estimated permissible range of change of
Mn in the weld metal with 0.5, 1 and 2%
initial Mn for Linde 80 flux.
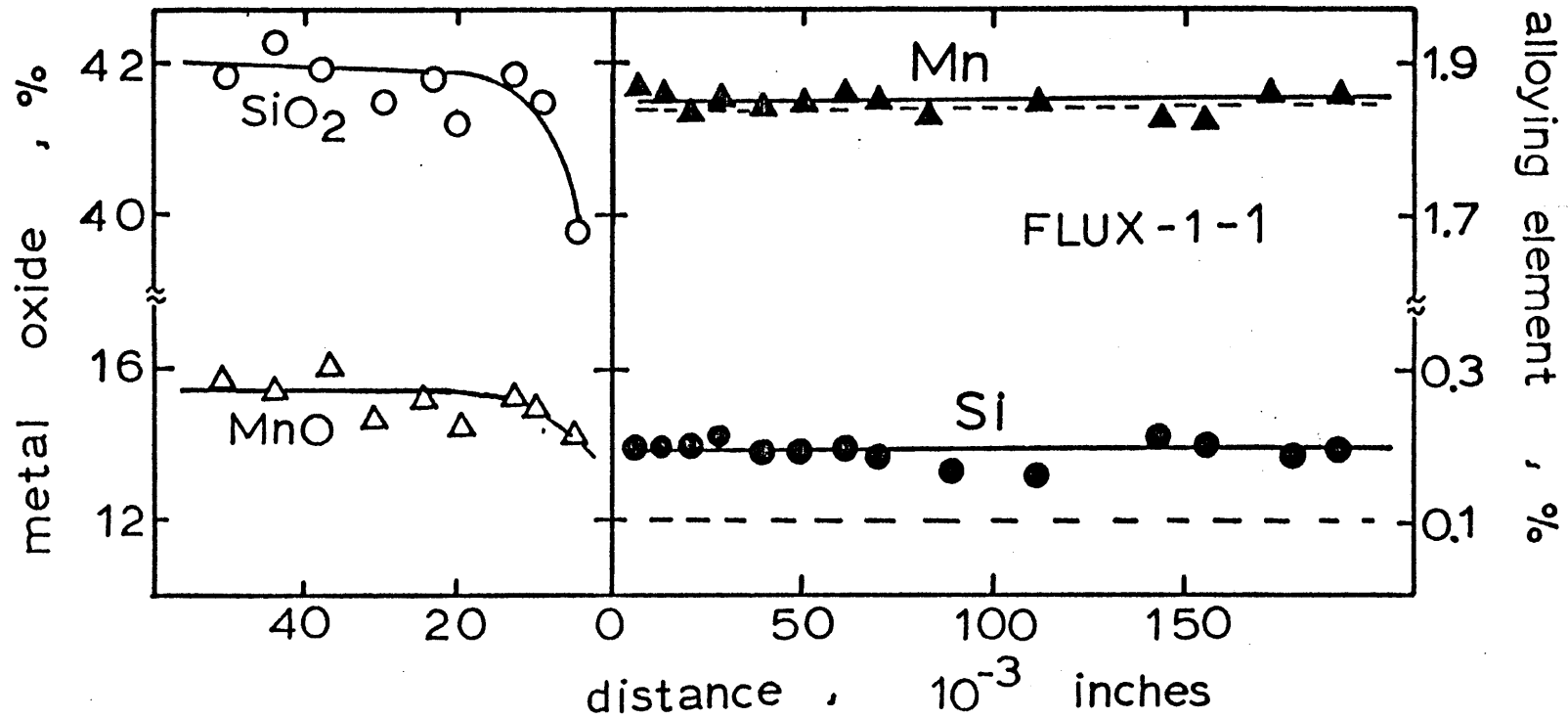
Appendix 6-a: The spatial distribution of Mn and Si in both the metal and slag phases for weld 1-1. Dashed lines are the initial values.
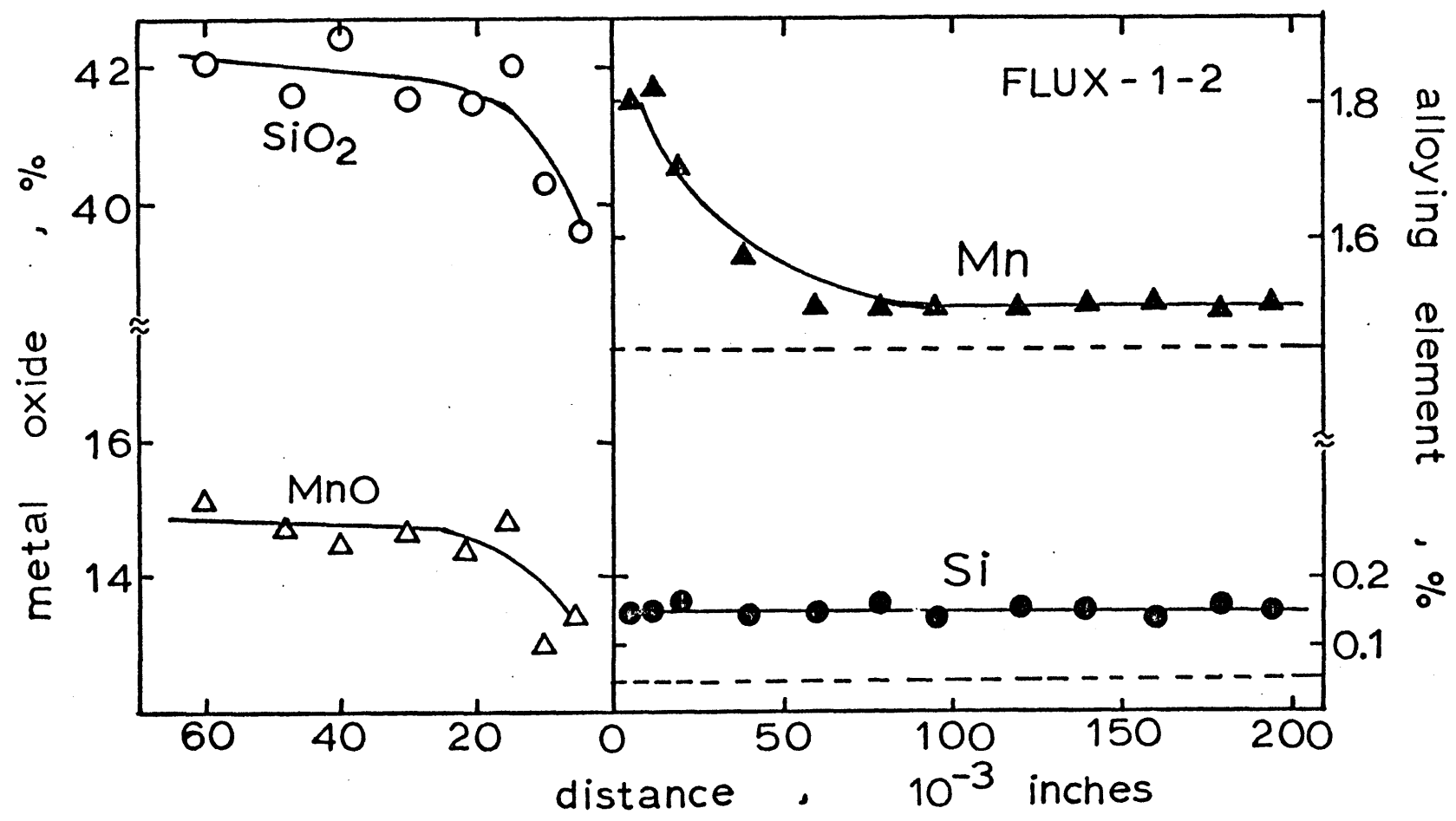
Appendix 6-b: The spatial distribution of Mn and Si in both the metal and slag phases for weld 1-2. Dashed lines are the initial values.
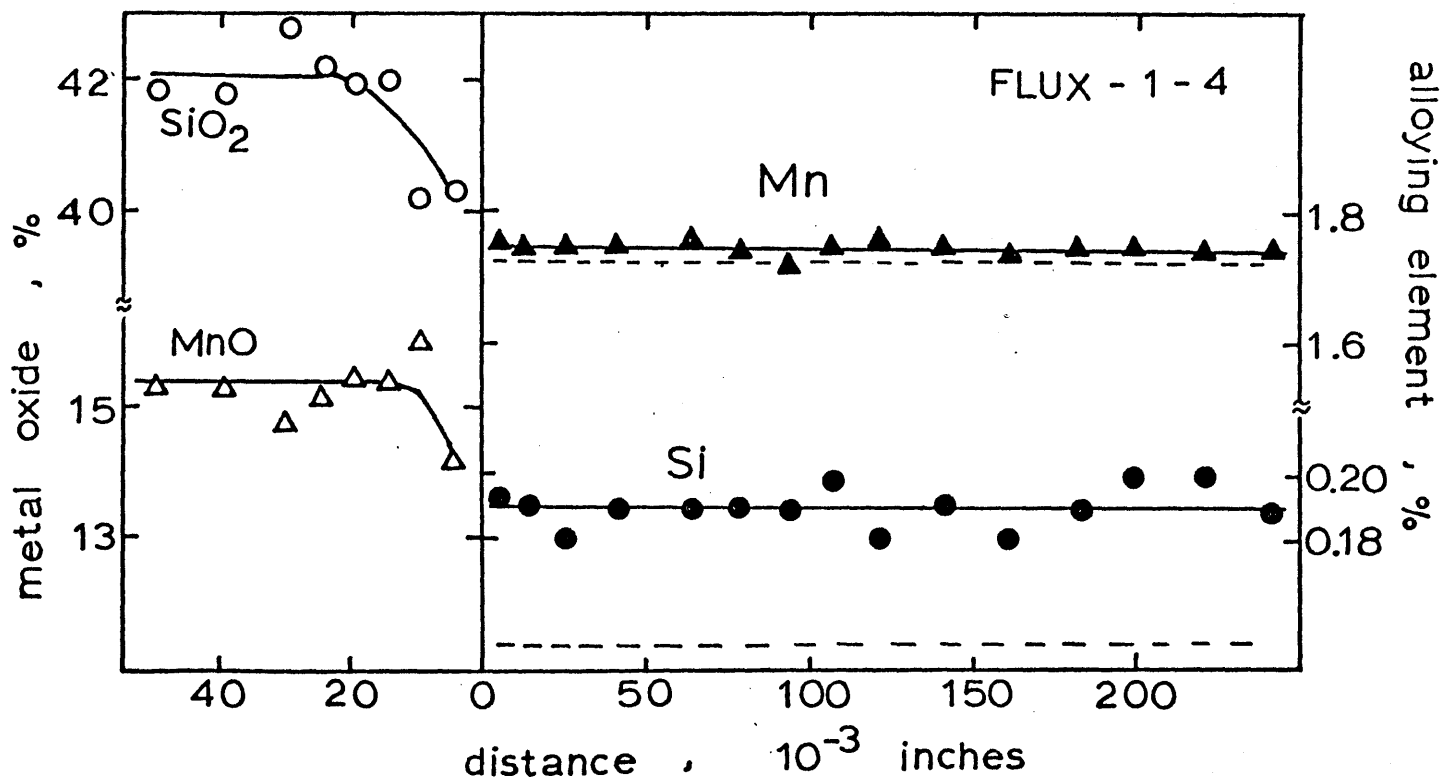
Appendix 6-c: The spatial distribution of Mn and Si in both the slag and metal phases for weld 1-4. Dashed lines are the initial values.
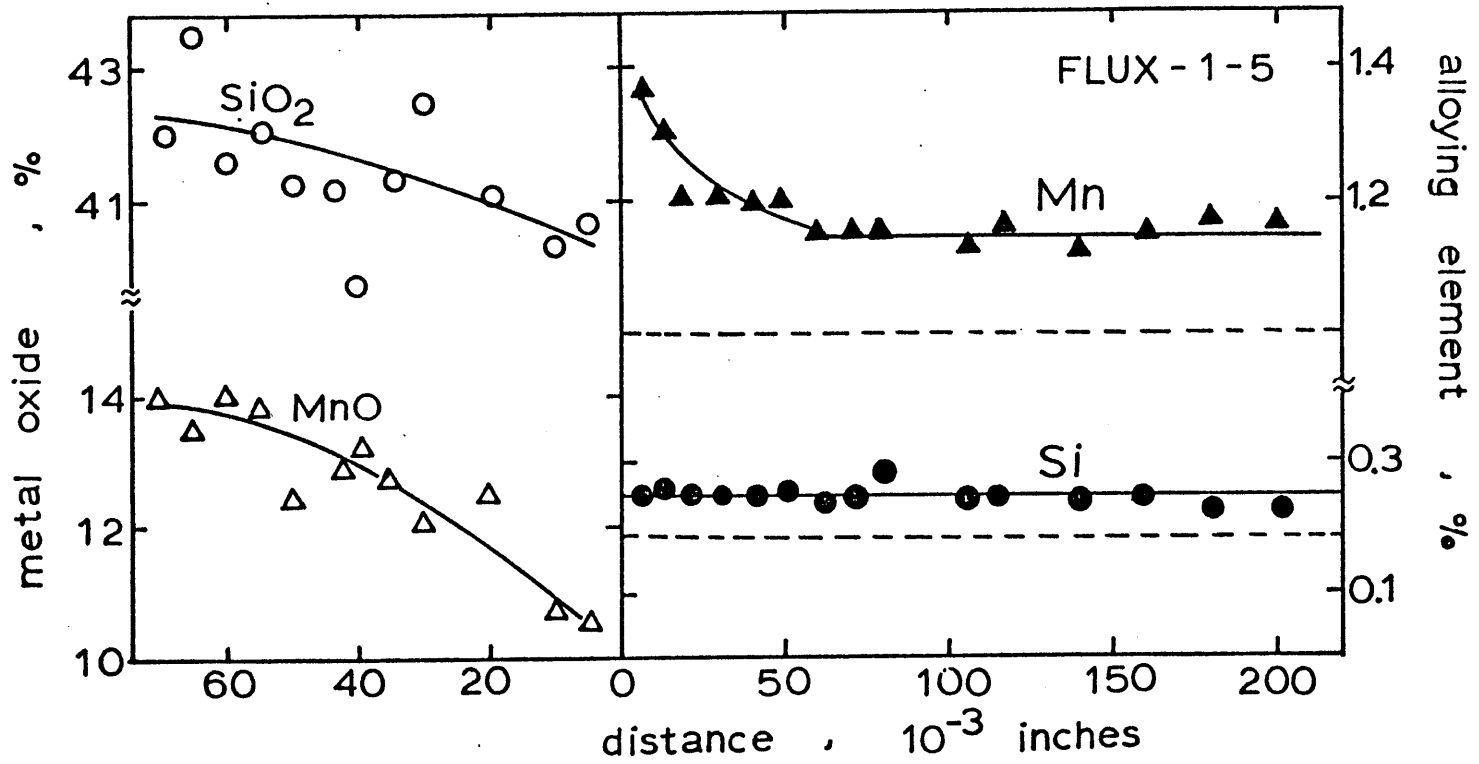
Appendix 6-d: The spatial distribution of Mn and Si in both the slag and the metal phases for weld 1-5. Dashed lines are the initial values.
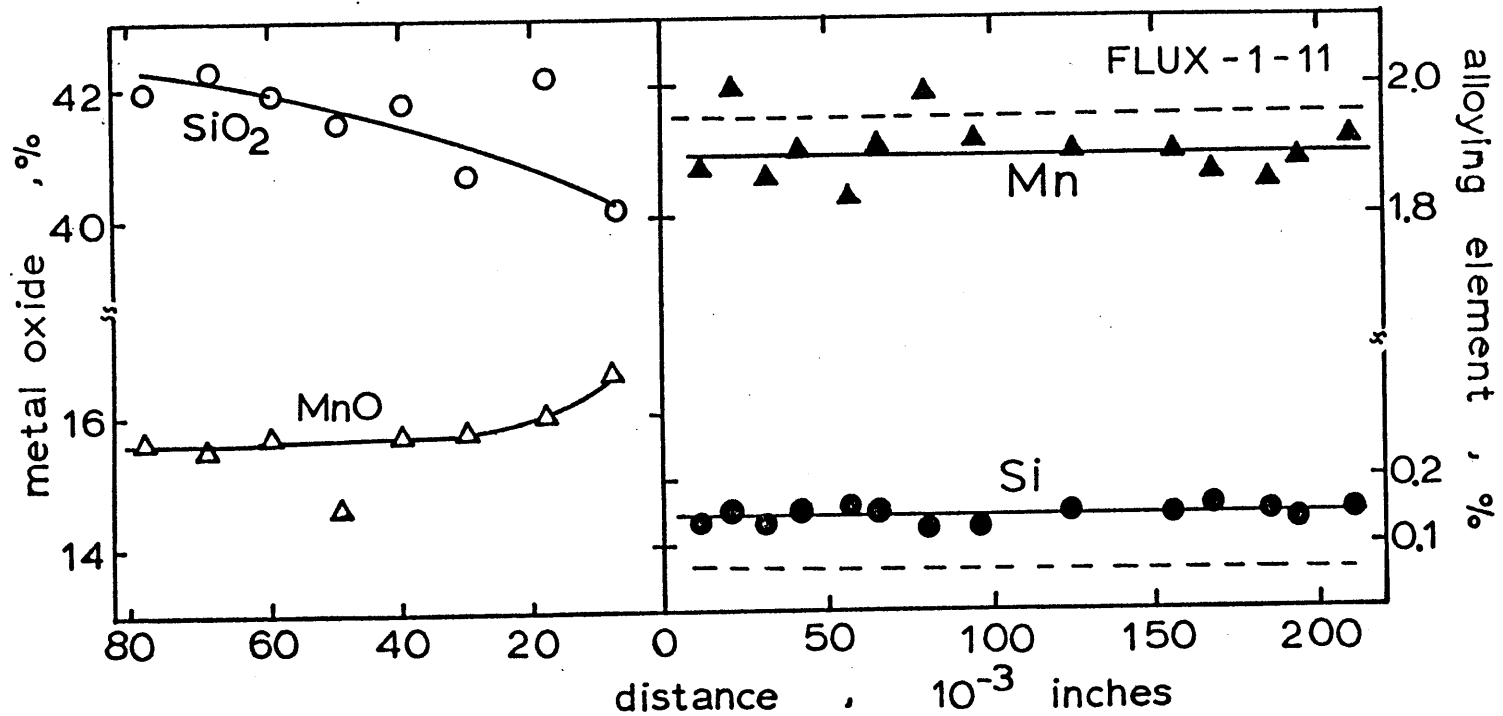
Appendix 6-e: The spatial distribution of Mn and Si in both the slag and the metal phases for weld 1-11. Dashed lines are the initial values.
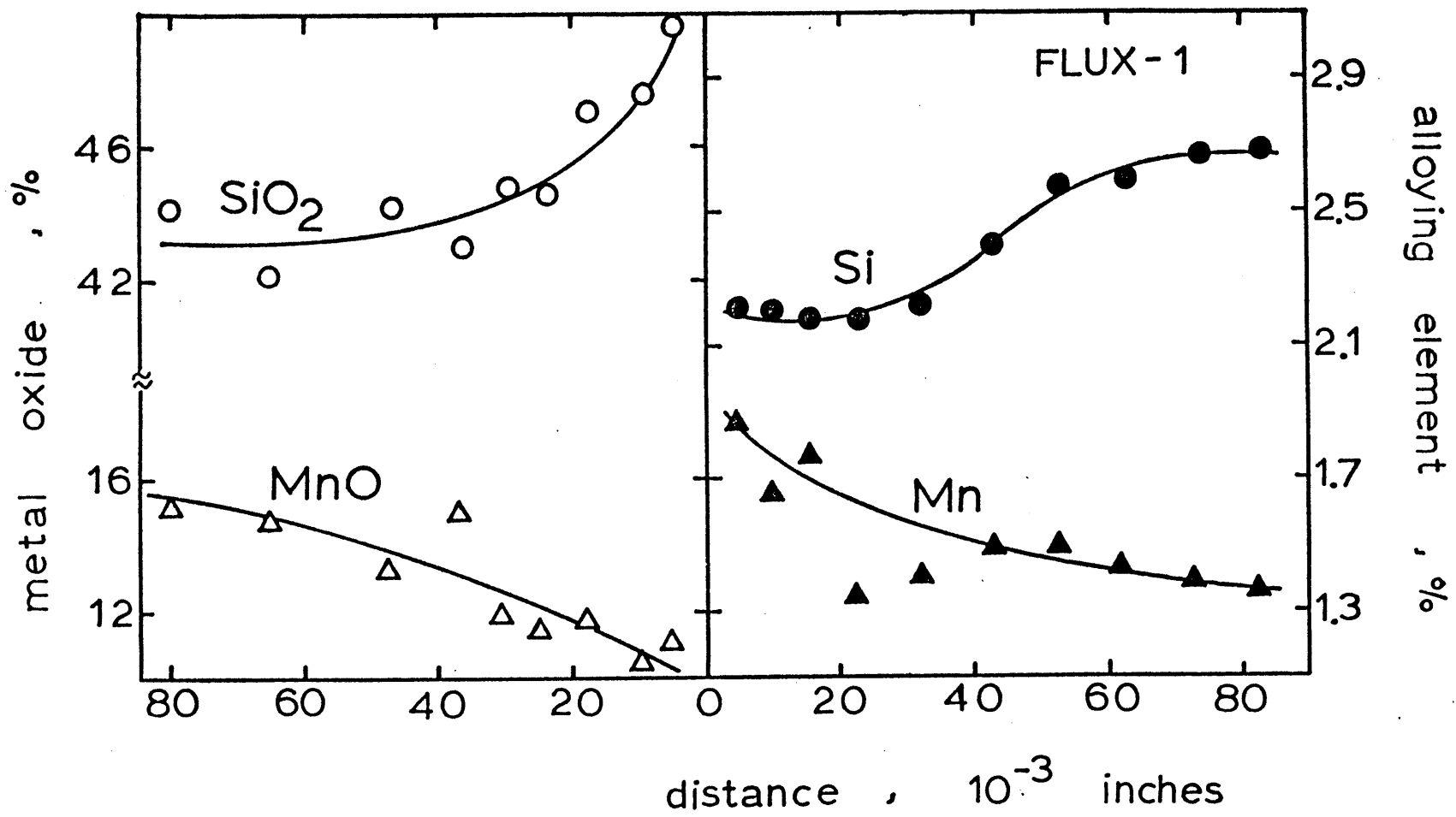
Appendix 6-f: The spatial distribution of Mn and Si in both the slag and metal phases for weld made with Flux-1 and 3.22% Si plate.
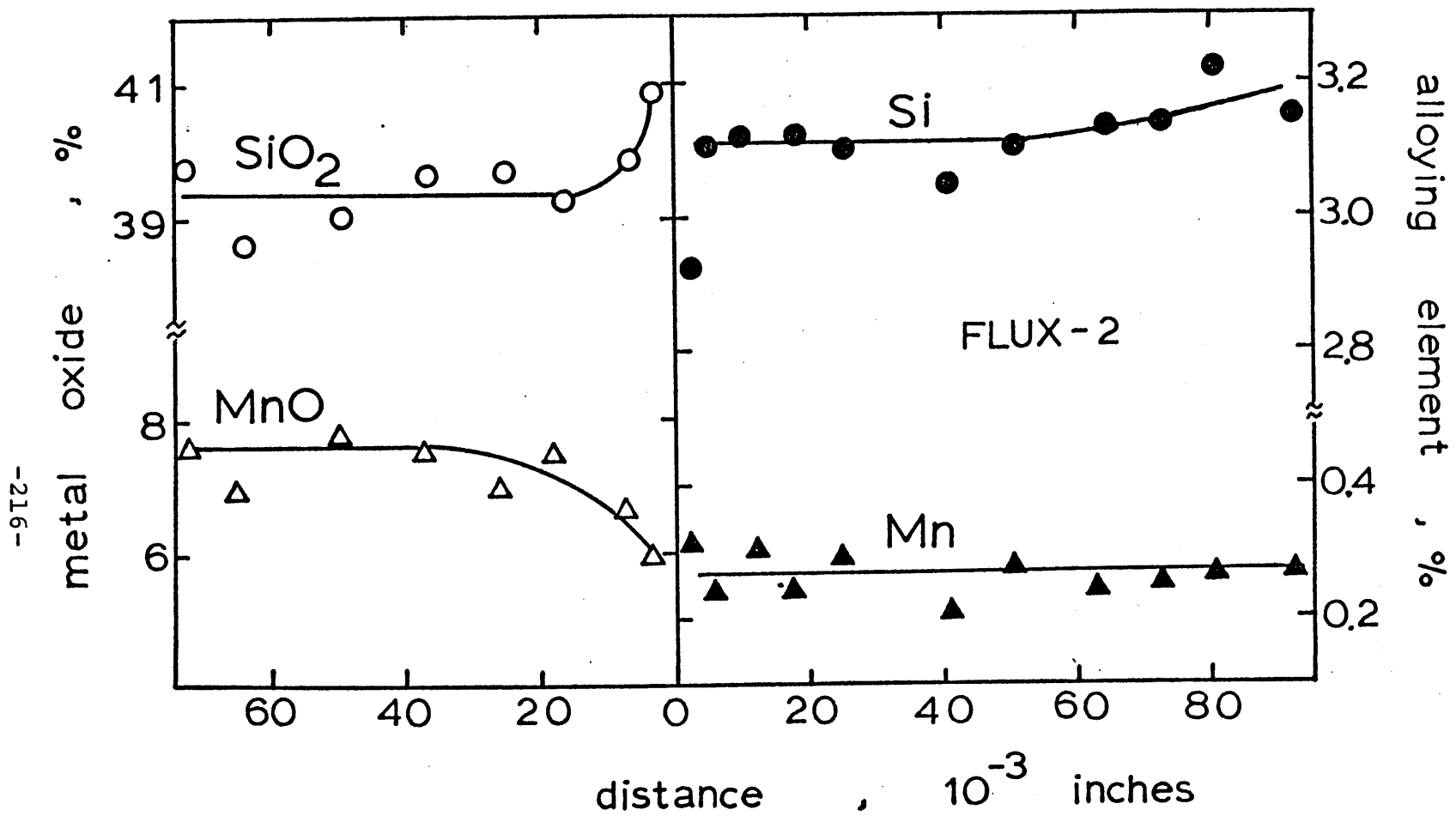
Appendix 6-g: The spatial distribution of Mn and Si in both the slag and the metal phases for weld made with Flux-2 and 3.22% Si plate.
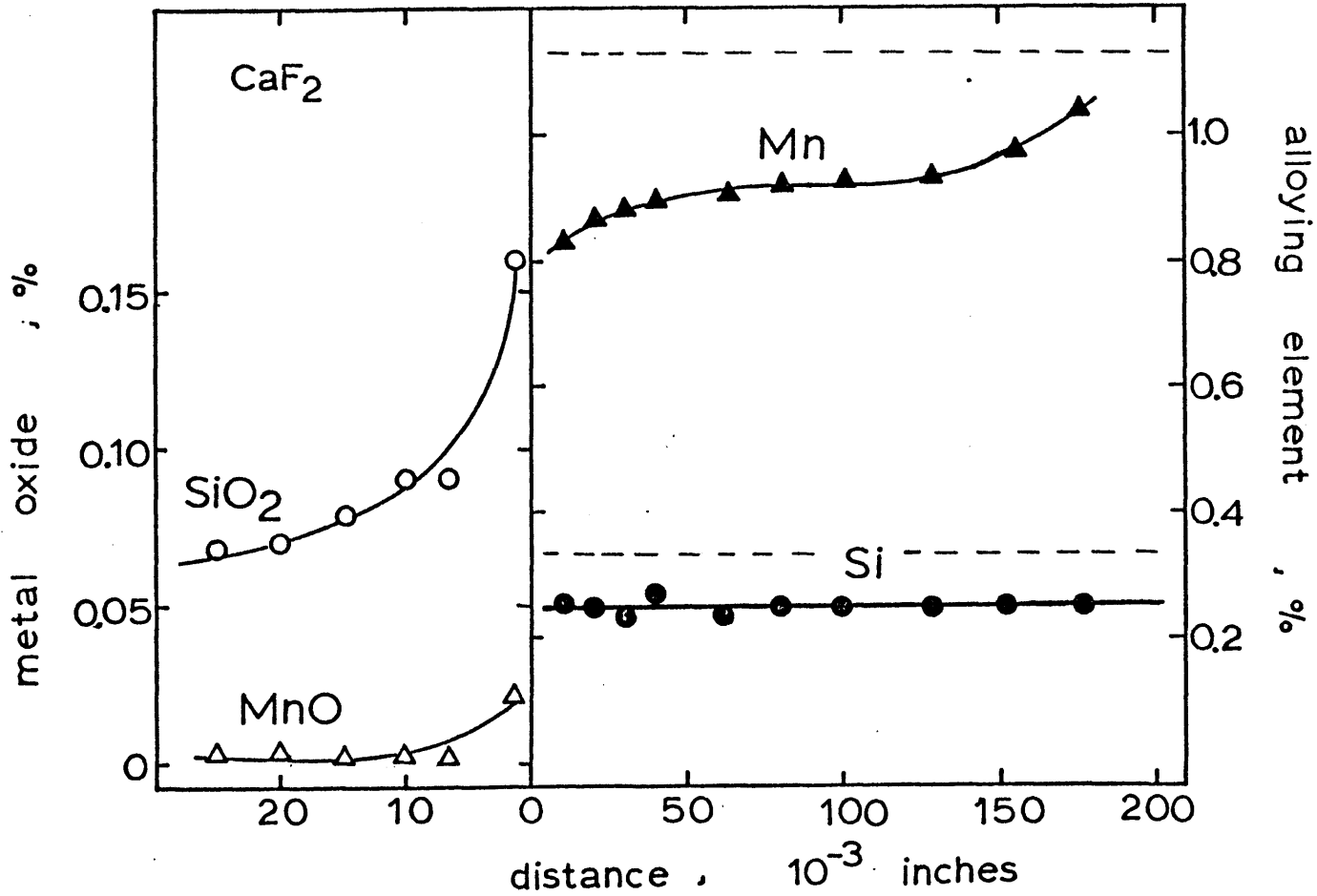
Appendix 6-h: The spatial distribution of Mn and Si in both the slag and the metal phases for weld made with pure CaF_2 flux. Dashed lines are the initial values.
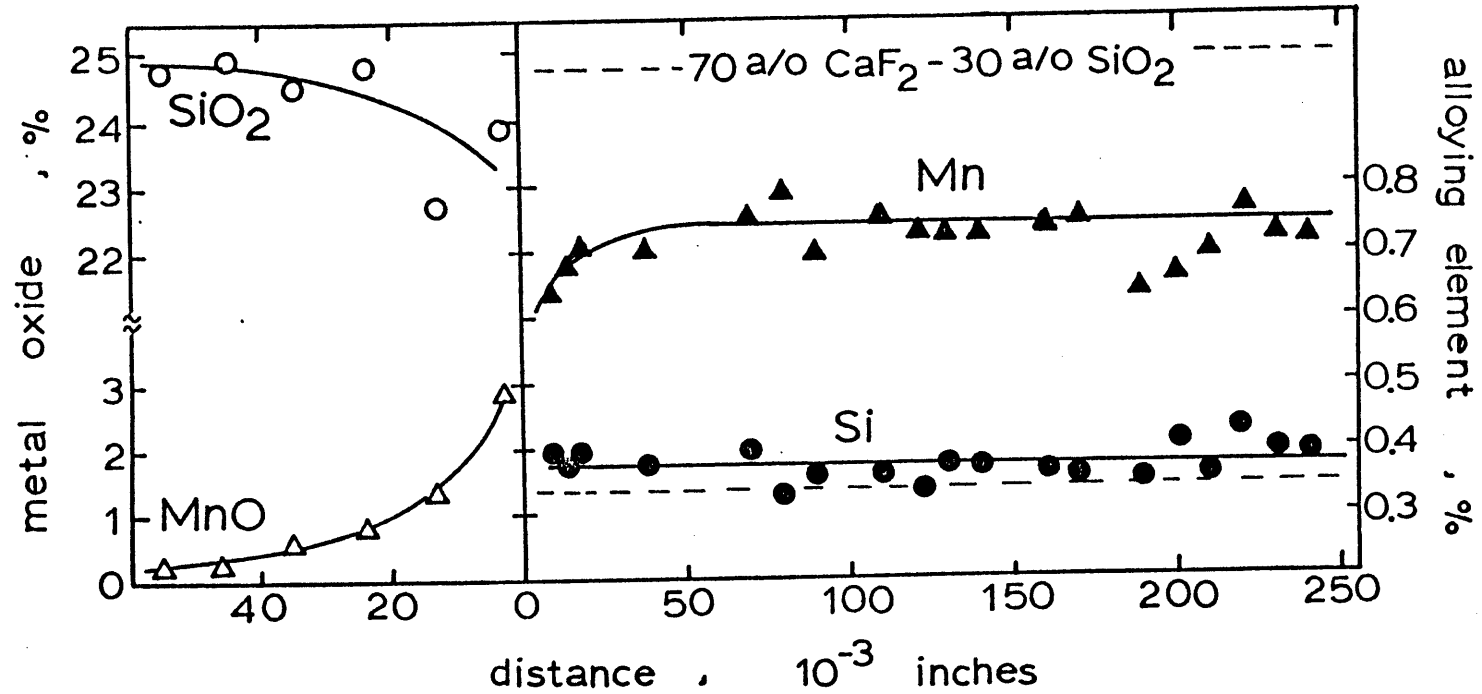
Appendix 6-i: The spatial distribution of Mn and Si in both the slag and the metal phases for weld made with 70%CaF$_2$-30%SiO$_2$ flux. Dashed lines are the initial values.

Appendix 6-j: The spatial distribution of Mn and Si in both the slag and the metal phases for weld made with 70%CaF$_2$-30%MgO flux. Dashed lines are the initial values.

Appendix 7: Results of the artificial baseplate experiment
using Flux F-1 and F-2

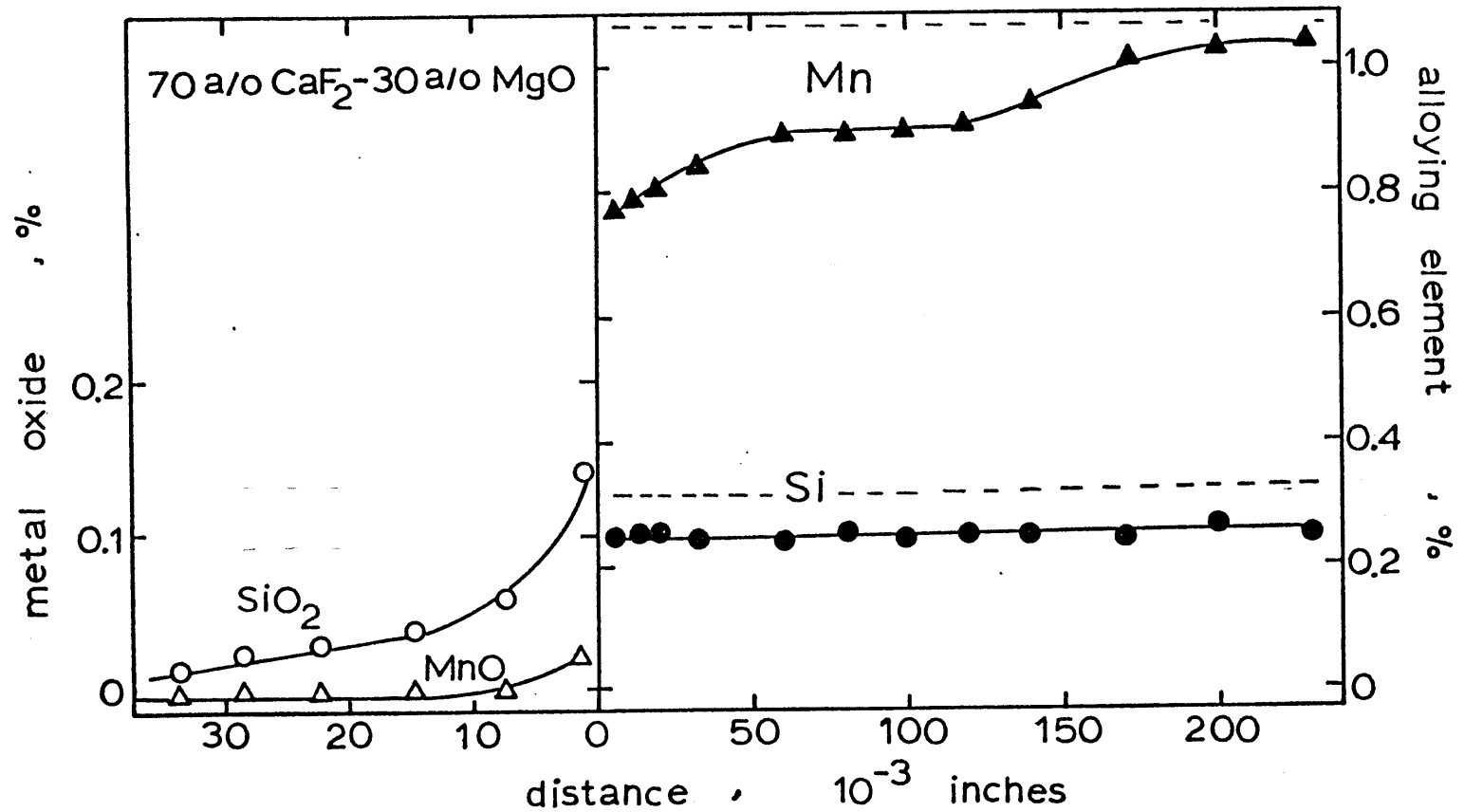| weld no.	Weld metal phase					Slag phase		Metallic mist in slag phase		
	Si,i (%)	Si,f (%)	Mn,i (%)	Mn,f (%)	O (%)	SiO_2 (%)	MnO (%)	Mn (%)	Si (%)	volume fraction of metallic mist (%)
1-1	0.10	0.19	1.85	1.85	0.050	41.83	15.60	0.93	0.83	1.5
1-2	0.05	0.15	1.40	1.50	0.047	42.00	14.23	---	---	2.31
1-3	0.04	0.09	0.08	0.48	0.068	---	---	0.71	0.86	1.06
1-4	0.10	0.19	1.74	1.75	0.072	42.00	15.51	1.03	1.80	0.6
1-5	0.19	0.25	1.00	1.15	0.052	41.79	12.76	0.71	0.69	0.46
1-6	0.21	0.27	0.85	1.20	0.062	42.13	12.51	0.84	1.05	0.86
1-7	0.06	0.08	0.07	0.40	0.035	---	---	---	---	0.71
1-8	0.27	0.27	0.94	1.27	0.030	42.40	12.95	0.83	0.96	0.43
1-9	0.54	0.49	0.98	1.40	0.049	---	---	0.78	1.10	0.78
1-10	0.08	0.13	0.64	1.00	0.060	---	---	---	---	2.98
1-11	0.07	0.15	1.95	1.90	0.046	41.58	15.83	0.83	0.72	1.87
1-12	0.24	0.26	0.88	1.10	0.056	42.41	10.59	0.65	0.91	2.10
1-13	0.02	0.06	2.30	2.16	0.050	---	---	---	---	0.60
1-14	0.32	0.29	1.06	1.16	0.038	42.46	15.31	---	---	1.05
1-15	0.39	0.36	0.93	1.20	0.040	---	---	---	---	1.95
2-1	0.23	0.27	1.07	0.86	0.070	37.80	8.20	0.40	0.66	0.19
2-2	0.01	0.11	0.49	0.44	0.099	38.34	7.80	---	---	0.06
2-3	0.65	0.61	1.38	1.02	0.078	39.68	8.35	---	---	0.14
2-4	0.02	0.11	2.04	1.33	0.096	---	---	---	---	0.94
2-5	0.21	0.26	1.03	0.76	0.102	37.70	8.25	0.74	1.24	0.39
2-6	0.63	0.53	1.34	0.98	0.080	39.93	8.58	---	---	0.17
2-7	0.06	0.15	1.07	0.92	0.107	---	---	---	---	1.55
2-8	0.09	0.11	2.24	1.67	0.072	36.85	8.83	0.77	1.43	0.12
2-9	0.18	0.19	1.18	0.90	0.085	---	---	---	---	0.25
2-10	0.01	0.04	0.79	0.69	0.085	38.53	7.84	0.47	0.76	0.25
2-11	0.02	0.14	2.30	1.56	0.096	38.10	9.45	---	---	0.22
2-12	0.02	0.23	2.33	1.58	0.069	---	---	0.93	1.70	0.62
2-13	0.01	0.11	0.28	0.38	0.099	38.34	7.40	---	---	1.25
2-14	0.12	0.21	0.40	0.44	0.082	38.65	7.15	---	---	1.50
2-15	0.33	0.30	0.78	0.62	0.078	39.63	8.00	---	---	0.18
2-16	0.42	0.39	1.74	1.34	0.080	39.64	8.40	---	---	2.15

Appendix 7: (continued) Results of the artificial
baseplate experiment using Flux F-3 and F-4

weld	Mn,i (%)	Mn.f (%)	Si,i (%)	Si,f (%)
3-1	0.79	1.06	0.01	0.20
3-2	1.18	1.26	0.18	, 0.26
3-3	1.06	1.18	0.26	0.39
3-4	1.07	1.17	0.29	0.38
3-5	1.10	1.12	0.33	0.39
3-6	1.34	1.26	0.63	0.68
3-7	0.91	1.07	0.06	0.35
3-8	1.03	1.20	0.21	0.38
3-9	1.40	1.29	0.50	0.61
4-1	0.79	0.58	0.01	0.06
4-2	1.18	0.87	0.15	0.18
4-3	1.07	0.94	0.29	0.28
4-4	1.07	0.88	0.29	0.26
4-5	1.10	0.93	0.31	0.28
4-6	1.34	0.87	0.63	0.45
4-7	1.07	1.02	0.06	0.17
4-8	1.03	0.55	0.21	0.22
4-9	1.40	1.00	0.50	0.40

Appendix 7: (continued) Results of the artificial
baseplate experiment using Flux
MIT-1 and MIT-2

weld No.	Mn,i(%)	Mn,f(%)	Si,i(%)	Si,f(%)
MIT-1-B-1	1.03	0.76	0.21	0.16
MIT-1-B-2	0.79	0.58	0.01	0.08
MIT-1-B-3	1.07	0.82	0.06	0.16
MIT-1-B-4	1.07	0.96	0.23	0.16
MIT-1-B-5	0.45	0.30	0.03	0.04
MIT-1-B-6	1.18	0.92	0.18	0.16
MIT-1-B-7	0.49	0.28	0.01	0.04
MIT-1-B-8	1.34	0.96	0.63	0.43
MIT-1-B-9	0.07	0.16	0.02	0.04
MIT-1-B-10	0.63	0.42	0.30	0.20
MIT-1-B-11	0.16	0.16	0.02	0.04
MIT-1-B-12	0.35	0.28	0.10	0.15
MIT-1-F-1	1.03	0.82	0.21	0.26
MIT-1-F-2	0.79	0.65	0.01	0.11
MIT-1-F-3	1.07	0.90	0.06	0.23
MIT-1-F-4	1.07	1.01	0.23	0.26
MIT-1-F-5	0.45	0.34	0.03	0.05
MIT-1-F-6	1.18	1.10	0.18	0.22
MIT-1-F-7	0.49	0.32	0.01	0.05
MIT-1-F-8	1.34	1.10	0.63	0.45
MIT-1-F-9	0.07	0.17	0.02	0.07
MIT-1-F-10	0,63	0.51	0.30	0.26
MIT-1-F-11	0.16	0.17	0.02	0.04
MIT-1-F-12	0.35	0.26	0.10	0.20
MIT-2-B-1	1.07	0.48	0.23	0.51
MIT-2-B-2	1.34	0.55	0.63	0.69
MIT-2-B-3	0.63	0.62	0.30	0.67
MIT-2-B-4	1.78	0.57	0.70	1.08
MIT-2-B-5	1.40	0.31	0.42	0.93
MIT-2-F-1	1.07	0.50	0.23	0.47
MIT-2-F-2	1.34	0.54	0.63	0.69
MIT-2-F-3	0.63	0.45	0.30	0.76
MIT-2-F-4	1.78	0.45	0.70	1.18
MIT-2-F-5	1.40	0.32	0.42	0.94

Appendix 8:Volume fraction of slag
            inclusions investigated
            in this study

weld no.	Volume fraction of slag inclusions (%)
1-1	5.5
1-4	3.86
1-5	10.3
1-6	3.56
1-8	3.57
1-12	3.61
2-1	8.72
2-5	3.8
2-8	6.8
2-10	3.99

Appendix 9: Comparison between k(expriment) and
k(theory) which was calculated from
both the Mn and the Si balance.
(positive sign represents weld metal gains
element, negative sign means weld metal loses
element)

| weld no. | k(exp) | k(theory) | |
		k(Mn balance)	k(Si balance)
1-1	0.34	0	+0.3
1-2	0.46	+0.08	+0.4
1-4	0.46	+0.07	+0.36
1-5	0.25	+0.07	+0.17
1-6	0.38	+0.14	+0.32
1-8	0.57	+0.16	0
1-11	0.41	-0.50	+0.18
1-12	0.31	+0.07	+0.35
1-14	0.51	+0.33	-0.58
2-1	0.57	+0.55	+0.05
2-2	0.53	-0.56	+0.18
2-3	0.59	-0.57	-0.72
2-5	0.46	-0.64	+0.06
2-8	0.53	-0.65	+0.02
2-10	0.53	-0.92	+0.06
2-11	0.48	-0.55	+0.18
2-13	0.52	+0.43	+0.18
2-14	0.44	+0.22	+0.09
2-15	0.54	-0.69	-0.64
2-16	0.51	-0.74	-0.58

Appendix 10: References of symbols used in Figures 17,18,20,35,36 and 47.

symbol	reference in Fig.17	reference in Fig.18	reference in Fig.20	reference in Fig.35	reference in Fig.36	reference in Fig.47
●	38	12	38	F-1	F-d	12
⊗	45	45	45	---	---	45
△	18	48	18	F-2	F-c	48
▣	44	44	44	---	F-e	---
▢	15	15	---	---	F-e	15
○	43	43	43	F-1	F-d	---
◉	17	17	---	---	---	17
⬡	47	47	---	---	---	---
⊞	42	---	---	---	---	---
◬	41	---	---	---	---	---
⊠	40	---	---	---	---	---
✕	46	---	---	---	---	---
▽	14	14	---	---	F-f	14
▲	this study	this study	---	---	---	this study
▼	---	14	---	---	F-f	---
▲	---	38	---	F-2	F-c	---